frontiers | Research Topics

Virology today in Spain. *Selected topics from the XVI Spanish virology*

Edited by
Covadonga Alonso and Josep Quer

Published in
Frontiers in Cellular and Infection Microbiology

ISSN 1664-8714
ISBN 978-2-8325-4424-2
DOI 10.3389/978-2-8325-4424-2

About Frontiers

Frontiers is more than just an open access publisher of scholarly articles: it is a pioneering approach to the world of academia, radically improving the way scholarly research is managed. The grand vision of Frontiers is a world where all people have an equal opportunity to seek, share and generate knowledge. Frontiers provides immediate and permanent online open access to all its publications, but this alone is not enough to realize our grand goals.

Frontiers journal series

The Frontiers journal series is a multi-tier and interdisciplinary set of open-access, online journals, promising a paradigm shift from the current review, selection and dissemination processes in academic publishing. All Frontiers journals are driven by researchers for researchers; therefore, they constitute a service to the scholarly community. At the same time, the *Frontiers journal series* operates on a revolutionary invention, the tiered publishing system, initially addressing specific communities of scholars, and gradually climbing up to broader public understanding, thus serving the interests of the lay society, too.

Dedication to quality

Each Frontiers article is a landmark of the highest quality, thanks to genuinely collaborative interactions between authors and review editors, who include some of the world's best academicians. Research must be certified by peers before entering a stream of knowledge that may eventually reach the public - and shape society; therefore, Frontiers only applies the most rigorous and unbiased reviews. Frontiers revolutionizes research publishing by freely delivering the most outstanding research, evaluated with no bias from both the academic and social point of view. By applying the most advanced information technologies, Frontiers is catapulting scholarly publishing into a new generation.

What are Frontiers Research Topics?

Frontiers Research Topics are very popular trademarks of the *Frontiers journals series*: they are collections of at least ten articles, all centered on a particular subject. With their unique mix of varied contributions from Original Research to Review Articles, Frontiers Research Topics unify the most influential researchers, the latest key findings and historical advances in a hot research area.

Find out more on how to host your own Frontiers Research Topic or contribute to one as an author by contacting the Frontiers editorial office: frontiersin.org/about/contact

Virology today in Spain. *Selected topics from the XVI Spanish virology*

Topic editors

Covadonga Alonso – Spanish National Research Council (CSIC), Spain

Josep Quer – Vall d'Hebron University Hospital, Spain

Citation

Alonso, C., Quer, J., eds. (2024). *Virology today in Spain. Selected topics from the XVI Spanish virology*. Lausanne: Frontiers Media SA.

doi: 10.3389/978-2-8325-4424-2

Table of contents

frontiers | Frontiers in Cellular and Infection Microbiology

TYPE Editorial
PUBLISHED 25 January 2024
DOI 10.3389/fcimb.2024.1367322

OPEN ACCESS

EDITED AND REVIEWED BY
Yousef Abu Kwaik,
University of Louisville, United States

*CORRESPONDENCE
Covadonga Alonso
calonso@inia.csic.es

RECEIVED 08 January 2024
ACCEPTED 12 January 2024
PUBLISHED 25 January 2024

CITATION
Alonso C, Quer J and García-Dorival I (2024) Editorial: Virology today in Spain. Selected topics from *Spanish virology*. *Front. Cell. Infect. Microbiol.* 14:1367322. doi: 10.3389/fcimb.2024.1367322

Editorial: Virology today in Spain. Selected topics from *Spanish virology*

Covadonga Alonso[1]*, Josep Quer[2,3,4] and Isabel García-Dorival[1]

[1]Departmento de Biotecnología, INIA-CSIC, Centro Nacional Instituto Nacional de Investigación y Tecnología Agraria y Alimentaria, Ctra. de la Coruña, Madrid, Spain, [2]Liver Diseases-Viral Hepatitis, Liver Unit, Vall d'Hebron Institut de Recerca (VHIR), Vall d'Hebron Hospital Universitari, Barcelona, Spain, [3]Centro de Investigación Biomédica en Red de Enfermedades Hepáticas y Digestivas (CIBERehd), Instituto de Salud Carlos III, Madrid, Spain, [4]Biochemistry and Molecular Biology Department, Universitat Autònoma de Barcelona (UAB), Bellaterra, Spain

KEYWORDS

virus host, emerging viral infection, hepatitis C virus (HCV), African swine fever virus (ASFV), Adeno associated virus, West Nile virus (WNV), MERS- and SARS-CoV

Editorial on the Research Topic
Editorial: Virology today in Spain. *Selected topics from Spanish virology*

The field of virology plays a pivotal role in our understanding of "One Health", encompassing animals, humans and the environment, influencing from public health strategies to advancements in medical treatments. This editorial introduces a series of 10 articles that delve into various aspects of virology, providing readers with a comprehensive and up-to-date overview of the field in this area. It includes interesting original articles about MERS-CoV, West Nile, Usutu, hepatitis C and African swine fever virus, between others, but also includes timely reviews on Coronaviruses (CoV), the origin of pediatric severe acute hepatitis, and antivirals against COVID-19 and human respiratory viruses.

Article by Barrado-Gil et al. investigates the intricate interplay between viruses and their hosts at the molecular level uncovering lipid host factors that influence endocytosis for African swine fever virus infection. Also, an article by García-Crespo et al. explores the mechanisms driving hepatitis C virus (HCV) evolution and adaptation, focusing on the HCV-fitness dependent implications in virus-host interactions and liver disease.

This Research Topic also examines the dynamics of emerging viral threats and discuss the strategies to anticipate and monitor such risks for health.

A clinical threat to the healthcare system was the occurrence of several cases of severe acute hepatitis (not A-E) in 37 countries in July 2022 that the article by Rodríguez-Frias et al. reviews.

Their conclusions pointed out that it was caused by Adeno-associated virus 2 (AAV2) infection, associated with a helper virus, and coincident with a determined genetic profile.

The emergence of the largest number of human cases of West Nile virus (WNV) infection occurred in Extremadura, Spain, with six human cases, is reported by Macias et al. These cases occurred in areas were WNV infections have been previously reported, suggesting the definition of an endemic area. Surveillance with early detection methods is encouraged in such regions.

Another research article by Llorente et al., communicates the experimental results regarding the susceptibility of certain bird species, such as red-legged partridges, to WNV strains, while being not competent for transmission of Usutu virus strains.

A review from Luis Enjuanes laboratory, summarizes the current knowledge of human CoV accessory proteins emphasizing their relevant contribution to pathogenesis (Hurtado-Tamayo et al.). Besides, Labiod et al., discuss on the role of DC-SIGN in MERS-CoV dissemination and pathogenesis.

Another study by Fernández-García et al., involved metagenomic sequencing, molecular characterization, and phylogenetics of the vaccine-derived poliovirus strain that caused disease in a patient in Senegal. It was confirmed to be an imported circulating type.

The Research Topic "*Vaccines and Antiviral Therapies*" was also covered by two reports in the antiviral activity of the HRA2pl fusion peptide against paramyxoviruses by Meza et al., and pneumoviruses by and another in the use of Plitidepsin in adult patients of COVID-19 by Varona et al.

This special issue reflects the immense diversity and quality of the research presented and discussed during the congress of the Spanish Society of Virology. Additionally, it serves as a small yet significant example of virology research conducted in Spain, actively promoted by the SEV.

Author contributions

CA: Conceptualization, Writing – original draft, Writing – review & editing. JQ: Conceptualization, Writing – original draft, Writing – review & editing. IG: Conceptualization, Writing – original draft, Writing – review & editing.

Conflict of interest

The authors declare that the research was conducted in the absence of any commercial or financial relationships that could be construed as a potential conflict of interest.

The author(s) declared that they were an editorial board member of Frontiers, at the time of submission. This had no impact on the peer review process and the final decision.

Publisher's note

frontiers | Frontiers in Cellular and Infection Microbiology

TYPE Original Research
PUBLISHED 22 February 2023
DOI 10.3389/fcimb.2023.1097809

OPEN ACCESS

EDITED BY
Josep Quer,
Vall d'Hebron Research Institute (VHIR), Spain

REVIEWED BY
Benjamin Florian Koch,
Goethe University Frankfurt, Germany
Francisco López Medrano,
Research Institute Hospital 12 de Octubre, Spain

*CORRESPONDENCE
Jose F. Varona
jfvarona@hmhospitales.com

SPECIALTY SECTION
This article was submitted to Clinical Microbiology, a section of the journal Frontiers in Cellular and Infection Microbiology

RECEIVED 14 November 2022
ACCEPTED 27 January 2023
PUBLISHED 22 February 2023

CITATION
Varona JF, Landete P, Paredes R, Vates R, Torralba M, Guisado-Vasco P, Porras L, Muñoz P, Gijon P, Ancochea J, Saiz E, Meira F, Jimeno JM, Lopez-Martin JA and Estrada V (2023) Plitidepsin in adult patients with COVID-19 requiring hospital admission: A long-term follow-up analysis. *Front. Cell. Infect. Microbiol.* 13:1097809. doi: 10.3389/fcimb.2023.1097809

Plitidepsin in adult patients with COVID-19 requiring hospital admission: A long-term follow-up analysis

Jose F. Varona[1,2*], Pedro Landete[3,4], Roger Paredes[5,6], Roberto Vates[7], Miguel Torralba[8,9], Pablo Guisado-Vasco[10,11], Lourdes Porras[12], Patricia Muñoz[13], Paloma Gijon[13], Julio Ancochea[3,4], Elena Saiz[14], Fernanda Meira[14], Jose M. Jimeno[14], Jose A. Lopez-Martin[14] and Vicente Estrada[15,16]

[1]Departamento de Medicina Interna, Hospital Universitario HM Monteprincipe, HM Hospitales, Madrid, Spain, [2]Facultad de Medicina, Universidad San Pablo-Centro de Estudios Universitarios (CEU), Madrid, Spain, [3]Departamento de Neumología, Hospital Universitario La Princesa, Madrid, Spain, [4]Facultad de Medicina, Universidad Autónoma de Madrid, Madrid, Spain, [5]Infectious Diseases Department, IrsiCaixa Acquired Immunodeficiency Syndrome (AIDS) Research Institute, Barcelona, Spain, [6]Servicio de Enfermedades Infecciosas Hospital Germans Trias I Pujol, Barcelona, Spain, [7]Internal Medicine Department, Hospital Universitario de Getafe, Madrid, Spain, [8]Medicine Department, Health Sciences Faculty, University of Alcalá, Madrid, Spain, [9]Internal Medicine Department, Guadalajara University Hospital, Guadalajara, Spain, [10]Internal Medicine Department, Hospital Universitario Quironsalud Madrid, Madrid, Spain, [11]Departamento de Medicina, Facultad de Ciencias Biomédicas y de la Salud, Universidad Europea, Madrid, Spain, [12]Internal Medicine, Hospital General de Ciudad Real, Ciudad Real, Spain, [13]Clinical Microbiology and Infectious Diseases Department, Instituto de Investigación Sanitaria Gregorio Marañón (IiSGM), Hospital General Universitario Gregorio Marañón, Madrid, Spain, [14]Virology Unit, PharmaMar, SA, Madrid, Spain, [15]Departamento de Medicina Interna Hospital Clínico San Carlos, Madrid, Spain, [16]Facultad de Medicina, Universidad Complutense de Madrid, Madrid, Spain

Introduction: The APLICOV-PC study assessed the safety and preliminary efficacy of plitidepsin in hospitalized adult patients with COVID-19. In this follow-up study (E-APLICOV), the incidence of post-COVID-19 morbidity was evaluated and any long-term complications were characterized.

Methods: Between January 18 and March 16, 2022, 34 of the 45 adult patients who received therapy with plitidepsin in the APLICOV-PC study were enrolled in E-APLICOV (median time from plitidepsin first dose to E-APLICOV enrollment, 16.8 months [range, 15.2–19.5 months]). All patients were functionally autonomous with regard to daily living (Barthel index: 100) and had normal physical examinations.

Results: From the APLICOV-PC date of discharge to the date of the extension visit, neither Common Terminology Criteria for Adverse Events version 5.0 (CTCAE v5) grade 3-4 complications nor QT prolongation or significant electrocardiogram (EKG) abnormalities were reported. Five (14.7%) patients had another COVID-19 episode after initial discharge from APLICOV-PC, and in 2 patients (5.9%), previously unreported chest X-ray findings were documented. Spirometry and lung-diffusion tests were normal in 29 (85.3%) and 27 (79.4%) patients, respectively,

and 3 patients needed additional oxygen supplementation after initial hospital discharge. None of these patients required subsequent hospital readmission for disease-related complications.

Discussion: In conclusion, plitidepsin has demonstrated a favorable long-term safety profile in adult patients hospitalized for COVID-19. With the constraints of a low sample size and a lack of control, the rate of post-COVID-19 complications after treatment with plitidepsin is in the low range of published reports. (ClinicalTrials.gov Identifier: NCT05121740; https://clinicaltrials.gov/ct2/show/NCT05121740).

KEYWORDS

plitidepsin, COVID-19, SARS-CoV-2, long COVID, post-COVID-19 complications

Introduction

As of 2 October 2022, the severe acute respiratory syndrome coronavirus 2 (SARS-CoV-2) pandemic has resulted in more than 615 million infections and 6.5 million deaths, at significant costs to healthcare systems and societies worldwide (World Health Organization, 2022). Though initial public health responses focused on reducing the acute burden of coronavirus disease 2019 (COVID-19), it has become increasingly apparent that SARS-CoV-2 infection can also provoke longer-term mental and physical health consequences, thus heightening the concern of the healthcare systems (Greenhalgh et al., 2020; National Institute for Health and Care Research, 2020; National Institute for Health and Care Excellence, 2020). The persistence of symptoms –such as fatigue, dyspnea, chest pain, cognitive disturbances, or arthralgia – 3 months after SARS-CoV-2 infection is referred to as post-COVID-19 disease or "long COVID" (National Institute for Health and Care Excellence, 2020). Between 10 and 25% of patients will experience long COVID, resulting in a significant limitation of daily activities, an increase in long-term sick leave from work, and the appearance of sequelae that may continue for more than one year (Carfì et al., 2020; Augustin et al., 2021).

Post-COVID-19 sequelae in patients who required hospitalization due to a severe SARS-CoV-2 infection are generally a consequence of structural damage to different organs by the infection itself and/or associated complications. Various studies point to sequelae not only restricting the respiratory apparatus but also affecting the cardiovascular system, the kidneys and the central and peripheral nervous system (Carfì et al., 2020; Salehi et al., 2020; Vindegaard and Benros, 2020; Ojha et al., 2020; Sudre et al., 2021; Huang et al., 2021). Psychiatric and psychological sequelae have also been documented (Vindegaard and Benros, 2020).

Risk factors for post-COVID-19 sequelae include the severity of acute COVID-19 infection, age, biological sex and sex hormones, and the presence of pre-existing conditions (Koc et al., 2022). Furthermore, it has been reported that viral load during acute COVID-19 may correlate with the severity of long COVID manifestation, and a rapid drop in the viral load of patients with acute COVID-19 infection may be protective from long COVID responses (Koc et al., 2022). Treatments that facilitate rapid resolution of the acute infection could therefore be protective against the effects of long COVID.

The APLICOV-PC proof-of-concept study (NCT04382066) assessed the safety and preliminary efficacy of 3 dose levels of plitidepsin (1.5 mg, 2.0 mg and 2.5 mg) administered for three consecutive days in hospitalized adult patients with COVID-19 (Varona et al., 2022). The trial met the primary endpoint of safety and feasibility of the 3 plitidepsin doses administered. In addition, results from APLICOV-PC suggested that plitidepsin was associated with reductions of viral load (mean 3.25-$\log_{10}$ reduction in baseline viral load by Day 15), inducing recovery (87% of the patients had moderate to severe illness when they entered the study; by Day 15, 82% of the patients had been discharged), and providing relevant impact on lymphocyte reconstitution and other inflammatory parameters (Varona et al., 2022).

The E-APLICOV study (NCT05121740) described herein was designed to evaluate whether plitidepsin treatment in patients hospitalized for COVID-19 could have a relevant impact on the emergence of long-term sequelae resulting from SARS-CoV-2 infection.

Methods

Study design and participants

APLICOV-PC was conducted in 10 hospital centers in Spain between May 12, 2020 and November 26, 2020 (second COVID-19 pandemic wave). Details and results of the study have been previously published (Varona et al., 2022). This multi-site extension of the APLICOV-PC clinical study (ran from January 18, 2022 to March 16, 2022) invited patients who received previous therapy with plitidepsin for COVID-19. Patients were enrolled after signing informed consent to participate in this extension study. The patients included in the extension study received no treatment whatsoever in relation to the study.

Procedures

The sites participating in the study were supervised by monitors appointed by the sponsor. Monitors performed periodic visits to the site before, during and at the end of the trial, or failing that, by telephone contact or written communication. Remote verification of source data were performed in agreement with the participating centers.

Data were collected through electronic case report forms (eCRFs) from each center participating in the study, and were provided by the Clinical Research Organization (CRO). The data was collected and processed with the appropriate precautions to guarantee confidentiality and compliance with the current legislation regarding data privacy (EU Regulation 2016/679 of the European Parliament and of the Council of 27 April 2016 on the protection of natural persons with regard to the processing of personal data and on the free movement of such data and with Organic Law 03/2018 on protection of personal data and guarantee of digital rights).

Study objective

The main objective of this study was to evaluate the incidence of post-COVID-19 morbidity and characterize the profile of complications in patients who participated in the APLICOV-PC study, assessing the incidence of post-COVID-19 complications after exposure to therapeutic intervention with plitidepsin at flat doses of 1.5, 2.0, and 2.5 mg/day, for 3 consecutive days as a 90-min IV infusion (Varona et al., 2022).

To complete this objective, the following information was gathered for the time spanning from the patient's last visit in the APLICOV-PC study through the end of the extension study: 1) readmissions to hospitals and their causes; 2) the need for oxygen therapy and duration of the same; and 3) the incidence of complications (See Supplementary Table 1).

Statistical analysis

All data has been analyzed with the SAS statistical analysis system, version 9.4. All analyses have been carried out mainly by descriptive statistical methods. Continuous endpoints have been described using maximum, minimum, Q1 and Q3, mean, median and standard deviation. Categorical endpoints have been described with frequencies and percentages as well as the exact 95% confidence interval of the relevant study variables. All demographic and patient characteristics are reported using the initiation of the E-APLICOV study as baseline unless otherwise noted.

Results

Of the 45 adult patients who received therapy with plitidepsin in the APLICOV-PC study, 34 were enrolled into this extension (Figure 1). Of those included in E-APLICOV, 5 (14.7%), 19 (55.9%) and 10 (29.4%) patients had mild, moderate, and severe COVID-19 (FDA criteria), respectively, at the time of treatment with plitidepsin (Table 1). A median of 16.8 months (range 15.2 – 19.5 months) had elapsed from the time patients received their first dose of plitidepsin to the start of this extension (Table 1). Most patients were male (23 patients, 67.6%) and Caucasian (23 patients, 67.6%) (Table 1). Their

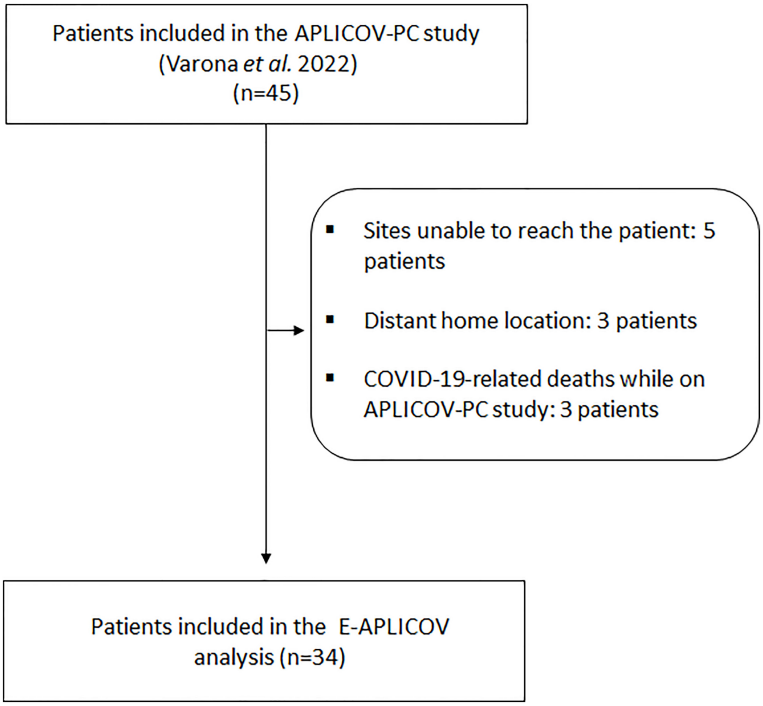

FIGURE 1
Flowchart of exclusions.

10.3389/fcimb.2023.1097809

TABLE 1 Demographic and baseline characteristics for the 34 patients included in the E-APLICOV study.

	1.5 mg N=9	2.0 mg N=14	2.5 mg N=11	Total N=34
Age, median (range) years	53 (33-70)	52,5 (36-72)	54 (43-68)	53 (33-72)
Gender, n (%) male	7 (77.8)	10 (71.4)	6 (54.5)	23 (67.6)
Ethnicity, n (%)				
Caucasian	7 (77.8)	9 (64.3)	7 (63.6)	23 (67.6)
Latin	2 (22.2)	3 (21.4)	4 (36.4)	9 (26.5)
North African	–	1 (7.1)	–	1 (2.9)
Asian	–	1 (7.1)	–	1 (2.9)
Body mass index, median (range) kg/m^2	27.7 (18.4-34.2)	30.3 (22.0-46.2)	29.8 (21.9-41.5)	29.7 (18.4-46.2)
Median (range) time from plitidepsin first dose to E-APLICOV inclusion, months	17.6 (15.3-19.5)	17.2 (15.7-18.6)	16.2 (15.2-17.8)	16.8 (15.2-19.5)
Number of comorbidities, n (%)				
None	3 (33.3)	2 (14.3)	0 (0)	5 (14.7)
One	1 (11.1)	6 (42.9)	6 (54.5)	13 (38.2)
Two or more	5 (55.6)	6 (42.9)	5 (45.5)	16 (47.1)
Disease status at randomization, n (%) [A]				
Mild COVID-19	1 (11.1)	3 (21.4)	1 (9.1)	5 (14.7)
Moderate COVID-19	5 (55.6)	7 (50)	7 (63.6)	19 (55.9)
Severe COVID-19	3 (33.3)	4 (28.6)	3 (27.3)	10 (29.4)
Vaccination status (COVID-19)				
Non-vaccinated patients, n (%)	1 (11.1)	–	–	1 (2.9)
Vaccinated patients, n (%)	8 (88.9)	14 (100)	11 (100)	33 (97.1)
1 dose	1 (11.1)	4 (28.6)	1 (9.1)	6 (17.6)
2 doses	4 (44.4)	7 (50.0)	10 (90.9)	21 (61.8)
3 doses	3 (33.3)	3 (21.4)	–	6 (17.6)
Serostatus against SARS-CoV-2, n (%)				
Negative	1 (11.1)	1 (7.1)	1 (9.1)	3 (8.8)
Positive	8 (88.9)	13 (92.9)	10 (90.9)	31 (91.2)

[A] Estimated using baseline assessments recorded in Electronic Data Capture using severity definitions in FDA Guidance for Industry "COVID-19: Developing Drugs and Biological Products for Treatment or Prevention": mild (no shortness of breath or dyspnea, $SpO_2 \geq 95\%$, respiratory rate < 20 breaths/min, heart rate < 90 bpm), moderate (shortness of breath with exertion, $SpO_2 > 93\%$ but < 95%, respiratory rate ≥ 20 breaths/min or heart rate ≥ 90 bpm), and severe (shortness of breath at rest or respiratory distress, $SpO_2 \leq 93\%$, respiratory rate ≥ 30 breaths/min, heart rate ≥ 125 bpm).
bpm, beats per minute; FDA, Food and Drug Administration; Kg, kilogram; m^2, square meter; mg, milligram; min, minutes; N, n, number; SpO_2, oxygen saturation.
–, No patients.

median age was 53 years (range: 33-72 years) and their median body-mass index (BMI) was 29.7 kg/m^2 (range: 18.4-46.2 kg/m^2) (Table 1). Obesity (BMI > 30 kg/m^2) was observed in 16 (47%) patients. Sixteen (47.1%) patients had two or more co-morbidities at randomization (Table 1). Eighty-five percent of patients had received some form of pharmacological treatment at E-APLICOV study entry. Thirty-eight percent of all patients were treated with lipid modifying agents and 35.3% with drugs used in diabetes. Analgesics (23.5% of patients) and anti-inflammatory and antirheumatic products (23.5% of patients) were also among the most frequently used medications for patients included in the study (See Supplementary Table 2). There was only 1 (2.9%) unvaccinated patient at the start of E-APLICOV, whereas 6 (17.6%), 21 (61.8%), and 6 (17.6%) patients, respectively, had received 1, 2, and 3 doses of a COVID-19 vaccine since the conclusion of the initial study (Table 1). A total of 3 patients were seronegative (8.8%) at entry into the extension study (Table 1). The median values of analytical parameters relevant to COVID-19 at study entry are shown in Supplementary Table 3. Patients in this analysis had a median total lymphocyte count of 1.98 x10^9 cells/L (interquartile range [IQR], 1.56–2.56), C-reactive protein [CRP] of 1.36 mg/dL (IQR, 0.9–2.9) and D-dimer of 240.5 ng/mL (IQR, 201–343).

At study entry, none of the patients showed functional limitations for their daily living activities (Barthel index: 100) and there were no reports of physical and neurological abnormalities. There were no

CTCAE v5 grade 3–4 complications from the date of APLICOV-PC discharge to the date of the extension visit. Nearly 15% of patients (n=5) were diagnosed with COVID-19 after the completion of the APLICOV-PC study (approximately 13-15 months after the last patient inclusion in the APLICOV-PC study). Among the post-COVID-19 complications occurring in the patients analyzed in the study (See Supplementary Tables 4, 5), the investigators found the following events, reported as grade 2 disease-related complications, in one patient each (2.9%): alopecia, cough, diabetic metabolic decompensation, hyperglycemia, and interstitial lung disease. Grade 2 asthenia was described in 2 patients (5.9%) (Table 2). There were no reports on clinically relevant abnormalities in hematological parameters. None of the patients experienced a thromboembolic event.

Two patients (5.9%) presented chest X-ray findings (hilar adenopathies and bilateral micronodules, impingement of the left lateral costophrenic sinus and calcified atheromatosis of the aortic arch) not reported previously. Electrocardiogram (EKG) abnormalities (e.g., atrial fibrilation, left axis deviation or sinus

TABLE 2 Summary of post-COVID-19 complications, related to study disease, overall. Worst grade per patient.

Post-COVID-19 complications	Grade						Total	
	Missing		G1		G2			
	N	%	N	%	N	%	N	%
Alanine aminotransferase increased	.	.	1	2.9	.	.	1	2.9
Alopecia	.	.	.	.	1	2.9	1	2.9
Anxiety	.	.	2	5.9	.	.	2	5.9
Aspartate aminotransferase increased	.	.	1	2.9	.	.	1	2.9
Asthenia	.	.	11	32.4	2	5.9	13	38.2
Attention deficit	.	.	5	14.7	.	.	5	14.7
Back pain	.	.	1	2.9	.	.	1	2.9
Blood cholesterol increased	.	.	1	2.9	.	.	1	2.9
Blood triglycerides increased	.	.	1	2.9	.	.	1	2.9
COVID-19 pneumonia	.	.	1	2.9	.	.	1	2.9
Chest pressure	.	.	1	2.9	.	.	1	2.9
Cough	.	.	4	11.8	1	2.9	5	14.7
Diabetic metabolic decompensation	.	.	.	.	1	2.9	1	2.9
Diarrhea	.	.	1	2.9	.	.	1	2.9
Dizziness	1	2.9	3	8.8	.	.	4	11.8
Dyspnea	.	.	1	2.9	.	.	1	2.9
Febricula	.	.	1	2.9	.	.	1	2.9
Fibrin D-dimer increased	.	.	1	2.9	.	.	1	2.9
Gamma-glutamyltransferase increased	.	.	2	5.9	.	.	2	5.9
General malaise	.	.	5	14.7	.	.	5	14.7
Headaches	.	.	3	8.8	.	.	3	8.8
Hyperglycemia	.	.	.	.	1	2.9	1	2.9
Interstitial lung disease	.	.	.	.	1	2.9	1	2.9
Joint pains	.	.	2	5.9	.	.	2	5.9
Low mood	.	.	3	8.8	.	.	3	8.8
Memory lapses	.	.	4	11.8	.	.	4	11.8
Muscle aches and pains	.	.	3	8.8	.	.	3	8.8
Palpitations	.	.	2	5.9	.	.	2	5.9
Serum ferritin increased	.	.	2	5.9	.	.	2	5.9
Tingling in extremity	.	.	5	14.7	.	.	5	14.7

G, grade; N, number.
–, No patients.

10.3389/fcimb.2023.1097809

TABLE 3 Pulmonary function assessment.

Pulmonary function assessment			1.5 mg		2 mg		2.5 mg		Total	
			N	%	N	%	N	%	N	%
Spirometry	**FVC result**	**Normal**	7	77.8	14	100.0	11	100.0	32	94.1
		Reduced	2	22.2	.	.	.	.	2	5.9
	FEV_1 result	**Normal**	7	77.8	13	92.9	9	81.8	29	85.3
		Reduced	2	22.2	1	7.1	2	18.2	5	14.7
	FEV_1/FVC result	**Normal**	9	100.0	12	85.7	8	72.7	29	85.3
		Reduced	.	.	2	14.3	3	27.3	5	14.7
Dyspnea assessment	**mMRC**	**0**	5	55.6	7	50.0	9	81.8	21	61.8
		1	2	22.2	6	42.9	2	18.2	10	29.4
		2	.	.	1	7.1	.	.	1	2.9
		3	2	22.2	.	.	.	.	2	5.9
Lung-diffusion testing	**DLCO result**	**Normal**	9	100.0	10	71.4	8	72.7	27	79.4
		High	.	.	3	21.4	2	18.2	5	14.7
		Low	.	.	1	7.1	1	9.1	2	5.9

0 (Symptoms: Little; Description: Dyspnea only with strenuous exercise); 1 (Symptoms: Mild; Description: Dyspnea when hurrying or walking up a slight hill); 2 (Symptoms: Moderate; Description: Walks slower than people of the same age because of dyspnea or has to stop for breath when walking at own pace); 3 (Symptoms: Many; Description: Stops for breath after walking just under 100 m (100 yards) or after a few minutes); 4 (Symptoms: Very much; Description: Too dyspneic to leave house or breathless when dressing) DLCO, diffusing capacity of the lungs for carbon monoxide; FEV_1, forced expiratory volume in one second; FVC, forced vital capacity; mg, milligram; mMRC, modified Medical Research Council; N, number.
., No patients.

tachycardia) were found in 5 patients (14.7%) but were not judged as clinically significant. No QT prolongation was described in any of the 34 patients.

Spirometry and lung-diffusion tests were normal in 29 (85.3%) and 27 (79.4%) patients, respectively, at study entry (Table 3). The pre-test 6-minute walk test scored 0–2 (no or slight dyspnea) in all patients (Borg scale). After the test, 24 (70.6%) patients had scores of 0–2, 6 (17.6%) patients of 2.5–4 (moderate dyspnea), and 4 (11.8%) patients had severe dyspnea (Supplementary Table 6). Only 2 patients, 1 with moderate COVID-19 and 1 in the severe group, stopped or paused during the test and none of the patients experienced symptoms at the end of the exercise.

Subsequent hospital readmission for disease-related complications was not required for any of the patients. Three patients (8.82%, 2 with severe and 1 with moderate COVID-19 disease) required additional oxygen supplementation, *via* nasal cannula or Venturi mask, after initial hospital discharge.

Discussion

Treatments to manage or prevent the development of sequelae arising from acute SARS-CoV-2 infection are urgently needed. Growing evidence suggests that the pathophysiologic model underlying post-COVID-19 sequelae stems from a dysregulated immune system that, after acute infection, continues releasing aberrantly high levels of proinflammatory cytokines that lead to chronic low-grade inflammation and multiorgan symptomatology (Buonsenso et al., 2022). Further, the hypothesis that a rapid reduction in SARS-CoV-2 viral load during acute infection may reduce the risk of post-COVID-19 complications is increasingly gaining strength (Rajan et al., 2021).

The previous APLICOV-PC proof-of-concept study confirmed plitidepsin safety in adult COVID-19 patients requiring hospital admission. Data gathered suggested that treatment of hospitalized patients with plitidepsin could sharply reduce SARS-CoV-2 viral load, promote recovery, and positively impact on the absolute lymphocyte counts and other inflammatory parameters (Varona et al., 2022). This trend toward increasing the total number of lymphocytes is of utmost importance given that the depth of lymphopenia may be associated with poor prognosis, including higher COVID-19 mortality (Lee et al., 2021). To the best of our knowledge, an increase in lymphocyte counts has not been reported with other antiviral therapies (Barratt-Due et al., 2021).

Due to plitidepsin's putative effect on rapidly reducing the SARS-CoV-2 viral load and normalizing certain immune system parameters, we sought to characterize the incidence of post-COVID-19 morbidity and long-term complications in patients who participated in APLICOV-PC. As the last patient in the APLICOV-PC study was enrolled in November 2020, there was already an extensive margin of follow-up time of almost 12 months to evaluate these parameters in this study. Despite the relatively high severity of COVID-19 (85% were graded as moderate to severe in the original study) and prevalence of comorbidity (85% of patients had ≥1 comorbidity), we observed few long-term complications in this group of patients previously treated with plitidepsin. None of the patients included in the E-APLICOV study had experienced functional restrictions in performing physical actions needed in everyday life. Reports of neurological Grade 1 post-COVID-19 complications, deemed to be related to study disease, included attention deficit (n=5; 14.7%), memory lapses (n=4; 11.8%),

low mood (n=3; 8.8%), headaches (n=3; 8.8%), and anxiety (n=2; 5.9%). These low rates are in contrast with reports from an electronic follow-up record of 236,379 patients during the first six months following COVID-19 diagnosis, in which neuropsychiatric complications emerged in 34% of cases, not including headache. The most commonly reported complications include mood and anxiety disorders and psychoses (24%), neuropathies (2.1%), and dementia (0.67%) (Taquet et al., 2021). On the other hand, the most frequent neurological symptoms are headache and cognitive changes, described in up to 68% and 81% of patients, respectively, with some sort of neurological symptoms after week 12 following acute infection (Graham et al., 2021).

In patients who present with severe COVID-19, the main sequelae is the development of pulmonary fibrosis. According to a recent meta-analysis, approximately 30% of patients hospitalized with pneumonia due to SARS-CoV-2 have shown fibrotic changes that persist for the first 12 months after discharge from the hospital (Fabbri et al., 2022). In this study, grade 1 COVID-19 pneumonia was reported in only 1 patient (2.9%) and only 2 patients (5.9%) presented chest X-ray findings, which were not suggestive of pulmonary fibrosis. None of the patients experienced a pulmonary embolism.

Finally, it should be highlighted that the dose range proposed in the APLICOV-PC study, which was based on pharmacokinetic/pharmacodynamic modeling, anticipated that antiviral concentrations of plitidepsin would be reached in distal anatomical compartments. *In-vivo* biodistribution of plitidepsin confirms that key organs in SARS-CoV-2 are exposed to therapeutic concentrations. Considering that SARS-CoV-2 infection is a systemic process that goes beyond affecting the respiratory tract, the biodistribution of plitidepsin might result in a widespread reduction of organ dysfunction, potentially protecting SARS-CoV-2-affected organs (Machhi et al., 2020; Rajan et al., 2021). Indeed, data from the COVERSCAN study conducted in the United Kingdom, which carried out serial Magnetic Resonance Imaging (MRI) scanning in a sample of 201 generally-healthy, middle-aged individuals, with COVID-19, showed evidence of mild organ impairment of the heart (32%), lungs (33%), kidneys (12%), liver (10%), pancreas (17%), and spleen (6%) (Rajan et al., 2021). Significant heart injuries, including myocarditis with reduced systolic function and arrhythmias, have been documented in patients with severe forms of COVID-19. Myocardial injury has been reported, which may be due to direct damage to the cardiomyocytes, systemic inflammation, myocardial interstitial fibrosis, and hypoxia (Babapoor-Farrokhran et al., 2020). Due to significant myocardial injuries in patients with severe COVID-19 symptoms, the morbidity and lethality of the illness could be high (Aggarwal et al., 2020; Clerkin et al., 2020; Bansal, 2020). Moreover, it has been shown that right ventricular abnormalities can occur after SARS-CoV-2 infection and likely reflect the consequences of COVID-19-associated severe pneumonia (Singh et al., 2022). It should be noted, however, that no clinically significant functional heart abnormalities were found in patients of the E-APLICOV study. At the E-APLICOV study entry, spirometry and lung-diffusion tests were abnormal in only 14.7% and 20.6% of the patients, respectively, percentages below the COVID-19-derived lung dysfunction rates previously described in the literature (Rajan et al., 2021).

In summary, considering the absence of CTCAE v5 grade 3-4 complications and of clinically significant EKG abnormalities, as well as the low rate of disease-related complications, chest X-ray findings and requirement of oxygen supplementation in patients included in this study, plitidepsin has demonstrated long-term safety in adult patients hospitalized for COVID-19. Despite the limitations of a low sample size and a lack of control group in APLICOV-PC, the rate of post-COVID-19 complications after treatment with plitidepsin appears to be in the lower limit of the 95% confidence interval of the prevalence of post-COVID-19 complications reported in a recent meta-analysis [80% (95% CI 65–92)] (Lopez-Leon et al., 2021).

Data availability statement

The original contributions presented in the study are included in the article/Supplementary Material. Further inquiries can be directed to the corresponding author.

Ethics statement

The studies involving human participants were reviewed and approved by CEIm HM Hospitales. The patients/participants provided their written informed consent to participate in this study.

Author contributions

The specific additional participation of each author is as follows: JV: conceptualization, investigation, writing and reviewing of the original draft. PL: investigation. RP: conceptualization and investigation. RV, MT, PG-V, LP, PM, PG, and JA: Investigation. ES and FM: data supervision. JJ: conceptualization, formal analysis, supervision, validation, investigation, methodology, and writing & critical review of the article. JL-M: conceptualization, data curation, software, formal analysis, supervision, validation, investigation, visualization, methodology, writing & critical review of the article. VE: conceptualization and investigation. All authors contributed to the article and approved the submitted version.

Funding

This study has been funded by Pharma.Mar, S.A. (Madrid, Spain).

Acknowledgments

We are indebted to the women and men that gave their consent to participate in this study, and to their relatives, for understanding their decision in these exceptional circumstances. We would like to thank Alvaro Belgrano for data curation and Timothy Silverstein and Raquel Lloris for providing editorial support.

Conflict of interest

VE has received personal fees from Janssen, Gilead, and ViiV and grants from MSD. RP has participated in Advisory Boards from Gilead, MSD, ViiV Healthcare, and Theratechnologies. MT has received consulting fees as a member of Advisory Committee and honoraria and speaking fees from Gilead, Janssen, MSD, and ViiV Companies. PG-V received speaker fees from FLS Science, Pharma Mar SA Madrid, Spain and GlaxoSmithKline Spain; consulting fees from Angelini Pharma and Pharma Mar SA; served as an advisory board member for Berlin Cures GmbH and Pharma Mar SA; and meeting grants from GlaxoSmithKline and Pharma Mar SA. JJ holds stocks of Pangaea Oncology, has a non-remunerated role in the Scientific Advisory Board and holds stocks of Promontory Therapeutics, and is a full-time employee of Pharmamar, SA Madrid, Spain and owns stocks. JL-M is a full-time employee and shareholder of Pharmamar, SA Madrid, Spain. ES and FM are full-time employees of Pharmamar, SA Madrid, Spain. JL-M is a co-inventor of a patent for plitidepsin WO2008135793A1. JJ is a co-inventor on a patent for didemnin WO99/42125 and on patents for aplidine WO03/033013 and WO 2004/080421.

The remaining authors declare that the research was conducted in the absence of any commercial or financial relationships that could be construed as a potential conflict of interest.

Publisher's note

All claims expressed in this article are solely those of the authors and do not necessarily represent those of their affiliated organizations, or those of the publisher, the editors and the reviewers. Any product that may be evaluated in this article, or claim that may be made by its manufacturer, is not guaranteed or endorsed by the publisher.

Supplementary material

The Supplementary Material for this article can be found online at: https://www.frontiersin.org/articles/10.3389/fcimb.2023.1097809/full#supplementary-material

References

Aggarwal, G., Cheruiyot, I., Aggarwal, S., Wong, J., Lippi, G., Lavie, C. J., et al. (2020). Association of cardiovascular disease with coronavirus disease 2019 (COVID-19) severity: A meta-analysis. *Curr. Probl Cardiol.* 45 (8), 100617. doi: 10.1016/j.cpcardiol.2020.100617

Augustin, M., Schommers, P., Stecher, M., Dewald, F., Gieselmann, L., Gruell, H., et al. (2021). Post-COVID syndrome in non-hospitalised patients with COVID-19: a longitudinal prospective cohort study. *Lancet Reg. Health Eur.* 6, 100122. doi: 10.1016/j.lanepe.2021.100122

Babapoor-Farrokhran, S., Gill, D., Walker, J., Rasekhi, R. T., Bozorgnia, B., and Amanullah, A. (2020). Myocardial injury and COVID-19: Possible mechanisms. *Life Sci.* 253, 117723. doi: 10.1016/j.lfs.2020.117723

Bansal, M. (2020). Cardiovascular disease and COVID-19. *Diabetes Metab. Syndr.* 14 (3), 247–250. doi: 10.1016/j.dsx.2020.03.013

Barratt-Due, A., Olsen, I. C., Nezvalova-Henriksen, K., Kåsine, T., Lund-Johansen, F., Hoel, H., et al. (2021). Evaluation of the effects of remdesivir and hydroxychloroquine on viral clearance in COVID-19: A randomized trial. *Ann. Intern. Med.* 174 (9), 1261–1269. doi: 10.7326/M21-0653

Buonsenso, D., Piazza, M., Boner, A. L., and Bellanti, J. A. (2022). Long COVID: A proposed hypothesis-driven model of viral persistence for the pathophysiology of the syndrome. *Allergy Asthma Proc.* 43 (3), 187–193. doi: 10.2500/aap.2022.43.220018

Carfì, A., Bernabei, R., and Landi, F. (2020). Gemelli against COVID-19 post-acute care study group. persistent symptoms in patients after acute COVID-19. *JAMA.* 324 (6), 603–605. doi: 10.1001/jama.2020.12603

Clerkin, K. J., Fried, J. A., Raikhelkar, J., Sayer, G., Griffin, J. M., Masoumi, A., et al. (2020). COVID-19 and cardiovascular disease. *Circulation.* 141 (20), 1648–1655. doi: 10.1161/CIRCULATIONAHA.120.046941

Fabbri, L., Moss, S., Khan, F. A., Chi, W., Xia, J., Robinson, K., et al. (2022). Parenchymal lung abnormalities following hospitalisation for COVID-19 and viral pneumonitis: A systematic review and meta-analysis. *Thorax* 78(2), 191–201. doi: 10.1136/thoraxjnl-2021-218275

Graham, E. L., Clark, J. R., Orban, Z. S., Lim, P. H., Szymanski, A. L., Taylor, C., et al. (2021). Persistent neurologic symptoms and cognitive dysfunction in non-hospitalized covid-19 "long haulers". *Ann. Clin. Transl. Neurol.* 8 (5), 1073–1085. doi: 10.1002/acn3.51350

Greenhalgh, T., Knight, M., A'Court, C., Buxton, M., and Husain, L. (2020). Management of post-acute covid-19 in primary care. *BMJ* 370, m3026. doi: 10.1136/bmj.m3026

Huang, C., Huang, L., Wang, Y., Li, X., Ren, L., Gu, X., et al. (2021). 6-month consequences of COVID-19 in patients discharged from hospital: a cohort study. *Lancet.* 397 (10270), 220–232. doi: 10.1016/S0140-6736(20)32656-8

Koc, H. C., Xiao, J., Liu, W., Li, Y., and Chen, G. (2022). Long COVID and its management. *Int. J. Biol. Sci.* 18 (12), 4768–4780. doi: 10.7150/ijbs.75056

Lee, J., Park, S. S., Kim, T. Y., Lee, D. G., and Kim, D. W. (2021). Lymphopenia as a biological predictor of outcomes in COVID-19 patients: A nationwide cohort study. *Cancers* 13 (3), 471. doi: 10.3390/cancers13030471

Lopez-Leon, S., Wegman-Ostrosky, T., Perelman, C., Sepulveda, R., Rebolledo, P. A., Cuapio, A., et al. (2021). More than 50 long-term effects of COVID-19: A systematic review and meta-analysis. *Sci. Rep.* 11, 16144. doi: 10.1038/s41598-021-95565-8

Machhi, J., Herskovitz, J., Senan, A. M., Dutta, D., Nath, B., Oleynikov, M. D., et al. (2020). The natural history, pathobiology, and clinical manifestations of SARS-CoV-2 infections. *J. Neuroimmune Pharmacol.* 15 (3), 359–386. doi: 10.1007/s11481-020-09944-5

National Institute for Health and Care Excellence (2020) *COVID-19 rapid guideline: Managing the long-term effects of COVID-19*. Available at: https://www.nice.org.uk/guidance/ng188 (Accessed October 2022).

National Institute for Health and Care Research (2020) *Living with Covid19*. Available at: https://evidence.nihr.ac.uk/themedreview/living-with-covid19/ (Accessed October 2022).

Ojha, V., Mani, A., Pandey, N. N., Sharma, S., and Kumar, S. (2020). CT in coronavirus disease 2019 (COVID-19): A systematic review of chest CT findings in 4410 adult patients. *Eur. Radiol.* 30 (11), 6129–6138. doi: 10.1007/s00330-020-06975-7

Rajan, S., Khunti, K., Alwan, N., Steves, C., MacDermott, N., Morsella, A., et al. (2021). *In the wake of the pandemic: Preparing for long COVID* (Copenhagen (Denmark: European Observatory on Health Systems and Policies).

Salehi, S., Reddy, S., and Gholamrezanezhad, A. (2020). Long-term pulmonary consequences of coronavirus disease 2019 (COVID-19): What we know and what to expect. *J. Thorac. Imaging* 35 (4), W87–W89. doi: 10.1097/RTI.0000000000000534

Singh, T., Kite, T. A., Joshi, S. S., Spath, N. B., Kershaw, L., Baker, A., et al. (2022). MRI And CT coronary angiography in survivors of COVID-19. *Heart.* 108 (1), 46–53. doi: 10.1136/heartjnl-2021-319926

Sudre, C. H., Murray, B., Varsavsky, T., Graham, M. S., Penfold, R. S., Bowyer, R. C., et al. (2021). Attributes and predictors of long COVID. *Nat. Med.* 27 (4), 626–631. doi: 10.1038/s41591-021-01292-y

Taquet, M., Geddes, J. R., Husain, M., Luciano, S., and Harrison, P. J. (2021). 6-month neurological and psychiatric outcomes in 236 379 survivors of COVID-19: a retrospective cohort study using electronic health records. *Lancet Psychiatry* 8 (5), 416–427. doi: 10.1016/S2215-0366(21)00084-5

Varona, J. F., Landete, P., Lopez-Martin, J. A., Estrada, V., Paredes, R., Guisado-Vasco, P., et al. (2022). Preclinical and randomized phase I studies of plitidepsin in adults hospitalized with COVID-19. *Life Sci. Alliance* 5 (4), e202101200. doi: 10.26508/lsa.202101200

Vindegaard, N., and Benros, M. E. (2020). COVID-19 pandemic and mental health consequences: Systematic review of the current evidence. *Brain Behav. Immun.* 89, 531–542. doi: 10.1016/j.bbi.2020.05.048

World Health Organization (2022) *Weekly epidemiological and operational updates October 2022*. Available at: https://www.who.int/emergencies/diseases/novel-coronavirus-2019/situation-reports (Accessed October 2022).

frontiers | Frontiers in Cellular and Infection Microbiology

TYPE Original Research
PUBLISHED 13 March 2023
DOI 10.3389/fcimb.2023.1057082

OPEN ACCESS

EDITED BY
Josep Quer,
Vall d'Hebron Research Institute (VHIR), Spain

REVIEWED BY
Miguel Angel Martinez,
IrsiCaixa, Spain
Maria I. Costafreda,
University of Barcelona, Spain

*CORRESPONDENCE
Esteban Domingo
edomingo@cbm.csic.es
Aurora Sánchez-Pacheco
asanchez@iib.uam.es
Celia Perales
celia.perales@cnb.csic.es

†These authors have contributed equally to this work

SPECIALTY SECTION
This article was submitted to Clinical Microbiology, a section of the journal Frontiers in Cellular and Infection Microbiology

RECEIVED 29 September 2022
ACCEPTED 28 February 2023
PUBLISHED 13 March 2023

CITATION
García-Crespo C, Francisco-Recuero I, Gallego I, Camblor-Murube M, Soria ME, López-López A, de Ávila AI, Madejón A, García-Samaniego J, Domingo E, Sánchez-Pacheco A and Perales C (2023) Hepatitis C virus fitness can influence the extent of infection-mediated epigenetic modifications in the host cells. *Front. Cell. Infect. Microbiol.* 13:1057082. doi: 10.3389/fcimb.2023.1057082

Hepatitis C virus fitness can influence the extent of infection-mediated epigenetic modifications in the host cells

Carlos García-Crespo[1,2†], Irene Francisco-Recuero[3†], Isabel Gallego[1,2], Marina Camblor-Murube[3], María Eugenia Soria[1,2,4], Ana López-López[3], Ana Isabel de Ávila[1,2], Antonio Madejón[1,5], Javier García-Samaniego[2,5], Esteban Domingo[1,2*], Aurora Sánchez-Pacheco[3*] and Celia Perales[2,4,6*]

[1]Department of Interactions with the Environment, Centro de Biología Molecular "Severo Ochoa" (CSIC-UAM), Consejo Superior de Investigaciones Científicas (CSIC), Campus de Cantoblanco, Madrid, Spain, [2]Centro de Investigación Biomédica en Red de Enfermedades Hepáticas y Digestivas (CIBERehd), Instituto de Salud Carlos III, Madrid, Spain, [3]Department de Biochemistry, UAM, Instituto de Investigaciones Biomédicas Alberto Sols, CSIC-UAM, Madrid, Spain, [4]Department of Clinical Microbiology, IIS-Fundación Jiménez Díaz, UAM, Madrid, Spain, [5]Hepatology Unit Hospital Universitario La Paz/Carlos III, Instituto de Investigación Sanitaria "La Paz", Madrid, Spain, [6]Department of Molecular and Cell Biology, Centro Nacional de Biotecnología (CNB-CSIC), Consejo Superior de Investigaciones Científicas (CSIC), Madrid, Spain

Introduction: Cellular epigenetic modifications occur in the course of viral infections. We previously documented that hepatitis C virus (HCV) infection of human hepatoma Huh-7.5 cells results in a core protein-mediated decrease of Aurora kinase B (AURKB) activity and phosphorylation of Serine 10 in histone H3 (H3Ser10ph) levels, with an affectation of inflammatory pathways. The possible role of HCV fitness in infection-derived cellular epigenetic modifications is not known.

Methods: Here we approach this question using HCV populations that display a 2.3-fold increase in general fitness (infectious progeny production), and up to 45-fold increase of the exponential phase of intracellular viral growth rate, relative to the parental HCV population.

Results: We show that infection resulted in a HCV fitness-dependent, average decrease of the levels of H3Ser10ph, AURKB, and histone H4 tri-methylated at Lysine 20 (H4K20m3) in the infected cell population. Remarkably, the decrease of H4K20m3, which is a hallmark of cellular transformation, was significant upon infection with high fitness HCV but not upon infection with basal fitness virus.

Discussion: Here we propose two mechanisms —which are not mutually exclusive— to explain the effect of high viral fitness: an early advance in the number of infected cells, or larger number of replicating RNA molecules per cell. The implications of introducing HCV fitness as an influence in virus-host

interactions, and for the course of liver disease, are warranted. Emphasis is made in the possibility that HCV-mediated hepatocellular carcinoma may be favoured by prolonged HCV infection of a human liver, a situation in which viral fitness is likely to increase.

KEYWORDS

virus-host interaction, histone modification, viral quasispecies, hepatocellular carcinoma, viral fitness, hepatitis C virus, aurora kinase B

Introduction

Epigenetic modifications modulate gene expression programs, with implications that have been extensively studied for the phenotypic profile of cancer cells, and their functional heterogeneity [reviewed in (Ilango et al., 2020; Ramon et al., 2020)]. Host cell epigenetic signatures are also altered during infection by DNA and RNA viruses, with consequences for viral persistence and latency (Milavetz and Balakrishnan, 2015; Lynch et al., 2019). Hepatitis C virus (HCV) participates of the double branch of epigenetic implications since they may affect the course of the infection itself, and the development of post-infection sequels such as hepatocellular carcinoma (HCC), often linked to progression of liver cirrhosis. Epigenetic changes that involve aberrant methylation of genes and post-transcriptional histone modifications occur frequently, and some of them are being exploited for the development of molecular diagnostic signatures for HCC (Lin et al., 2015; Zheng et al., 2019).

Several studies have addressed the interference of HCV-encoded proteins exerted on epigenetic pathways, in the course of the infection (Hung et al., 2014). Our previous investigation of HCV-induced histone modifications at early stages of HCV infection revealed inhibition of phosphorylation of Ser10 in histone H3 (H3Ser10ph), associated with a decrease of Aurora Kinase B (AURKB) activity, mediated by a direct interaction between HCV core protein and AURKB. In addition, we showed that AURKB inhibition had an effect on transcription of genes related to inflammatory pathways such as *NF-κB* and *COX-2* (Madejón et al., 2015). Aurora B is involved in chromosome segregation, spindle-checkpoint and cytokinesis, and alteration of each of these mitotic processes could induce aneuploidy, one of main features of cancer cells (Hegyi and Mehes, 2012; Chieffi, 2018). Chronic HCV infection also induces genome-wide changes in H3K27 acetylation, dependent on the liver fibrosis stage (Hamdane et al., 2019). Moreover, significant HCV infection-associated changes in active chromatin markers H3K4Me3 and H3K9Ac and silent chromatin marker H3K9Me3 seem to be associated with alteration of expression of genes involved in HCC development (Perez et al., 2019). Therefore, several lines of evidence suggest that epigenetic modifications as a result of chronic HCV infection may contribute to cancer risk (Mann, 2014; Madejón et al., 2015; Lohmann and Bartenschlager, 2019; Perez et al., 2019).

In the studies on the effect of HCV infection on host epigenetic modifications, the influence of viral replicative fitness is unknown. Yet, viral fitness, defined as the capacity of a viral population to produce infectious progeny, can have profound effects in the virus-host relationship, infection outcome, and response to antiviral treatment [reviewed in (Domingo and Holland, 1997; Quiñones-Mateu and Arts, 2006; Wargo and Kurath, 2011; Domingo et al., 2019; Domingo et al., 2020)]. Complex HCV quasispecies distributions evolve in infected patients (Farci, 2011; Quarleri and Oubina, 2016) with multiple implications for viral pathogenesis (Yan et al., 2008; Domingo et al., 2012).

Most studies on HCV population dynamics have not considered viral fitness, presumably due to difficulties for its quantification *in vivo*. Prolonged replication of a clonal population of HCV (termed HCV p0, obtained by transcription of plasmid Jc1FLAG2(p7-nsGLuc2A) (Marukian et al., 2008; Perales et al., 2013), resulted in populations HCV p100 and HCV p200 (which are HCV p0 passaged 100 and 200 times, respectively, in Huh-7.5 cells) that exhibited significant increases in viral replication, calculated relative to HCV p0 (Moreno et al., 2017) (Figure 1). Taking HCV p0 as reference for fitness measurements (arbitrarily assigned a fitness value of 1) in growth-competition experiments in Huh-7.5 cells, HCV p100 and HCV p200 attained a fitness value of 2.3 (Sheldon et al., 2014; Moreno et al., 2017).

In serial passages in Huh-7.5 cells, HCV p100 and HCV p200 displayed a 1.8-fold and 2.8-fold, respectively, higher infectious progeny yield per passage than HCV p0, while the maximum extracellular infectivity level was 1.17-fold higher for HCV p100 and HCV p200 that for HCV p0, over a broad range of multiplicity of infection (MOI) (Moreno et al., 2017). Thus, while the relative fitness of HCV p100 and HCV p200 was the same according to growth-competition assays for fitness measurement (Domingo and Holland, 1997), the exponential intracellular growth rate was 2.6-fold larger for HCV p200 than for HCV p100 (Moreno et al., 2017) (Figure 1).

Fitness gain of HCV resulted in genetically and phenotypically heterogeneous population displaying broad mutant spectra (Domingo et al., 2020; Gallego et al., 2020; Delgado et al., 2021). Attainment of high fitness was related to mutant spectrum complexity, itself previously identified as a determinant of disease progression and response to treatment of HCV infections *in vivo* (Farci et al., 2000; Farci, 2011). In the cell culture system, high HCV fitness confers resistance to antiviral agents used in therapy (Sheldon et al., 2014; Gallego et al., 2016). There is evidence that fitness-enhancing substitutions may be also involved in treatment failures *in vivo* (Wang et al., 2013; Soria et al., 2020). Directly

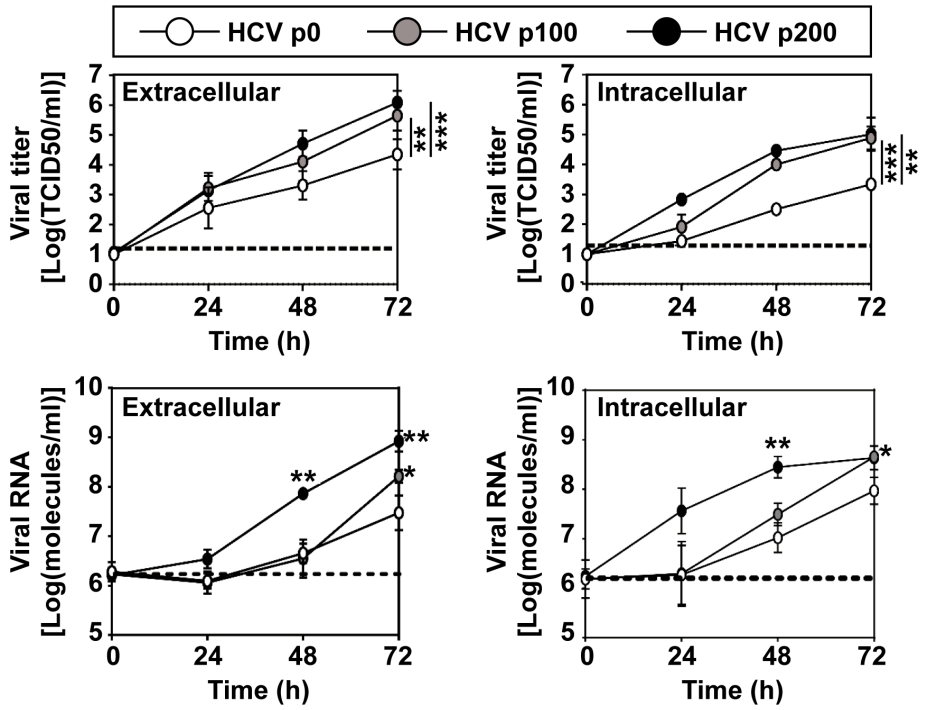

FIGURE 1
Kinetics of viral progeny production by HCV p0, HCV p100 and HCV p200. Huh 7.5 cells were either mock-infected or infected with the indicated virus (top box) at a MOI of 0.03 $TCID_{50}$/cell (4 x 10^3 Huh-7.5 cells infected with 1.2 x 10^4 $TCID_{50}$ of virus). Extracellular and intracellular infectivity and viral RNA were quantified. Results are the average of three independent experiments (biological triplicate). Data were transformed to the logarithmic values as indicated in ordinate. The statistical significance of the differences was calculated using the ANCOVA test (*p < 0.05; **p < 0.01; ***p < 0.001). Data on viral titers (upper two panels), have been previously published in (Moreno et al., 2017), and are included here to complement information on HCV fitness.

relevant to the virus-host relationship was the observation that high fitness HCV p100 and HCV p200 enhanced the shut-off of host cell protein synthesis relative to HCV p0, *via* increased phosphorylation of protein kinase R, and protein synthesis initiation factor eIF2α (Perales et al., 2013; Moreno et al., 2017). Given the multiple consequences of HCV fitness on host interactions, it was relevant to examine the possible influence of HCV fitness on host cell epigenetic signatures. Here we present comparative results with HCV p0, HCV p100 and HCV p200 that suggest such an influence. Mechanisms by which HCV fitness may modify quantitatively or even condition epigenetic modification in the host cells are discussed. The results render replicative fitness a relevant parameter for the interpretation of epigenetic modifications by this viral pathogen.

Materials and methods

Cell, viruses and infection

Huh-7.5 reporter cells were used for standard infections while Huh-7.5 cells were used for titration of virus infectivity. The origin of Huh-7.5 and Huh-7.5 reporter cell lines, and procedures for cell growth in Dulbecco's modification of Eagle's medium (DMEM), have been previously described (Blight et al., 2002; Jones et al., 2010; Perales et al., 2013); cells were cultured at 37°C and 5% CO_2.

The initial HCV was rescued from plasmid Jc1FLAG2(p7-nsGluc2A), and GNN from plasmid GNNFLAG2(p7nsGluc2A) (which carries a mutation in NS5B that renders the virus replication defective) and used as a negative infection control (Marukian et al., 2008). The preparation of the initial virus, HCV p0, has been previously described (Perales et al., 2013). HCV p100 and HCV p200 resulted from population HCV p0 passaged 100 and 200 times, respectively, in Huh-7.5 reporter cells, as described (Sheldon et al., 2014; Moreno et al., 2017). Mock-infected cells or GNN-infected cultures were included in parallel to ascertain the absence of contamination; no infectivity was detected in any of these control cultures. In all experiments, Huh-7.5 reporter cells were either mock-infected or infected with HCV p0, HCV p100 or HCV p200 (abbreviated as p0, p100 and p200, respectively) at an initial MOI of 0.03 $TCID_{50}$/cell, and processed 72, 96 or 144 hours after HCV infection, unless indicated in the relevant figure. Under these conditions 80-90% of the cells were infected as determined by live imaging (Jones et al., 2010).

Virus titration

Titration of infectious HCV was performed by serial dilution of cell culture supernatants and applying them to Huh-7.5 cell monolayers in 96-well plates (6,400 cells/well, seeded 16 h earlier). Three days after infection, the cells were washed with

PBS, fixed with ice-cold methanol, and stained to detect NS5A using anti-NS5A monoclonal antibody 9E10, as described previously (Lindenbach et al., 2005; Perales et al., 2013). Virus titers are expressed as $TCID_{50}$ per millilitre (Reed and Muench, 1938).

Western blot assays

Western blot assays were performed as previously described (Tardaguila et al., 2011). Blots were developed with the following antibodies: mouse monoclonal anti-core (ref. Sc-69937, Santa Cruz Biotechnology), mouse monoclonal anti-NS5A (ref. Sc-65458, Santa Cruz Biotechnology), rabbit polyclonal anti-H3Ser10ph (ref. 06-570, Millipore), rabbit polyclonal anti-AURKB (ref. Ab2254, Abcam), mouse monoclonal anti-β-Actin (ref. SAB1305567, Sigma), mouse monoclonal anti-tubulin (ref. T8328, Sigma), rabbit polyclonal anti-H4K20Me3 (ref. 07-463, Millipore), rabbit polyclonal anti-H3 (ref. 06-755, Millipore), mouse monoclonal anti-GADPH (ref. #CB1001, CallBiochem). Depending on the antibody, 5–30 μg of total protein was used in Western blot assays. β-Actin, tubulin, H3 or GADPH levels were used as loading control in Western blot assays. The values are the average of duplicate or triplicate determinations.

RNA extraction and quantification

Intracellular viral RNA was extracted from infected cells using the Qiagen RNeasy kit (Qiagen, Valencia, CA, USA), following the manufacturer's instructions. Viral RNA from cell culture supernatants was extracted using the Qiagen QIAamp viral RNA mini kit (Qiagen, Valencia, CA, USA).

HCV RNA quantification was performed by real-time quantitative RT-PCR (qRT-PCR) using the Light Cycler RNA Master SYBR green I kit (Roche) (Lindenbach et al., 2005; Perales et al., 2013). The 5' untranslated region (UTR) of the HCV genome was amplified using as oligonucleotide primers HCV-5UTR-F2 5'-TGAGGAACTACTGTCTTCACGCAGAAAG-3' (sense orientation; the 5' nucleotide corresponds to genomic residue 47; according to JFH-1, GenBank accession number #AB047639) and HCV-5UTR-R2 5'-TGCTCATGGTGCACGGTCTACGAG-3' (antisense orientation; the 5' nucleotide corresponds to genomic residue 347; according to JFH-1) (Perales et al., 2013). Quantification was relative to a standard curve obtained with known amounts of HCV RNA synthesized by *in vitro* transcription of plasmid GNNFLAG2(p7-nsGluc2A). Negative controls (without template RNA and RNA from mock-infected cells) were run in parallel with each amplification reaction to ascertain the absence of contamination with undesired templates.

Cellular mRNA quantification was performed by RNA retro-transcription (RT) and real-time quantitative (qPCR). Intracellular RNA was retro-transcribed using AMV reverse transcriptase (Promega) following manufacturer's instructions, and quantified using the NZYSpeedy qPCR Probe Master Mix (NZYTech). Each value was normalized against the GAPDH gene, and expressed as relative RNA abundance compared to mock-infected cells. The oligonucleotide primers used to amplify AURKB were 5'-GGGCGTCCTCTGCCCAAAGGC-3′ (sense orientation), 5′-GCCTGGATTTCGATCTCTC-3′ (antisense orientation), which resulted in amplification of nucleotides 360 to 511 of the AURKB gene. The oligonucleotide primers used to amplify GADPH were 5′-ACACTGCATGCCATCACTGCC-3′ (sense orientation), 5′-GCCTGCTTCACCACCTTCTTG-3′ (antisense orientation), which resulted in amplification of nucleotides 717 to 982 of the GADPH gene.

Statistics

Linear regression's test was performed using software R version 3.6.3. Student's t and Wilcoxon tests were performed using the SSC-Stat software (version 2.18; University of Reading, Reading, UK) and the IBM SPSS Statistic 19 software. The statistical significance of differences between groups was expressed by asterisks (*=p <0.05; **=p <0.01; ***=p <0.001).

Results

Alteration of histone H3 Ser10 phosphorylation by infection of human hepatoma cells with HCV of different fitness

A previous study indicated that at early times after infection with HCV p0 [the virus with a basal fitness level (Perales et al., 2013)] resulted in a reduction of H3Ser10ph (Madejón et al., 2015). To investigate the weight of HCV fitness in this reduction, Huh-7.5 cells were either mock-infected or infected with HCV p0, HCV p100 and HCV p200 at a multiplicity of infection (MOI) of 0.03 $TCID_{50}$/cell. H3Ser10ph levels were measured in cells lysed at 24h, 48h, and 72h post-infection, and compared with those of viral proteins NS5A and core as markers of the intracellular extent of the infection. Proteins were analysed by western blot assay using a specific polyclonal antibody for H3Ser10ph, a monoclonal antibody for NS5A, and a monoclonal antibody for core; β-actin, was used as loading control (see Materials and Methods for the origin of the antibodies). The results (Figures 2A-C) indicate that high HCV fitness accentuated the decrease of H3Ser10ph that reached a maximum of 5-fold with HCV p200 at late times post-infection; a reduction was observed at 48h post-infection with HCV p200, while a comparable effect required 72h with HCV p100 or HCV p0. The decrease correlated with an increase of intracellular infectivity and viral NS5A and core protein levels (Figures 2D-G). To reinforce the results, H3Ser10ph expression levels were compared between the low fitness HCV p0 population and the high fitness populations HCV p100 and HCV p200. The results showed again a significant decrease of H3Ser10ph levels comparing HCV p0 with HCV p100 and HCV p200 at late times post-infection (Figure S1A). Similar results were obtained for NS5A levels, while no significant differences were observed in core levels after infection with HCV p0 compared to HCV p200 (Figures S1B, C).

Since high viral fitness entails an increase of the intracellular level of viral RNA and its expression proteins, we examined the consequences for H3Ser10ph levels of infecting cells with HCV p0

10.3389/fcimb.2023.1057082

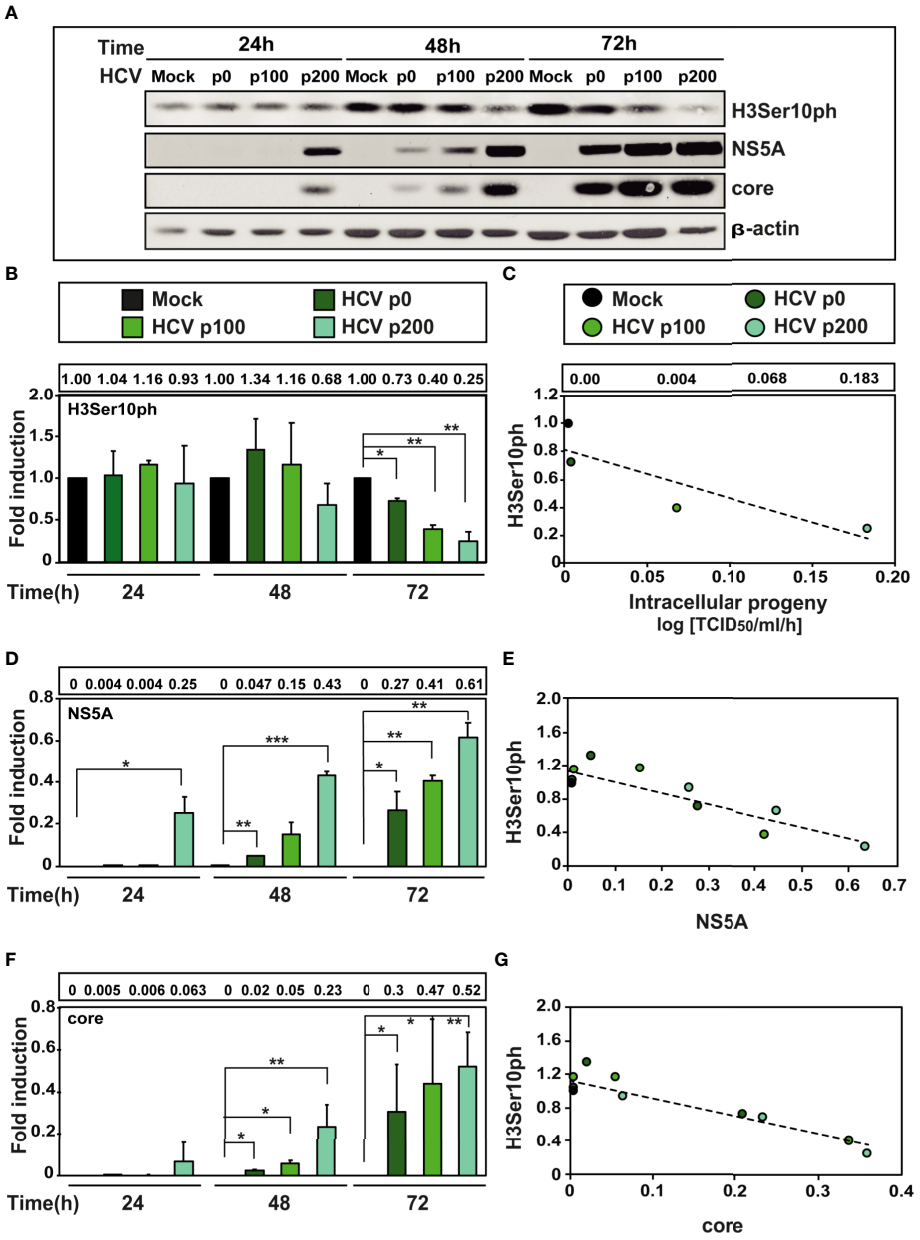

FIGURE 2
Effect of HCV fitness on the level of cellular protein H3Ser10ph and viral proteins NS5A and core. **(A)** Huh-7.5 reporter cells were either mock-infected or infected with HCV p0, HCV p100 or HCV p200 (abbreviated as p0, p100 and p200, respectively) at an initial MOI of 0.03 $TCID_{50}$/cell; protein extracts were prepared at the indicated times post-infection. Bands are those visualized by Western blot assays of cellular protein H3ser10ph and viral proteins NS5A and core (with β-actin as loading control). **(B)** H3Ser10ph levels in mock-infected or HCV-infected cells expressed as the fold induction relative to the corresponding value for the mock-infected cells; the infecting HCV (code in upper box), and the time post-infection at which extracts were prepared are given in the abscissa; the numerical densitometry values (measured relative to the mock-infected sample, taken as 1) are indicated in the upper box, next to the panel. Asterisks indicate statistical significance as follows: *p<0.05; **p<0,01; ***p<0.00; unpaired t-test. The values are the result of three independent experiments (biological triplicate). **(C)** Correlation between the increase of intracellular viral titer (code of infecting virus in upper box) expressed as log. 10 $TCID_{50}$/ml/h [data are from (28) and they are indicated in the box above the panel, for mock, HCV p0, HCV p100 and HCV p200, respectively] and the relative H3Ser10ph densitometry values at time 72 hours post-infection (given in panel B). The discontinuous line corresponds to function y=-3.45x+0.81 (R^2 = 0.77, p-value=0.1227; linear regression test). **(D)** Same as B but for viral protein NS5A. **(E)** Same as C but for the correlation between viral protein NS5A and cellular protein H3Ser10ph levels (densitometry values in panels B and D). The discontinuous line corresponds to function y=-1.33x+1,13 (R^2 = 0.77; p-value=0.00018; linear regression test). **(F)** Same as B but for viral core protein. **(G)** Same as C but for the correlation between viral core protein and H3Ser10 levels (densitometry values in panels B and F). The discontinuous line corresponds to function y=-2.13x+1.12 (R^2 = 0.85; p-value=0.000018; linear regression test).

and HCV p200 at MOIs that were up to 100-fold lower than that used in our standard infection protocol. The results (Figure 3) confirmed the effect of HCV fitness on H3Ser10ph depletion and its attenuation at low MOI that decreased the average level of intracellular NS5A. Similar results were obtained by comparing H3Ser10ph and NS5A levels between HCV p0 and HCV p200 (Figures 3F, G). Thus, HCV fitness is a determinant of the intracellular decrease of H3Ser10ph.

10.3389/fcimb.2023.1057082

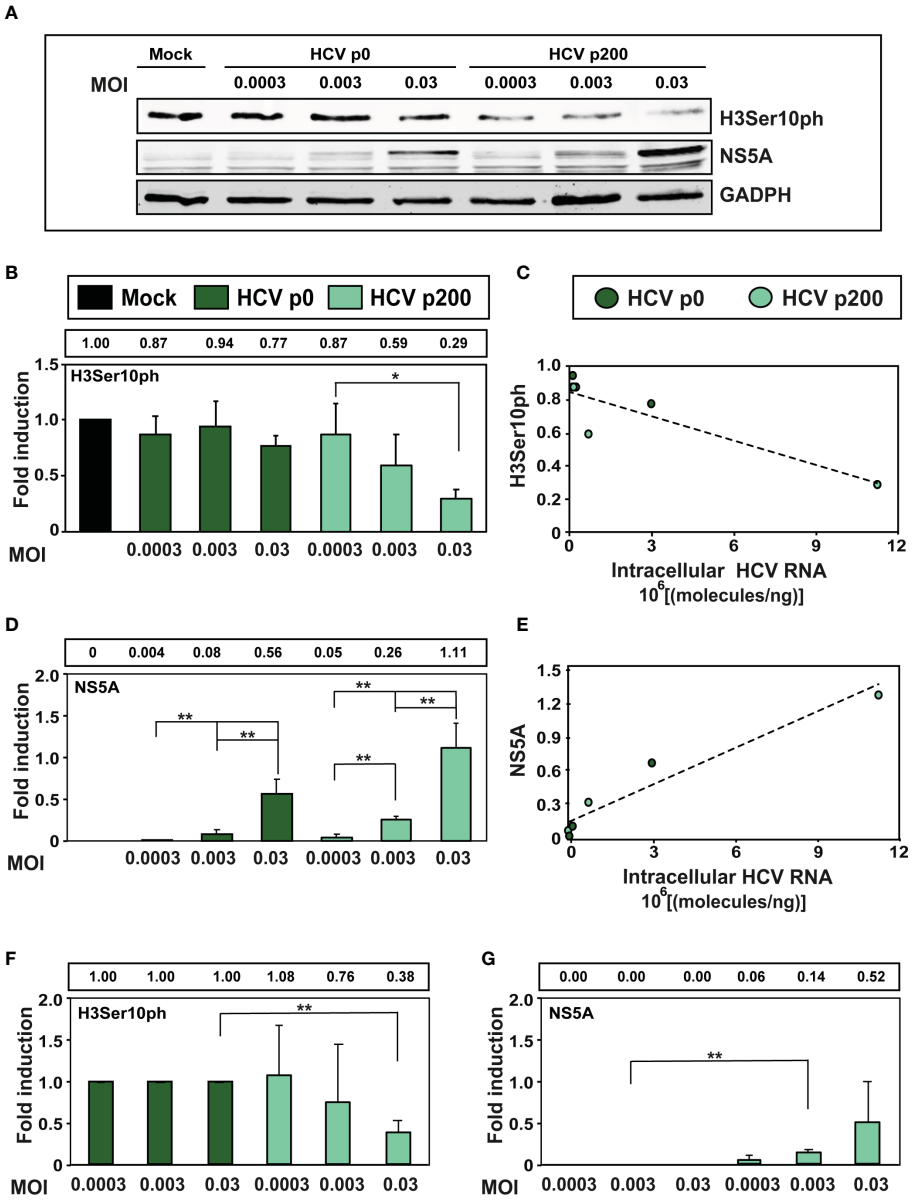

FIGURE 3
Effect of the multiplicity of infection (MOI) on the intracellular H3Ser10ph level. **(A)** Western blot analysis of extracts of cells that were either mock-infected or infected with HCV p0 or HCV p200 at the indicated MOI. Extracts were prepared at 72h post-infection. GAPDH was used as the loading control. **(B)** H3Ser10ph levels in mock-infected or HCV-infected cells, expressed as the fold induction relative to the corresponding value for the mock-infected cells. The values are the average (and standard deviations) of the densitometric quantifications of three independent western blots; the image of one of them is shown in **(A)** The MOI and infecting virus are indicated in abscissa, and the densitometry values (using as reference the corresponding value for the extract of mock-infected cells, taken as 1) are written in the box above the panel. **(C)** Correlation between the intracellular amount of viral RNA measured at 72h post-infection (abscissa) and the H3Ser10ph level determined by densitometry of the Western blots (ordinate). The discontinuous line corresponds to function $y=-5x10^{-0.8}x+0.85$ (R^2 = 0.78; p-value=0.02027, linear regression test). **(D)** Same as B but for viral protein NS5A. **(E)** Same as C but for viral protein NS5A. The discontinuous line corresponds to function $y=1x10^{-0.7}x + 0.12$ (R^2 = 0.918; p-value=0.0017, linear regression test). **(F, G)** Same as B and D but with the H3Ser10ph and NS5A levels in HCV-infected cells expressed as the fold induction relative to the corresponding value for the HCV p0 infected cells. The statistical significance of differences is as follows: *p<0.05; **p<0.01; unpaired t -test.

The effect of HCV fitness on the intracellular level of Aurora kinase B

AURKB is one of the enzymes that phosphorylates Ser10 of histone H3. Reduction of H3Ser10ph levels upon HCV infection is mediated by AURKB through its interaction with the viral core protein, as measured at early times post-infection (Madejón et al., 2015). To examine if HCV fitness affected the intracellular amount of AURKB, protein and intracellular RNA extracts were prepared from cells either mock-infected or infected with HCV p0 or HCV

p200 at a MOI of 0.03 $TCID_{50}$/cell. AURKB was detected by western blot using a specific polyclonal antibody. The results (Figures 4A, B) show significant reductions of AURKB at late times post-infection, that were more accentuated with HCV p200 than HCV p0; the difference between the two viruses reached 3.3-fold at 144 h post-infection. To examine if the decrease of AURKB proteins levels corresponded with a decrease in AURKB mRNA levels, RNA extracts were quantified by RT-qPCR. The results (Figures 4C, D) show a significant decrease in AURKB mRNA levels at late-times post-infection, and the decrease was enhanced with high fitness HCV p200. Therefore, a significant decrease was also observed by comparing ARUKB protein and mRNA levels between cells infected with HCV p0 or HCV p200 (Figures 4E, F). Therefore, AURKB kinase itself is affected by the replicative fitness of the infecting HCV.

The influence of HCV fitness on other epigenetic markers

HCV infection results in variation of several epigenetic markers (Madejón et al., 2015; Lohmann and Bartenschlager, 2019; Perez et al., 2019; Zheng et al., 2019). A particularly relevant signature is the tri-methylated form of lysine 20 of histone H4 (H4K20Me3) since its depletion is a common finding among tumor cells (Fraga et al., 2005). Therefore, we measured H4K20Me3 in extracts of cells

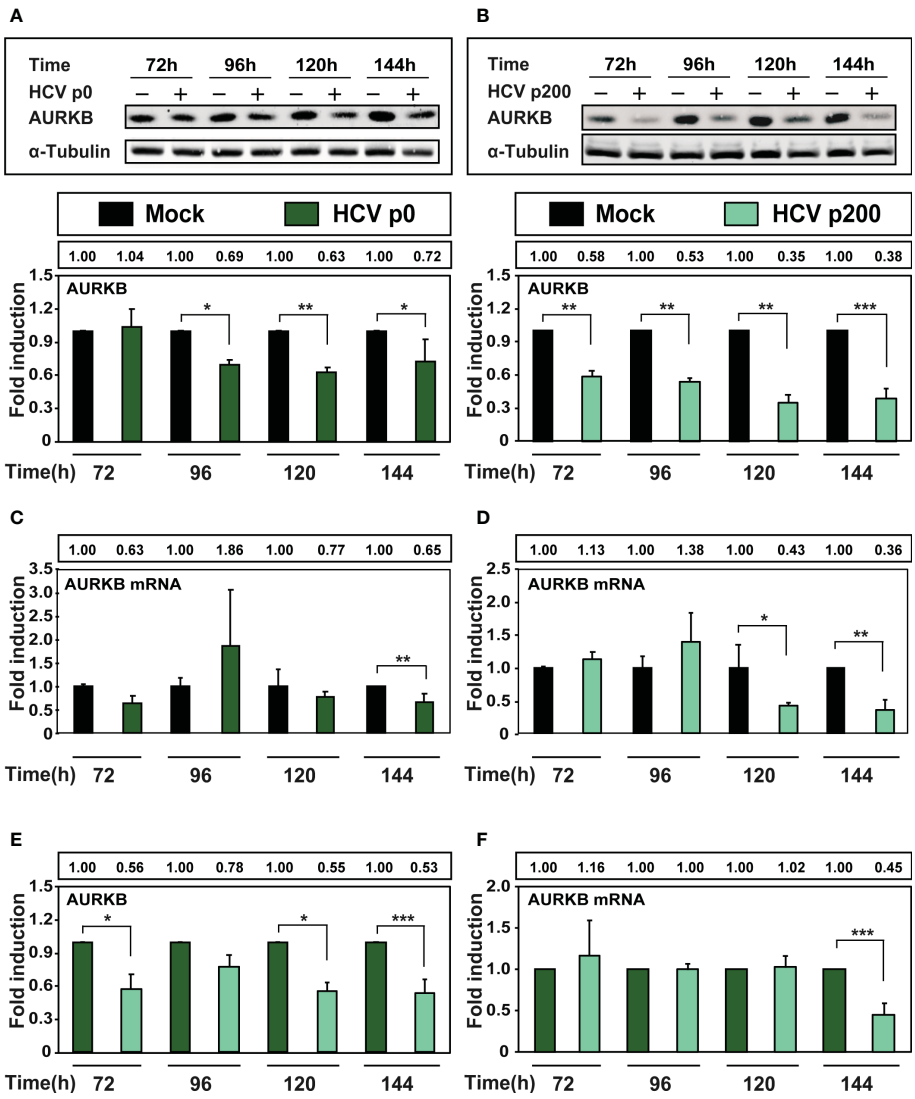

FIGURE 4
Effect of HCV infection on AURKB expression. Huh-7.5 reporter cells were either mock-infected or infected with HCV p0 and HCV p200 at a MOI of 0.03 $TCID_{50}$/cell. **(A)** Western blot with extracts of cells infected with HCV p0. Bands correspond to the cellular AURKB and α-tubulin used as loading control. The lower panel shows the densitometry quantification of the bands, taking as reference the corresponding value for mock-infected cells, numerical values are given in the box above the lower panel. Times post-infection are indicated in abscissa. **(B)** Same as A but for HCV p200-infected cells. **(C, D)** RT-qPCR measurements of AURKB mRNA using GADPH gene as control. **(E, F)** Same as A-D but with the AURKB and AURKB mRNA levels in HCV-infected cells expressed as the fold induction relative to the corresponding value for the HCV p0 infected cells. Results are the average of three independent experiments (biological triplicate). Asterisks indicate statistical significance as follows: *p<0.05; **p<0.01; ***p<0.001; unpaired t-test.

at late times after infection with HCV p0 or HCV p200 at a MOI of 0.03 $TCID_{50}$/cell, by western blot using a specific polyclonal antibody against H4K20Me3 (Figure 5). Interestingly, there was only a minor (but not statistically significant) decrease of H4K20Me3 upon infection with HCV p0, but a highly significant decrease at all times post-infection with HCV p200, that reached 4-fold at 144h post-infection (Figure 5). In addition, a significant decrease was also observed at late time post-infection comparing H4K20Me3 levels between cells infected with HCV p0 or HCV p200 (Figure 5C). Therefore, and most significant for the effect of HCV fitness on epigenetic signatures, depletion of H4K20Me3 was noted only upon infection with high fitness HCV.

Discussion

In the present investigation we have explored the effect of HCV fitness on several epigenetic markers at late times post-infection of Huh-7.5 cells, when the great majority of cells in the culture are infected, and the alterations of host gene expression are fully manifested (Moreno et al., 2017). The study has revealed two categories of fitness influence: (i) markers that are altered by HCV p0 (the population displaying basal fitness), with a significant accentuation when the cells are infected with high fitness HCV p200 (i.e. effects on H3Ser10ph and AURKB); (ii) a marker whose intensity was modified only in infections with high fitness HCV p200 (H4K20Me3). This distinction is circumscribed by the 2.3-fold fitness range that can be reached with our experimental system (Sheldon et al., 2014; Moreno et al., 2017). Additional differences might be revealed if HCV displaying larger fitness differences were compared.

One of the most frequent strategies used by some viruses to dysregulate host gene expression involve epigenetic mechanisms. This is true also of many plant viruses (Wang et al., 2019), as part of modulation of gene expression in infected plant cells. In the case of tobacco etch potyvirus, Elena and colleagues documented that viral fitness had a clear influence on the host transcriptome profile (Cervera et al., 2018). Regarding animal viruses, epigenetic changes evoked by hepatitis B virus (HBV) infection affected both viral cccDNA and host DNA expression, with implications for HBV-associated HCC (Levrero and Zucman-Rossi, 2016; Dandri, 2020). Epigenetic mechanisms probably contributed to suppression

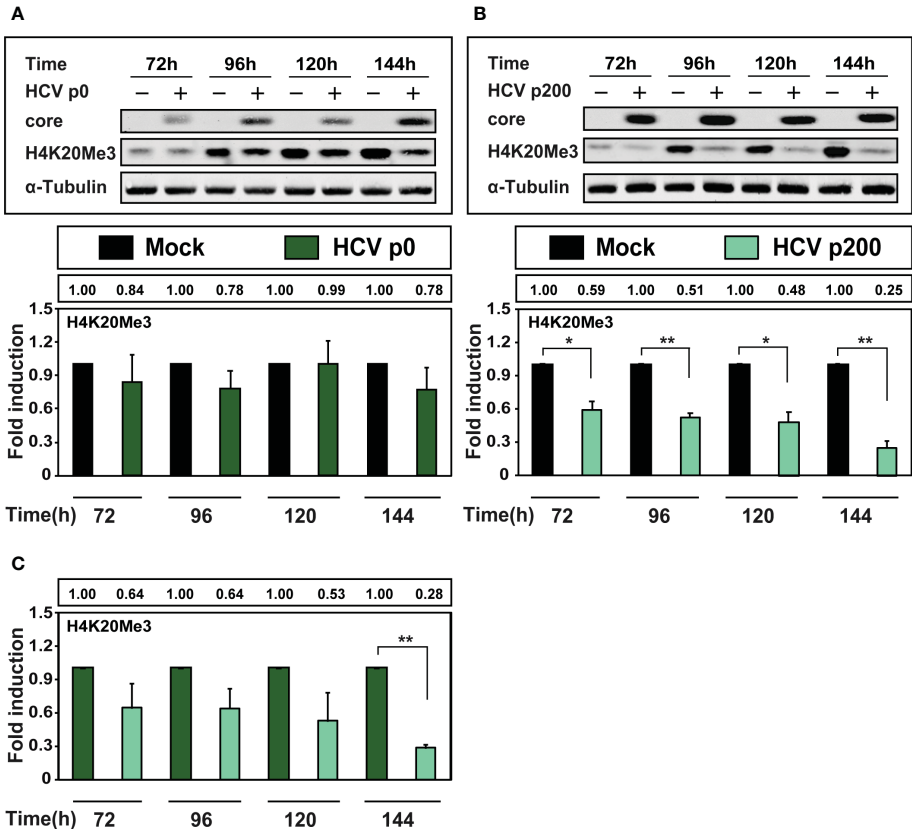

FIGURE 5
Comparison of the effect of HCV infection on the level of H4K20Me3. Huh-7.5 reporter cells were either mock-infected or infected with HCV p0 or HCV p200 at a MOI of 0.03 $TCID_{50}$/cell, and cellular extracts were prepared at the indicated times post-infection. Viral core protein, cellular H4K20Me3, and α-tubulin (used as loading control) were visualized by Western blot. **(A)** Upper panel: Western blot analysis of cells infected with HCV p0; below, densitometry quantifications (bars) with numerical values written in the box above the panel; Times post-infection are indicated in abscissa. **(B)** Same as A but for HCV p200-infected cells. **(C)** Same as **(A, B)** but with the H4K20Me3 levels in HCV-infected cells expressed as the fold induction relative to the corresponding value for the HCV p0 infected cells. Results are the average of three independent experiments (biological triplicate). Asterisks indicate statistical significance as follows: *p<0.05; **p<0.01; unpaired t-test.

of the IFN response during rabies virus infection of mice (Abdulazeez et al., 2020). Histone modifications affected herpes simplex virus 1 (HSV-1) gene expression in THP-1 cells (Gao et al., 2020). Viral respiratory infections, particularly by rhinovirus and respiratory syncytial virus, may participate in the exacerbation of airway inflammatory disease through DNA methylation and histone modifications of cells from the airway epithelium (Caixia et al., 2019; Tan et al., 2020). Likewise, modifications of epigenetic signatures have been associated with arbovirus infections (de Aguiar et al., 2019). In the studies with several DNA and RNA animal viral pathogens, fitness was not taken into consideration, and its possible relevance in the interpretation of types and extent of epigenetic modifications remains unknown.

Our study has established fitness as a relevant parameter with regard to the occurrence and intensity of epigenetic modifications underwent by the host cells. The results are in line with the fact that such modifications are often dependent on the amount of intracellular viral proteins that interact with cellular proteins, and high fitness virus provide a larger supply of interacting proteins (Sheldon et al., 2014; Moreno et al., 2017). Viral fitness may be also relevant to epigenetic therapeutic approaches (Ramos and Lossos, 2011; Dandri, 2020) because they target proteins that produce or recognize epigenetic marks, whose extent may be dependent on fitness of the effector virus. Thus, there is a variety of scenarios in which the types of influences revealed by our study may be pertinent.

A limitation of our study is that we cannot define in a precise way the molecular mechanism which is responsible of the observed fitness effects. Despite HCV p0 and HCV p200 belonging to the same evolutionary lineage, the mutant spectrum composition and the dominant sequences differ considerably between the two populations (Gallego et al., 2020; Delgado et al., 2021). Therefore, the repertoire of genomes and their expression products that intracellularly may act on the epigenetic mark effectors differ between HCV p0 and HCV p200. A second, non-mutually exclusive influence may be exerted by the number of Huh-7.5 cells that were infected at the times when the epigenetic marks were measured, following the initial infections at a MOI of 0.03 $TCID_{50}$/cell (see Materials and Methods).

Measurement of the number of infected cells using the anti-NS5A monoclonal antibody 9E10 indicated a significantly larger percentage of infected cells with HCV p200 than HCV p0, although the difference was not significant at 144 h post-infection (Figure S2). Yet a third non-mutually exclusive influence is the intracellular viral load which was quantified as being 2 to 3 logarithms larger for HCV p200 than HCV p0 at early (up to 21 h) and late (up to 72 h) post-infection (Moreno et al., 2017). Viral fitness is a parameter that captures several features of virus-host interactions (Domingo and Holland, 1997; Domingo et al., 2019), and the three effects outlined here may contribute to triggering epigenetic differences among host cells. A limitation of this work is the use of a tumorigenic human hepatoma cell line because this is the cell line in which HCV with higher fitness was obtained. However, similar results were obtained after the expression of HCV core in human primary hepatocytes (Madejón et al., 2015).

Persisting epigenetic changes following HCV infection may lead to HCC, and its recurrence in some patients with advanced fibrosis (Hamdane et al., 2019). Of the epigenetic signatures that were modified due to HCV fitness, AURKB and H4K20Me3 are especially noteworthy for their implication in cancer. AURKB is the effector of H3Ser10 phosphorylation (Goto et al., 2002), and the decrease of both H3Ser10ph and of AURKB was HCV fitness-dependent. AURKB is altered in several types of tumor cells, including HCC (Tanaka et al., 2008; Lin et al., 2010; Zhou et al., 2018). This kinase has been suggested as an independent molecular marker predicting tumor invasion of HCC (Tanaka et al., 2008). Previous report from our group indicated that the inhibition of AURKB could be one of the mechanisms by which HCV decreases cell proliferation and viability (Madejón et al., 2015). A striking case was a remarkable 4-fold depletion of H4K20Me3 produced by high fitness HCV and not by the basal fitness HCV population. This marker is involved in repression of transcription and genomic instability, an established specific process related to cancer development (Wang et al., 2008) and gene silencing (Schotta et al., 2004). Its depletion is common among tumor cells (Fraga et al., 2005), and it has been also reported among the epigenetic alterations associated with nonalcoholic steatohepatitis-related HCC in Stelic animal model mice, a system in which the course of disease resembles that of humans (de Conti et al., 2017). It is remarkable that in our cell culture system the decrease of H4K20Me3 was only seen with high fitness virus.

Our study establishes HCV fitness as a relevant parameter for epigenetic modifications and raises several questions which are presently under study. One is the duration of the epigenetic modifications observed once the virus is no longer present in the hepatic cell, and whether the fitness-dependent alterations are reverted. To solve this question poses the challenge that high fitness HCV cannot be extinguished by treatment with anyone of the HCV inhibitors that we have previously tested individually (Gallego et al., 2016; Gallego et al., 2018), and that the antiviral agents themselves can affect epigenetic marks (Giovannini et al., 2020). Our recent studies on HCV population dynamics in cell culture have documented that fitness gain was accompanied of a broadening of mutant spectra composed of many co-dominant genomes with comparable fitness (Domingo et al., 2020; Gallego et al., 2020). If these observations in population dynamics applied to HCV replication in the liver, they would suggest that chronicity may favor HCV fitness increase, with its concomitant elevated probability of epigenetic perturbations conductive to HCC. Fitness of the HCV that initially infects a patient may also have an effect on HCC development. However, comparative measurements of HCV fitness *in vivo* are presently not attainable, and the same virus may display dissimilar fitness in different host individuals.

Data availability statement

The raw data supporting the conclusions of this article will be made available by the authors, without undue reservation.

Author contributions

AS-P, AM, JG-S, ED and CP conceived, designed, and supervised the project. CG-C, IF-R, IG, MC, MS, AL, AA performed the experiments, analyzed the results and performed the statistical analyses. AM, JG-S, ED, AS-P and CP wrote the manuscript. All authors contributed to the article and approved the submitted version.

Funding

The work at CBMSO was supported by grants SAF2014-52400-R from Ministerio de Economía y Competitividad (MINECO), SAF2017-87846-R, BFU2017-91384-EXP from Ministerio de Ciencia, Innovación y Universidades (MCIU), project 525/C/2021 from Fundació La Marató de TV3, PID2020-113888RB-I00 from Ministerio de Ciencia e Innovación, PI18/00210 and PI21/00139 from Instituto de Salud Carlos III, S2013/ABI-2906, (PLATESA from Comunidad de Madrid/FEDER) and S2018/BAA-4370 (PLATESA2 from Comunidad de Madrid/FEDER). This research work was also funded by the European Commission–NextGenerationEU (regulation EU 2020/2094), through the CSIC's Global Health Platform (PTI Salud Global). CP is supported by the Miguel Servet program of the Instituto de Salud Carlos III (CP14/00121 and CPII19/00001) cofinanced by the European Regional Development Fund (ERDF). CIBERehd (Centro de Investigación en Red de Enfermedades Hepáticas y Digestivas) is funded by Instituto de Salud Carlos III. Institutional grants from the Fundación Ramón Areces and Banco Santander to the CBMSO are also acknowledged. The team at CBMSO belongs to the Global Virus Network (GVN). C. G.-C. is supported by predoctoral contract PRE2018-083422 from MCIU. The work at the UAM was supported by grant from Comunidad de Madrid IND2018/BMD9499. IF-R was supported by fellowships from Postgraduates studies from Universidad Autonoma de Madrid and from Ministerio de Educación Cultura y Deporte (MECD) FPU13/00945. The work at La Paz hospital was partially supported by grant PI12/02146 from "Fondo de Investigaciones Sanitarias".

Conflict of interest

The authors declare that the research was conducted in the absence of any commercial or financial relationships that could be construed as a potential conflict of interest.

Publisher's note

Supplementary material

The Supplementary Material for this article can be found online at: https://www.frontiersin.org/articles/10.3389/fcimb.2023.1057082/full#supplementary-material

SUPPLEMENTARY FIGURE 1
Effect of HCV fitness on the level of cellular protein H3Ser10ph and viral proteins NS5A and core. Huh-7.5 reporter cells were either mock-infected or infected with HCV p0, HCV p100 or HCV p200 (abbreviated as p0, p100 and p200, respectively) at an initial MOI of 0.03 TCID50/cell; protein extracts were prepared at the indicated times post-infection. **(A)** H3Ser10ph levels in HCV-infected cells expressed as the fold induction relative to the corresponding value for the HCV p0 infected cells; the infecting HCV (code in bottom right part), and the time post-infection at which extracts were prepared are given in the abscissa; the numerical densitometry values (measured relative to the HCV p0-infected sample, taken as 1) are indicated in the upper box, next to the panel. The values are the result of three independent experiments (biological triplicate). **(B)** Same as A but for viral protein NS5A. **(C)** Same as B but for the viral protein core. Asterisks indicate statistical significance as follows: *=p.

SUPPLEMENTARY FIGURE 2
Percentage of infected cells upon infection with HCV p0 and HCV p200. Cells were infected with the viruses HCV p0 or HCV p200 at a MOI of 0.03 TCID50/cell and were fixed with methanol at a different times post-infection. Cells were stained to detect NS5A using anti-NS5A monoclonal antibody 9E10. **(A)** Images of the stained cells at a different times post-infection. The images were taken using the LSM900 Upright Confocal Microscope. The different times post-infection are indicated in the upper boxes. The infecting viruses are indicated in the right boxes. **(B)** Percentage of infected cells at a different times post-infections. The number of infected cells was calculated using the software "Image Fiji". The infecting virus is indicated in the upper box. The percentage of infected cells is indicated in the ordinate while the time post-infection is indicated in the abscissa. Numerical values are given in the box above the lower panel. Asterisks indicate statistical significance as follows: *** =p.

References

Abdulazeez, M., Kia, G. S. N., Abarshi, M. M., Muhammad, A., Ojedapo, C. E., Atawodi, J. C., et al. (2020). Induction of rabies virus infection in mice brain may up and down regulate type II interferon gamma *via* epigenetic modifications. *Metab. Brain Dis.* 35 (5), 819–827. doi: 10.1007/s11011-020-00553-y

Blight, K. J., McKeating, J. A., and Rice, C. M. (2002). Highly permissive cell lines for subgenomic and genomic hepatitis c virus RNA replication. *J. Virol.* 76 (24), 13001–13014. doi: 10.1128/JVI.76.24.13001-13014.2002

Caixia, L., Yang, X., Yurong, T., and Xiaoqun, Q. (2019). Involvement of epigenetic modification in epithelial immune responses during respiratory syncytial virus infection. *Microb. Pathog.* 130, 186–189. doi: 10.1016/j.micpath.2019.03.019

Cervera, H., Ambros, S., Bernet, G. P., Rodrigo, G., and Elena, S. F. (2018). Viral fitness correlates with the magnitude and direction of the perturbation induced in the host's transcriptome: The tobacco etch potyvirus-tobacco case study. *Mol. Biol. Evol.* 35 (7), 1599–1615. doi: 10.1093/molbev/msy038

Chieffi, P. (2018). Aurora b: A new promising therapeutic target in cancer. *Intract. Rare. Dis. Res.* 7 (2), 141–144. doi: 10.5582/irdr.2018.01018

Dandri, M. (2020). Epigenetic modulation in chronic hepatitis b virus infection. *Semin. Immunopathol.* 42 (2), 173–185. doi: 10.1007/s00281-020-00780-6

de Aguiar, G., Leite, C., Dias, B., Vasconcelos, S. M. M., de Moraes, R. A., de Moraes, M. E. A., et al. (2019). Evidence for host epigenetic signatures arising from arbovirus infections: A systematic review. *Front. Immunol.* 10. doi: 10.3389/fimmu.2019.01207

de Conti, A., Dreval, K., Tryndyak, V., Orisakwe, O. E., Ross, S. A., Beland, F. A., et al. (2017). Inhibition of the cell death pathway in nonalcoholic steatohepatitis (NASH)-related hepatocarcinogenesis is associated with histone H4 lysine 16 deacetylation. *Mol. Cancer Res.* 15 (9), 1163–1172. doi: 10.1158/1541-7786.MCR-17-0109

Delgado, S., Perales, C., Garcia-Crespo, C., Soria, M. E., Gallego, I., de Avila, A. I., et al. (2021). A two-level, intramutant spectrum haplotype profile of hepatitis c virus revealed by self-organized maps. *Microbiol. Spectr.* 9 (3), e0145921. doi: 10.1128/Spectrum.01459-21

Domingo, E., de Avila, A. I., Gallego, I., Sheldon, J., and Perales, C. (2019). Viral fitness: history and relevance for viral pathogenesis and antiviral interventions. *Pathog. Dis.* 77 (2):ftz021. doi: 10.1093/femspd/ftz021

Domingo, E., and Holland, J. J. (1997). RNA Virus mutations and fitness for survival. *Annu. Rev. Microbiol.* 51, 151–178. doi: 10.1146/annurev.micro.51.1.151

Domingo, E., Sheldon, J., and Perales, C. (2012). Viral quasispecies evolution. *Microbiol. Mol. Biol. Rev.* 76 (2), 159–216. doi: 10.1128/MMBR.05023-11

Domingo, E., Soria, M. E., Gallego, I., de Avila, A. I., Garcia-Crespo, C., Martinez-Gonzalez, B., et al. (2020). A new implication of quasispecies dynamics: Broad virus diversification in absence of external perturbations. *Infect. Genet. Evol.* 82, 104278. doi: 10.1016/j.meegid.2020.104278

Farci, P. (2011). New insights into the HCV quasispecies and compartmentalization. *Semin. Liver. Dis.* 31 (4), 356–374. doi: 10.1055/s-0031-1297925

Farci, P., Shimoda, A., Coiana, A., Diaz, G., Peddis, G., Melpolder, J. C., et al. (2000). The outcome of acute hepatitis c predicted by the evolution of the viral quasispecies. *Science* 288 (5464), 339–344. doi: 10.1126/science.288.5464.339

Fraga, M. F., Ballestar, E., Villar-Garea, A., Boix-Chornet, M., Espada, J., Schotta, G., et al. (2005). Loss of acetylation at Lys16 and trimethylation at Lys20 of histone H4 is a common hallmark of human cancer. *Nat. Genet.* 37 (4), 391–400. doi: 10.1038/ng1531

Gallego, I., Gregori, J., Soria, M. E., Garcia-Crespo, C., Garcia-Alvarez, M., Gomez-Gonzalez, A., et al. (2018). Resistance of high fitness hepatitis c virus to lethal mutagenesis. *Virology* 523, 100–109. doi: 10.1016/j.virol.2018.07.030

Gallego, I., Sheldon, J., Moreno, E., Gregori, J., Quer, J., Esteban, J. I., et al. (2016). Barrier-independent, fitness-associated differences in sofosbuvir efficacy against hepatitis c virus. *Antimicrob. Agents Chemother.* 60 (6), 3786–3793. doi: 10.1128/AAC.00581-16

Gallego, I., Soria, M. E., Garcia-Crespo, C., Chen, Q., Martinez-Barragan, P., Khalfaoui, S., et al. (2020). Broad and dynamic diversification of infectious hepatitis c virus in a cell culture environment. *J. Virol.* 94 (6), e01856-19. doi: 10.1128/JVI.01856-19

Gao, C., Chen, L., Tang, S. B., Long, Q. Y., He, J. L., Zhang, N. A., et al. (2020). The epigenetic landscapes of histone modifications on HSV-1 genome in human THP-1 cells. *Antiviral Res.* 176, 104730. doi: 10.1016/j.antiviral.2020.104730

Giovannini, C., Fornari, F., Indio, V., Trere, D., Renzulli, M., Vasuri, F., et al. (2020). Direct antiviral treatments for hepatitis c virus have off-target effects of oncologic relevance in hepatocellular carcinoma. *Cancers* 12 (9):2674. doi: 10.3390/cancers12092674

Goto, H., Yasui, Y., Nigg, E. A., and Inagaki, M. (2002). Aurora-b phosphorylates histone H3 at serine28 with regard to the mitotic chromosome condensation. *Genes Cells* 7 (1), 11–17. doi: 10.1046/j.1356-9597.2001.00498.x

Hamdane, N., Juhling, F., Crouchet, E., El Saghire, H., Thumann, C., Oudot, M. A., et al. (2019). HCV-induced epigenetic changes associated with liver cancer risk persist after sustained virologic response. *Gastroenterology* 156 (8), 2313–2329.e2317. doi: 10.1053/j.gastro.2019.02.038

Hegyi, K., and Mehes, G. (2012). Mitotic failures in cancer: Aurora b kinase and its potential role in the development of aneuploidy. *Pathol. Oncol. Res.* 18 (4), 761–769. doi: 10.1007/s12253-012-9534-8

Hung, S. Y., Lin, H. H., Yeh, K. T., and Chang, J. G. (2014). Histone-modifying genes as biomarkers in hepatocellular carcinoma. *Int. J. Clin. Exp. Pathol.* 7 (5), 2496–2507.

Ilango, S., Paital, B., Jayachandran, P., Padma, P. R., and Nirmaladevi, R. (2020). Epigenetic alterations in cancer. *Front. Biosci.* 25 (6), 1058–1109. doi: 10.2741/4847

Jones, C. T., Catanese, M. T., Law, L. M., Khetani, S. R., Syder, A. J., Ploss, A., et al. (2010). Real-time imaging of hepatitis c virus infection using a fluorescent cell-based reporter system. *Nat. Biotechnol.* 28 (2), 167–171. doi: 10.1038/nbt.1604

Levrero, M., and Zucman-Rossi, J. (2016). Mechanisms of HBV-induced hepatocellular carcinoma. *J. Hepatol.* 64 (1 Suppl), S84–S101. doi: 10.1016/j.jhep.2016.02.021

Lin, Z. Z., Jeng, Y. M., Hu, F. C., Pan, H. W., Tsao, H. W., Lai, P. L., et al. (2010). Significance of aurora b overexpression in hepatocellular carcinoma. aurora b overexpression in HCC. *BMC Cancer* 10, 461. doi: 10.1186/1471-2407-10-461

Lin, M. V., King, L. Y., and Chung, R. T. (2015). Hepatitis c virus-associated cancer. *Annu. Rev. Pathol.* 10, 345–370. doi: 10.1146/annurev-pathol-012414-040323

Lindenbach, B. D., Evans, M. J., Syder, A. J., Wolk, B., Tellinghuisen, T. L., Liu, C. C., et al. (2005). Complete replication of hepatitis c virus in cell culture. *Science* 309 (5734), 623–626. doi: 10.1126/science.1114016

Lohmann, V., and Bartenschlager, R. (2019). Indelibly stamped by hepatitis c virus infection: Persistent epigenetic signatures increasing liver cancer risk. *Gastroenterology* 156 (8), 2130–2133. doi: 10.1053/j.gastro.2019.04.033

Lynch, K. L., Gooding, L. R., Garnett-Benson, C., Ornelles, D. A., and Avgousti, D. C. (2019). Epigenetics and the dynamics of chromatin during adenovirus infections. *FEBS Lett.* 593 (24), 3551–3570. doi: 10.1002/1873-3468.13697

Madejón, A., Sheldon, J., Francisco-Recuero, I., Perales, C., Dominguez-Beato, M., Lasa, M., et al. (2015). Hepatitis c virus-mediated aurora b kinase inhibition modulates inflammatory pathway and viral infectivity. *J. Hepatol.* 63 (2), 312–319. doi: 10.1016/j.jhep.2015.02.036

Mann, D. A. (2014). Epigenetics in liver disease. *Hepatology* 60 (4), 1418–1425. doi: 10.1002/hep.27131

Marukian, S., Jones, C. T., Andrus, L., Evans, M. J., Ritola, K. D., Charles, E. D., et al. (2008). Cell culture-produced hepatitis c virus does not infect peripheral blood mononuclear cells. *Hepatology* 48 (6), 1843–1850. doi: 10.1002/hep.22550

Milavetz, B. I., and Balakrishnan, L. (2015). Viral epigenetics. *Methods Mol. Biol.* 1238, 569–596. doi: 10.1007/978-1-4939-1804-1_30

Moreno, E., Gallego, I., Gregori, J., Lucia-Sanz, A., Soria, M. E., Castro, V., et al. (2017). Internal disequilibria and phenotypic diversification during replication of hepatitis c virus in a noncoevolving cellular environment. *J. Virol.* 91, e02505–16 (10). doi: 10.1128/JVI.02505-16

Perales, C., Beach, N. M., Gallego, I., Soria, M. E., Quer, J., Esteban, J. I., et al. (2013). Response of hepatitis c virus to long-term passage in the presence of alpha interferon: multiple mutations and a common phenotype. *J. Virol.* 87 (13), 7593–7607. doi: 10.1128/JVI.02824-12

Perez, S., Kaspi, A., Domovitz, T., Davidovich, A., Lavi-Itzkovitz, A., Meirson, T., et al. (2019). Hepatitis c virus leaves an epigenetic signature post cure of infection by direct-acting antivirals. *PloS Genet.* 15 (6), e1008181. doi: 10.1371/journal.pgen.1008181

Quarleri, J. F., and Oubina, J. R. (2016). Hepatitis c virus strategies to evade the specific-T cell response: a possible mission favoring its persistence. *Ann. Hepatol.* 15 (1), 17–26. doi: 10.5604/16652681.1184193

Quiñones-Mateu, M. E., and Arts, E. (2006). Virus fitness: concept, quantification, and application to HIV population dynamics. *Curr. Topics. Microbiol. Immunol.* 299, 83–140. doi: 10.1007/3-540-26397-7_4

Ramon, Y. C. S., Sese, M., Capdevila, C., Aasen, T., De Mattos-Arruda, L., Diaz-Cano, S. J., et al. (2020). Clinical implications of intratumor heterogeneity: challenges and opportunities. *J. Mol. Med.* 98 (2), 161–177. doi: 10.1007/s00109-020-01874-2

Ramos, J. C., and Lossos, I. S. (2011). Newly emerging therapies targeting viral-related lymphomas. *Curr. Oncol. Rep.* 13 (5), 416–426. doi: 10.1007/s11912-011-0186-8

Reed, L. J., and Muench, H. (1938). A simple method for estimating fifty per cent endpoint. *Am. J. Hyg.* 27, 493–497.

Schotta, G., Lachner, M., Sarma, K., Ebert, A., Sengupta, R., Reuter, G., et al. (2004). A silencing pathway to induce H3-K9 and H4-K20 trimethylation at constitutive heterochromatin. *Genes Dev.* 18 (11), 1251–1262. doi: 10.1101/gad.300704

Sheldon, J., Beach, N. M., Moreno, E., Gallego, I., Pineiro, D., Martinez-Salas, E., et al. (2014). Increased replicative fitness can lead to decreased drug sensitivity of hepatitis c virus. *J. Virol.* 88 (20), 12098–12111. doi: 10.1128/JVI.01860-14

Soria, M. E., Garcia-Crespo, C., Martinez-Gonzalez, B., Vazquez-Sirvent, L., Lobo-Vega, R., de Avila, A. I., et al. (2020). Amino acid substitutions associated with treatment failure for hepatitis c virus infection. *J. Clin. Microbiol.* 58 (12):e01985-20. doi: 10.1128/JCM.01985-20

Tan, K. S., Lim, R. L., Liu, J., Ong, H. H., Tan, V. J., Lim, H. F., et al. (2020). Respiratory viral infections in exacerbation of chronic airway inflammatory diseases: Novel mechanisms and insights from the upper airway epithelium. *Front. Cell Dev. Biol.* 8. doi: 10.3389/fcell.2020.00099

Tanaka, S., Arii, S., Yasen, M., Mogushi, K., Su, N. T., Zhao, C., et al. (2008). Aurora kinase b is a predictive factor for the aggressive recurrence of hepatocellular carcinoma after curative hepatectomy. *Br. J. Surg.* 95 (5), 611–619. doi: 10.1002/bjs.6011

Tardaguila, M., Gonzalez-Gugel, E., and Sanchez-Pacheco, A. (2011). Aurora kinase b activity is modulated by thyroid hormone during transcriptional activation of pituitary genes. *Mol. Endocrinol.* 25 (3), 385–393. doi: 10.1210/me.2010-0446

Wang, C., Sun, J. H., O'Boyle, D. R., Nower, P., Valera, L., Roberts, S., et al. (2013). Persistence of resistant variants in hepatitis c virus-infected patients treated with the NS5A replication complex inhibitor daclatasvir. *Antimicrob. Agents Chemother.* 57 (5), 2054–2065. doi: 10.1128/AAC.02494-12

Wang, C., Wang, C., Zou, J., Yang, Y., Li, Z., and Zhu, S. (2019). Epigenetics in the plant-virus interaction. *Plant Cell Rep.* 38 (9), 1031–1038. doi: 10.1007/s00299-019-02414-0

Wang, Z., Zang, C., Rosenfeld, J. A., Schones, D. E., Barski, A., Cuddapah, S., et al. (2008). Combinatorial patterns of histone acetylations and methylations in the human genome. *Nat. Genet.* 40 (7), 897–903. doi: 10.1038/ng.154

Wargo, A. R., and Kurath, G. (2011). *In vivo* fitness associated with high virulence in a vertebrate virus is a complex trait regulated by host entry, replication, and shedding. *J. Virol.* 85 (8), 3959–3967. doi: 10.1128/JVI.01891-10

Yan, X. B., Mei, L., Feng, X., Wan, M. R., Chen, Z., Pavio, N., et al. (2008). Hepatitis c virus core proteins derived from different quasispecies of genotype 1b inhibit the growth of Chang liver cells. *World J. Gastroenterol.* 14 (18), 2877–2881. doi: 10.3748/wjg.14.2877

Zheng, Y., Hlady, R. A., Joyce, B. T., Robertson, K. D., He, C., Nannini, D. R., et al. (2019). DNA Methylation of individual repetitive elements in hepatitis c virus infection-induced hepatocellular carcinoma. *Clin. Epigenet.* 11 (1), 145. doi: 10.1186/s13148-019-0733-y

Zhou, Y., Li, M., Yu, X., Liu, T., Li, T., Zhou, L., et al. (2018). Butein suppresses hepatocellular carcinoma growth *via* modulating aurora b kinase activity. *Int. J. Biol. Sci.* 14 (11), 1521–1534. doi: 10.7150/ijbs.25334

frontiers | Frontiers in Cellular and Infection Microbiology

TYPE Original Research
PUBLISHED 20 April 2023
DOI 10.3389/fcimb.2023.1125135

OPEN ACCESS

EDITED BY
Josep Quer,
Vall d'Hebron Research Institute (VHIR), Spain

REVIEWED BY
Tanya Allen Miura,
University of Idaho, United States
Carlos Cabello-Gutierrez,
National Institute of Respiratory Diseases-Mexico (INER), Mexico

*CORRESPONDENCE
Rocio Tirado Mendoza
rtirado@facmed.unam.mx

†Deceased

SPECIALTY SECTION
This article was submitted to Clinical Microbiology, a section of the journal Frontiers in Cellular and Infection Microbiology

RECEIVED 15 December 2022
ACCEPTED 29 March 2023
PUBLISHED 20 April 2023

CITATION
Meza UC, Lara NP, Gómez LC, Rodríguez MS, Hernández JRA and Mendoza RT (2023) The HRA2pl fusion peptide exerts *in vitro* antiviral activity against human respiratory paramyxoviruses and pneumoviruses.
Front. Cell. Infect. Microbiol. 13:1125135.
doi: 10.3389/fcimb.2023.1125135

The HRA2pl fusion peptide exerts *in vitro* antiviral activity against human respiratory paramyxoviruses and pneumoviruses

Uriel Cruz Meza[1], Norvell Perezbusta Lara[1], Laura Chávez Gómez[1], Marcela Solís Rodríguez[2], Javier R. Ambrosio Hernández[1†] and Rocio Tirado Mendoza[1*]

[1]Department of Microbiology and Parasitology, Faculty of Medicine, Universidad Nacional Autónoma de México (UNAM), Mexico City, Mexico, [2]Pharmaceutical Chemistry Department, University of Kansas, Douglas, KS, United States

Acute respiratory infections are a group of diseases caused by viruses, bacteria, and parasites that mainly affect children until the age of 5 and immunocompromised senior adults. In Mexico, these infections are the main cause of morbidity in children, with more than 26 million cases of respiratory infections reported by the Secretariat of Health, in 2019. The human respiratory syncytial virus (hRSV), the human metapneumovirus (hMPV), and the human parainfluenza-2 (hPIV-2) are responsible for many respiratory infections. Currently, palivizumab, a monoclonal antibody against the fusion protein F, is the treatment of choice against hRSV infections. This protein is being studied for the design of antiviral peptides that act by inhibiting the fusion of the virus and the host cell. Therefore, we examined the antiviral activity of the HRA2pl peptide, which competes the heptad repeat A domain of the F protein of hMPV. The recombinant peptide was obtained using a viral transient expression system. The effect of the fusion peptide was evaluated with an *in vitro* entry assay. Moreover, the effectiveness of HRA2pl was examined in viral isolates from clinical samples obtained from patients with infections caused by hRSV, hMPV, or hPIV-2, by evaluating the viral titer and the syncytium size. The HRA2pl peptide affected the viruses' capacity of entry, resulting in a 4-log decrease in the viral titer compared to the untreated viral strains. Additionally, a 50% reduction in the size of the syncytium was found. These results demonstrate the antiviral potential of HRA2pl in clinical samples, paving the way toward clinical trials.

KEYWORDS

acute respiratory infections, human respiratory virus, paramyxovirus, pneumovirus, fusion peptide, syncytium size

1 Introduction

Acute respiratory tract infections (ARTIs) represent a persistent public health problem (Lu et al., 2013b) and one of the main causes of morbidity and mortality in both neonates and infants (Yang et al., 2017). These infections range from asymptomatic to moderate and, in some cases, produce a severe infection. ARTIs affect the upper respiratory tract by causing colds, rhinosinusitis, pharyngitis, laryngitis, tracheitis, and otitis media (Schwarze, 2010), and the lower respiratory tract by causing tracheitis, wheezing, bronchitis, bronchiolitis, and pneumonia (Zappa et al., 2008). The latter three are considered the most frequent complications and death causes of ARTIs (Bicer et al., 2013; Perezbusta-Lara et al., 2020b). The etiological agents of ARTIs are primarily bacteria and viruses. Among the most common respiratory viruses are the human respiratory syncytial virus (hRSV), the human parainfluenza type 2 (hPIV-2), and emerging viruses, such as the human metapneumovirus (hMPV) (García-García et al., 2017). Recently, other respiratory viruses have been identified as etiological agents of ARTIs, such as the human bocavirus (Allander et al., 2005), the human coronaviruses NL63 and HKU1, the new human enterovirus, parechovirus, and rhinovirus strains (Berry et al., 2015).

The World Health Organization estimates that approximately 25% of hospitalizations of children are due to ARTIs (Perezbusta-Lara et al., 2020b). hRSV (subgroup A and subgroup B) is responsible for 80% of ARTIs, followed by hMPV with a share of 5–15% (Price et al., 2019; Rodríguez et al., 2020). These agents affect the pediatric population throughout the year (Perezbusta-Lara et al., 2020b). However, from December to February, an increased incidence of respiratory pathologies caused by infections occurs in children younger than 5 years old (Özgür and Demet, 2021). Premature newborns and infants with asthma, congenital heart disease, or bronchopulmonary dysplasia are more susceptible to these infections, usually presenting more severe clinical symptoms compared to children without comorbidities (Shachor-Meyouhas et al., 2011; Manzoni et al., 2017). Moreover, these respiratory infections are relevant in the context of high-risk populations such as the elderly and immunosuppressed patients (Takeuchi and Akira, 2009; Pierangeli et al., 2018).

Unfortunately, effective therapy is not yet available for these viral infections. To date, ribavirin and hRSV immunoglobulin are the only approved drugs for the treatment and prevention of hRSV in high-risk patients (Perezbusta-Lara et al., 2020b). In addition, various monoclonal antibodies are in use for the inhibition of viral entry to cells. Palivizumab is a humanized monoclonal antibody against the hRSV fusion protein F. It is approved as a preventive treatment against serious hRSV disease in infants with specific risk factors (Madhi et al., 2020). Nevertheless, its use has some limitations, including the administration of multiple doses, an efficacy of approximately 45% to 55% among high-risk infants (Madhi et al., 2020), and high costs (Morris et al., 2009). Other monoclonal antibodies against hRSV's F protein exist, like motavizumab (O'Brien et al., 2015) and nirsevimab (Muñoz et al., 2019). Both underwent clinical trials and demonstrated protective properties against hRSV infection (Madhi et al., 2020). The partial efficacy of the F protein monoclonal antibodies highlights the need to develop new, effective, and safe alternative drugs for the treatment of these infections (Shang et al., 2021).

Antiviral peptides are an alternative to expensive treatments such as monoclonal antibodies (Madhi et al., 2020). In this vein, Guy Boivin's research group in Canada tested several recombinant fragments of the heptad repeats (HR) A and B (conserved domains of the F protein) of hMPV expressed in *Escherichia coli*. Among them, HRA2 showed the best rates of inhibition of syncytia when tested against hMPV (Deffrasnes et al., 2008). The structure of this peptide suggests the interruption of fusion mechanism. More specifically, HRA and HRB rearrange the stable beam of six helices, a phenomenon that leads to the fusion of the membranes through the placement of the N-terminal of the fusion peptide next to the transmembrane C-terminal domain of the protein (Yin et al., 2005; Melero and Mas, 2015). Previous research suggests that the mechanism of action of the HRA2pl peptide is through its interaction with HRB when the F protein is refolded at the post-fusion state, which can result in a deficient fusion process. The HRB sequence is FNVALDQVFESIENSQALVDQSNRILSSAE.

In this study, we tested the antiviral activity of HRA2 expressed in *Nicotiana benthamiana* plants by a transient expression system (Márquez-Escobar et al., 2015). The effect of the fusion peptide was evaluated with an entry assay, while the viral titer and the size of the syncytium were determined with or without the peptide treatment. According to our data we could suggest that the HRA2pl peptide diminish the process of fusion for the entry of the virus and a 4-log decrease in the viral titer of the hRSV, hMPV, and hPIV-2 strains. These findings led us to study the effectiveness of HRA2pl on viral isolates from clinical samples of respiratory infection, where a 50% reduction in the size of the syncytium was found.

2 Materials and methods

2.1 Cells and viruses

Human laryngeal epithelial type 2 cells (HEp-2; ATCC CCL23, USA, which reported a contamination with HeLa cells) (Galvan et al, 2014) and Vero cells (normal adult African green monkey kidney cells; ATCC CCL81) were used to multiply the viral stocks for the viral titer test. They were propagated as described in Payment and Trudel (1993). The viruses hRSV Long [subgroup A (hRSV-A; ATCC® VR-26™)], hRSV 18537 [subgroup B (hRSV-B; ATCC® VR-1400™)], hPIV-2 (ATCC® VR-92™), and hMPV were isolated from clinical samples in our laboratory (Cerezo et al., 2016) The procedures for propagating the viruses and assessing the viral infectivity are described in Payment and Trudel (1993).

2.2 Clinical samples

The samples were retrieved from a bank of pharyngeal and nasopharyngeal specimens that were obtained from pediatric

patients (0–14 years) with an acute respiratory infection, between August 30, 2004, and February 13, 2014. The viral isolates obtained from the clinical samples were tested by endpoint RT-PCR as described in Perezbusta-Lara et al., 2020b. All subjects provided informed consent, and the study was reviewed and approved by the Research and Ethics Committee of the Faculty of Medicine, National Autonomous University of Mexico (UNAM; 089/2014; registry code: FMED/CI/SPLR/134/2014).

2.3 Fusion recombinant peptide HRA2pl

The sequence was based on Deffrasnes et al. (2008). The construction of the HRA2pl recombinant peptide (viral vector pICH11599 with the HRA2pl peptide coding sequence: HHHHHHSSGLVPRGSMKETAAAKFERQ HMDSPDL GTDDDDKAMADI GSEFENLYQGAKTIRLESEVTAIKNALKKT NEAVSTLGNGVRVLATAVRELKDFVSKN) and other two vectors required for the transient transformation (viral vector pICH4851 with the RNA-dependent polymerase (RdRp) coding sequence and the viral vector pICH10881 with the integrase coding sequence). were made by Veronica Marquez Escobar (Ph.D.). Six-week-old *N. benthamiana* plants were transiently transformed to express HRA2pl, which was subsequently purified by affinity chromatography with imidazole gradient through a zinc column. Two samples, B1 (172.31 ng/µL, imidazole 500 mM) and B2 (182.9 ng/µL, imidazole 250 mM), were provided by the Alpuche Solís Laboratory (Instituto Potosino de Investigación Científica y Tecnológica) for the fusion assays.

2.4 Cytotoxicity assay

The cytotoxic effect of the fusion peptide HRA2pl on HEp-2 and Vero cells was determined using AlamarBlue protocol as described elsewhere (O'Brien et al., 2000). Briefly, confluent monolayers of HEp-2 cells (1×10^5 cells per well) or Vero cells (1×10^5 cells per well) were seeded into 96-well culture plates and were incubated overnight at 37°C under 5% CO_2.) and were cultured overnight with DMEM containing 5% of fetal bovine serum (FBS) at 37 and °C under 5% CO_2. For the kinetics of cell viability (0 h, 24 h and 48 h) the medium with 5% FBS was removed, and HRA2pl (B1: 172.31 ng/µL; B2: 182.9 ng/µL), were applied in the presence of fresh DMEM without serum. Simultaneously, AlamarBlue reagent was added. The kinetics of cell viability was evaluated by spectrophotometry at 0 h, 24 h, and 48 h. The control of cell viability assay were done in parallel for both cell lines (Hep-2 cells or Vero cells), that were cultured with DMEM without serum and without peptide. The assays were conducted in triplicate (i.e., three experiments per assay). The kinetics of cell viability was evaluated by spectrophotometry at 0 h, 24 h, and 48 h. The absorbance was read at 570 nm. The viability was calculated as follows:

$$Cell\ \ viability = \frac{absorbance\ \ with\ \ treatment}{absorbance\ \ without\ \ treatment} \times 100$$

2.5 Determination of the optimal concentration of HRA2pl

The optimal concentration of the fusion peptides HRA2pl B1 and B2 was determined by measuring the reduction of the viral titer expressed as $TCID_{50}$/ml (Payment and Trudel, 1993). Confluent HEp-2 and Vero cell monolayers were treated with different concentrations of HRA2pl B1 or B2 (3.2 µg/ml, 2.1 µg/ml, and 1.8 µg/ml) against hRSV (1.9×10^4 $TCID_{50}$/ml), hMPV (clinically isolated), or hPIV-2 (1×10^5 $TCID_{50}$/ml). The treated cell monolayers were incubated with the mixtures previously described for 4 h at 4°C to avoid virus internalization. Afterwards, the 96-well culture plates were incubated for 2 h at 37°C under 5% CO_2 to allow the internalization of viral particles. Subsequently, the treated cultures were incubated for 72 h at 37°C (Lupini et al., 2009; Chang et al., 2013; Visintini Jaime et al., 2013; Lelešius et al., 2019) and the effect of HRA2pl on the viral titer was determined by the TCID50 assay (Payment and Trudel, 1993). The outcome of the HRA2pl treatment against hMPV was studied by measuring the size and number of the distinctive syncytia, corresponding to the cytopathic effect (CPE). To visualize CPE, the monolayers were fixed with methanol for 5 min. To stain the cells, the solution of crystal violet was added for 4 min at room temperature with constant stirring. The stain solution was removed, and the plate was rinsed with running water. The size of the syncytium was measured with the software ImageJ 1.5b. The assays were conducted in triplicate (i.e., three experiments per assay).

2.6 Entry assay

To test the virucidal activity of HRA2pl, we evaluated its effect on viral entry with the TCID50 assay for the hRSV and hPIV-2 strains or the reduction of CPE for the hMPV (Lupini et al., 2009; Chang et al., 2013; Visintini Jaime et al., 2013; Lelešius et al., 2019). Briefly, HEp-2 or Vero cells were grown in 96-well culture plates and incubated for 24 h under 5% CO_2. The confluent monolayers were treated with a mixture of hRSV (1.9×10^4 $TCID_{50}$/ml), hMPV (virus isolated from clinical samples), or hPIV-2 (1×10^5 $TCID_{50}$/ml) and 3.2 µg/ml of HRA2pl. Then, the treated cell monolayers were incubated with the mixtures previously described for 4 h at 4° C to avoid virus internalization. Subsequently, the plates were incubated with the mixture described above for 2 h at 37°C under 5% CO_2 to allow the internalization of viral particles. Next, the inoculum was removed, and 150 µl of fresh DMEM (without serum) per well were added for 48 h at 37°C under 5% CO_2. Subsequently, the viral titer was determined by the TCID50 assay as described elsewhere (Payment and Trudel, 1993) For hMPV, the changes in CPE (size and number of the distinctive syncytia) were determined.

The virucidal activity of HRA2pl was tested against viral isolates from clinical samples of respiratory infections. Briefly, Hep-2 or Vero cells were grown in 96-well culture plates and incubated for 24 h under 5% CO_2. The 96 plates were divided into two sections:

one was infected with the viral isolates without treatment with the peptide, and the other one was treated with both the viral isolates and 3.2 µg/ml of HRA2pl. The plates were then incubated at 4°C for 4 h. The assay followed the steps that are previously described in the above section. The effect of HRA2pl on the clinical samples was calculated as the change in the size and/or the number of distinctive syncytia in 10 microscopic fields per clinical sample. The controls of this assay were a mixture of DMEM and HRA2pl, DMEM and clinical viral isolates, and DMEM and cells. These controls were used for the statical analysis described in section 2.7.

2.7 Statistical analysis

The data were analyzed with one-way analyses of variance (ANOVA) and Student's t-test. The differences among the mean values were tested for significance using the Tukey test. All results were considered significant when $p \leq 0.05$. The data were analyzed and visualized using the statistical software GraphPad Prism 5.0.

3 Results

3.1 HRA2pl peptides did not have a cytotoxic effect on HEp-2 and Vero cells

Before evaluating B1 and B2 HRA2pl's antiviral activity, the peptide's innocuity on the HEp-2 and Vero cells was examined with a 48-h kinetics of cytotoxicity assay. B1 and B2 were not cytotoxic according to the measurement of cell viability, independently of the peptide's concentration (Figure 1). About our data, particularly the time 0 h of the kinetic cell viability assay, showed a decrease in the cell viability, result that took our attention. So, we tried to explain this result considering that the assay was done in deprivation of serum and this factor could affect the cell proliferation, considering that, the previous 24 h, we cultured both cell lines with DMEM containing 5% of FBS. The peptide did not affect the cell viability because the cell lines recover their proliferation for the following points of the kinetics. It is important to consider that besides the deprivation of serum (claimed before) the cell monolayers probably lose some cells during the development of the assay because the monolayer was washed before we began the peptide treatment.

3.2 HRA2pl reduced the viral titer of hRSV and hPIV-2

The antiviral effect of HRA2pl against hRSV and hPIV-2 was measured as the reduction of the viral titer. Three different concentrations of purified B1 or B2 (3.2 µg/ml, 2.1 µg/ml, 1.8 µg/ml) were tested. The viral titer of hRSV and hPIV-2 decreased at all tested concentrations. However, the most prominent reduction in viral production was observed at the concentration of 3.2 µg/ml of either B1 or B2. In the case of hRSV, the viral titer reduced from 1.9×10^4 to 5.9×10^1 $TCID_{50}$/ml (Figure 2A) when applying B1. As for B2, the viral production reduced from 1.9×10^4 to 2.5 $TCID_{50}$/ml (Figure 2B). Similarly, in the case of hPIV-2, the B1 peptide reduced the viral titer from 1×10^5 to 3.1×10^1 $TCID_{50}$/ml (Figure 2C), and the B2 peptide reduced it from 1×10^5 to 1.5×10^1 $TCID_{50}$/ml (Figure 2D). Thus, the HRA2pl B2 peptide had the best antiviral activity against the production of viral particles of hRSV and hPIV-2.

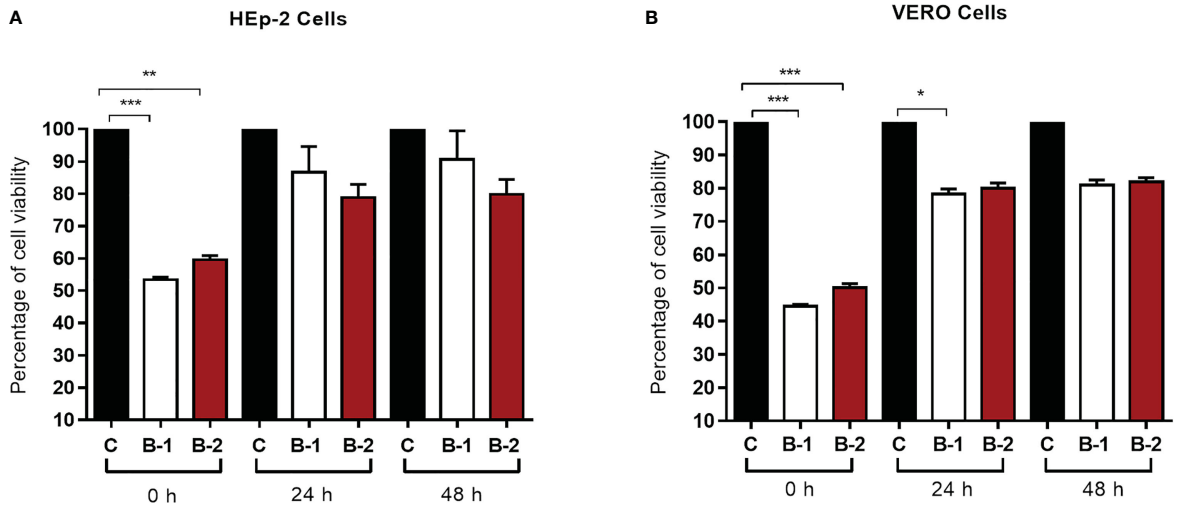

FIGURE 1
The HRA2pl peptide does not affect cell viability of **(A)** HEp-2 and **(B)** Vero cultures. For the assay, a confluent monolayer of HEp-2 and Vero cells (95%–100%) was treated with 90 µL of HRA2pl purified in DMEM (B1: 172.31 ng/µL; B2: 182.9 ng/µL) and 10 µL of AlamarBlue to measure the absorbance at 0 h, 24 h, and 48 h. *NS*: Nonsignificant; *$p< 0.05$;**$p< 0.01$; ***$p< 0.001$.

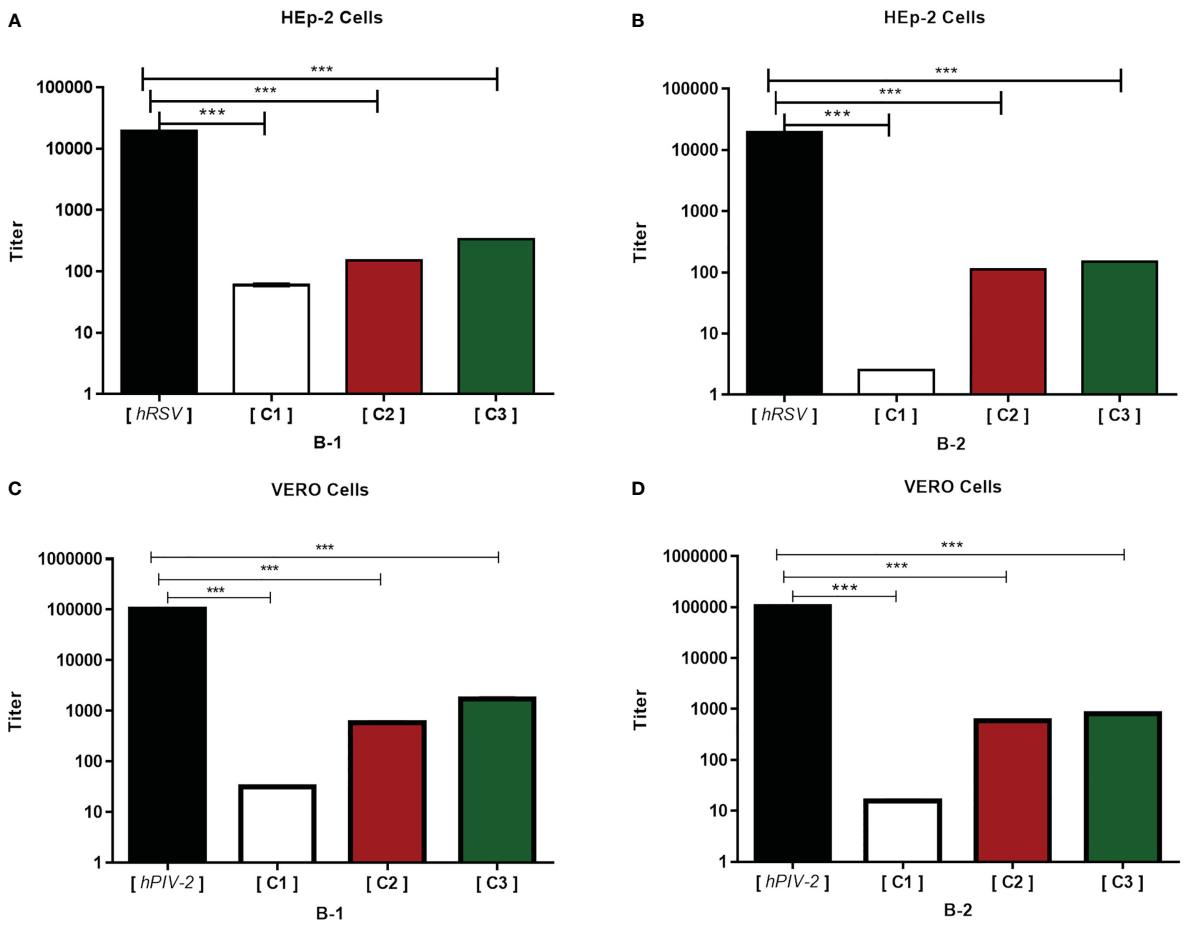

FIGURE 2
HRA2pl reduces the viral titer. For the assay, a confluent monolayer of HEp-2 **(A, B)** and Vero **(C, D)** cells (95%–100%) was treated with HRA2pl purified in DMEM at three different concentrations (C1: 3.2 μg/mL; C2: 2.1 μg/mL; C3: 1.8 μg/mL). The monolayers were treated with a mixture of C1, C2, or C3 and hRSV (1.9×10^4 $TCID_{50}$/ml) and hPIV-2 (1×10^5 $TCID_{50}$/ml). The reduction in the viral titer was established by $TCID_{50}$/ml.***$p<$ 0.001.

3.3 HRA2pl treatment reduced the syncytium size of clinical isolates

To test the peptide's effect on pediatric patients' samples, 40 clinical viral isolates, a representative sample of our viral bank, were studied. HRA2pl B2 treatment induced the reduction of the size of the syncytium. After treatment with the peptide, the hRSV-positive samples' syncytium size reduced to 52.87% of the control syncytium size (Figure 3A). The size of the syncytium without treatment ranged from 15.05 mm to 19.83 mm (average: 17.59 mm). Meanwhile, treatment with the peptide produced a reduction in the size of the syncytium, reaching a size that ranged from 7.20 mm to 10.52 mm (average: 8.29 mm). A similar result was observed on the clinical samples typified as hMPV-positive. They showed a reduction of 54.33% compared to the samples without treatment (Figure 3B). The average syncytium size without treatment was 18.13 mm, while after treatment, it reached 8.28 mm. Finally, the effect of the peptide on the hPIV-2 clinical samples showed a reduction of the syncytium (53.88% of the control samples) (Figure 3C). The average size without treatment was 24.59 mm, which reached 11.34 mm after treatment with the peptide. Therefore, the HRA2pl peptide acts as an inhibitor of viral fusion by competition against the respiratory viruses hRSV, hMPV, and hPIV-2.

3.4 HRA2pl treatment modified the number of syncytia

Even though treatment with HRA2pl caused a significant reduction in the size of the syncytium, an increase in the number of syncytia was observed. This was probably associated with deficient fusion resulting from the competition between the viral fusion protein of the viral isolates versus the HRA2pl fusion peptide. In the case of the hRSV-positive samples, an increase from 2.41 to 5.31 syncytia per field was found after treatment with the peptide (Figure 4A). The hMPV samples presented an increase from 2.69 to 3.73 syncytia per field after treatment (Figure 4B). Nonetheless, a reduction in the number of syncytia per field was recorded in the case of hPIV-2 clinical samples (without treatment: 4.28 syncytia per field; with treatment: 3.16 syncytia per field; Figure 4C).

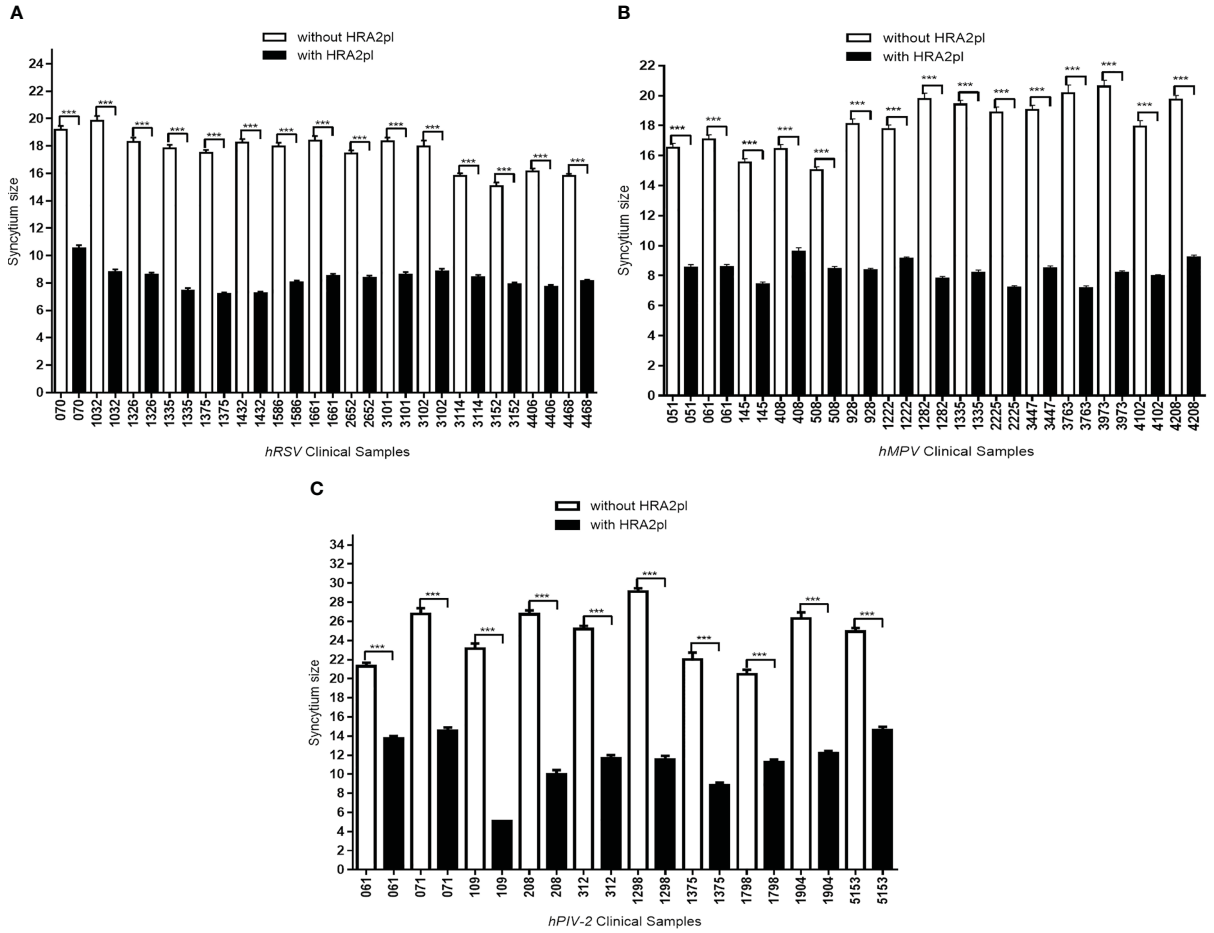

FIGURE 3
The syncytium size was reduced after treatment with HRA2pl B2. In HEp-2 cultures infected with **(A)** hRSV or **(B)** hMPV viral isolates, and **(C)** in Vero cultures infected with hPIV-2 viral isolates, treatment with HRA2pl significantly reduced the syncytium size. ***$p < 0.001$.

4 Discussion

In this study, we demonstrated that the HRA2pl peptide efficiently blocks the viral fusion of hRSV, hMPV, and hPIV-2 in an *in vitro* model, resulting in the reduction of the syncytium size. Moreover, we proved that the HRA2pl peptide reduced the number of syncytia in the hPIV2-positive clinical samples, contrary to the hRSV- or hMPV-positive samples. As for the latter, although the number of syncytia was not reduced, the reduction in their size is a noteworthy biological event that indicates the antiviral potential of HRA2pl in clinical samples.

The global presence of the hRSV, hMPV, and hPIV-2 viruses that are responsible for respiratory diseases, impacts the health of thousands of children and adults. Despite the relevance of viral ARTIs as a global persistent public health problem (Lu et al., 2013b) and the subsequent high risk of morbidity and mortality (Taylor, 2017), no prophylactic vaccines or effective antiviral treatments against them are currently available, with those applied providing only limited protection (Takeuchi and Akira, 2009). The production of a safe, efficient, and low-cost treatment against these viruses is a challenge to be faced.

The HRA2pl peptide inhibits the *in vitro* entry of hMPV at the fusion stage (Márquez-Escobar et al., 2015). In this context, we aimed to study whether HRA2pl can inhibit the entrance of not only hMPV but also other human respiratory viruses, like hRSV or hPIV-2, at the fusion stage. Our results demonstrate that the HRA2pl peptide produced a reduction in the size of the syncytium in all clinical samples independently of the type of respiratory viruses. This is in line with the fact that F proteins are phylogenetically close to each other (Russell et al., 2003) and are conserved across the families of *Pneumoviridae* and *Paramyxoviridae* (Aggarwal and Plemper, 2020).

F proteins are synthesized as an F0 precursor without fusion activity; their transition from F0 to F1–F2 is produced by the host cell's furin-type proteases residing in the Golgi apparatus (Aggarwal and Plemper, 2020). The F1 subunit contains the fusion peptide, a domain of hydrophobic amino acids, and the highly conserved amphipathic α-helical regions with 3–4 HR patterns adjacent to the fusion peptide, called the HRA and HRB domains (Aggarwal et al., 2020). Previous research showed that the recombinant HRA peptides were more efficient than HRB in inhibiting the fusion of hMPV and the virus' entry to the host cell, even at low concentrations (Deffrasnes et al., 2008). Here, we conclude that the HRA2pl decreased the size of the syncytium of hRSV, hMPV, and hPIV-2 viral isolates by up to 50% in HEp-2 and Vero cells.

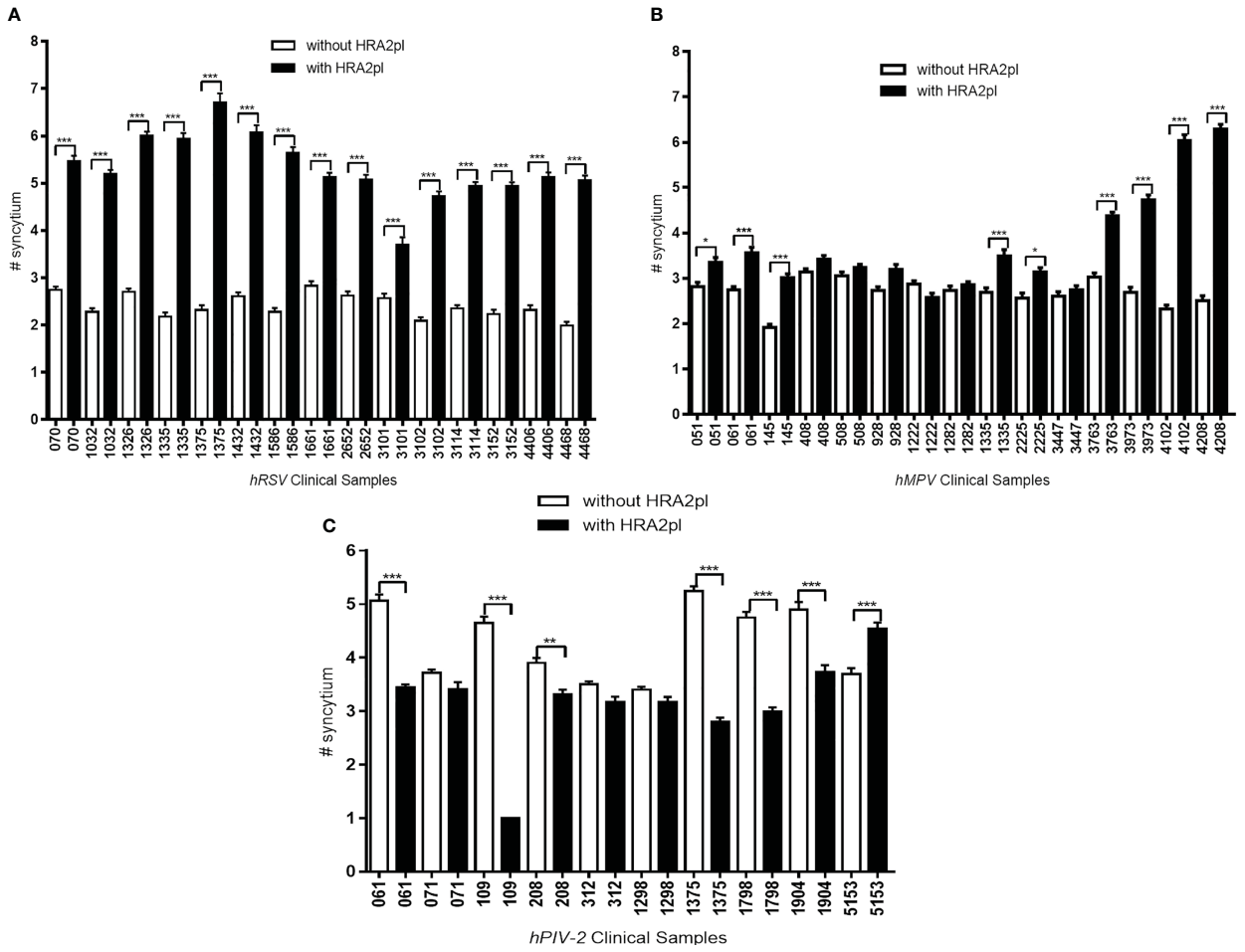

FIGURE 4
The changes in the number of syncytia after HRA2pl B2 treatment varied according to the viral infection. HRA2pl treatment increased the number of syncytia in **(A)** HEp-2 cells infected with hRSV viral isolates. **(B)** Some, but not all, HEp-2 cell cultures infected with hMPV viral isolates showed an increased number of syncytia after treatment with HRA2pl. **(C)** Treatment with the HRA2pl peptide decreased the number of syncytia in Vero cells infected with hPIV-2 viral isolates. NS, Nonsignificant; *p< 0.05; **p< 0.01; ***p< 0.001.

Our findings contribute to the literature concerning the therapeutic effects of interference with viral fusion proteins, paving the way toward clinical trials.

Data availability statement

The raw data supporting the conclusions of this article will be made available by the authors, without undue reservation.

Ethics statement

The study was conducted in accordance with the bi-osafety regulations of the World Medical Association's Declaration of Helsinki regarding the ethical conduct of research involving humans and was approved by the Research Ethics Board of Facultad de Medicina, UNAM (project number 101-2012). The informed consent letters were approved by the Committee of Ethics and Research of the División de Investigación de la Facultad de Medicina de la UNAM (FMED/CI/SPLR/004/2016).

Author contributions

Conceptualization, RT, UC and MS. Methodology, UC, NP, LC and MS. Validation UC, NP, LC and MS. Formal analysis, RT, UC and MS. Investigation, UC and RT. Resources, JH. Data curation, RT, UC and MS. Statistical analysis, UC, and LC. Writing, MS and RT. Supervision, RT and JH Project administration, JH, and RT. Funding acquisition, JH. All authors contributed to the article and approved the submitted version. JH passed away by COVID a year ago.

Funding

This research was funded by Dirección General de Asuntos del Personal Académico (DGAPA; IN-217519), UNAM, and Facultad de Medicina, UNAM.

Acknowledgments

The authors want to thank Dr. Diana Ríos for her assistance in the revision and preparation of the manuscript, Dr. Ángel Alpuche Solís for providing the HRA2pl peptide, and Ilektra Anagnostou for proofreading and editing the English version of the manuscript.

Conflict of interest

The authors declare that the research was conducted in the absence of any commercial or financial relationships that could be construed as a potential conflict of interest.

Publisher's note

References

Aggarwal, M., and Plemper, R. K. (2020). Structural insight into paramyxovirus and pneumovirus entry inhibition. *Viruses.* 12 (3), 342. doi: 10.3390/v12030342

Allander, T., Tammi, M. T., Eriksson, M., Bjerkner, A., Tiveljung-Lindell, A., and Andersson, B. (2005). Cloning of a human parvovirus by molecular screening of respiratory tract samples. *PNAS.* 102 (36), 12891–12896. doi: 10.1073/pnas.0504666102

Berry, M., Gamieldien, J., and Fielding, B. (2015). Identification of new respiratory viruses in the new millennium. *Viruses.* 7 (3), 996–1019. doi: 10.3390/v7030996

Bicer, S., Giray, T., Çöl, D., Erdağ, G. I., Vitrinel, A., Gürol, Y., et al. (2013). Virological and clinical characterizations of respiratory infections in hospitalized children. *Ital. J. Pediatr.* 39 (1), 22. doi: 10.1186/1824-7288-39-22

Cerezo, L. G., Zárate, C. K., Alpuche-Lazcano, S., et al. (2016). Diagnóstico molecular para la detección de metapneumovirus humano a partir de aislados virales en pacientes pediátricos con infección respiratoria aguda. *Investigación en Discapacidad* 5 (2), 88–95.

Chang, J. S., Wang, K. C., Yeh, C. F., Shieh, D. E., and Chiang, L. C. (2013). Fresh ginger (Zingiber officinale) has anti-viral activity against human respiratory syncytial virus in human respiratory tract cell lines. *J. Ethnopharmacol.* 145 (1), 146–151. doi: 10.1016/j.jep.2012.10.043

Deffrasnes, C., Hamelin, M. E., Prince, G. A., and Boivin, G. (2008). Identification and evaluation of a highly effective fusion inhibitor for human metapneumovirus. *Antimicrob. Agents Chemother.* 52 (1), 279–287. doi: 10.1128/aac.00793-07

Galvan, M. A., Cabello, C., Mejia, F., Valle, L., Valencia, E., and Manjarrez, M. E. (2014). Parainfluenza virus type 1 induces epithelial IL-8 production *via* p38-MAPK signalling. *J. Immunol. Res.* 2014, 1–12. doi: 10.1155/2014/515984

García-García, M. L., Calvo, C., Rey, C., Díaz, B., Molinero, M. D. M., Pozo, F., et al. (2017). Human metapnuemovirus infections in hospitalized children and comparison with other respiratory viruses. 2005-2014 prospective study. *PloS One* 12 (3), e0173504. doi: 10.1371/journal.pone.0173504

Lelešius, R., Karpovaitė, A., Mickienė, R., Drevinskas, T., Tiso, N., Ragažinskienė, O., et al. (2019). *In vitro* antiviral activity of fifteen plant extracts against avian infectious bronchitis virus. *BMC Vet. Res.* 15 (1), 178. doi: 10.1186/s12917-019-1925-6

Lu, Y., Wang, S., Zhang, L., Xu, C., Bian, C., Wang, Z., et al. (2013b). Epidemiology of human respiratory viruses in children with acute respiratory tract infections in jinan, China. *Clin. Dev. Immunol.* 2023, 1–8. doi: 10.1155/2013/210490

Lupini, C., Cecchinato, M., Scagliarini, A., Graziani, R., and Catelli, E. (2009). *In vitro* antiviral activity of chestnut and quebracho woods extracts against avian reovirus and metapneumovirus. *Res. Vet. Sci.* 87 (3), 482–487. doi: 10.1016/j.rvsc.2009.04.007

Madhi, S. A., Polack, F. P., Piedra, P. A., Munoz, F. M., Trenholme, A. A., Simões, E. A., et al. (2020). Respiratory syncytial virus vaccination during pregnancy and effects in infants. *NEJM.* 383 (5), 426–439. doi: 10.1056/nejmoa1908380

Manzoni, P., Figueras-Aloy, J., Simões, E. A. F., Checchia, P. A., Fauroux, B., Bont, L., et al. (2017). Defining the incidence and associated morbidity and mortality of severe respiratory syncytial virus infection among children with chronic diseases. *Infect. Dis. Ther.* 6 (3), 383–411. doi: 10.1007/s40121-017-0160-3

Márquez-Escobar, V. A., Tirado-Mendoza, R., Noyola, D. E., Gutiérrez-Ortega, A., and Alpuche-Solís, N. G. (2015). HRA2pl peptide: a fusion inhibitor for human metapneumovirus produced in tobacco plants by transient transformation. *Planta.* 242 (1), 69–76. doi: 10.1007/s00425-015-2277-5

Melero, J. A., and Mas, V. (2015). The pneumovirinae fusion (F) protein: A common target for vaccines and antivirals. *Virus Res.* 209, 128–135. doi: 10.1016/j.virusres.2015.02.024

Morris, S. K., Dzolganovski, B., Beyene, J., and Sung, L. (2009). A meta-analysis of the effect of antibody therapy for the prevention of severe respiratory syncytial virus infection. *BMC Infect. Dis.* 9 (1), 106. doi: 10.1186/1471-2334-9-106

Muñoz, F. M., Swamy, G. K., Hickman, S. P., Agrawal, S., Piedra, P. A., Glenn, G. M., et al. (2019). Safety and immunogenicity of a respiratory syncytial virus fusion (F) protein nanoparticle vaccine in healthy third-trimester pregnant women and their infants. *J. Infect. Dis.* 220 (11), 1802–1815. doi: 10.1093/infdis/jiz390

O'Brien, K. L., Chandran, A., Weatherholtz, R., Jafri, H. S., Griffin, M. P., Bellamy, T., et al. (2015). Efficacy of motavizumab for the prevention of respiratory syncytial virus disease in healthy native American infants: a phase 3 randomised double-blind placebo-controlled trial. *Lancet Infect. Dis.* 15 (12), 1398–1408. doi: 10.1016/s1473-3099(15)00247-9

O'Brien, J., Wilson, I., Orton, T., and Pognan, F. (2000). Investigation of the alamar blue (resazurin) fluorescent dye for the assessment of mammalian cell cytotoxicity. *Eur. J. Biochem.* 267 (17), 5421–5426. doi: 10.1046/j.1432-1327.2000.01606.x

Özgür, Ç., and Demet, Ç. (2021). Viral respiratory tract pathogens during the COVID-19 pandemic. *Eurasian J. Med.* 53 (2), 123–126. doi: 10.5152/eurasianjmed.2021.20459

Payment, P., and Trudel, M. (1993). 'Isolation and identification of viruses' in *Methods and techniques in virology.* N.Y. *USA: Marcel Dekker Inc* pp, 309–310. doi: 10.1002/rmv.1980040308

Perezbusta-Lara, N., Tirado-Mendoza, R., and Ambrosio-Hernández, J. R. (2020b). Respiratory infections and coinfections: geographical and population patterns. *Gaceta México.* 156 (4), 263–269. doi: 10.24875/gmm.m20000396

Pierangeli, A., Scagnolari, C., and Antonelli, G. (2018). Respiratory syncytial virus in infants. *Minerva Pediatr.* 70 (6), 553–565. doi: 10.23736/S0026-4946.18.05312-4

Price, R. H. M., Graham, C., and Ramalingam, S. (2019). Association between viral seasonality and meteorological factors. *Sci. Rep.* 9 (1), 8–11. doi: 10.1038/s41598-018-37481-y

Rodríguez, P. E., Frutos, M. C., Adamo, M. P., Cuffini, C., Cámara, J. A., Paglini, M. G., et al. (2020). Human metapneumovirus: Epidemiology and genotype diversity in children and adult patients with respiratory infection in córdoba, Argentina. *PloS One* 15 (12), e0244093. doi: 10.1371/journal.pone.0244093

Russell, C. J., Kantor, K. L., Jardetzky, T. S., and Lamb, R. A. (2003). A dual-functional paramyxovirus f protein regulatory switch segment. *JCB.* 163 (2), 363–374. doi: 10.1083/jcb.200305130

Schwarze, J. (2010). Respiratory viral infections in infants: Causes, clinical symptoms, virology, and immunology. *CMR.* 23 (1), 47–98. doi: 10.1128/cmr.00032-09

Shachor-Meyouhas, Y., Ben-Barak, A., and Kassis, I. (2011). Treatment with oral ribavirin and IVIG of severe human metapneumovirus pneumonia (HMPV) in immune compromised child. *Pediatr. Blood Cancer* 57 (2), 350–351. doi: 10.1002/pbc.23019

Shang, Z., Tan, S., and Ma, D. (2021). Respiratory syncytial virus: from pathogenesis to potential therapeutic strategies. *Int. J. Biol. Sci.* 17 (14), 4073–4091. doi: 10.7150/ijbs.64762

Takeuchi, O., and Akira, S. (2009). Innate immunity to virus infection. *Immunol. Rev.* 227 (1), 75–86. doi: 10.1111/j.1600-065x.2008.00737.x

Taylor, G. (2017). Animal models of respiratory syncytial virus infection. *Vaccine.* 35 (3), 469–480. doi: 10.1016/j.vaccine.2016.11.054

Visintini Jaime, M. F., Redko, F., Muschietti, L. V., Campos, R. H., Martino, V. S., and Cavallaro, L. V. (2013). *In vitro* antiviral activity of plant extracts from asteraceae medicinal plants. *Virol. J.* 10 (1), 245. doi: 10.1186/1743-422x-10-245

Yang, J., Hillson, E., Mauskopf, J., Copley-Merriman, C., Shinde, V., and Stoddard, J. (2017). The epidemiology of medically attended respiratory syncytial virus in older adults in the united states: A systematic review. *PloS One* 12 (8), e0182321. doi: 10.1371/journal.pone.0182321

Yin, H. S., Paterson, R. G., Wen, X., Lamb, R. A., and Jardetzky, T. S. (2005). Structure of the uncleaved ectodomain of the paramyxovirus (hPIV3) fusion protein. *Proc. Natl. Acad. Sci. U. S. A.* 102 (26), 9288–9293. doi: 10.1073/pnas.0503989102

Zappa, A., Perin, S., Amendola, A., Bianchi, S., Pariani, E., Ruzza, M. L., et al. (2008). Epidemiological and molecular surveillance of influenza and respiratory syncytial viruses in children with acute respiratory infections, (2004/2005 season). *Microbiologia Medica.* 23 (1), 7–21. doi: 10.4081/mm.2008.2592

frontiers | Frontiers in Cellular and Infection Microbiology

TYPE Review
PUBLISHED 01 May 2023
DOI 10.3389/fcimb.2023.1166839

OPEN ACCESS

EDITED BY
Josep Quer,
Vall d'Hebron Research Institute (VHIR), Spain

REVIEWED BY
Benjamin Florian Koch,
Goethe University Frankfurt, Germany
Luciana Jesus Da Costa,
Federal University of Rio de Janeiro, Brazil

*CORRESPONDENCE
Melissa Bello-Perez
mloreto@cnb.csic.es
Isabel Sola
isola@cnb.csic.es

†These authors contributed equally to this work and share senior authorship

RECEIVED 15 February 2023
ACCEPTED 11 April 2023
PUBLISHED 01 May 2023

CITATION
Hurtado-Tamayo J, Requena-Platek R, Enjuanes L, Bello-Perez M and Sola I (2023) Contribution to pathogenesis of accessory proteins of deadly human coronaviruses. *Front. Cell. Infect. Microbiol.* 13:1166839. doi: 10.3389/fcimb.2023.1166839

Contribution to pathogenesis of accessory proteins of deadly human coronaviruses

Jesus Hurtado-Tamayo, Ricardo Requena-Platek, Luis Enjuanes, Melissa Bello-Perez*† and Isabel Sola*†

Department of Molecular and Cell Biology, National Center of Biotechnology (CNB-CSIC), Campus Universidad Autónoma de Madrid, Madrid, Spain

Coronaviruses (CoVs) are enveloped and positive-stranded RNA viruses with a large genome (~ 30kb). CoVs include essential genes, such as the replicase and four genes coding for structural proteins (S, M, N and E), and genes encoding accessory proteins, which are variable in number, sequence and function among different CoVs. Accessory proteins are non-essential for virus replication, but are frequently involved in virus-host interactions associated with virulence. The scientific literature on CoV accessory proteins includes information analyzing the effect of deleting or mutating accessory genes in the context of viral infection, which requires the engineering of CoV genomes using reverse genetics systems. However, a considerable number of publications analyze gene function by overexpressing the protein in the absence of other viral proteins. This ectopic expression provides relevant information, although does not acknowledge the complex interplay of proteins during virus infection. A critical review of the literature may be helpful to interpret apparent discrepancies in the conclusions obtained by different experimental approaches. This review summarizes the current knowledge on human CoV accessory proteins, with an emphasis on their contribution to virus-host interactions and pathogenesis. This knowledge may help the search for antiviral drugs and vaccine development, still needed for some highly pathogenic human CoVs.

KEYWORDS

coronavirus, SARS-CoV, MERS-CoV, SARS-CoV-2, accessory proteins, pathogenesis, innate immune response

Introduction

Since the identification of the first human coronavirus (HCoV) in the 1960s (Kendall et al., 1962), seven HCoVs have been described. Four of them, HCoV-229E, HCoV-NL63, HCoV-OC43 and HCoV-HKU1, are low pathogenic and cause mild symptoms like a common cold, while three of them, SARS-CoV, MERS-CoV and SARS-CoV-2, are potentially deadly for humans.

HCoVs belong to the *Coronaviridae* family, included in the *Nidovirales* order (Zhou et al., 2021). The *Orthocoronavirinae* subfamily comprises viruses that infect mammals and birds, which are classified into four genera: *alphacoronavirus* and *betacoronavirus*, including viruses that infect humans and other mammals, *gammacoronavirus*, which

comprises viruses infecting birds, and *deltacoronavirus*, containing viruses that infect mammals and birds. HCoV-NL63 and HCoV-229E belong to the *alphacoronavirus* genus, while HCoV-OC43, HCoV-HKU1, SARS-CoV, MERS-CoV and SARS-CoV-2 belong to the *betacoronavirus* genus. This last genus has been recently subdivided into three subgenera: *Embecovirus* (HCoV-OC43 and HCoV-229E), *Sarbecovirus* (SARS-CoV and SARS-CoV-2) and *Merbecovirus* (MERS-CoV) (Gorbalenya et al., 2020; Kirtipal et al., 2020). The recent emergence of three highly pathogenic HCoVs during the 21th century (2002, 2012 and 2019, respectively) and the ongoing COVID-19 pandemic caused by SARS-CoV-2 have generated extensive interest in understanding the role of CoV proteins in pathogenesis.

CoVs possess a positive-sense single-strand RNA genome (~ 30 kb). The 5'-proximal two-thirds of the genome comprise two open reading frames (ORF1a and ORF1b), encoding two polyproteins that are processed by viral proteases into 16 non-structural proteins involved in viral continuous RNA synthesis or replication and discontinuous transcription (Sola et al., 2015). The 3' end of the genome contains genes that encode structural and accessory proteins. Four major structural proteins are homologous among all CoVs: spike (S), envelope (E), membrane (M) and nucleocapsid (N). Accessory genes, which encode structural and non-structural proteins, are variable in number, function and genome location among different CoV genera (Fang et al., 2021) (Figure 1). Accessory genes are interspersed among, or even overlapping, the structural genes. Accessory proteins are not essential for virus replication in cell cultures, although some of them may contribute to virus growth to some extent. However, they are involved in virus virulence *in vivo* by modulating cellular processes such as innate immunity, including the interferon (IFN) and proinflammatory responses, autophagy, cell cycle, apoptosis or stress pathways. In fact, alterations in these cell processes are often associated with the pathogenesis of deadly human CoVs, to which some accessory proteins contribute as virulence factors.

Understanding pathogenic virus-host interactions mediated by human deadly CoV accessory proteins is important to design antivirals that limit the severity of viral pathology. Monitoring mutations that these proteins undergo during viral evolution is essential to study changes in their interactions with cellular proteins. Moreover, deletion of accessory genes that behave as virulence factors from the viral genome provides a strategy to attenuate the virus for the development of vaccine candidates. Although other reviews have addressed the topic of SARS-CoV (Liu et al., 2014), MERS-CoV (Li et al., 2019) or SARS-CoV-2 (Redondo et al., 2021) accessory genes separately, this review is intended to provide a comparative description of the biological functions of accessory proteins from all three deadly human coronaviruses, including SARS-CoV and SARS-CoV-2 conserved proteins, with special emphasis on their contribution to pathogenesis. There is abundant literature describing the biological effects of CoV accessory proteins, but a significant proportion of these studies was performed by overexpressing a single protein. In the absence of other viral proteins, this ectopic expression may lead to non-physiological conditions with respect to subcellular localization, protein-protein interactions, or titration of host factors by the overexpressed protein, which could explain some controversial results. When possible, we will prioritize studies performed in the context of infection, which provide more physiological results.

Interferon and proinflammatory antiviral responses

The innate immune response represents the first line of defense against pathogens in vertebrates. Innate immunity includes a variety of cellular processes working coordinately to limit viral infection, including entry, translation and replication (Lokugamage et al., 2020). Innate immune response also contributes to identify and remove infected cells and to promote the adaptive immunity (Evans and Ozer, 1987). An essential component of innate immunity are cytokines, soluble factors that mediate the communication between cells and regulate different signaling pathways, such as the interferon (IFN) and pro-inflammatory responses. Type I IFN (IFNα and IFNβ) drives an antiviral state in non-immune cells and regulates antiviral responses to inhibit viral replication in infected cells (Lokugamage et al., 2020). IFN I activates the adaptive immune response by enhancing antigen presentation and promoting the action of T and B cells (Evans and Ozer, 1987; McNab et al., 2015). Pathogen-

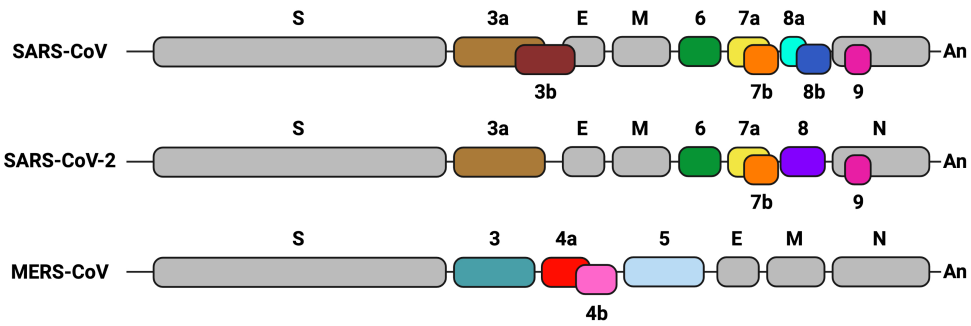

FIGURE 1
Genetic organization of the genome 3' end in highly pathogenic human CoVs. Structural and accessory genes are shown. Gray boxes indicate structural genes: spike (S), envelope (E), membrane (M) and nucleocapsid (N). Accessory genes are represented in different colors. Their names are indicated as numbers above or below the boxes. Sequence conservation of accessory genes is indicated with the same color. The Poly A sequence (An) is represented at the 3´end of each CoV genome. Created with BioRender.com.

associated molecular patterns (PAMPs) or danger-associated molecular patterns (DAMPS) are recognized by pattern-recognition receptors (PRRs) of immune and non-immune cells, expressed in both the cell membrane (toll-like receptors or TLR) and the cytoplasm (retinoic acid associated gene-I or RIG-I; melanoma differentiation-associated gene 5 or MDA-5; and cytosolic DNA sensors or CDSs). It was described that long dsRNAs generated during CoV replication were preferentially detected by MDA5. The presence of a cap structure on CoV mRNAs (Park et al., 2022; Yan et al., 2022), similarly to eukaryotic mRNAs, protects from exonucleases and promotes mRNA translation and evasion of the host immune response. In contrast, RIG-I is activated by short uncapped dsRNAs containing 5′-PPP or 5′-PP groups, usually found in the genomes of negative-strand RNA viruses (Roth-Cross et al., 2008; Sampaio et al., 2021). Upon viral sensing, PRRs initiate signalling cascades that converge on activation and subsequent nuclear localization of different families of transcription factors, including interferon regulatory factors (IRFs) (Mogensen TH., 2018) and NF-κB, which leads to pro-inflammatory responses (Chen et al., 2018). The IFN expression pathway is induced by IFN regulatory transcription factors 3 (IRF3) and 7 (IRF7) (Mogensen TH., 2018), whose activation depends on the phosphorylation induced by IκB kinases, specifically, the TANK-binding kinase 1 (TBK1) (Moser et al., 2015), resulting in transcription of IFN-β or IFNα genes and production of the first wave of IFN-I (Figure 2). IFNs activate a signal transduction cascade when interacting with their receptors (IFNAR) in an autocrine and paracrine manner. This interaction activates the JAK/STAT pathway that phosphorylates the signal transducer and activation of transcription 1 and 2 (STAT1 and STAT2), which interact with IRF9 to form the ISGF3 complex. Binding of ISGF3 to the Interferon-Stimulated Response Element (ISRE) present in many promoters initiates the expression of hundreds of interferon-stimulated genes (ISGs), which exert antiviral activities and recruit immune cells to facilitate viral clearance (Basler and Garcia-Sastre, 2002; Schneider et al., 2014; Schoggins, 2019). The relevance of the IFN system is emphasized by the fact that most viruses have evolved different mechanisms that antagonize IFN production or signaling to enhance IFN resistance (Garcia-Sastre et al., 1998; Basler et al., 2000; Park et al., 2003; Garcia-Sastre, 2017). NF-κB, activator protein-1 (AP-1), or JAK-STAT proinflammatory pathways lead to the production of inflammatory cytokines and chemokines for the recruitment of inflammatory cells, as well as for the induction of cell death to clear infected cells (Koyama et al., 2008; Takeuchi and Akira, 2010; Diamond and Kanneganti, 2022) (Figure 3). A crosstalk between innate immune pathways, such as IFN and inflammation, is involved in the complex regulation of antiviral activity. For instance, the activation of the NF-kB pathways not only induces the expression of pro-inflammatory cytokines, but also facilitates transcription of type I IFN early after infection (Basagoudanavar et al., 2011).

Interferon antagonism by deadly HCoV accessory proteins

Highly pathogenic HCoVs have developed strategies to evade the host IFN I response (Xue et al., 2021) in order to successfully infect their hosts (Figure 2). Inhibition of IFN production by individual accessory proteins from deadly HCoVs overexpressed in cell cultures has been extensively studied. SARS-CoV ORF3a inhibited

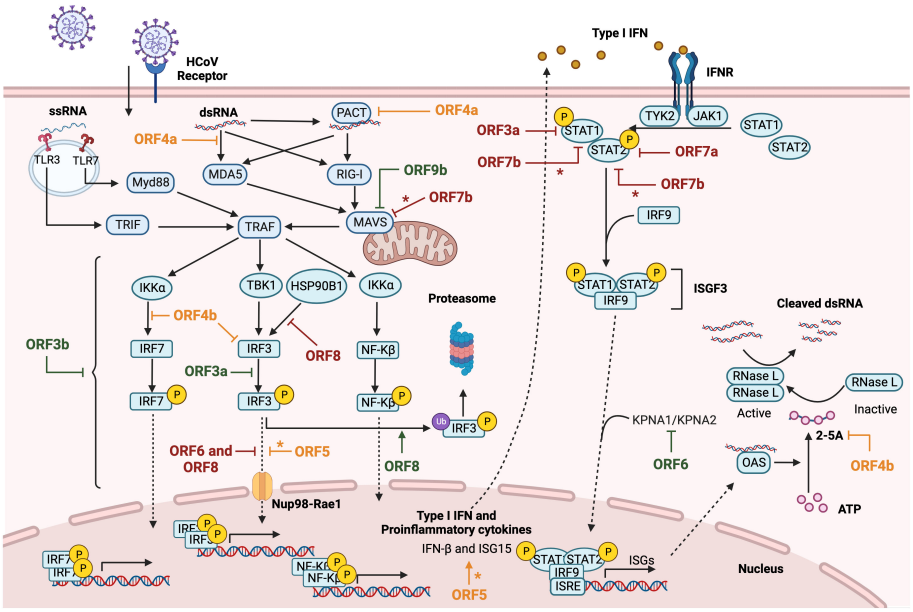

FIGURE 2
Modulation of IFN response by HCoVs accessory proteins. Diagram representing type I IFN and proinflammatory cytokines induction after cellular recognizing of HCoV RNA species by PRRs. After viral RNA sensing, MAVS-mediated nuclear transcription factor NF-Kβ and IRFs activation induce IFN and proinflammatory cytokines expression. The canonical autocrine or paracrine type I IFN signaling pathway triggers ISGs expression through ISGF3 complex activation. SARS-CoV accessory proteins are represented in green, MERS-CoV in orange and SARS-CoV-2 in red. The asterisk (*) indicates inconclusive results. Figure created with BioRender.com.

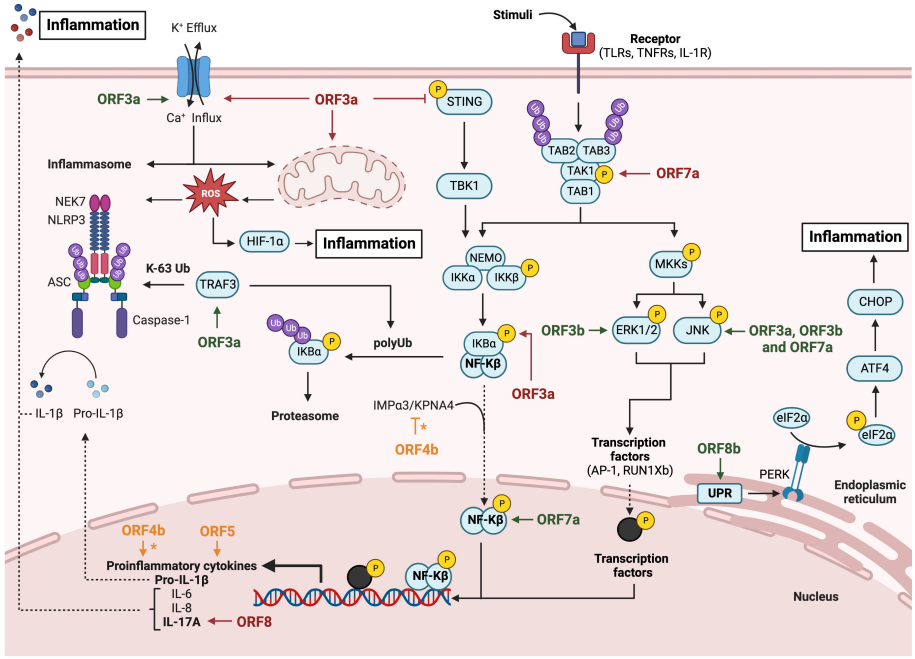

FIGURE 3
Modulation of inflammatory response pathway by HCoVs accessory proteins. Diagram representing the activation of the NLRP3 inflammasome pathway, the canonical NF-Kβ pathway and the canonical MAPKs pathway. The inflammatory inductors HIF-1α and CHOP activation are also represented via mitochondrial dysregulation and unfolded proteins response, respectively. SARS-CoV accessory proteins are represented in green, MERS-CoV in orange and SARS-CoV-2 in red. The asterisk (*) indicates inconclusive results. Figure created with BioRender.com.

phosphorylation of IRF-3 in HEK-293T, preventing the transcription of IFN-β gene (Kopecky-Bromberg et al., 2007). Other study described that overexpression of SARS-CoV ORF3b in HEK-293T cells inhibits type I IFN induction triggered by the overexpression of RIG-I or the mitochondrial antiviral signaling protein (MAVS), suggesting that 3b inhibits the IFN pathway at or downstream of the mitochondrial adaptor MAVS (Freundt et al., 2009). In addition, overexpressed SARS-CoV 8b and 8ab proteins induced degradation of IRF3 in a ubiquitin-proteasome-dependent manner, since IRF3 levels were partially restored in the presence of protease inhibitors (Wong et al., 2018). In agreement with this last result, the expression of 8b and 8ab SARS-CoV proteins by recombinant avian IBV viruses conferred a replication advantage to IBV in cells in which poly (I:C) induced the IFN response, suggesting a role for these proteins in the IFN antagonism. This effect was mediated by the down-regulation of IRF3 levels coupled to reduced IRF3 dimer formation.

SARS-CoV ORF6 regulates the IFN signaling, since infection with SARS-CoV blocks the nuclear trafficking of STAT1 in Vero cells transfected with STAT1-GFP, in contrast to deletion mutants lacking ORF6. A potential mechanism for this effect is that SARS-CoV ORF6 retains karyopherins, which are proteins involved in the transport of molecules between the cytoplasm and the nucleus, at the ER/Golgi membrane. During SARS-CoV infection, karyopherin 2 (KPNA2) in complex with KPNB1 were retained at the ER/Golgi, while KPNA2 was detected in the nucleus in SARS-CoV-Δ6 infection (Frieman et al., 2007). However, these results should be interpreted with caution because they were obtained in Vero cells, which are deficient in type I IFN production (Mosca and Pitha, 1986; Prescott et al., 2010).

Another SARS-CoV accessory protein described to inhibit MAVS is ORF9b. Overexpression of SARS-CoV 9b inhibited MAVS and reduced MAVS dependent-IRF3 phosphorylation. Moreover, it reduced in HEK-293 cells the levels of dynamin-like protein (DRP1), a host protein involved in mitochondrial fission, via a mechanism sensitive to proteasome inhibition. Lower DRP1 levels impaired the MAVS-induced IFN-β response (Shi et al., 2014).

SARS-CoV-2 infection induces in humans low levels of type I interferon (Blanco-Melo et al., 2020; Hojyo et al., 2020; Sa Ribero et al., 2020), suggesting that this CoV also encodes IFN antagonists. Similarly to SARS-CoV ORF3a, the overexpression of SARS-CoV-2 ORF3a in HEK-293T also inhibits IFN response, as expected from the high sequence conservation of 3a. In the case of SARS-CoV-2, two possible mechanisms have been suggested to inhibit the JAK/STAT signalling by ORF3, the suppression of STAT1 phosphorylation and nuclear translocation (Xia et al., 2020) or the upregulation of cytokine signalling 1 (SOCS1), a negative regulator of cytokine signalling (Wang et al., 2021). In agreement with these results, infection of human lung cells A549-hACE2 with SARS-CoV-2-Δ3a increased the expression levels of several ISGs (IFITM1, ISG56, OAS1 and PKR) as compared to the infection with the WT virus (Liu Y. et al., 2022).

The overexpression of all individual genes in HEK-293T cells transfected with an IFN-promoter reporter plasmid showed that ORF6 is the most potent IFN inhibitor of SARS-CoV-2 (Yuen et al., 2020). In this system, ORF6 directly binds the nuclear pore component Nup98-Rae1 and inhibits the nuclear translocation of activated STAT1 and IRF3 transcription factors, similarly to the

function previously proposed for ORF6 of SARS-CoV (Miorin et al., 2020). The crystal structure of SARS-CoV-2 ORF6 C-termini in complex with the Rae1–Nup98 heterodimer showed that ORF6 occupies the mRNA-binding groove, similarly to other viral proteins, indicating that this complex is a common target for different viruses to impair the nuclear mRNA export pathway (Li et al., 2021).

Using recombinant SARS-CoV mutants with the ORF6 deleted (rSARS-CoV-ΔORF6) or replaced by SARS-CoV-2 ORF6 (rSARS-$CoV_{ORF6\text{-}SARS\text{-}2}$), the IFN signaling pathway was evaluated in Vero E6 cells treated with IFN-I. Deletion of ORF6 significantly increased induction of IFN-stimulated genes *MX1* and ISG56, indicating that ORF6 was an antagonist of IFN-I signaling in the context of infection. rSARS-$CoV_{ORF6\text{-}SARS\text{-}2}$ suppressed induction of *MX1* and ISG56 to a lesser extent than the wild-type SARS-CoV, suggesting that SARS-CoV-2 ORF6 interferes less efficiently with human IFN signaling than SARS-CoV ORF6. Since both genes are homologous, differences at charged amino acids at positions 51 and 56 may be responsible for the differential phenotype (Schroeder et al., 2021).

ORF7a is a type I transmembrane protein highly conserved in SARS-CoV and SARS-CoV-2. SARS-CoV-2 ORF7a also antagonized IFN-I signaling in overexpression experiments in HEK293T and A549 cells, by blocking STAT2 phosphorylation (Xia et al., 2020; Garcia-Garcia et al., 2022). Another study showed that ubiquitination of ORF7a at residue K119 was required for IFN antagonism, as overexpression of an ubiquitination-defective ORF7a in HEK293T failed to inhibit ISG production (Cao et al., 2021). These results are in agreement with the fact that a SARS-CoV-2 isolated from patients containing a 7-nucleotide deletion (nt 301-307) in ORF7a, that truncates the C-terminal half of the protein, is deficient in antagonizing the IFN response. This isolate induced elevated type I IFN responses in HEK293T-hACE2 cells, including high levels of the toll-like receptor 7 sensor (TLR7), signal transducers (MYD88, OAS2), transcriptional regulators (IRF3, IRF5), and restriction factors (GBP1, IFITM3, MX1), as compared to infection with the WT virus (Nemudryi et al., 2021). Another function proposed for ORF7a protein is the inhibition of tetherin BST-2, a host ISG that inhibits the release of virions and limits viral spread (Taylor et al., 2015; Martin-Sancho et al., 2021).

The role of SARS-CoV-2 ORF7b in the IFN pathway is not clear yet, since discrepant results were obtained by overexpressing the protein in cell cultures. The most conclusive studies showed that overexpression of ORF7b inhibited the IFN production. In HEK 293T, the ORF7b inhibited the MAVS-induced IFN-I and IFN-III production, but not the interferon signaling (Shemesh et al., 2021). In line with this last study, overexpression of ORF7b in A549 cells did not inhibit the expression of ISGs like OASL, IFIT1 and IFIT2 (Garcia-Garcia et al., 2022). Additionally, a truncated ORF7b with a 382-nucleotide deletion (Δ382), derived from a SARS-CoV-2 natural isolate identified in Singapore and Taiwan in 2020 and associated with mild disease, lost the ability to suppress MAVS-induced type I IFN production (Shemesh et al., 2021).

SARS-CoV-2 ORF8 ectopically expressed in cell lines has been described as an antagonist of interferon production by decreasing the nuclear translocation of IRF3 (Li et al., 2020; Geng et al., 2021; Rashid et al., 2021a; Chen et al., 2022). The W45L mutation present in ORF8 of a natural isolate may help the virus to evade the immune response by increasing its binding affinity to IRF3, according to molecular docking analysis (Rashid et al., 2021b). Alternatively, the interaction of ORF8 and HSP90B1, a molecular chaperone that interacts with IRF3, observed after overexpression of ORF8 in HEK-293T cells, could explain the IFN antagonist activity. This hypothesis is supported by the observation that HSP90B1 knocking-down significantly decreased activation of IFN-I pathway by polyI:C (Chen et al., 2022). Unexpectedly, infection with rSARS-CoV-2-Δ8 of K18-hACE2 mice induced in the lungs higher levels of IFN-γ than rSARS-CoV-2-WT, although no difference in IFN-α levels was detected, indicating that ORF8 might have a limited impact on the IFN-I response *in vivo* (Silvas et al., 2021), in contrast to the results observed in overexpression experiments.

MERS-CoV-WT infection did not significantly induce either IFNβ or pro-inflammatory cytokines in Huh-7 and Calu-3 cells (Canton et al., 2018). In contrast, infection of MRC5 cells activated a potent innate immune response (Bello-Perez et al., 2022), suggesting cell type-specific differences in the IFN response. Interestingly, infection of knock-in mice expressing the human virus receptor (KI-hDPP4) induced moderate IFN-β levels. Therefore, deletion of accessory genes from the MERS-CoV genome is expected to have different effects on the host response depending on the experimental system.

MERS-CoV accessory genes 3, 4a, 4b and 5 are highly divergent in sequence to SARS-CoV accessory genes. MERS-CoV 4a protein includes a dsRNA binding domain (DRBD) highly conserved in host proteins such as protein kinase R (PKR) or the protein activator of PKR (PACT) (Siu et al., 2014). Stress granules (SGs) are dynamic cytoplasmic condensates of RNAs and proteins including mRNAs associated with stalled ribosome complexes and other RNA-binding proteins. SGs are proposed to contribute to the post-transcriptional regulation of gene expression under stress conditions and to exert specific antiviral functions, by providing a platform for interactions of proteins from innate immune signaling pathways (Wen et al., 2014). Activation of PERK/PKR either by ER-stress or dsRNA leads to eIF-2α phosphorylation and translation inhibition, which ultimately promotes SG formation (Shi et al., 2022). PKR is an IFN stimulated gene, while SGs are proposed to serve to the regulation of innate immune responses, thus illustrating the complex interplay of antiviral signaling pathways.

The overexpression of ORF4a in HeLa cells inhibited PKR activation, thus preventing stress granule formation (Rabouw et al., 2016). Accordingly, a recombinant MERS-CoV-Δ4ab lacking ORF4a and 4b induced SG formation in susceptible HeLa-hDPP4 cells, but not in Vero cells (Nakagawa et al., 2018), which are defective for IFN production, suggesting a relation between SGs and IFN response. In fact, ORF4a overexpression in HEK293T cells suggested a role in the antagonist of IFN (Niemeyer et al., 2013; Siu et al., 2014; Rabouw et al., 2016) by two possible mechanisms. ORF4a may inhibit the MDA5-induced IFN response by directly interacting with viral dsRNA via the ORF4a dsRNA binding domain (DRBD) (Niemeyer et al., 2013). A second model

proposes that ORF4a interacts with PACT in an RNA-dependent manner inhibiting PACT-induced activation of RIG-I and MDA5. MERS-CoV 4a protein might inhibit PACT, RIG-I and MDA5 by competing for dsRNA binding (Siu et al., 2014).

In the context of infection, ORF4a antagonizes IFN production and signaling, as $A549^{DPP4}$ cells infected with a recombinant MERS-CoV-Δ4a showed increased mRNA expression levels of interferon lambda (IFNL1) and ISGs OAS2 and IFIT1 (Comar et al., 2019; Comar et al., 2022). Unexpectedly, the specific deletion of ORF4a from MERS-CoV genome did not result in robust activation of either PKR and SG formation (Rabouw et al., 2016) or the IFN and oligoadenylate synthetase/ribonuclease L (OAS-RNase L) pathways, as compared to WT virus (Comar et al., 2019; Comar et al., 2022). These results suggest that other viral proteins present in MERS-CoV-Δ4a are inhibiting the host antiviral response during infection.

MERS-CoV 4b protein includes a nuclear localization signal and a phosphodiesterase (PDE) domain (Thornbrough et al., 2016; Canton et al., 2018). In Huh-7 and Calu-3 cells, deletion of ORF4b from the viral genome increased the induction of IFN- β. In contrast, in MRC-5 cells and in susceptible mice, 4b deletion reduced the IFN-β response and attenuated the virus (Canton et al., 2018; Bello-Perez et al., 2022). These differences underline the need to find alternative, more physiological experimental systems to study the host response induced by MERS-CoV. Differences in cell lines and times post infection, which may also be related to differences in viral titers, in the different studies might justify the diverse contribution of 4b protein to the innate immune response in mice and cell cultures.

MERS-CoV 4b protein phosphodiesterase activity antagonizes the OAS-RNase L pathway (Thornbrough et al., 2016) by degrading 2',5'-oligoadenylates (2-5A) required to activate RNase L, an antiviral system that cleaves viral and host single-stranded RNA and contributes to the control of replication and early spread of viruses (Choi et al., 2015). Infection of Calu-3 cells with the recombinant virus MERS-CoV-Δ4b did not completely restored rRNA degradation by RNase L, suggesting that MERS-CoV may include additional mechanisms of RNase L antagonism (Thornbrough et al., 2016). In agreement with these results, individual deletion of ORF4a and ORF4b had minor effects on RNaseL activity in $A549^{DPP4}$ cells (Comar et al., 2022). However, infection with double mutant viruses with an inactivated endoribonuclease (EndoU) along with deletion of ORF4a or inactivation of ORF4b PDE domain strongly inactivated dsRNA-induced innate immune pathways (Comar et al., 2022). Deletion of ORF4b in MERS-CoV reduced the IFN response in MRC5 lung cells and also in hDPP4-KI mice (Bello-Perez et al., 2022) at 4 and 6 dpi, as compared to the WT virus, suggesting that ORF4b was not an IFN antagonist at these time points. Since the IFN response in CoV infection varies with time, it cannot be excluded that ORF4b antagonizes IFN-β production at earlier times post infection (Bello-Perez et al., 2022).

MERS-CoV gene 5 is highly conserved in viruses isolated from humans and camels. However, virus adaptation to cell culture or mouse lungs led to mutations and deletions that prevented full-length protein expression, leading to a truncated protein that contains a 17-nucleotide (nt) deletion and a stop codon at position 108 (Gutierrez-Alvarez et al., 2021). There are controversial results published about the role of the ORF5 in the IFN system. ORF5 antagonized interferon in over-expression experiments in 293T cells and inhibited the nuclear translocation of the interferon transcription factor IRF-3. In line with these results, in cells infected with Sendai virus, a potent inducer of IFN, the overexpression of ORF5 led to the accumulation of IRF3 in the cytoplasm (Yang et al., 2013). In contrast, the deletion of ORF5 from MERS-CoV (rMERS-CoV-Δ5) led to a decreased IFN response both in hDPP4-KI mice lungs and in MRC-5 cells, as the mRNA levels of IFN-β and ISG15 were significantly reduced as compared to the parental rMERS-CoV virus expressing the truncated protein (Gutierrez-Alvarez et al., 2021). In addition, another study suggested no specific role of ORF5 in the IFN antagonism, since the replacement of ORF5 by a fluorescent gene failed to induce in Calu 3 cells robust type I and III IFN responses, at different times post-infection (Menachery et al., 2017). Differences among studies regarding the relevance of gene 5 to the IFN response highlight the importance of using physiological experimental systems that recapitulate the complexity of virus-host interactions in the context of viral infection at the organism level.

A relationship between interferon antagonism and viral pathogenesis has been established (Thornbrough et al., 2016). Viruses may inhibit the induction of the IFN response by blocking the IFN signaling, or by interfering with the antiviral activities induced by IFN. In highly pathogenic coronaviruses SARS-CoV and MERS-CoV, a late or prolonged IFN-β response increase virulence and decrease survival, while early IFN-ß production was associated with protection (Channappanavar et al., 2019).

Interference of deadly HCoV accessory proteins with the inflammatory response

Highly pathogenic human CoVs induce exacerbated inflammatory processes, which are a main determinant of pathogenesis (Lowery et al., 2021). A limited and delayed IFN-I and IFN-III response results in exacerbated proinflammatory cytokine production and in extensive cellular infiltrates in the respiratory tract, resulting in lung pathology. High levels of inflammatory markers, such as increased neutrophil-lymphocyte blood ratio or cytokine-chemokine serum levels have been associated with higher risk of severe disease in SARS-CoV-2 infections (Hu et al., 2021). It is known that SARS-CoV, MERS-CoV and SARS-CoV-2 infections dysregulate inflammation leading to cytokine storm and acute respiratory distress syndrome (ARDS), which are described as hyperinflammatory pathologies (Chien et al., 2006; Kim et al., 2016; Liu T. et al., 2021). Among HCoVs genes, accessory genes have been proposed to interfere with the innate immune response and particularly, with the inflammatory pathway (Figure 3).

Several SARS-CoV accessory proteins interfere with inflammatory processes. ORF3a and 8a are viroporins, viral transmembrane proteins with ion channel activity. ORF3a has

permeability to calcium, potassium and sodium ions, which has effects on cellular homeostasis. Additionally, protein 3a has a PDZ-binding motif (PBM), which can potentially participate in protein-protein interactions with over 400 cellular proteins that contain PDZ domains. SARS-CoV 3a protein was required for efficient SARS-CoV replication and virulence in mice, whereas viroporin 8a had only a minor impact on these activities (Castano-Rodriguez et al., 2018). A recombinant mouse adapted SARS-CoV-Δ3a-MA30 was attenuated in BALC/c mice, indicating that ORF3a was a virulence factor. However, individual mutants of ORF3a ion channel or PBM domains were not attenuated, suggesting that, separately, these activities did not play a key role in pathogenesis (Castano-Rodriguez et al., 2018).

In HeLa cells overexpressing SARS-CoV ORF3a, NLRP3 inflammasome was activated in an ion channel-activity dependent manner, leading to IL-1β secretion. Dysregulation of potassium flux by protein 3a, which alters cell homeostasis, and the production of reactive oxygen species from damaged mitochondria were required for NLRP3 activation (Chen et al., 2019). Another mechanism that may contribute to NLRP3 inflammasome activation is the canonical NF-kB signaling pathway. HEK293T and A549 cells overexpressing ORF3a showed activation of NF-κB and JNK1, which led to increased expression of IL-8 and RANTES (Kanzawa et al., 2006). Activation of the canonical NF-κB signalling pathway involves the participation of TNF receptor-associated factor 3 (TRAF3) in the degradation of the IkBα inhibitor and the processing of NF-kB p105 into p50, which promotes IL-1β transcription. ORF3a has been described to bind the inflammasome adapter protein ASC promoting its polyubiquitination, a critical step required for NLRP3 inflammasome activation (Siu et al., 2019). In line with the overexpression results, deletion of 3a gene from the viral genome (SARS-CoV-Δ3a) confirmed that ORF3a is necessary for NLRP3 inflammasome activation and IL-1β production, although this effect was independent of the ion-channel activity (Siu et al., 2019).

Another SARS-CoV accessory protein related to the activation of inflammatory pathways is ORF3b. Overexpression of ORF3b in Huh7 cells led to the activation of two MAPKs, JNK and ERK, which increased the activity of the transcription factor AP-1, leading to enhanced expression of proinflammatory mediators like the monocyte chemoattractant protein-1 (MCP-1 also known as CCL2) (Varshney and Lal, 2011). A more extensive analysis of interactions of overexpressed ORF3b with host factors in Huh7 cells, using yeast two-hybrid and co-immunoprecipitation techniques, identified the transcription factor RUNX1b as a partner of 3b. Physical interaction between ORF3b and RUNX1b increased its transactivation potential via ERK phosphorylation, leading to enhanced transcription of the macrophage inflammatory protein MIP-1α and the proinflammatory cytokine IL2 (Varshney et al., 2012). Monocyte cells are abortively infected by SARS-CoV. However, it is speculated that the expression of 3b protein from the viral genome in infected monocytic cells might induce inflammatory responses and contribute to SARS-CoV pathogenesis.

SARS-CoV ORF7a is also described as a proinflammatory accessory protein by enhancing NF-κB as well as JNK1 phosphorylation levels, which led to increased levels of proinflammatory cytokines IL-8 and RANTES in A549 cells overexpressing ORF7a (Kanzawa et al., 2006). In addition, SARS-CoV ORF8b has been described in overexpression systems as an insoluble accessory protein. Intracellular aggregates of ORF8b induced both endoplasmic reticulum and lysosomal stress leading to the accumulation and activation of the transcription factors CHOP and TFEB, both related to proinflammatory responses. This study also demonstrated that ORF8b activates NLRP3 inflammasome in macrophages and monocytes (Shi et al., 2019).

SARS-CoV-2 accessory proteins are also related to proinflammatory processes. As described for SARS-CoV, the highly conserved SARS-CoV-2 ORF3a activates the NLRP3 inflammasome (Xu et al., 2022). Overexpression of ORF3a in A549 cells induced potassium efflux, via ORF3a ion channel activity, which triggers the interaction of NLRP3 (Figure 3) with the activator kinase NEK7, leading to the recruitment of the inflammasome adapter protein ASC and pro-caspase 1 into the active inflammasome. In addition, ORF3a increased IL1-β levels due to NF-κB induction via IκBα phosphorylation (Xu et al., 2022). Another study related ORF3a overexpression in HEK293T cells to the inhibition of the proinflammatory response by preventing cGAS-STING immune activation (Rui et al., 2021). This inhibition may be due to the direct interaction between ORF3a and STING, as suggested by colocalization and coimmunoprecipitation studies. In fact, it was shown that ORF3a inhibited NF-κB induction by cGAS-STING antagonism (Rui et al., 2021). Furthermore, ORF3a overexpressed in HEK293T and Hela cells increased the levels of the transcription factor HIF-1α, by inducing mitochondrial damage and mitochondrial reactive oxygen species (Mito-ROS) signalling, ultimately promoting transcription of pro-inflammatory cytokines IL-6, and IL-1β (Tian et al., 2021).

SARS-CoV-2 ORF7a overexpressed in HeLa and A549 cells activated the NF-κB-dependent proinflammatory response, as it was previously described for SARS-CoV ORF7a (Su CM. et al., 2021) (Figure 3). Similar results were reported in HEK293T cells, leading to IL8 and IP-10 production. This study suggested that ORF7a induces the NF-κB pathway by binding and activating the ubiquitin-dependent kinase TAK1. ORF7a polyubiquitination, mediated by the E3 ubiquitin ligase RNF121, was required for NF-κB pathway activation. Polyubiquitinated ORF7a may need the K63-linked polyubiquitin binding activity of TAK1 binding proteins TAB2 and TAB3 to activate TAK1, which leads to NF-κB activation. In addition, binding of the NF-kB modulator NEMO to polyubiquitin was also needed for this activation (Nishitsuji et al., 2022).

The sequence identity between SARS-CoV and SARS-CoV-2 ORF8 is low (~26%) (Takatsuka et al., 2022), suggesting different roles in the immune response pathways. SARS-CoV-2 ORF8 acts as an IL17a mimetic by interacting with its receptor IL17RA, thereby activating this pathway (Lin et al., 2021; Wu et al., 2022). ORF8 overexpressed in HEK293T cells interacted with IL17a receptor (IL17RA and IL17RC), inducing a proinflammatory response. ORF8 amino acids Y42, E106, E171 and E176 played a critical role in this interaction (Wu et al., 2022). In another paper, adenoviruses expressing ORF8 rescued the IL17A phenotype in IL17A-deficient mice, suggesting that ORF8 mimics the pro-inflammatory function of IL17A (Lin et al., 2021).

The role of MERS-CoV accessory proteins on inflammatory pathways is cell type-dependent. MERS-CoV ORF4b has been related to NF-κB inhibition, thus reducing inflammatory responses in cells (Matthews et al., 2014; Munasinghe et al., 2022). One study in which ORF4b was overexpressed in HEK293T cells treated with TNF-α, showed a modest (two-fold) reduction in expression of genes regulated by NF-κB transcription factor (Matthews et al., 2014). Another study (Munasinghe et al., 2022) also described that ORF4b overexpression inhibited the NF-κB pathway by binding the host nuclear import protein IMPα3 (also known as karyopherin-α4), via the 4b nuclear localization sequence (NLS), which inhibited NF-κB nuclear translocation. Computational analysis showed the potential of ORF4b to competitively inhibit IMPα3 by binding the major NLS site of IMPα3, which is necessary for NF-KB p50 nuclear import (Munasinghe et al., 2022). The role of 4b protein in the pro-inflammatory response has also been demonstrated in the context of infection. Recombinant viruses, MERS-CoV-Δ4b and MERS-CoV-mNLS, in which the 4b gene was either deleted or its NLS inactivated by mutation, respectively, induced higher levels of NF-κB-dependent pro-inflammatory cytokines IL6, IL8 or TNF-α in Huh7 and Calu-3 cells, as compared to the rSARS-CoV-WT. This result indicated that 4b protein inhibits the inflammatory response during infection and its nuclear localization is necessary for NF-κB inhibition. The study described the interaction between ORF4b and karyopherin-α4 (KPNA4) in an NLS-dependent manner. KPNA4 is known to translocate the NF-κB protein complex from the cytoplasm into the nucleus. Binding of 4b to KPNA4 during infection inhibited its interaction with NF-κB-p65 subunit. Thereby, a model where 4b outcompetes NF-κB for KPNA4 binding and translocation into the nucleus was proposed as a mechanism of interference with the NF-κB-mediated response (Canton et al., 2018). *In vivo* experiments in the hDPP4-KI mouse model, using mouse-adapted recombinant viruses with identical ORF4b mutations, showed that 4b protein is a virulence factor, since MERS-CoV-Δ4b is completely attenuated, in contrast to MERS-CoV-WT, which causes 100% mortality. However, deletion of 4b significantly reduced the expression of pro-inflammatory cytokines and chemokines and the accumulation of cell infiltrates in the lungs of mice 3 and 6 dpi (Bello-Perez et al., 2022). The apparent discrepancy between the results of 4b protein during infection of cell lines or hDPP4-KI mice might be explained by the timing of the innate immune response. In cell lines, deletion of 4b increased the pro-inflammatory response at 24 hpi, while the reduced inflammation *in vivo* was detected at 3 and 6 dpi. Further studies would be required to confirm whether 4b deletion promoted *in vivo* an inflammatory response at earlier times with protective effects.

MERS-CoV ORF5 also dysregulates the inflammatory response. A recombinant mouse adapted MERS-CoV virus lacking ORF5 (rMERS-Δ5-MA15) induced delayed and dysregulated levels of proinflammatory cytokines in hDPP4-KI mice at 4 dpi. Similarly, lower levels of proinflammatory mediators were induced in MRC-5 cells at 18-24 hpi. This result suggests a role of ORF5 in inflammatory modulation. Interestingly, rMERS-Δ5-MA15 was more virulent in mice than WT, indicating a role of gene 5 in pathogenesis (Gutierrez-Alvarez et al., 2021).

Apoptosis

Apoptosis is a programmed cell death characterized by cell cycle arrest and controlled phagocytosis of cellular components, previously released following cell fragmentation in vesicles known as apoptotic bodies (Xu et al., 2019). The induction of this pathway is dependent on the activation of caspases (Figure 4), which are cysteine-aspartic proteases. Initiator caspases (caspases 8 and 9) are activated by proapoptotic proteins and induce effector caspases (caspases 3, 6 and 7), which initiate the apoptosis pathway. Once initiated, apoptotic cell DNA is fragmented by nucleases, while nuclear and cytoskeleton proteins are degraded and cellular components are cleared by phagocytic cells. Apoptosis is induced by two different pathways. The intrinsic pathway is modulated by the B cell lymphoma 2 (Bcl2) family of proteins. These proteins control the mitochondrial outer membrane permeability (MOMP), either by increasing permeability by proapoptotic factors like BAX and BAK, or by decreasing it by antiapoptotic factors like Bcl2, Bcl-xL and Mcl-1. MOMP increases the release of cytochrome C from the mitochondria to the cytoplasm, which activates the initiator caspase 9 and finally, the effector caspase 3. The extrinsic pathway is modulated by the binding of death ligands, like FasL or TNF-α, to death receptors present on the cell surface. This pathway activates the initiator caspase 8, which can both induce the effector caspases or coactivate the intrinsic pathway by the activation of proapoptotic Bid protein (Elmore, 2007).

Premature cell death induced by apoptosis is a potent antiviral pathway to limit viral spread (Shen and Shenk, 1995). Alternatively, some viruses induce an uncontrolled apoptosis that increases pathogenesis. This is the case of deadly HCoVs, which have been related to apoptosis induction (Yan et al., 2004; Yeung et al., 2016; Liu Y. et al., 2021). Although little information is available in the context of infection, apoptosis activation (Figure 4) may contribute to pathogenesis.

Among SARS-CoV accessory proteins, ORF3a has been proposed as an apoptosis inductor (Law et al., 2005; Padhan et al., 2008; Chan et al., 2009; Minakshi et al., 2009; Freundt et al., 2010). Despite the mechanism remains unclear, overexpression of ORF3a in Vero E6 cells activated the extrinsic pathway through caspase-8 activation (Law et al., 2005). In addition, overexpressed ORF3a induced the intrinsic pathway via activation of both caspase-8 and caspase-9 in Huh7 (Padhan et al., 2008) and Vero E6 cells (Chan et al., 2009). ORF3a C133S mutation, which disrupts ORF3a homo-dimer/-tetramer formation, and subsequently its ion channel activity, resulted in the loss of apoptosis induction, suggesting that ORF3a ion channel activity is the main contributor to its activity (Chan et al., 2009). ORF3a probably also activates apoptosis via the unfolded protein response (UPR) pathway (Minakshi et al., 2009). Huh7 cells overexpressing ORF3a activated PERK-eIF2α pathway, which induced translation of the activating transcription factor 4 (ATF4) that subsequently

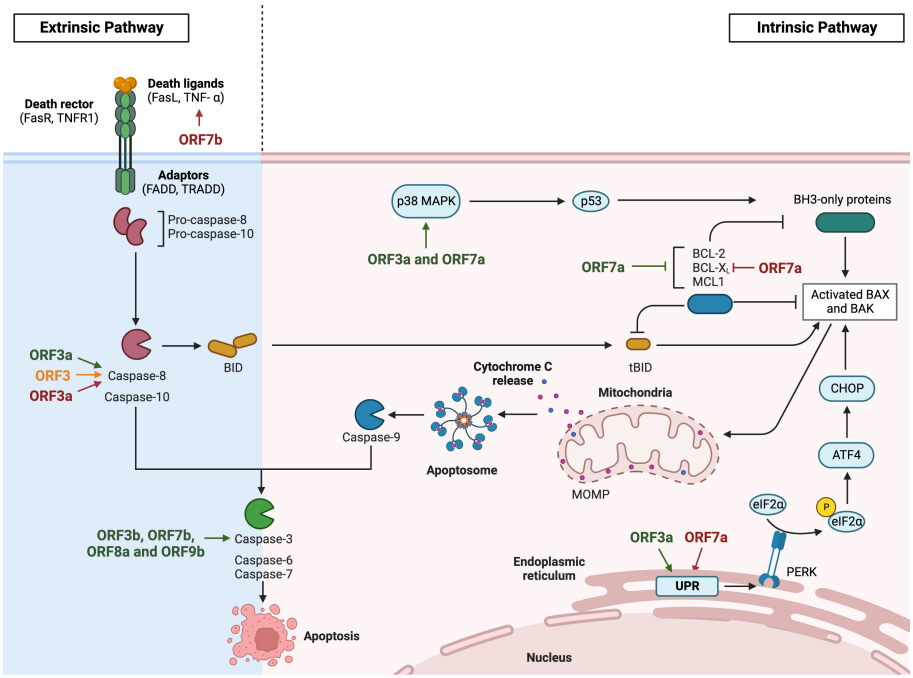

FIGURE 4
Modulation of apoptosis by HCoVs accessory proteins. Diagram representing the extrinsic and the intrinsic apoptosis pathway via death ligand recognition or viral induction respectively. The apoptosis inductor CHOP activation is represented via unfolded protein response. SARS-CoV accessory proteins are represented in green, MERS-CoV in orange and SARS-CoV-2 in red. Images created with BioRender.com.

promoted transcription of the C/EBP homologous protein (CHOP) (Figure 4). CHOP upregulated the transcription of BAK and BAX, which oligomerize and release apoptotic factors, such as cytochrome c and apoptosis-inducing factor (AIF), through mitochondria permeabilization, eventually causing cell death (Minakshi et al., 2009). According to overexpression results, Vero E6 cells infected with SARS-CoV-Δ3a showed lower cell death levels than WT infection, suggesting an implication of ORF3a in cell death pathways (Freundt et al., 2010).

The overexpression of SARS-CoV 7a, but not 3a or the viral structural proteins, N, M, and E, induced apoptosis via a caspase-dependent pathway in cell lines derived from different organs, including lung, kidney, and liver. These results indicate that apoptosis activation by overexpressed viral proteins could be cell type dependent (Tan et al., 2004). In addition, ORF7a overexpressed in HEK293T cells inhibited protein synthesis by inducing a stress response that activated the p38 MAPK pathway, which in turn, could induce the apoptosis pathway (Kopecky-Bromberg et al., 2006). In this line, a physical interaction between ORF7a and several prosurvival Bcl-2 family proteins like Bcl-xL, Bcl-2, Bcl-w, A1 and Mcl-1 was shown by coimmunoprecipitation in Vero E6 infected cells. ORF7a transmembrane domain was proposed as the major contributor to this interaction. This interaction with antiapoptotic, but not with proapoptotic proteins, may lead to apoptosis induction (Tan et al., 2007). Another possible mechanism for apoptosis activation by ORF7a is related to the interaction of 7a with Ap_4A-hydrolase, which plays a role in maintaining cell homeostasis by cleaving diadenosine tetraphosphate (Ap_4A) back into ATP and AMP. It was suggested that ORF7a may be downregulating Ap_4A-hydrolase activity, leading to increased Ap_4A levels (Vartanian et al., 2003), which have been previously related to apoptosis induction (Vasilenko et al., 2010). In contrast, one study in the context of infection showed similar apoptosis levels in Vero E6 cells infected with rSARS-CoV-ΔORF7ab or the WT virus. Therefore, despite overexpression of ORF7a or ORF7b in Vero E6 cells increased caspase-3 activation, these proteins did not significantly contributed to apoptosis in the context of infection, which would be induced by other viral proteins (Schaecher et al., 2007). This discrepancy may be due to an artifact related to overexpression. It is known that overexpression of proteins induces endoplasmic reticulum stress, leading to apoptosis indirectly (Szegezdi et al., 2006). Although the mechanisms were not explored, there are some papers relating caspase-3 activation with the presence of overexpressed SARS-CoV accessory proteins like ORF3b (Yuan et al., 2005; Khan et al., 2006), ORF8a (Chen et al., 2007) or ORF9b accumulation in the nucleus (Sharma et al., 2011).

Apoptosis induction has also been described in SARS-CoV-2 infections (Liu Y. et al., 2021), as observed in postmortem lung sections from COVID-19 patients and in lung tissues from a non-human primate model of SARS-CoV-2 infection. As previously reported for SARS-CoV, accessory proteins have been associated with apoptosis activation. Similar to SARS-CoV ORF3a, overexpression studies suggested SARS-CoV-2 ORF3a as a proapoptotic protein via the extrinsic pathway, by activating caspase-8, which led to Bid cleavage, cytochrome c release and ultimately, the activation of the intrinsic pathway. ORF3a C130/133S or Y160A mutants failed to induce significant apoptosis levels,

suggesting the relevance of the transmembrane domain in this function (Ren et al., 2020). In addition, overexpressed ORF7a induced apoptosis in HEK293T cells, by interacting with Bcl-xL, which was retained in the endoplasmic reticulum inhibiting its antiapoptotic activity (Liu Z. et al., 2022). This interaction was dependent on ORF7a C-terminal positively charged Lys117 and Lys119 residues, present in the extracellular domain (Liu Z. et al., 2022). The endoplasmic reticulum accumulation of ORF7a induced ER stress via PERK-eIF2α pathway, which upregulated the transcription factor CHOP, leading to the activation of the intrinsic pathway of apoptosis via BAK/BAX induction and cytochrome c release (Liu Z. et al., 2022). Finally, SARS-CoV-2 ORF7b overexpressed in Vero E6 and HEK293T cells was also related to apoptosis activation via the extrinsic pathway. An increase in TNF-α, which binds type I TNF receptor (TNFR1) and promote caspase-8 activation was described (Yang et al., 2021).

ORF3 is the only accessory protein of MERS-CoV that is related to apoptosis induction. Apoptosis analysis in HEK293T, BEASB2, Calu-3 and A549 cells overexpressing ORF3 demonstrated that ORF3 activates caspase-8 and caspase-3, but not BAX or Bcl-2 proteins, suggesting an effect in the apoptosis extrinsic pathway. It has been described that ORF3 was degraded via the ubiquitin-proteasome system, which limits the apoptosis induction. This polyubiquitination was performed by HUWE1, an E3 ligase that physically interacted with ORF3, thus preventing an exacerbated apoptosis activation (Zhou et al., 2022).

Regulation of antigen presentation

Viruses present a variety of mechanisms to evade the host immune system. One of them is the expression of proteins with immunoglobulin-like (Ig-like) domains that may interfere with multiple functions, including antigen presentation, cell-cell recognition and signal transduction in the immune system (Gewurz et al., 2001; Fu et al., 2011). SARS-CoV-2 ORF8 contains an Ig-like domain, suggesting its role in mediating macromolecular interactions in immune responses (Chen et al., 2021). Cytotoxic T lymphocytes (CTL) recognition of infected cells is crucial for viral clearance. Higher levels of the cytokines induced by T cells (IFN-γ, TNF-α, IL-2, and IL-5) were detected in patients infected with the attenuated isolate SARS-CoV-2-Δ382, in which a 382 nt deletion truncates 7b and abolishes ORF8 expression, suggesting improved T cell recognition of infected cells in the absence of ORF8 (Young et al., 2020). SARS-CoV-2 infection led to MHC-I downregulation in infected hACE2-HEK293T cell, similarly to overexpressing of ORF8 in the absence of infection (Zhang et al., 2021a; Matsuoka et al., 2022). In these cells, the interaction of ORF8 with MHC-I and LC3-labeled autophagosomes was confirmed by co-localization and co-immunoprecipitation experiments (Zhang et al., 2021a). Inhibition of autophagy significantly restored the MHC-I surface expression, suggesting that downregulation of MHC-I by ORF8 involves the autophagy pathway (Zhang et al., 2021a). Lower expression of MHC-I can result in impairment of CTL-mediated lysis of SARS-CoV-2–infected cells, therefore reducing the antiviral cytotoxic immune response of the host, which may increase virus virulence. In fact, ORF8 protects target cells from CTL lysis, as SARS-CoV-2-specific CD8+ T cells isolated from recovered patients eliminated ORF8-expressing target cells with lower efficiency than control cells (Zhang et al., 2021a). ORF8 of SARS-CoV-2 delta variant includes deletions of Asp119 and Phe120 amino acids, which result in structural instability of ORF8 dimers. Docking analysis revealed reduced interaction of mutant ORF8 with MHC-I, as compared to the WT ORF8, suggesting that delta variant might not be able to bind efficiently the MHC-I complex, thus limiting MHC-I degradation via autophagy, which might result in a better immune response against this SARS-CoV-2 variant. In addition to ORF8, the overexpression of SARS-CoV-2 ORF7a in HEK-293 T cells reduced 5-fold the MHC-I levels on the cell surface. However, this down-regulation was largely maintained in cells infected with a recombinant SARS-CoV-2 in which the ORF7 was replaced by a reporter gene (Zhang F. et al., 2022), suggesting additional mechanisms of MHC-I downregulation, possibly by ORF8. SARS-CoV-2 ORF8 has also been proposed to modulate the recognition of viral antigens via antigen presenting monocytes, as immune cell-binding assays showed a stronger interaction of ORF8 with monocytes than with other immune cells (Chen et al., 2021).

Histone mimic

CoVs use a variety of mechanisms to interfere with multiple host cell functions. One strategy is the interference with the epigenetic regulation of gene expression mediated by histone modification. SARS-CoV-2 ORF8 mimics the ARKS sequence present in histone H3, which is the most critical regulatory region for post-translational modifications (PTMs) (Kee et al., 2022). SARS-CoV-2 infection of A549 cells increased the levels of methylated histones H3K9me3 and H3K27me3 as compared with mock-infected cells (Kee et al., 2022). The complete deletion of ORF8, or just the ARKSAP motif, attenuated this effect, indicating that this motif was involved in histone modifications (Kee et al., 2022). In addition, infections with SARS-CoV-2-ΔORF8 or SARS-CoV-2-ΔARKSAP did not reduce the expression of the acetyltransferase histone KAT2A levels as in SARS-CoV-2-WT infection (Kee et al., 2022). The histone mimic function of ORF8 was also confirmed in post-mortem lung tissue samples from COVID19 patients, as infected cells showed stronger staining of methylated histone H3K9me3 than neighbouring cells or control tissues (Kee et al., 2022). The histone mimic function could contribute to the milder disease observed in patients infected with the SARS-CoV-2 isolate including a the ORF8 382-nt deletion. Remodeling of chromatin induced by acute viral infections can disrupt epigenetic regulation of gene expression with multiple effects on cellular processes, including the immune response (Kee et al., 2022). However, the implications of these chromatin modifications either in acute infection or in post-acute sequelae of SARS-CoV-2 are not well understood yet.

Autophagy regulation

Autophagy is an intracellular catabolic transport route highly conserved among all eukaryotic cells. Among its many functions, this

pathway plays a role in the defence against viruses. Autophagy sequesters viruses into double-membrane vesicles (autophagosomes) that subsequently fuse with lysosomes, forming the autolysosome, where viruses are degraded under acidic conditions (de Haan and Reggiori, 2008; Jackson, 2015; Choi et al., 2018; Bello-Perez et al., 2020). This process is orchestrated by Beclin 1, a scaffolding protein that regulates the lipid kinase Vps34 and interacts with ultraviolet irradiation resistance-associated gene (UVRAG) or the autophagy related gene 14 (Atg14) to form the PI3K3-C1 complex (Beclin 1-Vps34- Atg14) or PI3K3-C2 complex (Beclin1-Vsp34-UVRAG), which promote autophagosome formation or maturation, respectively (Qu et al., 2021). On the other hand, the autolysosome formation depends on the interaction between a specific SNARE (soluble N-ethylmaleimide-sensitive factor attachment protein receptor) called Syntaxin 17 (STX17) with the homotypic fusion and protein sorting (HOPS) complex (Jiang et al., 2014). The autophagy flux is measured by analyzing two markers: the conversion of microtubule-associated protein light chain 3 (LC3) to lipidated LC3-II, which correlates with the autophagosome formation, and the turnover of the autophagy substrate p62 (also known as SQSTM1). While the increase in LC3-II may reflect either increased autophagosome formation or accumulation due to decreased autolysosome degradation, p62 decrease indicates that autophagy is induced (Klionsky et al., 2021). Although many viruses inhibit autophagy to prevent their own degradation, others use this pathway to complete their morphogenesis. For this reason, autophagy could have either anti-viral or pro-viral effects (Prentice et al., 2004; Krejbich-Trotot et al., 2011; Tian et al., 2011).

Viral proteins, including accessory proteins, exploit different mechanisms to inhibit autophagy by blocking the progression of autophagosomes into autolysosomes. The incomplete autophagy induced by SARS-CoV-2 in infected HeLa-hACE2 and Vero E6 cells has been associated with ORF3a, because ORF3a overexpression inhibited the fusion between autophagosomes and lysosomes in multiple cell lines as HEK-293T (Hayn et al., 2021; Miao et al., 2021), A549 and HeLa-hACE2 (Zhang et al., 2021b). ORF3a directly sequesters the mediator of autophagy Vps39 on late endosomes and prevents its interaction with STX17, a membrane protein of autophagosomes that controls fusion with lysosomes, thereby blocking the autolysosome formation (Miao et al., 2021; Zhang et al., 2021b). In addition, ORF3a binds UVRAG, significantly reducing the interaction between autophagy factors UVRAG and Beclin 1, which may disrupt the formation of the PI3KC3-C2 complex involved in autophagosome maturation (Qu et al., 2021).

The overexpression of ORF7a causes the accumulation of autophagosomes in different cell lines, HEK-293T, Hela, Caco2 and Vero E6 (Koepke et al., 2021; Hou et al., 2022), as a consequence of the reduced acidity of lysosomes, which inhibited the autophagosomal degradation and prevented the autophagy flux (Koepke et al., 2021). Knock-down of ORF7a sgmRNA translation with specific short-hairpin RNAs (shRNAs) during infection decreased autophagy levels (Hou et al., 2022). Together, these results suggest that ORF7a initiates autophagy, but also limits the progression of the autophagy flux by activating caspase 3, which cleaves the SNAP29 membrane protein required for the fusion of autophagosomes and lysosomes (Hou et al., 2022). Consequently, ORF7a promotes viral replication by inhibiting autophagy progression.

Autophagy regulation was also shown to contribute to the virulence of CoVs. One study described that MERS-CoV 4b protein was a virulence factor, since deletion of 4b from the viral genome completely attenuated the virus in hDPP4-KI mice, without significant changes in the viral titers between WT and Δ4b virus in the lungs of mice. 4b protein inhibited autophagy both *in vivo*, in hDPP4-KI mice, and in the MRC5 human lung cell line (Bello-Perez et al., 2022). Additionally, deletion of 4b induced a significantly lower inflammatory response in the lungs of mice and in MRC5 cells, suggesting a link between autophagy and inflammation, with consequences in virus virulence (Bello-Perez et al., 2022). In fact, inhibition of autophagy increased the expression levels of pro-inflammatory cytokines in MERS-CoV infected cells (Bello-Perez et al., 2022). Autophagy has important effects on the induction and modulation of inflammatory processes. The cross-talk between inflammation and autophagy is an emerging field with implications for understanding viral pathogenesis and to identify potential antiviral targets (Netea-Maier et al., 2016). In another paper, MERS-CoV 4b and 5 proteins were shown to inhibit autophagy in Vero cells in the context of infection, using recombinant viruses in which either ORF4b or ORF5 had been deleted (Gassen et al., 2019). Inhibition of autophagy by 4b and 5 proteins was related with increased viral growth, suggesting that autophagy activation might also have an antiviral effect in MERS-CoV infection of Vero cells (Gassen et al., 2019).

Endoplasmic reticulum stress pathway

The endoplasmic reticulum (ER) plays a critical role in the synthesis, folding and structural maturation of most cellular proteins. ER folding capacity depends on ER size and secretory potential, which are different in each cellular type. The ER stress occurs when the ER protein-folding capacity is saturated, leading to misfolded protein accumulation and activation of the unfolded protein response (UPR) (Oakes and Papa, 2015). The UPR is initiated by three ER transmembrane proteins that activate different pathways. The inositol-requiring enzyme 1α (IRE1α), the pancreatic endoplasmic reticulum kinase (PERK) and the activating transcription factor 6 (ATF6) pathway. The main function of the UPR is to restore the cellular homeostasis by increasing ER biogenesis and transcription of protein-folding chaperones. Alternatively, when the ER-stress is not resolved, the prolonged unfolded protein response induces programmed cell death or apoptosis (Frakes and Dillin, 2017).

Commonly, ER stress induced by viral infections leads to UPR (Mehrbod et al., 2019). Human CoVs encode multiple proteins that localize in the ER and have been related to the activation of this stress pathway, among them there are some accessory proteins (Fung et al., 2014). SARS-CoV ORF3a induces ER stress when

overexpressed in Huh7 cells, as determined by the increase of grp78 transcription levels, a crucial ER chaperone. This work suggests that ORF3a specifically activates PERK, but not IRE1α or ATF6 branches of the unfolded-protein response, as determined by the increase of phosphorylated eIF2α levels (Minakshi et al., 2009). SARS-CoV ORF8b also triggered ER stress by forming intracellular aggregates, which upregulated the transcription factor CHOP, although the specific branch responsible for UPR activation still remains unclear (Shi et al., 2019). Among SARS-CoV-2 accessory proteins, ORF3a has also been related to ER stress. Although the mechanism is not clear, ORF3a overexpressed in HeLa cells activated the three UPR branches (Su WQ. et al., 2021). In addition, SARS-CoV-2 ORF3a has been reported to induce ER stress by activating BECN1 and RETREG1-dependent reticulophagy, an ER degradation process via autophagy. A549 cells transfected with ORF3a or infected with SARS-CoV-2 demonstrated to induce reticulophagy and the subsequent ER stress only in the presence of active BECN1 or RETREG1. These results suggest a new mechanism by which SARS-CoV-2 might induce ER stress in a reticulophagy dependent manner (Zhang X. et al., 2022). In addition, this same study includes results suggesting that autophagy could increase SARS-CoV-2 replication, as overexpression of ORF3a not only induces autophagy, but also increases the expression levels of viral genes S, N and RdRp (Hou et al., 2022).

Concluding remarks

Coronavirus accessory genes are not strictly required for viral replication, although some of them may contribute to virus growth to some extent. Several CoV accessory proteins have structural functions and participate in virion structure, like SARS-CoV ORFs 3a, 3b, 6, 7a or 7b (Liu et al., 2014). However, they are mostly involved in virus virulence by interfering with the host antiviral responses. Despite their diversity in sequence and mechanism of action, CoV accessory proteins contribute to virus pathogenesis by modulating the innate immune response, the host immune system or other pathways involved in host resistance to viral infections, like autophagy or apoptosis.

The virulence of highly pathogenic human CoVs, SARS-CoV, MERS-CoV and SARS-CoV-2 is associated with lung immunopathology, characterized by massive inflammatory cell infiltration and elevated pro-inflammatory cytokine and chemokine responses. As described in this review, experimental infections of animal models with deletion mutants of accessory genes have confirmed the relevance of these genes in virus-induced immunopathology.

Attenuation of human CoVs due to virus evolution may involve the loss of virus virulence factors, including accessory genes, as observed with deletions within ORF8 during SARS-CoV epidemic (Oostra et al., 2007) or in ORFs 7 and 8 in the current SARS-CoV-2 pandemic (Young et al., 2020). These mutations, leading to defects in the suppression of the host immune response, might confer an evolutionary disadvantage, which could explain why these mutations disappear in the immunocompetent population. Alternatively, mutations in CoV accessory genes that modulate the innate immune response and may enhance viral pathogenicity have also been identified (Hassan et al., 2022). The emergence of novel human CoVs that cross the species barrier from animal hosts may involve, not only significant changes in viral proteins required for cell entry (Forni et al., 2021; Montoya et al., 2021), but also in accessory proteins that modulate the innate immune response of the new host. Similarly, a 29-nt deletion in SARS-CoV ORF8, which split ORF8 into ORF8a and ORF8b, occurred soon after its zoonotic transmission from civets to humans and was considered a virus adaptation to humans (Oostra et al., 2007). MERS-CoV accessory genes also seem to be relevant to the interaction of the virus with specific hosts. MERS-CoV ORF5 is conserved in field isolates from camels and humans, while it is highly unstable in cell cultures, with the appearance of mutations and deletions leading to a truncated protein 5 (Gutierrez-Alvarez et al., 2021). Moreover, the identification of a variety of deletions in MERS-CoV ORF3 and ORF4b in samples from camels suggest that the virus is not fully adapted to this host yet (Chu et al., 2018; Peiris and Perlman, 2022). In addition, an *in-vitro* study of MERS-CoV persistent infection in bat cells showed that ORF5 acquired a 341 nt-deletion after 15 passages (Banerjee et al., 2020).

To understand the relevance of accessory genes in pathogenesis in the context of infection, *in vivo* assays with syngenic viruses just differing in the gene of interest are essential. The availability of animal models of infection and reverse genetics systems to engineer the CoV genome is crucial for these studies.

Overexpression of individual accessory genes, in the absence of infection, provides a complementary approach to identify or add further insight into the molecular mechanism of action of accessory proteins in virus-host interactions. However, it is important to consider that the ectopic overexpression of a single protein has a different biological impact on the host cell than infection with a virus. The overexpressed protein may be localized to different subcellular compartments and establish distinct interactions in the absence of the other viral components, with different functional consequences in virus-host interactions. To date, only a very limited number of studies about CoV accessory genes have been performed in the context of *in vivo* infection (Castaño-Rodriguez et al., 2021; Gutierrez-Alvarez et al., 2021; Silvas et al., 2021; Bello-Perez et al., 2022). Further analyses are required to determine the relevance of accessory genes in virus pathogenesis and to define their mechanism of action. This information will be helpful to identify new therapeutic interventions that ameliorate the severity of coronavirus diseases.

Author contributions

Conceptualization, MB-P and IS. Funding acquisition, LE and IS. Writing—original draft preparation, JH-T, RR-P, MB-P and IS. Writing—review and editing, JH-T, RR-P, LE, MB-P and IS. All

authors contributed to the article and approved the submitted version.

Funding

This work was supported by grants from the Government of Spain (PID2019-107001RB-I00 AEI/FEDER, UE; SEV 2017-0712 and PIE_INTRAMURAL_Ref.-202020E079), the CSIC (PIE_INTRAMURAL-202020E043), the European Commission (ISOLDA_848166 H2020-SC1-2019; MANCO_101003651 H2020-SC1-PHE-CORONAVIRUS-2020), and the U.S. National Institutes of Health (NIH_2P01AI060699). JH-T received a fellowship from PID2019-107001RB-I00 AEI/FEDER, UE. RR-P received a fellowship from Arnhold de la Camara Foundation. MB-P received a contract from ISOLDA Project and a Jose Castillejo fellowship for PhDs mobility. The funders had no role in study design, data collection and analysis, decision to publish, or preparation of the manuscript.

Acknowledgments

We thank Marga Gonzalez (CNB-CSIC) for her technical assistance.

Conflict of interest

The authors declare that the research was conducted in the absence of any commercial or financial relationships that could be construed as a potential conflict of interest.

Publisher's note

References

Banerjee, A., Subudhi, S., Rapin, N., Lew, J., Jain, R., Falzarano, D., et al. (2020). Selection of viral variants during persistent infection of insectivorous bat cells with middle East respiratory syndrome coronavirus. *Sci. Rep.* 10, 7257. doi: 10.1038/s41598-020-64264-1

Basagoudanavar, S. H., Thapa, R. J., Nogusa, S., Wang, J., Beg, A. A., and Balachandran, S. (2011). Distinct roles for the NF-kappa b RelA subunit during antiviral innate immune responses. *J. Virol.* 85, 2599–2610. doi: 10.1128/JVI.02213-10

Basler, C. F., and Garcia-Sastre, A. (2002). Viruses and the type I interferon antiviral system: induction and evasion. *Int. Rev. Immunol.* 21 (4-5), 305–337. doi: 10.1080/08830180213277

Basler, C. F., Wang, X., Muhlberger, E., Volchkov, V., Paragas, J., Klenk, H. D., et al. (2000). The Ebola virus VP35 protein functions as a type I IFN antagonist. *Proc. Natl. Acad. Sci. U.S.A.* 97 (22), 12289–12294. doi: 10.1073/pnas.220398297

Bello-Perez, M., Hurtado-Tamayo, J., Requena-Platek, R., Canton, J., Sanchez-Cordon, P. J., Fernandez-Delgado, R., et al. (2022). MERS-CoV ORF4b is a virulence factor involved in the inflammatory pathology induced in the lungs of mice. *PloS Pathog.* 18 (9), e1010834. doi: 10.1371/journal.ppat.1010834

Bello-Perez, M., Sola, I., Novoa, B., Klionsky, D. J., and Falco, A. (2020). Canonical and noncanonical autophagy as potential targets for COVID-19. *Cells.* 9 (7). doi: 10.3390/cells9071619

Blanco-Melo, D., Nilsson-Payant, B. E., Liu, W. C., Uhl, S., Hoagland, D., Moller, R., et al. (2020). Imbalanced host response to SARS-CoV-2 drives development of COVID-19. *Cell.* 181, 1036–45 e9. doi: 10.1016/j.cell.2020.04.026

Canton, J., Fehr, A. R., Fernandez-Delgado, R., Gutierrez-Alvarez, F. J., Sanchez-Aparicio, M. T., Garcia-Sastre, A., et al. (2018). MERS-CoV 4b protein interferes with the NF-kappaB-dependent innate immune response during infection. *PloS Pathog.* 14, e1006838. doi: 10.1371/journal.ppat.1006838

Cao, Z., Xia, H., Rajsbaum, R., Xia, X., Wang, H., and Shi, P. Y. (2021). Ubiquitination of SARS-CoV-2 ORF7a promotes antagonism of interferon response. *Cell Mol. Immunol.* 18 (3), 746–748. doi: 10.1038/s41423-020-00603-6

Castano-Rodriguez, C., Honrubia, J. M., Gutierrez-Alvarez, J., DeDiego, M. L., Nieto-Torres, J. L., Jimenez-Guardeno, J. M., et al. (2018). Role of severe acute respiratory syndrome coronavirus viroporins e, 3a, and 8a in replication and pathogenesis. *MBio.* 9, e2325-17. doi: 10.1128/mBio.02325-17

Castaño-Rodriguez, C., Honrubia, J. M., Gutiérrez-Álvarez, J., Sola, I., and Enjuanes, L. (2021). Viral PDZ binding motifs influence cell behavior through the interaction with cellular proteins containing PDZ domains. *Methods Mol. Biol.* 2256, 217–236. doi: 10.1007/978-1-0716-1166-1_13

Chan, C. M., Tsoi, H., Chan, W. M., Zhai, S., Wong, C. O., Yao, X., et al. (2009). The ion channel activity of the SARS-coronavirus 3a protein is linked to its pro-apoptotic function. *Int. J. Biochem. Cell Biol.* 41, 2232–2239. doi: 10.1016/j.biocel.2009.04.019

Channappanavar, R., Fehr, A. R., Zheng, J., Wohlford-Lenane, C., Abrahante, J. E., Mack, M., et al. (2019). IFN-I response timing relative to virus replication determines MERS coronavirus infection outcomes. *J. Clin. Invest.* 130, 3625–3639. doi: 10.1172/JCI126363

Chen, L., Deng, H., Cui, H., Fang, J., Zuo, Z., Deng, J., et al. (2018). Inflammatory responses and inflammation-associated diseases in organs. *Oncotarget.* 9, 7204–7218. doi: 10.18632/oncotarget.23208

Chen, J., Lu, Z., Yang, X., Zhou, Y., Gao, J., Zhang, S., et al. (2022). Severe acute respiratory syndrome coronavirus 2 ORF8 protein inhibits type I interferon production by targeting HSP90B1 signaling. *Front. Cell Infect. Microbiol.* 12, 899546. doi: 10.3389/fcimb.2022.899546

Chen, I. Y., Moriyama, M., Chang, M. F., and Ichinohe, T. (2019). Severe acute respiratory syndrome coronavirus viroporin 3a activates the NLRP3 inflammasome. *Front. Microbiol.* 10, 50. doi: 10.3389/fmicb.2019.00050

Chen, C. Y., Ping, Y. H., Lee, H. C., Chen, K. H., Lee, Y. M., Chan, Y. J., et al. (2007). Open reading frame 8a of the human severe acute respiratory syndrome coronavirus not only promotes viral replication but also induces apoptosis. *J. Infect. Dis.* 196 (3), 405–415. doi: 10.1086/519166

Chen, X., Zhou, Z., Huang, C., Zhou, Z., Kang, S., Huang, Z., et al. (2021). Crystal structures of bat and human coronavirus ORF8 protein ig-like domain provide insights into the diversity of immune responses. *Front. Immunol.* 12, 807134. doi: 10.3389/fimmu.2021.807134

Chien, J. Y., Hsueh, P. R., Cheng, W. C., Yu, C. J., and Yang, P. C. (2006). Temporal changes in cytokine/chemokine profiles and pulmonary involvement in severe acute respiratory syndrome. *Respirology.* 11, 715–722. doi: 10.1111/j.1440-1843.2006.00942.x

Choi, Y., Bowman, J. W., and Jung, J. U. (2018). Autophagy during viral infection - a double-edged sword. *Nat. Rev. Microbiol.* 16 (6), 341–354. doi: 10.1038/s41579-018-0003-6

Choi, U. Y., Kang, J. S., Hwang, Y. S., and Kim, Y. J. (2015). Oligoadenylate synthase-like (OASL) proteins: dual functions and associations with diseases. *Exp. Mol. Med.* 47 (3), e144. doi: 10.1038/emm.2014.110

Chu, D. K. W., Hui, K. P. Y., Perera, R., Miguel, E., Niemeyer, D., Zhao, J., et al. (2018). MERS coronaviruses from camels in Africa exhibit region-dependent genetic diversity. *Proc. Natl. Acad. Sci. U.S.A.* 115, 3144–3149. doi: 10.1073/pnas.1718769115

Comar, C. E., Goldstein, S. A., Li, Y., Yount, B., Baric, R. S., and Weiss, S. R. (2019). Antagonism of dsRNA-induced innate immune pathways by NS4a and NS4b accessory proteins during MERS coronavirus infection. *MBio.* 10, e00319–e00319. doi: 10.1128/mBio.00319-19

Comar, C. E., Otter, C. J., Pfannenstiel, J., Doerger, E., Renner, D. M., Tan, L. H., et al. (2022). MERS-CoV endoribonuclease and accessory proteins jointly evade host innate immunity during infection of lung and nasal epithelial cells. *Proc. Natl. Acad. Sci. U.S.A.* 119 (21), e2123208119. doi: 10.1073/pnas.2123208119

de Haan, C. A., and Reggiori, F. (2008). Are nidoviruses hijacking the autophagy machinery? *Autophagy* 4 (3), 276–279. doi: 10.4161/auto.5241

Diamond, M. S., and Kanneganti, T. D. (2022). Innate immunity: the first line of defense against SARS-CoV-2. *Nat. Immunol.* 23 (2), 165–176. doi: 10.1038/s41590-021-01091-0

Elmore, S. (2007). Apoptosis: a review of programmed cell death. *Toxicol. Pathol.* 35 (4), 495–516. doi: 10.1080/01926230701320337

Evans, S. S., and Ozer, H. (1987). Enhancement of a human antibody response *In vitro* mediated by interaction of interferon-alpha with T lymphocytes. *J. Immunol.* 138, 2451–2456. doi: 10.4049/jimmunol.138.8.2451

Fang, P., Fang, L., Zhang, H., Xia, S., and Xiao, S. (2021). Functions of coronavirus accessory proteins: overview of the state of the art. *Viruses.* 13 (6). doi: 10.3390/v13061139

Forni, D., Cagliani, R., Arrigoni, F., Benvenuti, M., Mozzi, A., Pozzoli, U., et al. (2021). Adaptation of the endemic coronaviruses HCoV-OC43 and HCoV-229E to the human host. *Virus Evol.* 7 (2), veab061. doi: 10.1093/ve/veab061

Frakes, A. E., and Dillin, A. (2017). The UPR(ER): sensor and coordinator of organismal homeostasis. *Mol. Cell.* 66 (6), 761–771. doi: 10.1016/j.molcel.2017.05.031

Freundt, E. C., Yu, L., Goldsmith, C. S., Welsh, S., Cheng, A., Yount, B., et al. (2010). The open reading frame 3a protein of severe acute respiratory syndrome-associated coronavirus promotes membrane rearrangement and cell death. *J. Virol.* 84, 1097–1109. doi: 10.1128/JVI.01662-09

Freundt, E. C., Yu, L., Park, E., Lenardo, M. J., and Xu, X. N. (2009). Molecular determinants for subcellular localization of the severe acute respiratory syndrome coronavirus open reading frame 3b protein. *J. Virol.* 83, 6631–6640. doi: 10.1128/JVI.00367-09

Frieman, M., Yount, B., Heise, M., Kopecky-Bromberg, S. A., Palese, P., and Baric, R. S. (2007). Severe acute respiratory syndrome coronavirus ORF6 antagonizes STAT1 function by sequestering nuclear import factors on the rough endoplasmic reticulum/Golgi membrane. *J. Virol.* 81 (18), 9812–9824. doi: 10.1128/JVI.01012-07

Fu, J., Li, L., and Bouvier, M. (2011). Adenovirus E3-19K proteins of different serotypes and subgroups have similar, yet distinct, immunomodulatory functions toward major histocompatibility class I molecules. *J. Biol. Chem.* 286 (20), 17631–17639. doi: 10.1074/jbc.M110.212050

Fung, T. S., Huang, M., and Liu, D. X. (2014). Coronavirus-induced ER stress response and its involvement in regulation of coronavirus-host interactions. *Virus Res.* 194, 110–123. doi: 10.1016/j.virusres.2014.09.016

Garcia-Garcia, T., Fernandez-Rodriguez, R., Redondo, N., de Lucas-Rius, A., Zaldivar-Lopez, S., Lopez-Ayllon, B. D., et al. (2022). Impairment of antiviral immune response and disruption of cellular functions by SARS-CoV-2 ORF7a and ORF7b. *iScience.* 25 (11), 105444. doi: 10.1016/j.isci.2022.105444

Garcia-Sastre, A. (2017). Ten strategies of interferon evasion by viruses. *Cell Host Microbe* 22, 176–184. doi: 10.1016/j.chom.2017.07.012

Garcia-Sastre, A., Egorov, A., Matassov, D., Brandt, S., Levy, D. E., Durbin, J. E., et al. (1998). Influenza a virus lacking the NS1 gene replicates in interferon-deficient systems. *Virology.* 252 (2), 324–330. doi: 10.1006/viro.1998.9508

Gassen, N. C., Niemeyer, D., Muth, D., Corman, V. M., Martinelli, S., Gassen, A., et al. (2019). SKP2 attenuates autophagy through Beclin1-ubiquitination and its inhibition reduces MERS-coronavirus infection. *Nat. Commun.* 10 (1), 5770. doi: 10.1038/s41467-019-13659-4

Geng, H., Subramanian, S., Wu, L., Bu, H. F., Wang, X., Du, C., et al. (2021). SARS-CoV-2 ORF8 forms intracellular aggregates and inhibits IFNgamma-induced antiviral gene expression in human lung epithelial cells. *Front. Immunol.* 12, 679482. doi: 10.3389/fimmu.2021.679482

Gewurz, B. E., Gaudet, R., Tortorella, D., Wang, E. W., Ploegh, H. L., and Wiley, D. C. (2001). Antigen presentation subverted: structure of the human cytomegalovirus protein US2 bound to the class I molecule HLA-A2. *Proc. Natl. Acad. Sci. U.S.A.* 98 (12), 6794–6799. doi: 10.1073/pnas.121172898

Gorbalenya, A. E., Baker, S. C., Baric, R. S., de Groot, R. J., Drosten, C., Gulyaeva, A. A., et al. (2020). The species severe acute respiratory syndrome-related coronavirus: classifying 2019-nCoV and naming it SARS-CoV-2. *Nat. Microbiol.* 5 (4), 536–544. doi: 10.1038/s41564-020-0695-z

Gutierrez-Alvarez, J., Wang, L., Fernandez-Delgado, R., Li, K., McCray, P. B.Jr., Perlman, S., et al. (2021). Middle East respiratory syndrome coronavirus gene 5 modulates pathogenesis in mice. *J. Virol.* 95, e01172-20. doi: 10.1128/JVI.01172-20

Hassan, S. S., Choudhury, P. P., Dayhoff, G. W.2nd, Aljabali, A. A. A., Uhal, B. D., Lundstrom, K., et al. (2022). The importance of accessory protein variants in the pathogenicity of SARS-CoV-2. *Arch. Biochem. Biophys.* 717, 109124. doi: 10.1016/j.abb.2022.109124

Hayn, M., Hirschenberger, M., Koepke, L., Nchioua, R., Straub, J. H., Klute, S., et al. (2021). Systematic functional analysis of SARS-CoV-2 proteins uncovers viral innate immune antagonists and remaining vulnerabilities. *Cell Rep.* 35 (7), 109126. doi: 10.1016/j.celrep.2021.109126

Hojyo, S., Uchida, M., Tanaka, K., Hasebe, R., Tanaka, Y., Murakami, M., et al. (2020). How COVID-19 induces cytokine storm with high mortality. *Inflammation Regen.* 40, 37. doi: 10.1186/s41232-020-00146-3

Hou, P., Wang, X., Wang, H., Wang, T., Yu, Z., Xu, C., et al. (2022). The ORF7a protein of SARS-CoV-2 initiates autophagy and limits autophagosome-lysosome fusion via degradation of SNAP29 to promote virus replication. *Autophagy* 19 (2), 551–569. doi: 10.1080/15548627.2022.2084686

Hu, B., Huang, S., and Yin, L. (2021). The cytokine storm and COVID-19. *J. Med. Virol.* 93 (1), 250–256. doi: 10.1002/jmv.26232

Jackson, W. T. (2015). Viruses and the autophagy pathway. *Virology* 479-480, 450–456. doi: 10.1016/j.virol.2015.03.042

Jiang, P., Nishimura, T., Sakamaki, Y., Itakura, E., Hatta, T., Natsume, T., et al. (2014). The HOPS complex mediates autophagosome-lysosome fusion through interaction with syntaxin 17. *Mol. Biol. Cell.* 25 (8), 1327–1337. doi: 10.1091/mbc.e13-08-0447

Kanzawa, N., Nishigaki, K., Hayashi, T., Ishii, Y., Furukawa, S., Niiro, A., et al. (2006). Augmentation of chemokine production by severe acute respiratory syndrome coronavirus 3a/X1 and 7a/X4 proteins through NF-kappaB activation. *FEBS Lett.* 580 (30), 6807–6812. doi: 10.1016/j.febslet.2006.11.046

Kee, J., Thudium, S., Renner, D. M., Glastad, K., Palozola, K., Zhang, Z., et al. (2022). SARS-CoV-2 disrupts host epigenetic regulation via histone mimicry. *Nature.* 610 (7931), 381–388. doi: 10.1038/s41586-022-05282-z

Kendall, E. J., Bynoe, M. L., and Tyrrell, D. A. (1962). Virus isolations from common colds occurring in a residential school. *Br. Med. J.* 2 (5297), 82–86. doi: 10.1136/bmj.2.5297.82

Khan, S., Fielding, B. C., Tan, T. H., Chou, C. F., Shen, S., Lim, S. G., et al. (2006). Over-expression of severe acute respiratory syndrome coronavirus 3b protein induces both apoptosis and necrosis in vero E6 cells. *Virus Res.* 122 (1-2), 20–27. doi: 10.1016/j.virusres.2006.06.005

Kim, E. S., Choe, P. G., Park, W. B., Oh, H. S., Kim, E. J., Nam, E. Y., et al. (2016). Clinical progression and cytokine profiles of middle East respiratory syndrome coronavirus infection. *J. Korean Med. Sci.* 31, 1717–1725. doi: 10.3346/jkms.2016.31.11.1717

Kirtipal, N., Bharadwaj, S., and Kang, S. G. (2020). From SARS to SARS-CoV-2, insights on structure, pathogenicity and immunity aspects of pandemic human coronaviruses. *Infect. Genet. Evol.* 85, 104502. doi: 10.1016/j.meegid.2020.104502

Klionsky, D. J., Abdel-Aziz, A. K., Abdelfatah, S., Abdellatif, M., Abdoli, A., Abel, S., et al. (2021). Guidelines for the use and interpretation of assays for monitoring autophagy (4th edition)(1). *Autophagy* 17 (1), 1–382. doi: 10.1080/15548627.2020.1797280

Koepke, L., Hirschenberger, M., Hayn, M., Kirchhoff, F., and Sparrer, K. M. (2021). Manipulation of autophagy by SARS-CoV-2 proteins. *Autophagy* 17 (9), 2659–2661. doi: 10.1080/15548627.2021.1953847

Kopecky-Bromberg, S. A., Martinez-Sobrido, L., Frieman, M., Baric, R. A., and Palese, P. (2007). Severe acute respiratory syndrome coronavirus open reading frame (ORF) 3b, ORF 6, and nucleocapsid proteins function as interferon antagonists. *J. Virol.* 81 (2), 548–557. doi: 10.1128/JVI.01782-06

Kopecky-Bromberg, S. A., Martinez-Sobrido, L., and Palese, P. (2006). 7a protein of severe acute respiratory syndrome coronavirus inhibits cellular protein synthesis and activates p38 mitogen-activated protein kinase. *J. Virol.* 80 (2), 785–793. doi: 10.1128/JVI.80.2.785-793.2006

Koyama, S., Ishii, K. J., Coban, C., and Akira, S. (2008). Innate immune response to viral infection. *Cytokine.* 43 (3), 336–341. doi: 10.1016/j.cyto.2008.07.009

Krejbich-Trotot, P., Gay, B., Li-Pat-Yuen, G., Hoarau, J. J., Jaffar-Bandjee, M. C., Briant, L., et al. (2011). Chikungunya triggers an autophagic process which promotes viral replication. *Virol. J.* 8, 432. doi: 10.1186/1743-422X-8-432

Law, P. T. W., Wong, C. H., Au, T. C. C., Chuck, C. P., Kong, S. K., Chan, P. K. S., et al. (2005). The 3a protein of severe acute respiratory syndrome-associated coronavirus induces apoptosis in vero E6 cells. *J. Gen. Virol.* 86 (Pt 7), 1921–1930. doi: 10.1099/vir.0.80813-0

Li, Y. H., Hu, C. Y., Wu, N. P., Yao, H. P., and Li, L. J. (2019). Molecular characteristics, functions, and related pathogenicity of MERS-CoV proteins. *Eng. (Beijing).* 5, 940–947. doi: 10.1016/j.eng.2018.11.035

Li, J. Y., Liao, C. H., Wang, Q., Tan, Y. J., Luo, R., Qiu, Y., et al. (2020). The ORF6, ORF8 and nucleocapsid proteins of SARS-CoV-2 inhibit type I interferon signaling pathway. *Virus Res.* 286, 198074. doi: 10.1016/j.virusres.2020.198074

Li, T., Wen, Y., Guo, H., Yang, T., Yang, H., and Ji, X. (2021). Molecular mechanism of SARS-CoVs Orf6 targeting the Rae1-Nup98 complex to compete with mRNA nuclear export. *Front. Mol. Biosci.* 8, 813248. doi: 10.3389/fmolb.2021.813248

Lin, X., Fu, B., Yin, S., Li, Z., Liu, H., Zhang, H., et al. (2021). ORF8 contributes to cytokine storm during SARS-CoV-2 infection by activating IL-17 pathway. *iScience.* 24, 102293. doi: 10.1016/j.isci.2021.102293

Liu, T., Feng, M., Wen, Z., He, Y., Lin, W., and Zhang, M. (2021). Comparison of the characteristics of cytokine storm and immune response induced by SARS-CoV, MERS-CoV, and SARS-CoV-2 infections. *J. Inflamm. Res.* 14, 5475–5487. doi: 10.2147/JIR.S329697

Liu, Z., Fu, Y., Huang, Y., Zeng, F., Rao, J., Xiao, X., et al. (2022). Ubiquitination of SARS-CoV-2 ORF7a prevents cell death induced by recruiting BclXL to activate ER stress. *Microbiol. Spectr.* 10 (6), e0150922. doi: 10.1128/spectrum.01509-22

Liu, D. X., Fung, T. S., Chong, K. K., Shukla, A., and Hilgenfeld, R. (2014). Accessory proteins of SARS-CoV and other coronaviruses. *Antiviral Res.* 109, 97–109. doi: 10.1016/j.antiviral.2014.06.013

Liu, Y., Garron, T. M., Chang, Q., Su, Z., Zhou, C., Qiu, Y., et al. (2021). Cell-type apoptosis in lung during SARS-CoV-2 infection. *Pathogens* 10 (5). doi: 10.3390/pathogens10050509

Liu, Y., Zhang, X., Liu, J., Xia, H., Zou, J., Muruato, A. E., et al. (2022). A live-attenuated SARS-CoV-2 vaccine candidate with accessory protein deletions. *Nat. Commun.* 13 (1), 4337. doi: 10.1038/s41467-022-31930-z

Lokugamage, K. G., Hage, A., de Vries, M., Valero-Jimenez, A. M., Schindewolf, C., Dittmann, M., et al. (2020). Type I interferon susceptibility distinguishes SARS-CoV-2 from SARS-CoV. *J. Virol.* 94, e01410–e01420. doi: 10.1128/JVI.01410-20

Lowery, S. A., Sariol, A., and Perlman, S. (2021). Innate immune and inflammatory responses to SARS-CoV-2: implications for COVID-19. *Cell Host Microbe* 29, 1052–1062. doi: 10.1016/j.chom.2021.05.004

Martin-Sancho, L., Lewinski, M. K., Pache, L., Stoneham, C. A., Yin, X., Becker, M. E., et al. (2021). Functional landscape of SARS-CoV-2 cellular restriction. *Mol. Cell.* 81 (12), 2656–68 e8. doi: 10.1016/j.molcel.2021.04.008

Matsuoka, K., Imahashi, N., Ohno, M., Ode, H., Nakata, Y., Kubota, M., et al. (2022). SARS-CoV-2 accessory protein ORF8 is secreted extracellularly as a glycoprotein homodimer. *J. Biol. Chem.* 298 (3), 101724. doi: 10.1016/j.jbc.2022.101724

Matthews, K. L., Coleman, C. M., van der Meer, Y., Snijder, E. J., and Frieman, M. B. (2014). The ORF4b-encoded accessory proteins of middle East respiratory syndrome coronavirus and two related bat coronaviruses localize to the nucleus and inhibit innate immune signalling. *J. Gen. Virol.* 95, 874–882. doi: 10.1099/vir.0.062059-0

McNab, F., Mayer-Barber, K., Sher, A., Wack, A., and O'Garra, A. (2015). Type I interferons in infectious disease. *Nat. Rev. Immunol.* 15, 87–103. doi: 10.1038/nri3787

Mehrbod, P., Ande, S. R., Alizadeh, J., Rahimizadeh, S., Shariati, A., Malek, H., et al. (2019). The roles of apoptosis, autophagy and unfolded protein response in arbovirus, influenza virus, and HIV infections. *Virulence* 10 (1), 376–413. doi: 10.1080/21505594.2019.1605803

Menachery, V. D., Mitchell, H. D., Cockrell, A. S., Gralinski, L. E., Yount, B. L.Jr., Graham, R. L., et al. (2017). MERS-CoV accessory ORFs play key role for infection and pathogenesis. *MBio* 8, e00665-17. doi: 10.1128/mBio.00665-17

Miao, G., Zhao, H., Li, Y., Ji, M., Chen, Y., Shi, Y., et al. (2021). ORF3a of the COVID-19 virus SARS-CoV-2 blocks HOPS complex-mediated assembly of the SNARE complex required for autolysosome formation. *Dev. Cell.* 56 (4), 427–42 e5. doi: 10.1016/j.devcel.2020.12.010

Minakshi, R., Padhan, K., Rani, M., Khan, N., Ahmad, F., and Jameel, S. (2009). The SARS coronavirus 3a protein causes endoplasmic reticulum stress and induces ligand-independent downregulation of the type 1 interferon receptor. *PloS One* 4, e8342. doi: 10.1371/journal.pone.0008342

Miorin, L., Kehrer, T., Sanchez-Aparicio, M. T., Zhang, K., Cohen, P., Patel, R. S., et al. (2020). SARS-CoV-2 Orf6 hijacks Nup98 to block STAT nuclear import and antagonize interferon signaling. *Proc. Natl. Acad. Sci. U.S.A.* 117, 28344–28354. doi: 10.1073/pnas.2016650117

Mogensen TH., I. R. F. (2018). And STAT transcription factors - from basic biology to roles in infection, protective immunity, and primary immunodeficiencies. *Front. Immunol.* 9, 3047. doi: 10.3389/fimmu.2018.03047

Montoya, V., McLaughlin, A., Mordecai, G. J., Miller, R. L., and Joy, J. B. (2021). Variable routes to genomic and host adaptation among coronaviruses. *J. Evol. Biol.* 34 (6), 924–936. doi: 10.1111/jeb.13771

Mosca, J. D., and Pitha, P. M. (1986). Transcriptional and posttranscriptional regulation of exogenous human beta interferon gene in simian cells defective in interferon synthesis. *Mol. Cell Biol.* 6, 2279–2783. doi: 10.1128/mcb.6.6.2279-2283.1986

Moser, C. V., Stephan, H., Altenrath, K., Kynast, K. L., Russe, O. Q., Olbrich, K., et al. (2015). TANK-binding kinase 1 (TBK1) modulates inflammatory hyperalgesia by regulating MAP kinases and NF-kappaB dependent genes. *J. Neuroinflamm.* 12, 100. doi: 10.1186/s12974-015-0319-3

Munasinghe, T. S., Edwards, M. R., Tsimbalyuk, S., Vogel, O. A., Smith, K. M., Stewart, M., et al. (2022). MERS-CoV ORF4b employs an unusual binding mechanism to target IMPalpha and block innate immunity. *Nat. Commun.* 13 (1), 1604. doi: 10.1038/s41467-022-28851-2

Nakagawa, K., Narayanan, K., Wada, M., and Makino, S. (2018). Inhibition of stress granule formation by middle East respiratory syndrome coronavirus 4a accessory protein facilitates viral translation, leading to efficient virus replication. *J. Virol.* 92, e00902-18. doi: 10.1128/JVI.00902-18

Nemudryi, A., Nemudraia, A., Wiegand, T., Nichols, J., Snyder, D. T., Hedges, J. F., et al. (2021). SARS-CoV-2 genomic surveillance identifies naturally occurring truncation of ORF7a that limits immune suppression. *Cell Rep.* 35 (9), 109197. doi: 10.1016/j.celrep.2021.109197

Netea-Maier, R. T., Plantinga, T. S., van de Veerdonk, F. L., Smit, J. W., and Netea, M. G. (2016). Modulation of inflammation by autophagy: consequences for human disease. *Autophagy.* 12 (2), 245–260. doi: 10.1080/15548627.2015.1071759

Niemeyer, D., Zillinger, T., Muth, D., Zielecki, F., Horvath, G., Suliman, T., et al. (2013). Middle East respiratory syndrome coronavirus accessory protein 4a is a type I interferon antagonist. *J. Virol.* 87, 12489–12495. doi: 10.1128/JVI.01845-13

Nishitsuji, H., Iwahori, S., Ohmori, M., Shimotohno, K., and Murata, T. (2022). Ubiquitination of SARS-CoV-2 NSP6 and ORF7a facilitates NF-kappaB activation. *mBio.* 13 (4), e0097122. doi: 10.1128/mbio.00971-22

Oakes, S. A., and Papa, F. R. (2015). The role of endoplasmic reticulum stress in human pathology. *Annu. Rev. Pathol.* 10, 173–194. doi: 10.1146/annurev-pathol-012513-104649

Oostra, M., de Haan, C. A., and Rottier, P. J. (2007). The 29-nucleotide deletion present in human but not in animal severe acute respiratory syndrome coronaviruses disrupts the functional expression of open reading frame 8. *J. Virol.* 81 (24), 13876–13888. doi: 10.1128/JVI.01631-07

Padhan, K., Minakshi, R., Towheed, M. A. B. , and Jameel, S. (2008). Severe acute respiratory syndrome coronavirus 3a protein activates the mitochondrial death pathway through p38 MAP kinase activation. *J. Gen. Virol.* 89(Pt 8), 1960–1969. doi: 10.1099/vir.0.83665-0

Park, G. J., Osinski, A., Hernandez, G., Eitson, J. L., Majumdar, A., Tonelli, M., et al. (2022). The mechanism of RNA capping by SARS-CoV-2. *Nature.* 609, 793–800. doi: 10.1038/s41586-022-05185-z

Park, M. S., Shaw, M. L., Munoz-Jordan, J., Cros, J. F., Nakaya, T., Bouvier, N., et al. (2003). Newcastle Disease virus (NDV)-based assay demonstrates interferon-antagonist activity for the NDV V protein and the nipah virus V, W, and c proteins. *J. Virol.* 77 (2), 1501–1511. doi: 10.1128/JVI.77.2.1501-1511.2003

Peiris, M., and Perlman, S. (2022). Unresolved questions in the zoonotic transmission of MERS. *Curr. Opin. Virol.* 52, 258–264. doi: 10.1016/j.coviro.2021.12.013

Prentice, E., Jerome, W. G., Yoshimori, T., Mizushima, N., and Denison, M. R. (2004). Coronavirus replication complex formation utilizes components of cellular autophagy. *J. Biol. Chem.* 279 (11), 10136–10141. doi: 10.1074/jbc.M306124200

Prescott, J., Hall, P., Acuna-Retamar, M., Ye, C., Wathelet, M. G., Ebihara, H., et al. (2010). New world hantaviruses activate IFNlambda production in type I IFN-deficient vero E6 cells. *PloS One* 5, e11159. doi: 10.1371/journal.pone.0011159

Qu, Y., Wang, X., Zhu, Y., Wang, W., Wang, Y., Hu, G., et al. (2021). ORF3a-mediated incomplete autophagy facilitates severe acute respiratory syndrome coronavirus-2 replication. *Front. Cell Dev. Biol.* 9, 716208. doi: 10.3389/fcell.2021.716208

Rabouw, H. H., Langereis, M. A., Knaap, R. C., Dalebout, T. J., Canton, J., Sola, I., et al. (2016). Middle East respiratory coronavirus accessory protein 4a inhibits PKR-mediated antiviral stress responses. *PloS Pathog.* 12, e1005982. doi: 10.1371/journal.ppat.1005982

Rashid, F., Dzakah, E. E., Wang, H., and Tang, S. (2021a). The ORF8 protein of SARS-CoV-2 induced endoplasmic reticulum stress and mediated immune evasion by antagonizing production of interferon beta. *Virus Res.* 296, 198350. doi: 10.1016/j.virusres.2021.198350

Rashid, F., Suleman, M., Shah, A., Dzakah, E. E., Wang, H., Chen, S., et al. (2021b). Mutations in SARS-CoV-2 ORF8 altered the bonding network with interferon regulatory factor 3 to evade host immune system. *Front. Microbiol.* 12, 703145. doi: 10.3389/fmicb.2021.703145

Redondo, N., Zaldivar-Lopez, S., Garrido, J. J., and Montoya, M. (2021). SARS-CoV-2 accessory proteins in viral pathogenesis: knowns and unknowns. *Front. Immunol.* 12, 708264. doi: 10.3389/fimmu.2021.708264

Ren, Y., Shu, T., Wu, D., Mu, J., Wang, C., Huang, M., et al. (2020). The ORF3a protein of SARS-CoV-2 induces apoptosis in cells. *Cell Mol. Immunol.* 17 (8), 881–883. doi: 10.1038/s41423-020-0485-9

Roth-Cross, J. K., Bender, S. J., and Weiss, S. R. (2008). Murine coronavirus mouse hepatitis virus is recognized by MDA5 and induces type I interferon in brain macrophages/microglia. *J. Virol.* 82, 9829–9838. doi: 10.1128/JVI.01199-08

Rui, Y., Su, J., Shen, S., Hu, Y., Huang, D., Zheng, W., et al. (2021). Unique and complementary suppression of cGAS-STING and RNA sensing- triggered innate immune responses by SARS-CoV-2 proteins. *Signal. Transduct. Target. Ther.* 6 (1), 123. doi: 10.1038/s41392-021-00515-5

Sampaio, N. G., Chauveau, L., Hertzog, J., Bridgeman, A., Fowler, G., Moonen, J. P., et al. (2021). The RNA sensor MDA5 detects SARS-CoV-2 infection. *Sci. Rep.* 11 (1), 13638. doi: 10.1038/s41598-021-92940-3

Sa Ribero, M., Jouvenet, N., Dreux, M., and Nisole, S. (2020). Interplay between SARS-CoV-2 and the type I interferon response. *PloS Pathog.* 16 (7), e1008737. doi: 10.1371/journal.ppat.1008737

Schaecher, S. R., Touchette, E., Schriewer, J., Buller, R. M., and Pekosz, A. (2007). Severe acute respiratory syndrome coronavirus gene 7 products contribute to virus-induced apoptosis. *J. Virol.* 81 (20), 11054–11068. doi: 10.1128/JVI.01266-07

Schneider, W. M., Chevillotte, M. D., and Rice, C. M. (2014). Interferon-stimulated genes: a complex web of host defenses. *Annu. Rev. Immunol.* 32, 513–545. doi: 10.1146/annurev-immunol-032713-120231

Schoggins, J. W. (2019). Interferon-stimulated genes: what do they all do? *Annu. Rev. Virol.* 6, 567–584. doi: 10.1146/annurev-virology-092818-015756

Schroeder, S., Pott, F., Niemeyer, D., Veith, T., Richter, A., Muth, D., et al. (2021). Interferon antagonism by SARS-CoV-2: a functional study using reverse genetics. *Lancet Microbe* 2 (5), e210–e2e8. doi: 10.1016/S2666-5247(21)00027-6

Sharma, K., Akerstrom, S., Sharma, A. K., Chow, V. T., Teow, S., Abrenica, B., et al. (2011). SARS-CoV 9b protein diffuses into nucleus, undergoes active Crm1 mediated nucleocytoplasmic export and triggers apoptosis when retained in the nucleus. *PloS One* 6, e19436. doi: 10.1371/journal.pone.0019436

Shemesh, M., Aktepe, T. E., Deerain, J. M., McAuley, J. L., Audsley, M. D., David, C. T., et al. (2021). SARS-CoV-2 suppresses IFNbeta production mediated by NSP1, 5, 6, 15, ORF6 and ORF7b but does not suppress the effects of added interferon. *PloS Pathog.* 17 (8), e1009800. doi: 10.1371/journal.ppat.1009800

Shen, Y., and Shenk, T. E. (1995). Viruses and apoptosis. *Curr. Opin. Genet. Dev.* 5 (1), 105–111. doi: 10.1016/S0959-437X(95)90061-6

Shi, J., Li, Z., Xu, R., Zhang, J., Zhou, Q., Gao, R., et al. (2022). The PERK/PKR-eIF2alpha pathway negatively regulates porcine hemagglutinating encephalomyelitis virus replication by attenuating global protein translation and facilitating stress granule formation. *J. Virol.* 96, e01695-21. doi: 10.1128/JVI.01695-21

Shi, C. S., Nabar, N. R., Huang, N. N., and Kehrl, J. H. (2019). SARS-coronavirus open reading frame-8b triggers intracellular stress pathways and activates NLRP3 inflammasomes. *Cell Death Discov.* 5, 101. doi: 10.1038/s41420-019-0181-7

Shi, C. S., Qi, H. Y., Boularan, C., Huang, N. N., Abu-Asab, M., Shelhamer, J. H., et al. (2014). SARS-coronavirus open reading frame-9b suppresses innate immunity by targeting mitochondria and the MAVS/TRAF3/TRAF6 signalosome. *J. Immunol.* 193, 3080–3089. doi: 10.4049/jimmunol.1303196

Silvas, J. A., Vasquez, D. M., Park, J. G., Chiem, K., Allue-Guardia, A., Garcia-Vilanova, A., et al. (2021). Contribution of SARS-CoV-2 accessory proteins to viral pathogenicity in K18 human ACE2 transgenic mice. *J. Virol.* 95, e00402–e00421. doi: 10.1128/JVI.00402-21

Siu, K. L., Yeung, M. L., Kok, K. H., Yuen, K. S., Kew, C., Lui, P. Y., et al. (2014). Middle East respiratory syndrome coronavirus 4a protein is a double-stranded RNA-binding protein that suppresses PACT-induced activation of RIG-I and MDA5 in innate antiviral response. *J. Virol.* 88, 4866–4876. doi: 10.1128/JVI.03649-13

Siu, K. L., Yuen, K. S., Castano-Rodriguez, C., Ye, Z. W., Yeung, M. L., Fung, S. Y., et al. (2019). Severe acute respiratory syndrome coronavirus ORF3a protein activates the NLRP3 inflammasome by promoting TRAF3-dependent ubiquitination of ASC. *FASEB J.* 33, fj201802418R. doi: 10.1096/fj.201802418R

Sola, I., Almazán, F., Zúñiga, S., and Enjuanes, L. (2015). Continuous and discontinuous RNA synthesis in coronaviruses. *Annu. Rev. Virol.* 2, 265–288. doi: 10.1146/annurev-virology-100114-055218

Su, C. M., Wang, L., and Yoo, D. (2021). Activation of NF-kappaB and induction of proinflammatory cytokine expressions mediated by ORF7a protein of SARS-CoV-2. *Sci. Rep.* 11, 13464. doi: 10.1038/s41598-021-92941-2

Su, W. Q., Yu, X. J., and Zhou, C. M. (2021). SARS-CoV-2 ORF3a induces incomplete autophagy via the unfolded protein response. *Viruses* 13 (2), 2467. doi: 10.3390/v13122467

Szegezdi, E., Logue, S. E., Gorman, A. M., and Samali, A. (2006). Mediators of endoplasmic reticulum stress-induced apoptosis. *EMBO Rep.* 7 (9), 880–885. doi: 10.1038/sj.embor.7400779

Takatsuka, H., Fahmi, M., Hamanishi, K., Sakuratani, T., Kubota, Y., and Ito, M. (2022). In silico analysis of SARS-CoV-2 ORF8-binding proteins reveals the involvement of ORF8 in acquired-immune and innate-immune systems. *Front. Med. (Lausanne).* 9, 824622. doi: 10.3389/fmed.2022.824622

Takeuchi, O., and Akira, S. (2010). Pattern recognition receptors and inflammation. *Cell.* 140 (6), 805–820. doi: 10.1016/j.cell.2010.01.022

Tan, Y. J., Fielding, B. C., Goh, P. Y., Shen, S., Tan, T. H., Lim, S. G., et al. (2004). Overexpression of 7a, a protein specifically encoded by the severe acute respiratory syndrome coronavirus, induces apoptosis via a caspase-dependent pathway. *J. Virol.* 78 (24), 14043–14047. doi: 10.1128/JVI.78.24.14043-14047.2004

Tan, Y. X., Tan, T. H., Lee, M. J., Tham, P. Y., Gunalan, V., Druce, J., et al. (2007). Induction of apoptosis by the severe acute respiratory syndrome coronavirus 7a protein is dependent on its interaction with the bcl-XL protein. *J. Virol.* 81 (12), 6346–6355. doi: 10.1128/JVI.00090-07

Taylor, J. K., Coleman, C. M., Postel, S., Sisk, J. M., Bernbaum, J. G., Venkataraman, T., et al. (2015). Severe acute respiratory syndrome coronavirus ORF7a inhibits bone marrow stromal antigen 2 virion tethering through a novel mechanism of glycosylation interference. *J. Virol.* 89 (23), 11820–11833. doi: 10.1128/JVI.02274-15

Thornbrough, J. M., Jha, B. K., Yount, B., Goldstein, S. A., Li, Y., Elliott, R., et al. (2016). Middle East respiratory syndrome coronavirus NS4b protein inhibits host RNase l activation. *MBio.* 7, e00258. doi: 10.1128/mBio.00258-16

Tian, M., Liu, W., Li, X., Zhao, P., Shereen, M. A., Zhu, C., et al. (2021). HIF-1alpha promotes SARS-CoV-2 infection and aggravates inflammatory responses to COVID-19. *Signal. Transduct. Target. Ther.* 6 (1), 308. doi: 10.1038/s41392-021-00726-w

Tian, Y., Sir, D., Kuo, C. F., Ann, D. K., and Ou, J. H. (2011). Autophagy required for hepatitis b virus replication in transgenic mice. *J. Virol.* 85 (24), 13453–13456. doi: 10.1128/JVI.06064-11

Varshney, B., Agnihothram, S., Tan, Y. J., Baric, R., and Lal, S. K. (2012). SARS coronavirus 3b accessory protein modulates transcriptional activity of RUNX1b. *PloS One* 7, e29542. doi: 10.1371/annotation/64ae6047-0f9b-4d17-a065-e08c153aa435

Varshney, B., and Lal, S. K. (2011). SARS-CoV accessory protein 3b induces AP-1 transcriptional activity through activation of JNK and ERK pathways. *Biochemistry* 50, 5419–5425. doi: 10.1021/bi200303r

Vartanian, A. A., Suzuki, H., and Poletaev, A. I. (2003). The involvement of diadenosine 5',5"'-P1,P4-tetraphosphate in cell cycle arrest and regulation of apoptosis. *Biochem. Pharmacol.* 65 (2), 227–235. doi: 10.1016/S0006-2952(02)01481-8

Vasilenko, N., Moshynskyy, I., and Zakhartchouk, A. (2010). SARS coronavirus protein 7a interacts with human Ap4A-hydrolase. *Virol. J.* 7, 31. doi: 10.1186/1743-422X-7-31

Wang, R., Yang, X., Chang, M., Xue, Z., Wang, W., Bai, L., et al. (2021). ORF3a protein of severe acute respiratory syndrome coronavirus 2 inhibits interferon-activated janus Kinase/Signal transducer and activator of transcription signaling via elevating suppressor of cytokine signaling 1. *Front. Microbiol.* 12, 752597. doi: 10.3389/fmicb.2021.752597

Wen, X., Huang, X., Mok, B. W., Chen, Y., Zheng, M., Lau, S. Y., et al. (2014). NF90 exerts antiviral activity through regulation of PKR phosphorylation and stress granules in infected cells. *J. Immunol.* 192, 3753–3764. doi: 10.4049/jimmunol.1302813

Wong, H. H., Fung, T. S., Fang, S., Huang, M., Le, M. T., and Liu, D. X. (2018). Accessory proteins 8b and 8ab of severe acute respiratory syndrome coronavirus suppress the interferon signaling pathway by mediating ubiquitin-dependent rapid degradation of interferon regulatory factor 3. *Virology* 515, 165–175. doi: 10.1016/j.virol.2017.12.028

Wu, X., Xia, T., Shin, W. J., Yu, K. M., Jung, W., Herrmann, A., et al. (2022). Viral mimicry of interleukin-17A by SARS-CoV-2 ORF8. *mBio.* 13 (2), e0040222. doi: 10.1128/mbio.00402-22

Xia, H., Cao, Z., Xie, X., Zhang, X., Chen, J. Y., Wang, H., et al. (2020). Evasion of type I interferon by SARS-CoV-2. *Cell Rep.* 33, 108234. doi: 10.1016/j.celrep.2020.108234

Xu, H., Akinyemi, I. A., Chitre, S. A., Loeb, J. C., Lednicky, J. A., McIntosh, M. T., et al. (2022). SARS-CoV-2 viroporin encoded by ORF3a triggers the NLRP3 inflammatory pathway. *Virology.* 568, 13–22. doi: 10.1016/j.virol.2022.01.003

Xu, X., Lai, Y., and Hua, Z. C. (2019). Apoptosis and apoptotic body: disease message and therapeutic target potentials. *Biosci. Rep.* 39 (1). doi: 10.1042/BSR20180992

Xue, W., Ding, C., Qian, K., and Liao, Y. (2021). The interplay between coronavirus and type I IFN response. *Front. Microbiol.* 12, 805472. doi: 10.3389/fmicb.2021.805472

Yan, L., Huang, Y., Ge, J., Liu, Z., Lu, P., Huang, B., et al. (2022). A mechanism for SARS-CoV-2 RNA capping and its inhibition by nucleotide analog inhibitors. *Cell.* 185, 4347–60 e17. doi: 10.1016/j.cell.2022.09.037

Yan, H., Xiao, G., Zhang, J., Hu, Y., Yuan, F., Cole, D. K., et al. (2004). SARS coronavirus induces apoptosis in vero E6 cells. *J. Med. Virol.* 73 (3), 323–331. doi: 10.1002/jmv.20094

Yang, Y., Zhang, L., Geng, H., Deng, Y., Huang, B., Guo, Y., et al. (2013). The structural and accessory proteins m, ORF 4a, ORF 4b, and ORF 5 of middle East respiratory syndrome coronavirus (MERS-CoV) are potent interferon antagonists. *Protein Cell.* 4, 951–961. doi: 10.1007/s13238-013-3096-8

Yang, R., Zhao, Q., Rao, J., Zeng, F., Yuan, S., Ji, M., et al. (2021). SARS-CoV-2 accessory protein ORF7b mediates tumor necrosis factor-alpha-Induced apoptosis in cells. *Front. Microbiol.* 12, 654709. doi: 10.3389/fmicb.2021.654709

Yeung, M. L., Yao, Y., Jia, L., Chan, J. F., Chan, K. H., Cheung, K. F., et al. (2016). MERS coronavirus induces apoptosis in kidney and lung by upregulating Smad7 and FGF2. *Nat. Microbiol.* 1 (3), 16004. doi: 10.1038/nmicrobiol.2016.4

Young, B. E., Fong, S. W., Chan, Y. H., Mak, T. M., Ang, L. W., Anderson, D. E., et al. (2020). Effects of a major deletion in the SARS-CoV-2 genome on the severity of infection and the inflammatory response: an observational cohort study. *Lancet.* 396 (10251), 603–611. doi: 10.1016/S0140-6736(20)31757-8

Yuan, X., Shan, Y., Zhao, Z., Chen, J., and Cong, Y. (2005). G0/G1 arrest and apoptosis induced by SARS-CoV 3b protein in transfected cells. *Virol. J.* 2, 66. doi: 10.1186/1743-422X-2-66

Yuen, C. K., Lam, J. Y., Wong, W. M., Mak, L. F., Wang, X., Chu, H., et al. (2020). SARS-CoV-2 nsp13, nsp14, nsp15 and orf6 function as potent interferon antagonists. *Emerg. Microbes Infect.* 9, 1418–1428. doi: 10.1080/22221751.2020.1780953

Zhang, Y., Chen, Y., Li, Y., Huang, F., Luo, B., Yuan, Y., et al. (2021a). The ORF8 protein of SARS-CoV-2 mediates immune evasion through down-regulating MHC-iota. *Proc. Natl. Acad. Sci. U.S.A.* 118 (23). doi: 10.1073/pnas.2024202118

Zhang, Y., Sun, H., Pei, R., Mao, B., Zhao, Z., Li, H., et al. (2021b). The SARS-CoV-2 protein ORF3a inhibits fusion of autophagosomes with lysosomes. *Cell Discov* 7 (1), 31. doi: 10.1038/s41421-021-00268-z

Zhang, X., Yang, Z., Pan, T., Long, X., Sun, Q., Wang, P. H., et al. (2022). SARS-CoV-2 ORF3a induces RETREG1/FAM134B-dependent reticulophagy and triggers sequential ER stress and inflammatory responses during SARS-CoV-2 infection. *Autophagy* 18 (11), 2576–2592. doi: 10.1080/15548627.2022.2039992

Zhang, F., Zang, T. M., Stevenson, E. M., Lei, X., Copertino, D. C., Mota, T. M., et al. (2022). Inhibition of major histocompatibility complex-I antigen presentation by sarbecovirus ORF7a proteins. *Proc. Natl. Acad. Sci. U.S.A.* 119 (41), e2209042119. doi: 10.1073/pnas.2209042119

Zhou, Z., Qiu, Y., and Ge, X. (2021). The taxonomy, host range and pathogenicity of coronaviruses and other viruses in the nidovirales order. *Anim. Dis.* 1 (1), 5. doi: 10.1186/s44149-021-00005-9

Zhou, Y., Zheng, R., Liu, S., Disoma, C., Du, A., Li, S., et al. (2022). Host E3 ligase HUWE1 attenuates the proapoptotic activity of the MERS-CoV accessory protein ORF3 by promoting its ubiquitin-dependent degradation. *J. Biol. Chem.* 298 (2), 101584. doi: 10.1016/j.jbc.2022.101584

frontiers | Frontiers in Cellular and Infection Microbiology

TYPE Original Research
PUBLISHED 02 May 2023
DOI 10.3389/fcimb.2023.1168355

OPEN ACCESS

EDITED BY
Josep Quer,
Vall d'Hebron Research Institute (VHIR), Spain

REVIEWED BY
Graham John Belsham,
University of Copenhagen, Denmark
Karen Kyuregyan,
Russian Medical Academy of Continuous Professional Education & Mechnikov Research Institute for Vaccines and Sera, Russia

*CORRESPONDENCE
Maria Dolores Fernandez-Garcia
mdfernandez@isciii.es

RECEIVED 17 February 2023
ACCEPTED 11 April 2023
PUBLISHED 02 May 2023

CITATION
Fernandez-Garcia MD, Faye M, Diez-Fuertes F, Moreno-Docón A, Chirlaque-López MD, Faye O and Cabrerizo M (2023) Metagenomic sequencing, molecular characterization, and Bayesian phylogenetics of imported type 2 vaccine-derived poliovirus, Spain, 2021. *Front. Cell. Infect. Microbiol.* 13:1168355. doi: 10.3389/fcimb.2023.1168355

Metagenomic sequencing, molecular characterization, and Bayesian phylogenetics of imported type 2 vaccine-derived poliovirus, Spain, 2021

Maria Dolores Fernandez-Garcia[1,2]*, Martin Faye[3], Francisco Diez-Fuertes[4,5], Antonio Moreno-Docón[6,7], Maria Dolores Chirlaque-López[2,7,8], Ousmane Faye[3] and Maria Cabrerizo[1,2]

[1]Enterovirus and Viral Gastroenteritis Unit/National Polio Laboratory, National Centre for Microbiology, Instituto de Salud Carlos III, Madrid, Spain, [2]Consortium of Epidemiology and Public Health (CIBERESP), Instituto de Salud Carlos III, Madrid, Spain, [3]Virology Department, Institut Pasteur de Dakar, Dakar, Senegal, [4]AIDS Immunopathogenesis Unit, Instituto de Salud Carlos III, Madrid, Spain, [5]Consortium of Infectious Diseases, Instituto de Salud Carlos III, Madrid, Spain, [6]Microbiology Department, Hospital U. Virgen de la Arrixaca, Murcia, Spain, [7]Instituto Murciano de Investigación Biosanitaria (IMIB)-Arrixaca, Murcia University, Murcia, Spain, [8]Department of Epidemiology, Murcia Regional Health Council, Murcia, Spain

Introduction: In 2021, a type 2 vaccine-derived poliovirus (VDPV2) was isolated from the stool of a patient with acute flaccid paralysis (AFP) admitted to Spain from Senegal. A virological investigation was conducted to characterize and trace the origin of VDPV2.

Methods: We used an unbiased metagenomic approach for the whole-genome sequencing of VDPV2 from the stool (pre-treated with chloroform) and from the poliovirus-positive supernatant. Phylogenetic analyses and molecular epidemiological analyses relying on the Bayesian Markov Chain Monte Carlo methodology were used to determine the geographical origin and estimate the date of the initiating dose of the oral poliovirus vaccine for the imported VDPV2.

Results: We obtained a high percentage of viral reads per total reads mapped to the poliovirus genome (69.5% for pre-treated stool and 75.8% for isolate) with a great depth of sequencing coverage (5,931 and 11,581, respectively) and complete genome coverage (100%). The two key attenuating mutations in the Sabin 2 strain had reverted (A481G in the 5'UTR and Ile143Thr in VP1). In addition, the genome had a recombinant structure between type-2 poliovirus and an unidentified non-polio enterovirus-C (NPEV-C) strain with a crossover point in the protease-2A genomic region. VP1 phylogenetic analysis revealed that this strain is closely related to VDPV2 strains circulating in Senegal in 2021. According to Bayesian phylogenetics, the most recent common ancestor of the imported VDPV2 could date back 2.6 years (95% HPD: 1.7–3.7) in Senegal. We suggest that all VDPV2s circulating in 2020–21 in Senegal, Guinea, Gambia, and Mauritania have an ancestral origin in Senegal estimated around 2015. All 50 stool samples

from healthy case contacts collected in Spain (n = 25) and Senegal (n = 25) and four wastewater samples collected in Spain were poliovirus negative.

Discussion: By using a whole-genome sequencing protocol with unbiased metagenomics from the clinical sample and viral isolate with high sequence coverage, efficiency, and throughput, we confirmed the classification of VDPV as a circulating type. The close genomic linkage with strains from Senegal was consistent with their classification as imported. Given the scarce number of complete genome sequences for NPEV-C in public databases, this protocol could help expand poliovirus and NPEV-C sequencing capacity worldwide.

KEYWORDS

vaccine-derived polio virus, whole-genome, metagenomics, recombination, molecular epidemiology, OPV (oral polio vaccine), Bayesian phylogenetic analysis

Introduction

Poliomyelitis is caused by poliovirus, a human enterovirus (family *Picornaviridae*, genus *Enterovirus*, species *Enterovirus C*). Since the Global Polio Eradication Initiative (GPEI) was launched in 1988, polio cases have been reduced by more than 99% (Global Polio Eradication Initiative). The GPEI managed to eradicate wild poliovirus (WPV) type 2 in 2015 and type 3 in 2019. The main strategies for eradication were mass immunization with the oral poliovirus vaccine (OPV) and surveillance of acute flaccid paralysis (AFP) cases and their contacts (Global Polio Eradication Initiative). OPV is a live-attenuated vaccine (with the three Sabin poliovirus serotypes) that replicates in the gut for a short time. Here, parental Sabin strains can mutate and be excreted into the environment ***via*** feces (Kew et al., 2005). Therefore, if polio vaccine coverage is low in a community and sanitation is inadequate, the mutated viruses may be transmitted in unimmunized and under-immunized populations, leading to genetic drift and the emergence of new pathogenic strains known as circulating vaccine-derived polioviruses (cVDPVs) (Kew et al., 2005). VDPVs currently constitute a major challenge to the polio eradication endgame, given their potential to cause paralysis and/or persistent circulation in human communities. Because most cVDPVs are type 2, in April 2016, a global switch from the trivalent oral polio vaccine to a bivalent oral polio vaccine containing only types 1 and 3 was implemented to remove all live-attenuated type 2 vaccines and their associated risk. The switch and delays in introducing a dose of inactivated polio vaccine (IPV) into essential immunization in all regions led to decreasing immunity to type 2 poliovirus (PV-2) (World Health Organization, 2021a). Decreasing immunity, together with the use of monovalent vaccine OPV2 in outbreak control campaigns, failures to control movements of VDPVs between countries, and difficulties in maintaining adequate vaccination coverage due to COVID-19, all resulted in a rapid growth of cVDPV2 outbreaks, with more cases of cVDPV2 than WPV1 annually since 2017 (Alleman et al., 2021; World Health Organization, 2021a).

If poliomyelitis is not eradicated globally, the risk of the virus being reintroduced in Europe remains. Two EU/EEA countries (Poland and Romania) and one neighboring country (Ukraine) are considered at risk of sustained poliovirus transmission following WPV importation or the emergence of cVDPV due to significant gaps in population immunity (World Health Organization, 2021b). In Spain, OPV was replaced by IPV in 2004, and national coverage of three doses in children's first year of age exceeds 95% (Ministry of Health, Social Services and Equality, 2023). The National Action Plan for Poliomyelitis Eradication (NAPPE) was first established in 1998, and the study of AFP cases is the cornerstone of poliovirus surveillance, along with non-polio enterovirus (NPEV) surveillance (Masa-Calles et al., 2018). Since the OPV was replaced, only two VDPV have been identified, one in 2005 and the other in 2019 (Avellón et al., 2008; Informe anual, 2019). Both VDPVs were imported and isolated from immunocompromised patients. However, in September 2021, an imported paralysis case from Senegal was notified in Spain, identifying VDPV2 in a stool sample of the patient. All measures taken and actions carried out were within the framework of the NAPPE and the recommendations issued under the ongoing Public Health Emergency of International Concern on the risk of international spread of poliovirus (López et al., 2021). Molecular characterization of poliovirus isolates detected through AFP and environmental surveillance activities is key to distinguishing vaccine-related from WPV, and identifying genetic linkages between isolates to identify patterns of circulation (Classification and reporting of vaccine-derived polioviruses (VDPV), 2016). This molecular characterization is routinely based on Sanger sequencing of the viral protein 1 (VP1) capsid region. However, surveillance of poliovirus based on the whole genome has proven an essential tool for the final stages of polio eradication (Montmayeur et al., 2017). In this report, we describe the virological study of the case based on the VP1 and the whole-genome analyses of the detected VDPV2.

Materials and methods

The AFP case

Briefly, a child under the age of 6 years from Senegal traveled to Murcia, in the southeast of Spain, on August 2021, to be admitted to the hospital to continue treatment of an AFP with unknown origin and

onset of symptoms in July 2021 in Senegal. The child was discharged from the hospital after showing clinical improvement. The diagnosis was acute anterior meningomyeloradiculitis because of an enterovirus infection (coxsackievirus B4 was detected in a respiratory sample during hospitalization). The child stayed with a local family until September 2021, then returned to Senegal. The case's vaccination card showed four doses of OPV (received in the first year of life; last OPV dose: August 2016), followed by one dose of IPV. All of them were received during the first year of age. The case had no evidence of primary immunodeficiency. The AFP case was notified retrospectively in September, and a stool sample collected in August was sent to the National Polio Laboratory (NPL) of the National Centre for Microbiology (CNM) for a poliovirus study (López et al., 2021).

Virological methods

The AFP case was laboratory investigated according to the isolation assay algorithm recommended by WHO (World Health Organization, 2004a) and the Spanish NAPPE (Ministerio de Sanidad, Asuntos Sociales e Igualdad, 2016). In addition to the single sample from the case, two stool samples from 25 healthy close contacts of the patient were examined. Analysis of the presence of poliovirus in all samples was performed by culture on RD and L20B cell lines following the 14-day algorithm (World Health Organization, 2004a; World Health Organization, 2004b). In addition, real-time RT-PCR (Cabrerizo et al., 2014) was used for the detection of enterovirus/poliovirus in clinical samples. Four RT-nested PCRs on the 3'VP1 region (specific for enterovirus species A to D) followed by sequencing were applied subsequently to those enterovirus-positive samples or isolates for genotyping (Cabrerizo et al., 2008). Finally, characterization of the detected poliovirus (WPV, OPV, or VDPV) was carried out using intratypic differentiation (ITD) assays (Gerloff et al., 2018), as was amplification and sequencing of the complete VP1 region of the viral genome. In Senegal, 25 contacts of the AFP case were studied by the WHO-accredited reference polio laboratory at the Institut Pasteur of Dakar, as previously described (Faye. et al., 2022).

Wastewater samples

The presence of poliovirus was also analyzed in four raw wastewater samples collected at two inlet points of the wastewater treatment plant from the area where the case stayed on two different days (15 and 20 September). The same culture and molecular methods applied to clinical samples were used. Samples had been processed and concentrated previously using a protocol based on precipitation with $AlCl_3$ (Randazzo et al., 2020).

Metagenomic sequencing and bioinformatic analysis

Full-genome sequences of cVDPV2 from the AFP case were obtained from fecal suspension and from the L20B-positive supernatant. Fecal samples were prepared according to WHO standard procedures (World Health Organization, 2004a). Briefly, fecal samples were pre-treated with chloroform, to which enteroviruses are resistant, to remove bacteria and fungi. This was clarified at 4,000 rpm for 20 min at 4°C, contributing to the removal of host cellular debris and bacteria. This fecal suspension was used to inoculate cell cultures. Culture supernatants were frozen, thawed three times, and clarified. RNA was extracted from both stool-clarified suspension and clarified supernatant using the Quick RNA viral kit (Zymo). Sample library preparation was conducted using the NEBNext Ultra II Directional RNA Library Prep Kit for Illumina with NEBNext Multiplex Oligos for Illumina Set 3 (New England BioLabs Inc., USA) from a total concentration of 10 ng of RNA quantified using the QuantiFluor RNA System (E3310, Promega). Both libraries were sequenced using an Illumina MiSeq Reagent Kit v2 Nano on a MiSeq sequencer (300 cycles). The resulting data was analyzed using PikaVirus, a NextFlow pipeline openly available at https://github.com/BU-ISCIII/PikaVirus, and consisted of the following steps: quality control of the samples using FastQC (v. 0.11.9) and MultiQC (v. 1.9) for quality assessment, and FastP (v. 0.20.1) for trimming; potential viral genomes identification within the trimmed reads using MASH screening (v. 2.3) against the full GenBank viral assemblies database (release 248, downloaded on 2 April 2022); mapping of potentially present viral genomes against the samples using BowTie2 (v. 2.4.4); and obtention of coverage statistics using SamTools (v. 1.12); and BedTools (v. 2.30.0). Human host reads were subtracted by performing a kmer-based mapping of the trimmed reads with the GRCh38 NCBI human genome using Kraken2 v.2.1.2 (Wood et al., 2019). Reads that aligned to the human genome were excluded from further analysis. Spades v3.14.0 in *rnaviral* mode was used to perform a *de novo* assembly of non-host reads. Contigs taxonomic annotation was based on alignment to NCBI's viral database using BLAST v2.9.0+. Results were visualized using Krona. For viral consensus genome reconstruction, we used the viralrecon pipeline v2.5 (https://github.com/nf-core/viralrecon) written in Nextflow (https://www.nextflow.io/) in collaboration with the nf-core (https://nf-co.re/) community and the Bioinformatics Unit of the Institute of Health Carlos III (BU-ISCIII) (https://github.com/BU-ISCIII) (Patel et al). The GenBank accession number of the isolate complete genome sequence is OQ401876.

Phylogenetic and recombination analysis

Phylogenetic trees were constructed by the neighbor-joining method with 1,000 bootstrap replicates using Molecular Evolutionary Genetic Analysis (MEGA version 10) software (https://www.megasoftware.net/). We used published VP1 coding sequences available in GenBank, retrieved in November 2022. Nucleotide (nt) sequence alignment was performed by the ClustalW multiple alignment program within the BioEdit Sequence Alignment Editor package. Similarity plot analysis was performed by using the Simplot program, v3.5.1 with the Kimura distance model and a window size of 400 bp moving in 40 nt steps with 1,000 resamplings.

Estimation of dates of the initiating OPV dose

The date and location of the OPV that initiated the emergence of the SPA866 case were estimated using a Bayesian Markov chain Monte Carlo (MCMC) approach. Root-to-tip genetic distances against sample collection dates were examined in a preliminary analysis with TempEst v.1.5.3 to identify the temporal signal of the VP1 nt sequence data. The Bayesian analysis was performed with BEAST software v1.10.4 (Rambaut et al., 2016) using the nt-substitution model described by Shapiro et al. (2006) with a discrete gamma distribution to accommodate rate variation among sites in the alignment and allowing different rates of substitution for the first plus second versus the third codon position. Lineage-specific rate heterogeneity was taken into account by using the uncorrelated relaxed molecular clock model with a lognormal rate distribution (Drummond et al., 2005). A Bayesian Skyline coalescent model assuming that a small random sample from a large population is included in the data set was selected. Two independent MCMC runs of 100 million states sampling every 10,000 steps were computed and mixed. The convergence of MCMC chains was checked using Tracer v.1.7.1, ensuring that the effective sample size values were greater than 200 for each estimated parameter (Rambaut et al., 2018). The maximum clade credibility trees were obtained from the tree posterior distribution using TreeAnnotator v.1.10.4 after a 10% burn-in. Phylogenetic trees were visualized and annotated with FigTree v.1.4.4 to indicate the mean estimated values and 95% highest posterior density (HPD) intervals for OPV dose dates and the posterior probability values for the most probable location.

Results

The AFP case: Poliovirus detection and initial molecular characterization of the stool isolate

The poliovirus was identified first by the presence of a cytopathic effect on both L20B and RD cell lines. Viral RNA extracted directly from stool suspension and from L20B-positive supernatant tested positive for enterovirus by real-time RT-PCR and RT-nested PCR. Genotyping in the 3'-VP1 region indicated that the enterovirus was a PV-2. The ITD assays, performed simultaneously at the CNM and at the Regional Polio Laboratory at the Robert Koch Institute (RKI) in Berlin, confirmed it was a PV-2 (both in the L20B-positive supernatant and in the stool sample). The isolate is hereinafter referred to as SPA866. Sanger sequencing of the complete VP1 region (903 nt) of the PV-2 detected in the L20B supernatant was performed in CNM and RKI simultaneously with identical results. The complete VP1 coding sequence differed from Sabin 2 (AY184220) by 5.1% (46 nt changes), confirming its classification as VDPV-2 according to WHO-adopted criteria (>0.6% genetic divergence in the complete genomic region) (Classification and reporting of vaccine-derived polioviruses (VDPV), 2016). Among the seven amino acid changes found in the VP1, one was the Ile143Thr substitution (encoded by the $U_{2909} \rightarrow C$ nt mutation), which represents the reversion of a key attenuation determinant of Sabin 2 (Ren et al., 1991).

Whole-genome sequencing of the detected VDPV-2

Complete genomic sequencing of strain SPA866 was performed using a sequence-independent metagenomic approach from the pre-treated stool suspension and from the L20B-positive supernatant. For the stool suspension, a total of 439,714 reads were obtained. Of these, the percentage of viral reads that mapped to the targeted poliovirus genome accounted for 69.5% (n = 305,565), with a median deep coverage of 5,931 and a coverage >10× of 100%. For the isolate, a total of 777,948 reads were obtained. Of these, viral reads mapped to the poliovirus genome accounted for 75.8% (n = 589,645), with a median deep coverage of 11,581 and a coverage >10× of 100%. Performing *de novo* assembly of reads, no coinfecting pathogens were detected in the samples (only commensal bacteria of Mycoplasma spp.). Metagenomics in both samples yielded the same full-genome VDPV-2 sequence. The VP1 Sanger sequence described in the previous section was identical to that obtained by metagenomic sequencing. The consensus sequence was 7,427 nt in length, including a 5′ untranslated region (UTR) of 738 nt, a single open reading frame (ORF) of 6621 nt encoding a single polyprotein of 2,207 aa, and a 3'UTR of 71 nt. The whole-genome sequence was compared to the Sabin-2 vaccine reference strain (Table 1). Strain SPA866 differed from that of Sabin-2 by 12.7% (846 nt and 66 aa substitutions) in the open reading frame, by 13% (96 nt substitutions) in the 5′UTR and by 4.2% (3 nt substitutions) in the 3′UTR. A key determinant of the Sabin-2 attenuated phenotype at nt 481 of the 5'UTR reverted in strain SPA866 (A-to-G substitution). Nt substitutions were widely distributed throughout the P1 region. A majority (87.5%, 119/136) occurred in the third codon position. Four amino acid (aa) substitutions in the P1 capsid region mapped in virion surface residues form the neutralizing antigenic sites (Table 1).

Analysis of recombination events

Although the P1 capsid genomic region was similar to that of Sabin-2 (5.1% nt divergence), the nonstructural regions of the genome (P2 and P3) were dissimilar (18.8% and 17% nt divergence, respectively) (Table 1). This suggested that the strain SPA866 was a vaccine/non-vaccine recombinant. Similarly, the 5'UTR sequence of SPA866 was apparently derived from non-OPV viruses (13% difference from the Sabin 2 strain). To confirm the existence of recombination events, similarity plot analysis was conducted against complete sequences closely related to strain SPA866 (Figure 1). These closely related strains were screened against the NCBI non-redundant nt database using BLASTn (http://www.ncbi.nlm.nih.gov/). The structural P1 coding region and nonstructural P2 and P3 regions of strain SPA866 were used as queries for BLASTn, and sequences with the highest homologies and complete genomes were used in the recombination analysis

TABLE 1 Nucleotide and amino acid substitutions in strain SPA866 in comparison to Sabin 2.

Genomic region		Nucleotides		Amino acid		Relevant mutations*
		No. substitutions	Divergence (%)	No. substitutions	Divergence (%)	
5'UTR		96	13	NA	NA	A481G (Attenuation)
P1 region	**VP4**	19	9.2	1	1.4	
	VP2	37	4.5	2	0.7	
	VP3	34	4.7	4	1.7	Ser73Asn (NAg site 3), Thr75Met (NAg site 3)
	VP1	46	5.1	7	2.3	Arg103Lys (NAg site 1), Ile143Thr (Attenuation), Ser222Pro (NAg site 2)
P2 region		325	18.8	25	4.3	
P3 region		384	17	27	3.6	
3'UTR		3	4.2	NA	NA	

*Relevant mutations refer to relevant sites in the Sabin-2 genome described as being involved in Sabin-2 attenuation (Ren et al., 1991) or those predicted neutralizing antigenic (NAg) sites important for immune recognition (Shulman et al., 2000; Adu et al., 2007).
NA, not applicable.

(Supplementary Table 1). A majority of closely related strains found in public databases were type 2 VDPVs from Nigeria, the Central African Republic, Russia, and Ukraine, and only one strain was a non-polio species C enterovirus (coxsackievirus A20 from Nigeria). Similarity plot analysis revealed that the nt similarity in the 3' half of the genome was <90%. The potential recombination breakpoint was estimated to be in the protease 2A genomic region (position refers to alignment with Sabin-2) (Figure 1).

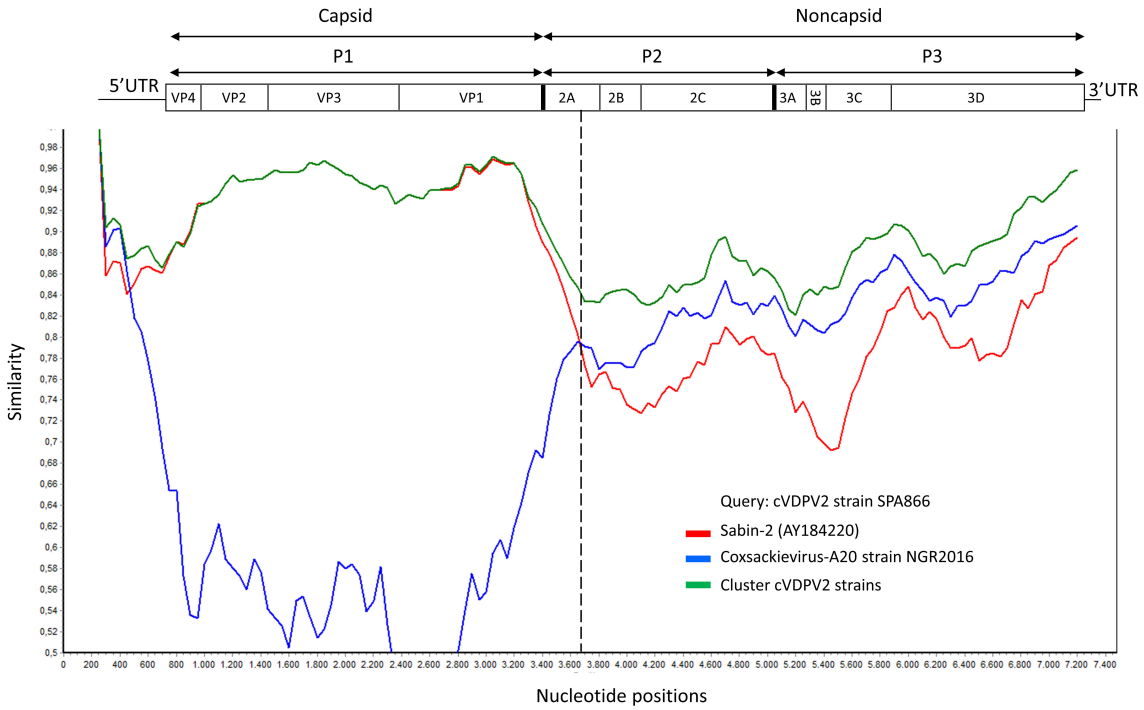

FIGURE 1
Plot of similarity of whole-genome nucleotide sequences of study strain SPA866 (query), Sabin-2 poliovirus strain, and closely related strains from NCBI. The enterovirus genetic organization is shown in the top panel. The breakpoint position of recombination is marked with a dashed line. cVDPV2 strains: MT432140, MG212462, JX275032, JX275140, JX275015, KJ170572, MG212459, KX162700, KX162714, KX162716, MG212490, MG212480, and MT432143; Coxsackievirus-A20 strain NGR2016: MH785183. cVDPV, type 2 circulating vaccine-derived poliovirus; UTR, untranslated region.

Phylogenetic analysis

Analysis of complete VP1 coding sequences showed that strain SPA866 branched closely (bootstrap value of 98%) with cVDPV2 strains obtained in Senegal in 2021, more precisely with those strains previously defined in clade 2 by Faye et al (Faye. et al., 2022). that comprised sequences from Dakar, Diourbel, Thiès, and Louga. Clade 2 strains from Senegal and strain SPA866 were highly similar (nt identity ≥97.2%; aa identity ≥96.7%) supporting that all are genetically related and have a common precursor (Figure 2). Strain SPA866 showed the closest relationship to strain ON604904 (bootstrap value of 92%, nt identity = 99.3%, aa identity = 100%), isolated from an AFP case in 2021 from Bambey, in the Diourbel medical region.

Estimation of the duration of replication of SPA866

The maximum clade credibility tree of the complete VP1 coding sequence was estimated for the study strain SPA866 and closely related sequences (clusters 1 and 2) observed in Figure 2 (Figure 3). The sequence SPA866 branched into a lineage (the SEN3 lineage) comprising 34 sequences from samples collected in the Diourbel and Thies regions of Senegal in 2021 (Figure 3). The time of the most recent common ancestor (tMRCA) of this lineage is 2.6 years (95% HPD: 1.7–3.7). Two other independent VDPV2 lineage groups were identified with samples from Senegal. The first lineage (SEN1 lineage) comprised sequences from Dakar (Senegal), Guinea, and Gambia, with Senegal being the most likely origin (PP = 0.94) and with a mean tMRCA of 2.9 years (95% HPD: 1.8–4.1). The other lineage (SEN2 lineage) included sequences from southern Senegal (regions of Fatick and Kaolack) and Mauritania, being Senegal the most probable origin (PP = 0.98) and with a mean tMRCA of 3.0 years (95% HPD: 1.8–4.4). These three independent lineages that have arisen approximately at the same time, around early 2018, in different regions of Senegal, share a common ancestor that was circulating in Senegal (PP = 0.96) with a mean tMRCA of 5.4 years (95% HPD: 3.6–7.5). The date of the OPV dose that initiated these three independent lineages observed in Senegal was estimated around 2015, about 5.4 years before 2021 (95% HPD: 3.6–7.5), with robust node support (a posterior probability value of 1).

Microbiological investigation of case contacts and environmental samples in Spain

All stool samples from 25 close contacts were negative for poliovirus, as were the four concentrated wastewater samples, although rhinoviruses (n = 8) or NPEV of A and B species (n = 6) were detected in some of them (Supplementary Tables 2, 3).

Microbiological investigation of case contacts in Senegal

Field investigations were conducted around the case in the Mbour medical district (Thies medical region) in Senegal. Stool samples collected from 25 contacts tested negative for polioviruses, while 32% of them (n = 8) tested positive for enterovirus B species.

Discussion

If there are cVDPVs that emerge and circulate due to person-to-person transmission in communities with low polio immunity, there remains the potential for international spread to polio-free countries with high vaccine coverage, such as Spain. Despite the worldwide reported decline in the number of cVDPV2 AFP cases since 2020 (1082 in 2020, 682 in 2021, and 478 in 2022 across 34 countries) (World Health Organization, 2022), the risk of the international spread of cVDPV2 remains quite high. Among these cVDPV2 AFP cases, 59%, 87%, and 72% were reported in Africa in 2020, 2021, and 2022, respectively (World Health Organization, 2022). In 2021, Senegal reported 29 cases of cVDPVs (including 17 paralytic cases), with more than 80% of cVDPV2 being reported in Dakar and Diourbel (UNICEF Senegal, 2022). In this context, in September 2021, a VDPV2 was identified in the stool of a case of AFP admitted to a Spanish hospital from Senegal.

This study describes the isolation and molecular characterization of VDPV2 detected and isolated (SPA866). We demonstrate by sequencing and phylogenetic analysis of the VP1 genomic region that the isolated virus is genetically linked to cVDPVs previously isolated in Diourbel, Senegal. We estimated that the initiating OPV dose for VDPV2s circulating in west Africa in 2020–21 was given around 2015 in Senegal, and it disseminated in early 2018 within the country and lately to nearby countries such as Mauritania, Guinea, and Gambia. Thus, the widespread circulation of cVDPV2s reveals gaps in immunity to PV2 in children across all these countries and their silent circulation until the first detection in wastewater samples in Dakar, Senegal, in December 2020 (Faye. et al., 2022). The Bayesian phylogenetic analysis suggests that the most probable origin of all VDPV2 isolates circulating in Senegal, Guinea, Gambia, and Mauritania was Senegal around 2015. Our results are consistent with previous findings that suggest that VDPV2s in Senegal in 2021 will spread to Gambia (Faye. et al., 2022), given that all VDPV2 strains from the Gambia branch are in the SEN1 lineage, which has Senegal as the most likely origin with a very high probability. Similarly, these results do not contradict the possibility that the origin of some independent VDPV2 introductions observed in Senegal recorded during 2020–21 was Guinea, Mali, and Côte d'Ivoire, as previously suggested (Faye. et al., 2022). It is to be noted that results may be biased given the lack of sequence data from other countries in West Africa.

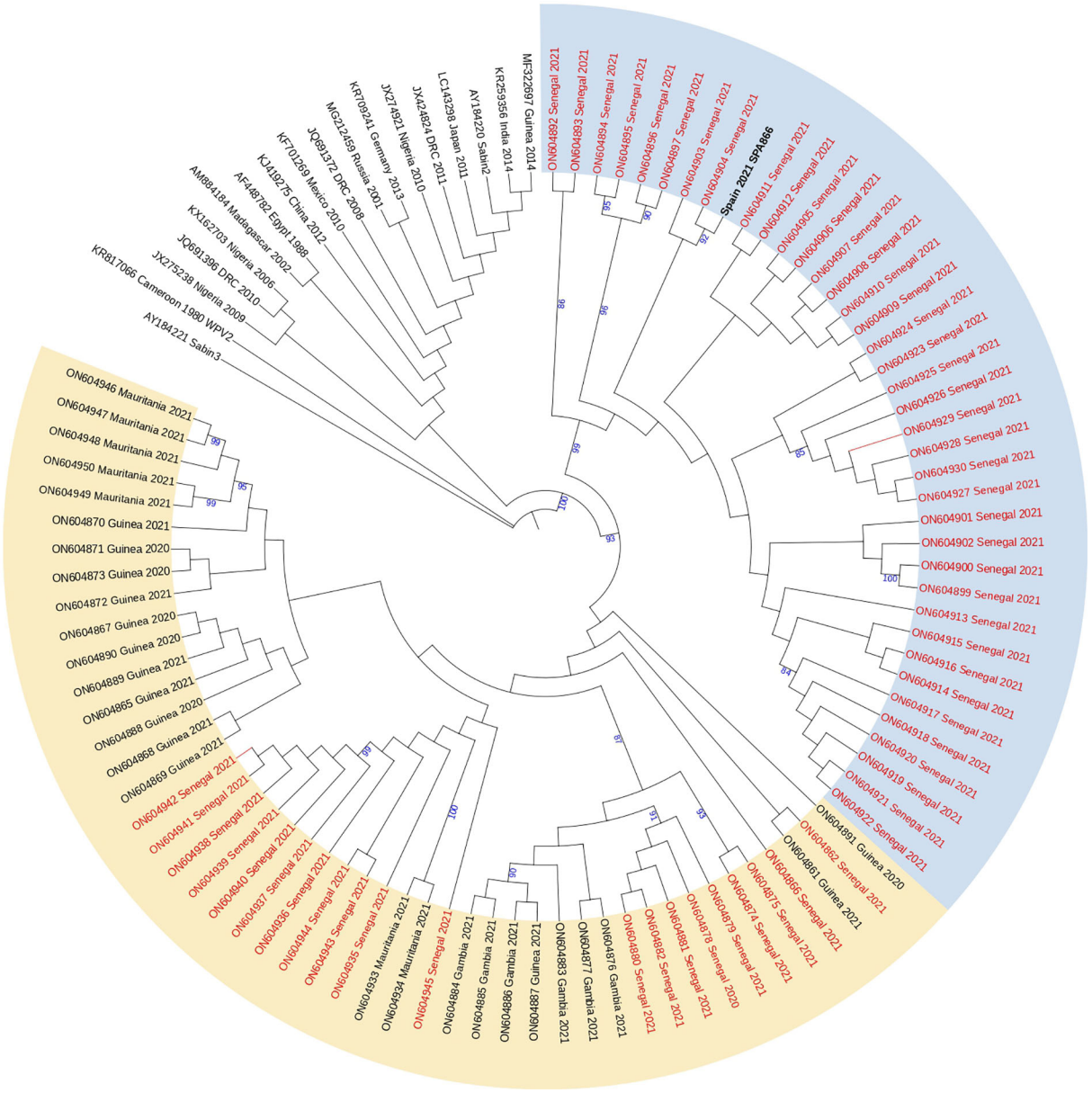

FIGURE 2
Phylogenetic tree of the complete VP1 coding sequences of VDPV2 study strain SPA866 and 104 sequences from previously described VDPV2 strains extracted from GenBank. The neighbor-joining tree was constructed using MEGA 10.0. Distances were computed using the Kimura 2-parameter model after excluding positions containing gaps and missing data from the alignments. The robustness of the nodes was tested by 1,000 bootstrap replications. Only bootstrap support values above 80% are shown in branch nodes. The scale bar represents nt substitutions per site. The tree is annotated with the classification proposed by Faye et al. for cVDPVs circulating in Senegal since their first introduction in 2020 (clade 1 in yellow and clade 2 in blue). Strains from Senegal are marked in red for clarity. The study strain is marked in bold black. The Sabin-3 poliovirus sequence was introduced as an outgroup.

Enteroviruses are characterized by a great deal of genetic variability, relying on two different evolutionary mechanisms: mutation and recombination (Muslin et al., 2019). In this study, we looked at both mechanisms. Regarding mutations in the complete VP1 coding sequence, we observed that strain SPA866 contained reverse mutations of nt481 (A to G) and nt2909 (Ile to Thr), which are associated with the phenotypic reversion of the attenuated Sabin 2 strain to neurovirulence. Besides mutations, RNA recombination is a molecular process during which genomic fragments from different RNA strands are combined into a single genome (Muslin et al., 2019). RNA recombination with cocirculating NPEV species C (NPEV-C) strains is thought to also contribute to the emergence of cVDPVs with enhanced transmissibility, replication, and/or neurovirulence (Jegouic et al., 2009; Bessaud et al., 2016). Most cVDPVs detected to date have recombinant genomes typically composed of a P1 region (encoding capsid proteins) derived from parental OPV and P2–P3 regions (encoding non-structural proteins) derived from non-vaccine viruses, most likely NPEV-C strains (Kew et al., 2005; Combelas et al., 2011). The NPEV-C sequences found in the P2–P3 regions of

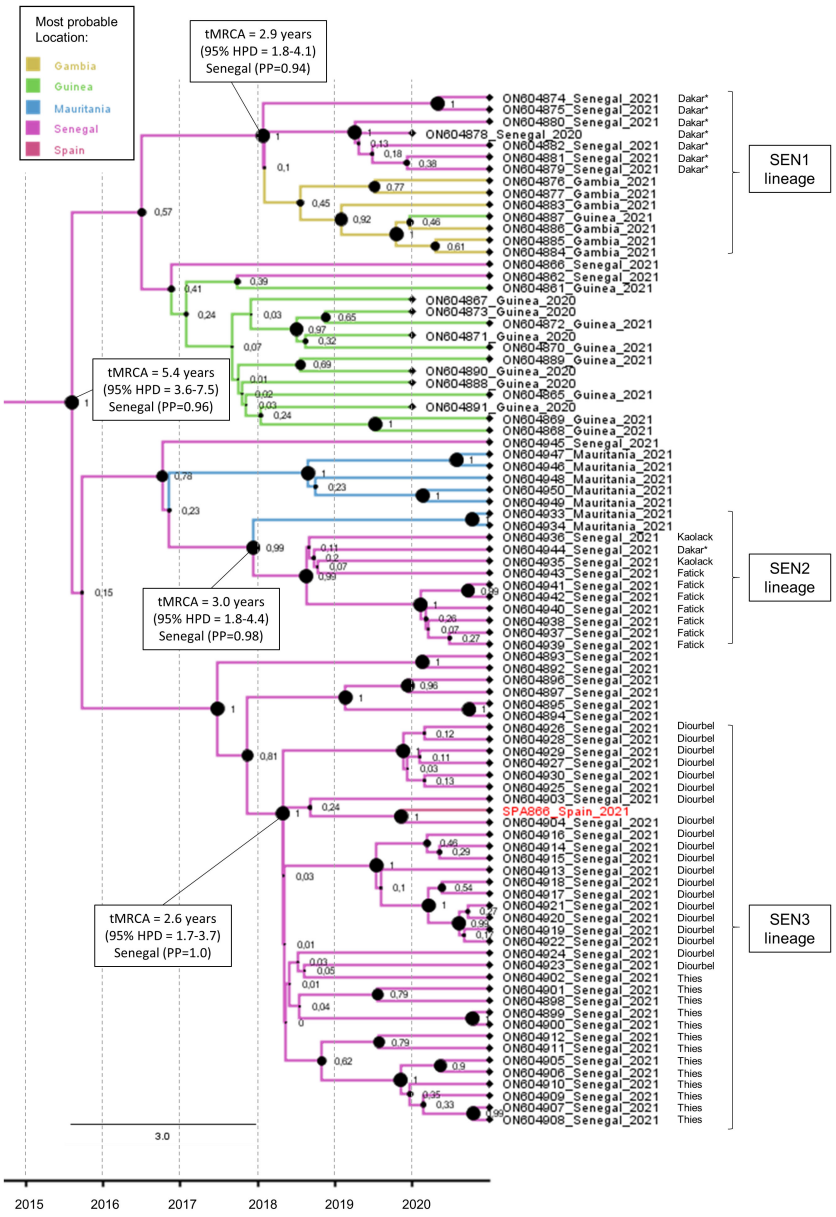

FIGURE 3
Maximum clade credibility (MCC) subtree of the 86 VP1 coding sequences branching with the SPA866 sequence. Branch colors indicate the most probable location of the MRCA. Node support values are indicated by their values and node size. The scale axis represents the estimated dating of the MRCA for each cluster. The regions within Senegal where samples were taken are indicated. Samples from sewage are indicated by an asterisk.

previously described pathogenic cVDPVs are CVA17, CVA20, CVA11, and CVA13 (Rakoto-Andrianarivelo et al., 2007; Faleye et al., 2019). In our study, we similarly observed that strain SPA866 may be a vaccine/non-vaccine recombinant given that P2–P3 regions showed high divergences (18.8% and 17%, respectively) with Sabin 2, suggesting that the putative non-OPV sequence of SPA866 was derived from co-circulating NPEV-C. However, the parental NPEV-C strain of the non-capsid sequence could not be identified. This could be due to the scarce number of complete genome sequences for NPEV-C in public databases. For instance, only seven full-genome CVA17 strains were found in GenBank, of which four were from Africa (Madagascar, 2001–2011). Similarly, only one CVA20 from West Africa was found in GenBank (Nigeria, 2016). Another major limitation for recombination analyses was that all NPEV-C sequences retrieved from GenBank were distant both geographically and in time from study strain SPA866 (imported from Senegal, 2021). Future whole-genome sequencing of co-circulating human NPEV-C strains from West African countries, such as Senegal, Guinea, and Mauritania, will provide a clearer picture of the contribution of recombinants to the emergence of West African VDPVs. Vaccine/non-vaccine breakpoints in the genomes of recombinant VDPVs are usually located at the end of the 2A- or 2B-coding sequences, although they may also be found close to the vaccine/non-vaccine junction or in the P3 region (Rakoto-Andrianarivelo et al., 2007; Bessaud et al., 2016; Faleye et al., 2019; Joffret et al., 2021). Here we show that the

likely site of recombination of strain SPA866 is in the 2A region, which is in accordance with previous studies describing breakpoints in the genomes of recombinant VDPVs type-2 from Madagascar, Nigeria, and the Central African Republic located at this position (Rakoto-Andrianarivelo et al., 2007; Faleye et al., 2019; Joffret et al., 2021).

A whole-genome sequence might be needed for a higher resolution molecular analysis of poliovirus and is important for the confirmation and classification of a VDPV (Classification and reporting of vaccine-derived polioviruses (VDPV), 2016). For the purposes of poliovirus surveillance, VDPVs are categorized as 1) circulating VDPVs, for which there is evidence of person-to-person transmission in the community, and 2) immunodeficiency-associated VDPVs (iVDPV), which are detected in persons with a primary immunodeficiency (Classification and reporting of vaccine-derived polioviruses (VDPV), 2016). Analysis of whole poliovirus genomes using unbiased metagenomics has important advantages. One is enabling the detection of recombinant genomes. This is useful to facilitate its classification as "circulating" VDPV, given that recombination is favorably favored during person-to-person transmission. Another advantage is the detection of mixtures of poliovirus genomes and genetic variants. This is useful to exclude its classification as iVDPV, given that these are characterized by complex mixtures of poliovirus strains and variants (Classification and reporting of vaccine-derived polioviruses (VDPV), 2016; Montmayeur et al., 2017). In this study, using metagenomics, we observed the recombinant structure of VDPV2 and that no other poliovirus genomes were present in the sample, confirming thus its classification as "circulating" VDPV2.

With our metagenomic protocol, a high percentage of viral reads mapping to the target poliovirus genome per total read (69.5% for stool and 75.8% for isolate) was obtained with a great depth of sequencing coverage (5,931 and 11,581, respectively). This result is in accordance with a previous study that obtained on average 68.5% ± 17.6% of viral reads mapping to reference poliovirus genomes per total read using the same NEB-RNA library kit on poliovirus isolates and a viral RNA kit for nucleic acid extraction (Montmayeur et al., 2017). However, we did not use DNase treatment after nucleic acid extraction to remove host DNA while obtaining highly efficient results and simplifying the steps in the protocol. The use of metagenomic protocols, which are increasingly accessible and affordable, in global poliovirus laboratories during the poliovirus endgame will help not only to expand poliovirus sequencing capacity worldwide but to sequence the whole genome of NPEV-C strains and thus serve in further cVDPV recombination analyses to study their contribution to the emergence of VDPVs.

Polio and NPEVs can remain infectious for as long as 2 months in the sewage. Environmental surveillance by testing wastewater samples is a valuable tool for tracking the distribution of these viruses (Global Polio Eradication Initiative). In Spain, environmental surveillance is not established nationwide but has been conducted in the capital since 1999 to maintain the techniques and protocols to be used when an event of poliovirus importation or an outbreak occurs, such as the one described in this article. Virological results in contacts and wastewater samples contributed to the dismissal poliovirus transmission in the community.

In conclusion, we used a whole-genome sequencing protocol using unbiased metagenomics directly from a clinical sample and from an isolate, obtaining high sequence coverage, efficiency, and throughput. By using this method, we generated the whole genome of an imported VDPV2 in 2021 from Spain. The rates of nt substitutions, the recombinant nature of the genome, and the close genomic linkage with strains from Senegal were consistent with the classification of VDPV2 as a circulating type imported from Senegal. We suggest an ancestral origin in Senegal around 2015 for all VDPV2s circulating in 2020–21 in Senegal, Guinea, Gambia, and Mauritania. Our findings also illustrate the importance of microbiological analysis of environmental samples to rule out further transmission.

Data availability statement

The datasets presented in this study can be found in online repositories. The names of the repository/repositories and accession number(s) can be found in the article/Supplementary Material.

Ethics statement

Ethical review and approval was not required for the study on human participants in accordance with the local legislation and institutional requirements. Written informed consent to participate in this study was provided by the participants' legal guardian/next of kin.

Author contributions

MF-G performed the whole-genome sequencing of the detected VDPV-2 together with phylogenetic and recombination analyses. MC led the National Polio Laboratory and performed the poliovirus virological study of the case and contacts in Spain. FD-F performed the phylogenetic analyses. AM-D led the microbiological laboratory in Murcia. OF and MF performed the microbiological poliovirus study of the case contacts in Senegal. MC-L contributed with the epidemiological data. MG drafted the first version of the manuscript. All authors listed have made a substantial, direct, and intellectual contribution to the work and approved it for publication.

Funding

This study was partially supported by two grants from the Instituto de Salud Carlos III [grant numbers PI18CIII-00017 and PI20CIII/00005].

Acknowledgments

We sincerely thank A. Otero, P. Higueras, and I. Bodega for their contribution to the laboratory investigations and all clinicians and laboratories participating in the Spanish Acute Flaccid Paralysis Surveillance System. We also thank the Genomics and the Bioinformatic Departments in the ISCIII for technical assistance. We thank Camille Jacqueline for technical assistance with phylogenetic analysis. Also thanks to all members of the national technical support group convened for case study and decision-making: B.R. Guzmán-Herrador, J. Masa-Calles, N. López-Perea, M.E. Alarcón-Linares, A. Allende, E. Aznar Cano, M.I. Barranco-Boada, E. Cantero-Gudino, S. Fernández-Balbuena, A. Fernández-Dueñas, L. García-Hernández, V. García-Ortúzar, E. Martínez-Salcedo, M. Ordobás-Gavín, I. Rodero-Garduño, M.J. Sierra Moros, F. Simón-Soria, A. Limia-Sánchez, B. Suárez-Rodríguez. The team at Institut Pasteur de Dakar thanks all the personnel of the WHO-accredited Reference Polio Laboratory for their technical support and the Division of Prevention at the Senegalese MoH in Senegal for sharing the field epidemiological data.

Conflict of interest

The authors declare that the research was conducted in the absence of any commercial or financial relationships that could be construed as a potential conflict of interest.

Publisher's note

All claims expressed in this article are solely those of the authors and do not necessarily represent those of their affiliated organizations, or those of the publisher, the editors and the reviewers. Any product that may be evaluated in this article, or claim that may be made by its manufacturer, is not guaranteed or endorsed by the publisher.

Supplementary material

The Supplementary Material for this article can be found online at: https://www.frontiersin.org/articles/10.3389/fcimb.2023.1168355/full#supplementary-material

References

Adu, F., Iber, J., Bukbuk, D., Gumede, N., Yang, S. J., Jorba, J., et al. (2007). Isolation of recombinant type 2 vaccine-derived poliovirus (VDPV) from a Nigerian child. *Virus Res.* 127 (1), 17–25. doi: 10.1016/j.virusres.2007.03.009

Alleman, M. M., Jorba, J., Henderson, E., Diop, O. M., Shaukat, S., Traoré, M. A., et al. (2021). *Update on vaccine-derived poliovirus outbreaks — worldwide, January 2020–June 2021. MMWR morbidity and mortality weekly report* (USA: Centers for Disease Control and Prevention).

Avellón, A., Cabrerizo, M., De Miguel, T., Pérez-Breña, P., Tenorio, A., Pérez, J. L., et al. (2008). Paralysis case and contact spread of recombinant vaccine-derived poliovirus, Spain. *Emerg Infect. Dis* 14 (11), 1807–1809. doi: 10.3201/eid1411.080517

Bessaud, M., Joffret, M.-L., Blondel, B., Delpeyroux, F., Paul, A. V., Wimmer, E., et al. (2016). Exchanges of genomic domains between poliovirus and other cocirculating species c enteroviruses reveal a high degree of plasticity. *Sci. Rep.* 6 (November), 38831. doi: 10.1038/srep38831

Cabrerizo, M., Calvo, C., Rabella, N., Muñoz-Almagro, C., del Amo, E., Pérez-Ruiz, M., et al. (2014). Design and validation of a real-time RT-PCR for the simultaneous detection of enteroviruses and parechoviruses in clinical samples. *J. Virol Methods* 208, 125–128. doi: 10.1016/j.jviromet.2014.08.008

Cabrerizo, M., Echevarria, J. E., Gonzalez, I., de Miguel, T., and Trallero, G. (2008). Molecular epidemiological study of HEV-b enteroviruses involved in the increase in meningitis cases occurred in Spain during 2006. *J. Med. Virol.* 80 (6), 1018–1024. doi: 10.1002/jmv.21197

Classification and reporting of vaccine-derived polioviruses (VDPV) (2016). *Global polio eradication initiative guidelines* (Geneva, Switzerland: WHO). Available at: http://polioeradication.org/wp-content/uploads/2016/09/Reporting-and-Classification-of-VDPVs.

Combelas, N., Holmblat, B., Joffret, M. L., Colbère-Garapin, F., and Delpeyroux, F. (2011). Recombination between poliovirus and coxsackie a viruses of species c: a model of viral genetic plasticity and emergence. *Viruses* 3 (8), 1460–1484. doi: 10.3390/v3081460

Drummond, A. J., Rambaut, A., Shapiro, B., and Pybus, O. G. (2005). Bayesian Coalescent inference of past population dynamics from molecular sequences. *Mol. Biol. Evol* 22 (5), 1185–1192. doi: 10.1093/molbev/msi103

Faleye, T. O. C., Adewumi, O. M., Olayinka, O. T., and Adeniji, J. A. (2019). Genomic characterization of a coxsackievirus A20 strain recovered from a child with acute flaccid paralysis in Nigeria. *Microbiol. Resource Announcements* 8 (42). doi: 10.1128/MRA.00849-19

Faye., M., Kébé, O., Diop, B., Ndiaye, N., Dosseh, A., Sam, A., et al. (2022). Importation and circulation of vaccine-derived poliovirus serotype 2, Senegal, 2020-2021. *Emerg. Infect. Dis.* 28 (10), 2027–2034. doi: 10.3201/eid2810.220847

Gerloff, N., Sun, H., Mandelbaum, M., Maher, C., Nix, W. A., Zaidi, S., et al. (2018). Diagnostic assay development for poliovirus eradication. *J. Clin. Microbiol* 56 (2). doi: 10.1128/JCM.01624-17

Global Polio Eradication Initiative. Available at: https://polioeradication.org/.

Informe anual (2019) *Vigilancia de la parálisis flácida aguda y vigilancia de enterovirus en españa*. Available at: https://www.isciii.es/QueHacemos/Servicios/VigilanciaSaludPublicaRENAVE/EnfermedadesTransmisibles/Documents (Accessed 31 Jan 2023).

Jegouic, S., Joffret, M. L., Blanchard, C., Riquet, F. B., Perret, C., Pelletier, I., et al. (2009). Recombination between polioviruses and co-circulating coxsackie a viruses: role in the emergence of pathogenic vaccine-derived polioviruses. *PloS Pathog.* 5 (5), e1000412. doi: 10.1371/journal.ppat.1000412

Joffret, M. L., Doté, J. W., Gumede, N., Vignuzzi, M., Bessaud, M., and Gouandjika-Vasilache, I. (2021). Vaccine-derived polioviruses, central African republic, 2019. *Emerg Infect. Dis* 27 (2), 620–623. doi: 10.3201/eid2702.203173

Kew, O. M., Sutter, R. W., De Gourville, E. M., Dowdle, W. R., and Pallansch, M. A. (2005). Vaccine-derived polioviruses and the endgame strategy for global polio eradication. *Annu. Rev. Microbiol* 59, 587–635. doi: 10.1146/annurev.micro.58.030603.123625

López, M. D. C., Cabrerizo, M., Herrador, B. R. G., Masa-Calles, J., Alarcón-Linares, M. E., Allende, A., et al. (2021). An imported case of vaccine-derived poliovirus type 2, Spain in the context of the ongoing polio public health emergency of international concern, September 2021. *Eurosurveillance* 26 (50), 2101068. doi: 10.2807/1560-7917.ES.2021.26.50.2101068

Masa-Calles, J., Torner, N., López-Perea, N., de Mier M de, V. T., Fernández-Martínez, B., Cabrerizo, M., et al. (2018). Acute flaccid paralysis (AFP) surveillance: challenges and opportunities from 18 years' experience, Spain, 1998 to 2015. *Eurosurveillance* 23 (47), 1700423. doi: 10.2807/1560-7917.ES.2018.23.47.1700423

Ministerio de Sanidad, Asuntos Sociales e Igualdad (2016) *Plan de acción en españa para la erradicación de la poliomielitis [Spanish polio eradication strategy]*. Available at: https://www.sanidad.gob.es/profesionales/saludPublica/prevPromocion/vacunacione.

Ministry of Health, Social Services and Equality (2023) *Coberturas de vacunación. datos estadísticos. [Vaccine coverage. statistical data]* (Madrid). Available at: https://pestadistico.inteligenciadegestion.sanidad.gob.es/publico (Accessed 31 Jan 2023).

Montmayeur, A. M., Ng, T. F., Schmidt, A., Zhao, K., Magana, L., Iber, J., et al. (2017). High-throughput next-generation sequencing of polioviruses. *J. Clin. Microbiol.* 55 (2), 606–615. doi: 10.1128/JCM.02121-16

Muslin, C., Mac Kain, A., Bessaud, M., Blondel, B., and Delpeyroux, F. (2019). Recombination in enteroviruses, a multi-step modular evolutionary process. *Viruses* 11 (9), E859. doi: 10.3390/v11090859

Patel, H., Varona, S., Monzón, S., Espinosa-Carrasco, J., Heuer, M. L., Underwood, A., et al. *Nf-core/viralrecon: nf-core/viralrecon v2.4.1 - plastered magnesium marmoset*.

Rakoto-Andrianarivelo, M., Guillot, S., Iber, J., Balanant, J., Blondel, B., Riquet, F., et al. (2007). Co-Circulation and evolution of polioviruses and species c enteroviruses in a district of Madagascar. *PloS Pathog.* 3 (12), e191. doi: 10.1371/journal.ppat.0030191

Rambaut, A., Drummond, A. J., Xie, D., Baele, G., and Suchard, M. A. (2018). Posterior summarization in Bayesian phylogenetics using tracer 1.7. *Systematic Biol.* 67 (5), 901–904. doi: 10.1093/sysbio/syy032

Rambaut, A., Lam, T. T., Carvalho, L. M., and Pybus, O. G. (2016). Exploring the temporal structure of heterochronous sequences using TempEst (formerly path-O-Gen). *Virus Evol* 67 (5), 901–904. doi: 10.1093/ve/vew007

Randazzo, W., Truchado, P., Cuevas-Ferrando, E., Simón, P., Allende, A., and Sánchez, G. (2020). SARS-CoV-2 RNA in wastewater anticipated COVID-19 occurrence in a low prevalence area. *Water Res* 181, 115942. doi: 10.1016/j.watres.2020.115942

Ren, R. B., Moss, E. G., and Racaniello, V. R. (1991). Identification of two determinants that attenuate vaccine-related type 2 poliovirus. *J. Virol.* 65 (3), 1377–1382. doi: 10.1128/jvi.65.3.1377-1382.1991

Shapiro, B., Rambaut, A., and Drummond, A. J. (2006). Choosing appropriate substitution models for the phylogenetic analysis of protein-coding sequences. *Mol. Biol. Evol* 23 (1), 7–9. doi: 10.1093/molbev/msj021

Shulman, L. M., Manor, Y., Handsher, R., Delpeyroux, F., McDonough, M. J., Halmut, T., et al. (2000). Molecular and antigenic characterization of a highly evolved derivative of the type 2 oral poliovaccine strain isolated from sewage in Israel. *J. Clin. Microbiol.* 38 (10), 3729–3734. doi: 10.1128/JCM.38.10.3729-3734.2000

UNICEF Senegal (2022). Available at: https://www.unicef.org/senegal/en/stories/kicking-polio-out-senegal.

Wood, D. E., Lu, J., and Langmead, B. (2019). Improved metagenomic analysis with kraken 2. *Genome Biol* 20 (1), 257. doi: 10.1186/s13059-019-1891-0

World Health Organization (2004a). *Polio laboratory manual. 4th edition* (Geneva, Switzerland: World Health Organization). Available at: http://apps.who.int/iris/bitstream/10665/68762/1/WHO_IVB_04.10.pdf.

World Health Organization (2004b). *An alternative test algorithm for poliovirus isolation and characterization. polio laboratory manual. 4th edition* (Geneva: World Health Organization). Available at: http://polioeradication.org/wp-content/uploads/2017/05/NewAlgorithmForPoliovirusIsola.

World Health Organization (2021a). *Polio eradication strategy 2022–2026: executive summary* (Geneva, Switzerland: World Health Organization). Available at: https://apps.who.int/iris/bitstream/handle/10665/341938/9789240024830-eng.pdf.

World Health Organization (2021b). *35th meeting of the European regional certification commission for poliomyelitis eradication* (Geneva, Switzerland: World Health Organization). Available at: https://www.who.int/europe/publications/i/item/WHO-EURO-2022-5197-44961-64000.

World Health Organization (2022). *Global circulating vaccine-derived poliovirus (cVDPVs)* (Geneva, Switzerland: World Health Organization). Available at: https://polioeradication.org/wp-content/uploads/2022/12/weekly-polio-analyses-cVDPV-20221220.pdf.

frontiers | Frontiers in Cellular and Infection Microbiology

TYPE Original Research
PUBLISHED 15 June 2023
DOI 10.3389/fcimb.2023.1163467

OPEN ACCESS

EDITED BY
Josep Quer,
Vall d'Hebron Research Institute (VHIR), Spain

REVIEWED BY
Shweta Saraswat,
Amity University, India
Sonia Zuñiga,
Spanish National Research Council (CSIC), Spain

*CORRESPONDENCE
Rafael Gutiérrez-López
rafael.gutierrez@inia.csic.es

RECEIVED 10 February 2023
ACCEPTED 23 May 2023
PUBLISHED 15 June 2023

CITATION
Llorente F, Gutiérrez-López R, Pérez-Ramirez E, Sánchez-Seco MP, Herrero L, Jiménez-Clavero MÁ and Vázquez A (2023) Experimental infections in red-legged partridges reveal differences in host competence between West Nile and Usutu virus strains from Southern Spain.
Front. Cell. Infect. Microbiol. 13:1163467.
doi: 10.3389/fcimb.2023.1163467

Experimental infections in red-legged partridges reveal differences in host competence between West Nile and Usutu virus strains from Southern Spain

Francisco Llorente[1], Rafael Gutiérrez-López[1]*, Elisa Pérez-Ramirez[1], María Paz Sánchez-Seco[2,3], Laura Herrero[2,3], Miguel Ángel Jiménez-Clavero[1,4] and Ana Vázquez[2,4]

[1]Centro de Investigación en Sanidad Animal (CISA-INIA), Consejo Superior de Investigaciones Científicas (CSIC), Valdeolmos, Madrid, Spain, [2]Centro Nacional de Microbiología, Instituto de Salud Carlos III, Majadahonda, Madrid, Spain, [3]CIBER Enfermedades Infecciosas (CIBERINFEC), Madrid, Spain, [4]CIBER Epidemiología y Salud Pública (CIBERESP), Madrid, Spain

Introduction: West Nile virus (WNV) and Usutu virus (USUV) are emerging zoonotic arboviruses sharing the same life cycle with mosquitoes as vectors and wild birds as reservoir hosts. The main objective of this study was to characterize the pathogenicity and course of infection of two viral strains (WNV/08 and USUV/09) co-circulating in Southern Spain in a natural host, the red-legged partridge (*Alectoris rufa*), and to compare the results with those obtained with the reference strain WNV/NY99.

Methods: WNV inoculated birds were monitored for clinical and analytical parameters (viral load, viremia, and antibodies) for 15 days post-inoculation.

Results and discussion: Partridges inoculated with WNV/NY99 and WNV/08 strains showed clinical signs such as weight loss, ruffled feathers, and lethargy, which were not observed in USUV/09-inoculated individuals. Although statistically significant differences in mortality were not observed, partridges inoculated with WNV strains developed significantly higher viremia and viral loads in blood than those inoculated with USUV. In addition, the viral genome was detected in organs and feathers of WNV-inoculated partridges, while it was almost undetectable in USUV-inoculated ones. These experimental results indicate that red-legged partridges are susceptible to the assayed Spanish WNV with pathogenicity similar to that observed for the prototype WNV/NY99 strain. By contrast, the USUV/09 strain was not pathogenic for this bird species and elicited extremely low viremia levels, demonstrating that red-legged partridges are not a competent host for the transmission of this USUV strain.

KEYWORDS

vector-borne diseases, arbovirus, flavivirus, birds, experimental infection

Introduction

West Nile virus (WNV) and Usutu virus (USUV) are arthropod-borne viruses belonging to the family *Flaviviridae*, genus *Flavivirus*. Both viruses belong to the Japanese encephalitis virus (JEV) antigenic complex (Calisher & Gould, 2003) and have a similar ecology. Their life cycle involves multiple bird species as amplifying hosts and a wide range of mosquitoes as vectors, with *Culex pipiens* as the main species involved (Busquets et al., 2008; Vázquez et al., 2011; Calzolari et al., 2012; Fros et al., 2015). Although horses and humans are susceptible to the infection (Castillo-Olivares and Wood, 2004; Gaibani et al., 2012; Aberle et al., 2018; Guerrero-Carvajal et al., 2021), they are not competent hosts due to their low and transient viremia, insufficient to transmit the virus to feeding mosquitoes (McLean et al., 2002; Vilibic-Cavlek et al., 2020).

West Nile virus is the etiological agent of a zoonotic disease with a severe impact on human and animal health (Nikolay, 2015). This emerging pathogen has broadly expanded during the last 20 years and is nowadays considered one of the most widespread arboviruses in the world, being present in all continents except Antarctica (Jiménez-Clavero, 2012; Paz, 2015). Although infection in humans is, in most cases, asymptomatic or results in mild clinical signs, a low percentage (<1%) of infected individuals develop severe neurological disease, including encephalitis or meningoencephalitis (Nash et al., 2001; Campbell et al., 2002). In Europe, WNV has been circulating with increasing intensity in the last two decades, spreading to most countries in the continent, except the Northernmost (European Centre for Disease Prevention and Control (ECDC), 2022). Important outbreaks of WNV lineages 1 and 2 in horses and humans have occurred also recently, mainly in eastern countries (2018), Spain (2020), and Italy (2022) (Bakonyi & Haussig, 2020; European Centre for Disease Prevention and Control (ECDC), 2022; Figuerola et al., 2022). Outbreaks in wild birds have also been observed to affect species such as the Northern goshawk (*Accipiter gentilis*) (Aguilera-Sepúlveda et al., 2022), snowy owl (*Bubo scandiacus*), Chinese merganser (*Mergus squamatus*), black-tailed gull (*Larus crassirostris*), great tit (*Parus major*) (Santos et al., 2022), griffon vulture (*Gyps fulvus*), the little owl (*Athene noctua*) (Bravo-Barriga et al., 2021). Although abundant information exists regarding experimental infections of birds with WNV, especially with the WNV/NY99 strain (Komar et al., 2003; Pérez-Ramírez et al., 2014), studies about the pathogenicity of Euro-Mediterranean strains in different avian species are still scarce (Sotelo et al., 2011; Dridi et al., 2013; Lim et al., 2014; Spedicato et al., 2015). In fact, the pathogenicity of new strains is worth to be studied in order to obtain a better understanding of the eco-epidemiology of WNV.

Usutu virus has spread to Europe over the last two decades mainly leading to avian mortalities (Weissenböck et al., 2002; Clé et al., 2019), and although infections in humans are considered asymptomatic or with mild clinical signs, encephalitis or meningoencephalitis cases have also been reported (Cavrini et al., 2009; Pecorari et al., 2009; Gaibani et al., 2013; Nagy et al., 2019; Pacenti et al., 2019). So far, eight lineages of USUV have been described: five European lineages (Europe 1–5) and three African lineages (Africa 1–3) (Cadar et al., 2017). Usutu virus has been identified from mosquitos (Busquets et al., 2008; Calzolari et al., 2012; Jöst et al., 2011; Vázquez et al., 2011) and birds, such as common blackbird (*Turdus merula*) and great gray owl (*Strix nebulosa*), and specific antibodies have been found in common blackbird (*T. merula*), carrion crow (*Corvus corone*), Eurasian magpie (*Pica pica*), house sparrow (*Passer domesticus*), red-legged partridge (*Alectoris rufa*), and common turkey (*Meleagris gallopavo*), among others (Figuerola et al., 2009; Llorente et al., 2013; Clé et al., 2019; Bravo-Barriga et al., 2021; Napp et al., 2021; Marzal et al., 2022). Although USUV distribution in Europe is increasing considerably (Cadar et al., 2017), scarce data from experimental infection in birds are available (Chvala et al., 2005; Chvala et al., 2006; Benzarti et al., 2020; Escribano-Romero et al., 2021; Kuchinsky et al., 2021; Kuchinsky et al., 2022).

In nature, WNV and USUV are often found co-circulating in the same areas, probably due to their similar ecology (Llorente et al., 2013). In Spain, the circulation of WNV and USUV has been known since 2003 (Figuerola et al., 2007) and 2006, respectively (Busquets et al., 2008). West Nile virus was isolated for the first time in Spain in 2007 from vertebrate hosts (golden eagle, *Aquila chrysaetos*; Jimenez-Clavero et al., 2008) and identified in vectors in 2006 (*C. pipiens*; Vázquez et al., 2010) and 2008 (*Culex perexiguus*; Vázquez et al., 2011). Usutu virus was detected in vectors in 2006 (*C. pipiens*; Busquets et al., 2008). In addition, in the south of Spain, serological evidence supports the co-circulation of both viruses in the same populations of red-legged partridge (Llorente et al., 2013). This fact could indicate that this species can play a relevant role in the epidemiology of these flaviviruses in Spain. Moreover, it has been shown as a suitable animal model for WNV experimental research. Notably, it was found to reach viremic levels high enough to infect mosquitoes (i.e., it is a competent host). Furthermore, it is useful to discriminate between WNV strains in terms of pathogenicity (Sotelo et al., 2011; Pérez-Ramírez et al., 2018; Gamino et al., 2021). However, the susceptibility of this wild bird species to USUV infection and disease, as well as its competence for virus transmission and overall epidemiological role, is still unclear.

In Southern Spain, WNV lineage 1 and a USUV Africa 2 lineage strains were detected from mosquitoes *C. perexiguus* in 2008 and 2009, respectively (Vázquez et al., 2011). In this area, co-circulation of WNV and USUV has been detected in birds and vectors (Llorente et al., 2013), and numerous human cases of WNV infections have been noted (Rodríguez-Alarcón et al., 2021). However, the pathogenicity of these WNV and USUV strains in wild bird hosts is still unknown.

Therefore, the main aim of this study is to evaluate the course of the infection of the WNV strain (WNV/08) and the USUV strain (USUV/09) isolated from Southwestern Spain in bird hosts by means of experimental inoculations in the red-legged partridge bird model. We examined mortality, morbidity, viremia, and virus load in blood, feathers, oral swabs, and organs and seroconversion in order to evaluate the pathogenic potential of these two flaviviruses and the potential role of the red-legged partridge as a competent reservoir host in nature.

Materials and methods

Viruses and virus preparations

Two strains of WNV (WNV/NY99, North American reference strain, and WNV/08 Spanish strain) and one Spanish strain of USUV (USUV/09) were used in this study. The origins of the Spanish strains can be consulted in Vázquez et al. (2011), and details about passage since isolation are described in Table 1. All the strains were titrated by plaque assay in Vero cells, and virus titers were given in plaque-forming units (pfu).

Experimental inoculations of red-legged partridges

Six-week-old red-legged partridges (*A. rufa*) (n = 39) were obtained from the Lugar Nuevo breeding facility (Estación de Referencia de la Perdiz Roja, Consejería de Medio Ambiente y Ordenación del Territorio-Junta de Andalucía, Andújar, Spain, 38° 16′N; 4°6′W). The partridges were transported to the biosafety level 3 (BSL-3) facilities at CISA-INIA (Centro de Investigación en Sanidad Animal, Valdeolmos, Spain) and distributed in four groups in wire mesh cages (three cages with 10 birds and another with 9) after external deparasitation. The partridges were provided with a commercial diet for game birds and water *ad libitum* throughout the experiment. Previous exposure of the individuals to WNV and USUV was evaluated serologically using a commercially available competitive ELISA (INgezim West Nile Compac, INGENASA, Madrid, Spain) and virologically by real-time RT-PCR (Del Amo et al., 2013).

After 7 days for acclimatization, three groups composed of 10, 10, and 9 red-legged partridges in their seventh week of age were inoculated subcutaneously in the neck (10^4 pfu/individual) with the strains WNV/NY99, WNV/08, and USUV/09, respectively. The inocula were diluted in 100 µl/individual of phosphate-buffered saline (PBS) with 0.2% bovine serum albumin (BSA). The fourth group (negative control group, n = 10) was sham-inoculated with an equivalent volume of PBS with 0.2% BSA and maintained in a separate cage.

Animal care, handling, and experimental procedures were authorized by the INIA Committee of Ethics and Animal Experimentation (reference: 10/033826).

Clinical follow-up and collection of samples

Partridges were observed daily for disease symptoms up to 15 days post-inoculation (dpi). All the birds were weighed at 1, 3, 5, 7, 9, 12, and 15 dpi. To assess the course of viremia and viral load in blood, samples were collected at 1, 3, 5, 7, and 9 dpi. Blood (0.1 ml) was collected in sterile polypropylene tubes filled with 0.9 ml of BA-1 diluent (Hanks M-199 salts, 0.05 M Tris, pH 7.6, 1% BSA, 0.35 g/L of sodium bicarbonate, 100 U/ml of penicillin, 100 µg/ml of streptomycin, and 1 µg/ml of amphotericin B) and stored at −80° C until analysis. To assess the antibody response, a second blood sample (0.1–0.2 ml/individual) was collected at 3, 5, 7, 9, 12, and 15 dpi in dry tubes and allowed to clot at 37°C for 1 h followed by overnight incubation at 4°C to obtain serum. Oropharyngeal swabs and immature rump feathers were collected at 1, 3, 5, 7, 9 12, and 15 dpi. Swabs were placed in sterile polypropylene tubes containing 1 ml of PBS, and feathers were collected in empty sterile polypropylene tubes. Both types of samples were stored at −80°C until analysis. At 15 dpi, three animals from each group were necropsied, and samples (approximately 0.1 g) of the brain, heart, kidney, spleen, and liver were collected in tubes containing 0.9 ml of PBS for PCR analysis. The individual that died during the experiment was necropsied, and samples of the brain, heart, kidney, spleen, and liver were collected. Single-use scalpels and forceps were used to avoid cross-contamination. Sham-inoculated (negative control group) partridges were handled, sampled, and analyzed in parallel, exactly in the same way as the virus-inoculated groups.

Virus detection assays

Viremia was measured by standard plaque formation assays as described (Payne et al., 2006). The viral genome was extracted following different previous preparation steps depending on the type of sample. Blood samples, diluted in 0.9 ml of BA-1 (see above), were centrifuged at 6,000 ×*g* for 5 min, and 200 µl from the supernatant was used for RNA extraction. For feathers, the vascular pulp was aseptically removed from the umbilicus with forceps and placed in tubes containing 0.9 ml of PBS (one pulp per sampling day and animal). Tissues from necropsies and feather pulps in PBS were homogenized for 2 min at 30 cycles/s using a TissueLyser

TABLE 1 Viral strains used in this study, origins, sources, and the number of passages in cell culture.

Virus strain	Geographic origin	Species	Year of isolation	Cell passage number	GenBank accession number	Source of the strain
WNV/NY99 (NY99crow-V76/1)	New York NY (USA)	American crow	1999	VR-6p	FJ51394	Diagnostic Virology Laboratory Dept. of Agriculture (USDA), Ames, IA, USA
WNV/08 (HU6365/08)	(Spain)	*Culex perexiguus*	2008	VR-2p	JF707789	Instituto de Salud Carlos III (ISCIII)
USUV/09 (HU10279/09)	(Spain)	*C. perexiguus*	2009	VR-4p	MN813489	Instituto de Salud Carlos III (ISCIII)

VR, vero cells.

homogenizer (QIAGEN, Valencia, CA, USA) followed by a centrifugation step at 6,000 ×*g* for 5 min to clarify homogenates. The swab suspensions were vortexed and then clarified at 6,000 ×*g* for 5 min. RNA from blood, organs, feathers, and swabs was extracted using BioSprint 15 platform (QIAGEN) and subjected to real-time RT-PCR (RRT-PCR), as described previously (Del Amo et al., 2013). Samples with Ct > 40.0 were considered negative (Del Amo et al., 2013).

Antibody detection assays

Virus-neutralizing antibodies in serum were titrated by virus neutralization test (VNT) in 96-well microplates as described (Llorente et al., 2019). Serum dilutions (from 1:5 to 1:1,280) were assayed in parallel against the reference strains WNV Eg-101 (GenBank accession number AF260968) or USUV SAAR-1776 (GenBank accession number AY453412).

Statistical analyses

The survival curves between the groups of partridges infected with the different strains were calculated by Kaplan–Meier analysis and analyzed by log-rank test using IBM SPSS (IBM Corporation). Differences in weight variations during the experiment (dependent variable) among groups were analyzed by means of linear mixed models. The variables day, viral strain, and the interaction between both were included as independent factors. Individual identity was included as a random factor. Differences in body weight variation among groups at specific dpi were analyzed by a pairwise t-test. Viral genome load in blood, feathers, and oral swabs were compared between the groups infected with WNV using the Kruskal–Wallis test. Statistical analyses were run in R software 3.2.5 (R Core Team, 2016) using the package *lme4* (Bates et al., 2015).

Results

Pathogenicity for red-legged partridge

All partridges inoculated with either WNV/08 or WNV/NY99 showed unspecific clinical signs (e.g., weight loss, ruffled feathers, and lethargy), while no clinical signs were observed in partridges inoculated with USUV/09. Statistically significant differences in weight variation during the infection were observed between groups. Weight gain throughout the experiment was significantly lower in the individuals infected with WNV/NY99 (estimate = −0.541; Std. error = 0.089; p-value < 0.001) or with WNV/08 (estimate = −0.478; Std. error = 0.087; p-value < 0.001) in comparison with the negative control group. However, the group infected with USUV/09 did not show a significant difference in weight during the experiment in comparison with the negative control group (estimate = −0.118; Std. error = 0.089; p-value = 0.181) (Figure 1). Statistically significant differences in body weight variation between the control and WNV/08-inoculated group were observed at specific dpi (at 7 dpi, p = 0.02; at 9 dpi, p = 0.02; at 12 dpi, p = 0.04) and between control and WNV/NY99 (at 7 dpi, p = 0.02; at 9 dpi, p = 0.02).

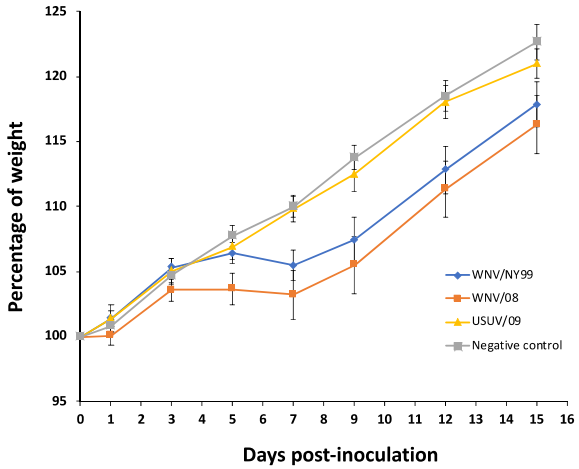

FIGURE 1
Weight curve of red-legged partridges after virus inoculation expressed as the percentage of initial weight through different days post-inoculation. Bars represent the standard error of the mean.

Only one bird infected with WNV/08 died at 7 dpi, but non-significant differences in mortality rate in this group in comparison with the other groups were detected (p = 0.317).

Birds inoculated with WNV/NY99 or WNV/08 strains started to show symptoms at 5–7 dpi. From this day on, surviving partridges started to gain weight, although the average weight in the WNV-inoculated groups remained lower than in the USUV group and the negative control group at the end of the experiment (Figure 1). The control group stayed healthy and steadily increased weight during the experiment as expected for the age of the birds (7 weeks old at the start of the experiment).

Viral detection in blood, feathers, oral swabs, and organs

All WNV-inoculated partridges developed a detectable virus genome in blood from 1 to 9 dpi, with a peak of viral RNA load at 3 dpi. Non-significant differences in average Ct values between WNV strains were found throughout the experiment (29.35 for WNV/NY99 and 29.11 for WNV/08) (χ^2 = 0.79, d.f. = 1, p-value = 0.37) (Figure 2). Regarding the USUV/09-inoculated group, viral RNA load in blood was detected, at a high Ct value (i.e., >36), in 60% (6/10) of the individuals at 3 or 5 dpi (Figure 2).

All inoculated partridges developed detectable viremia by plaque assay for both WNV strains analyzed. The viremia peak was observed at 3 dpi. Statistically significant differences were detected between the two WNV-inoculated groups, with WNV/08 giving higher viremia titers (1.97×10^6 pfu/ml) than WNV/NY99 (6×10^5 pfu/ml) (p = 0.04). Only three partridges developed detectable viremia at 3 dpi for USUV/09 and only one at 5 dpi. The viremia peak was also observed at 3 dpi with a mean of 8×10^2 pfu/ml (Figure 3).

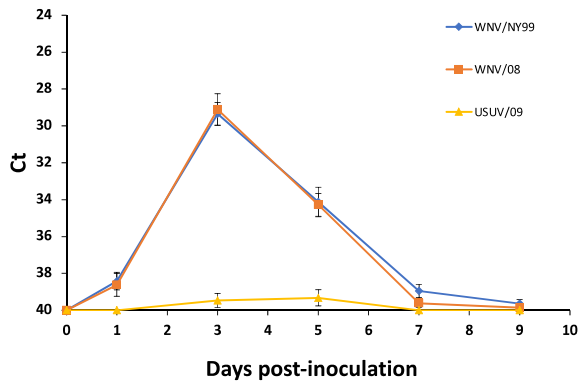

FIGURE 2
Mean daily blood viral genome load for the three inoculated virus groups. Each point represents the mean Ct obtained for the surviving individuals at different times post-inoculation. Bars represent the standard error of the mean.

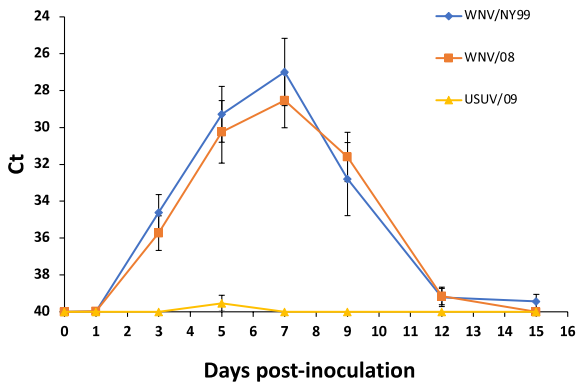

FIGURE 4
Viral genome load of feather pulps collected from the surviving individuals of the three inoculated virus groups at different days post-inoculation. Bars represent standard error of the mean.

In feathers, viral genome load was similar in WNV/NY99 and WNV/08 groups ($\chi^2 = 0.85$, d.f. = 1, p-value = 0.36), with the peak at 7 dpi with average Ct values of 26.99 for WNV/NY99 and 28.54 for WNV/08 (Figure 4). For USUV/09-infected birds, only one individual showed viral genome in feathers at 5 dpi with a Ct value of 35.86 (Figure 4).

West Nile virus genome was detected in oral swabs of the inoculated partridges from 3 dpi to the end of the experiment (15 dpi) but at lower viral RNA loads than in blood and feathers. Statistically significant differences were not observed in the two WNV-inoculated groups ($\chi^2 = 0.13$, d.f. = 1, p-value = 0.72). The peak of viral RNA load in swabs was reached at 7 dpi for both WNV strains at Ct values of 34.20 for WNV/NY99 and 33.72 for WNV/08 (Figure 5). In the USUV-inoculated group, the virus genome was detected in oral swabs only in two birds at 7 dpi at extremely low rates (Ct values of 39.49 and 39.97, respectively).

At the end of the experiment, in the WNV/NY99-inoculated group, low viral RNA loads were detected in some of the organs (brain, heart, kidney, or spleen) of the three animals analyzed. The highest viral RNA load was obtained in the brain, while the virus genome was completely absent from the liver. In the group inoculated with WNV/08, the viral genome was found only in the heart and spleen from one out of three analyzed birds at 15 dpi, with the highest viral RNA load detected in the heart. In the bird that succumbed to the WNV/08 infection at 7 dpi, the viral genome was detected in all the organs analyzed (brain, heart, liver, kidney, and spleen), with the highest viral RNA load in the kidney and the lowest in the liver. The Usutu virus genome was not detected in any of the organs of the three animals analyzed at 15 dpi (Table 2).

Seroconversion

All surviving partridges inoculated with WNV and USUV developed antibodies. Neutralizing antibodies were first observed at 5 dpi. By day 7, all inoculated individuals had seroconverted, reaching maximum neutralizing antibody titers at 9–15 dpi (Figure 6).

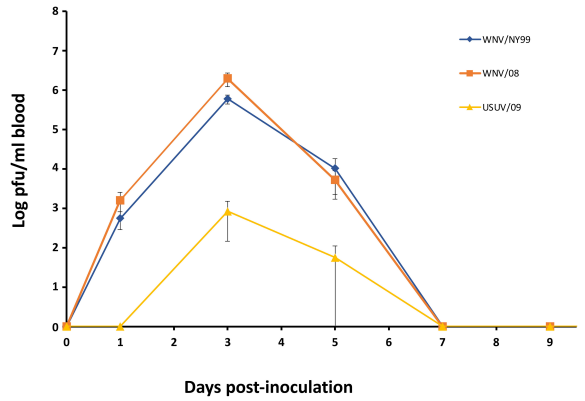

FIGURE 3
Mean daily viremia for the three inoculated virus groups. Each point represents the mean viremia for the surviving individuals at different times post-inoculation. Bars represent the standard error of the mean.

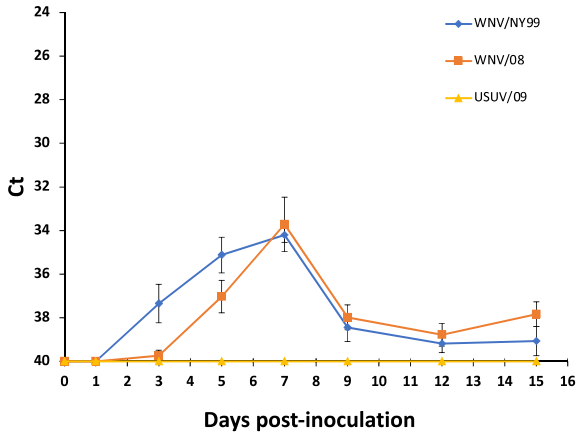

FIGURE 5
Viral genome load of oropharyngeal swabs collected from the surviving individuals of the three inoculated virus groups at different days post-inoculation. Bars represent standard error of the mean.

TABLE 2 Virus genome (Ct values) in organs by day post-inoculation and virus strain.

Virus strain	dpi	Brain	Heart	Kidney	Liver	Spleen
WNV/NY99	15	Neg.	37.9	Neg.	Neg.	Neg.
	15	33.8	Neg.	37.5	Neg.	Neg.
	15	36	Neg.	Neg.	Neg.	37.1
WNV/08	7*	26.6	26.7	24.6	37.9	26.4
	15	Neg.	32.9	Neg.	Neg.	35.2
	15	Neg.	Neg.	Neg.	Neg.	Neg.
	15	Neg.	Neg.	Neg.	Neg.	Neg.
USUV/09	15	Neg.	Neg.	Neg.	Neg.	Neg.
	15	Neg.	Neg.	Neg.	Neg.	Neg.
	15	Neg.	Neg.	Neg.	Neg.	Neg.

Ct values ≥40 are considered negative (neg.).
* Lethally infected partridge.

Discussion

Our results show that red-legged partridges are susceptible to WNV/NY99, WNV/08, and USUV/09 infection. However, on the basis of the observed viremia and viral loads in blood, it seems that this species is a competent host for analyzed WNV isolates but not for USUV.

Previous studies have evidenced that red-legged partridges are susceptible to infection and disease and are transmission-competent hosts for several L1 and L2 WNV strains (Sotelo et al., 2011; Pérez-Ramírez et al., 2018). In these studies, important differences in terms of host competence capacity and pathogenicity for the different strains studied were observed (Sotelo et al., 2011; Pérez-Ramírez et al., 2018). However, the WNV strains analyzed in our study (WNV/08 and WNV/NY99) did not differ in either viral loads in blood or pathogenicity for the infected animals. Both strains produced similar morbidity, and although one individual infected with WNV/08 died, this did not mean a significant difference in mortality between both strains. Indeed, viral load profiles in organs, feathers, and oropharyngeal swabs during the infection were also similar. Infection of both WNV strains analyzed (WNV/NY99 and WNV/08) induced viremia values over 10^5 pfu/ml, which is the value considered as the threshold necessary to infect a mosquito that may feed on an infected bird (see Komar et al., 2003). Consequently, the red-legged partridge would constitute a competent host for these two strains. Thus, our results support a potential role for the red-legged partridge in the transmission of WNV in Southern Spain, where this species is endemic and the virus circulates intensively with new cases reported in every transmission season (Figuerola et al., 2022).

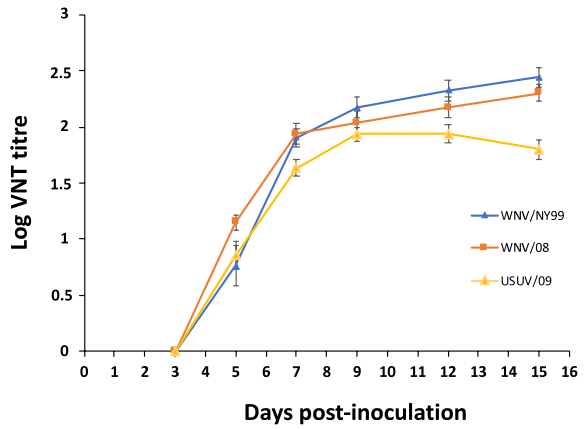

FIGURE 6
Neutralizing antibody response in serum of inoculated red-legged partridges measured by virus neutralization test. Bars represent standard error of the means.

Regarding USUV, the virus has caused numerous deaths in birds in European countries (Weissenböck et al., 2002; Ziegler et al., 2015; Vilibic-Cavlek et al., 2020), and USUV-specific antibodies have been found in a larger range of wild bird species (Figuerola et al., 2009; Manarolla et al., 2010; Becker et al., 2012; Llorente et al., 2013; Michel et al., 2019; Bravo-Barriga et al., 2021; Napp et al., 2021; Marzal et al., 2022), evidencing exposure to USUV infection and its circulation in different European countries. However, little is known about the competence capacity of different bird species for USUV transmission due to the very scarce experimental studies performed in wild birds, particularly in natural reservoir hosts. To our knowledge, USUV experimental infection trials have been carried out in only five avian species: domestic goose (*Anser anser* f. *domestica*) (Chvala et al., 2006), domestic chicken (*Gallus gallus domesticus*) (Chvala et al., 2005; Kuchinsky et al., 2021), domestic canary (*Serinus canaria*) (Benzarti et al., 2020), Eurasian magpie (Escribano-Romero et al., 2021), and house sparrow (Kuchinsky et al., 2022). Only canaries and sparrows developed viremia levels high enough to be considered competent hosts (Benzarti et al., 2020; Kuchinsky et al., 2022). However, domestic geese, Eurasian magpies, and domestic chickens infected with USUV did not show clinical signs and did not develop high viremia levels (Chvala et al., 2005; Chvala et al., 2006; Escribano-Romero et al., 2021).

From the data of viremia and viral load in blood obtained in this study, we have found out that the red-legged partridge is susceptible

to USUV infection. Nevertheless, only 30% of the infected animals showed detectable viremia, and the mean peak of viremia at 3 dpi is very low, under 10^3, being lower than the threshold necessary to infect a mosquito (Kuchinsky et al., 2022). Considering these data, partridge is not a competent host for USUV.

While we did not observe relevant differences in mortality rates between WNV and USUV, important differences were evidenced in terms of morbidity. West Nile virus-infected animals suffered a significant delay in weight gain as compared to the control birds. By contrast, USUV-infected partridges gained weight at a similar rate as the control group, which suggests that USUV is not pathogenic for red-legged partridges. Similar results were found for domestic canaries and house sparrows by Benzarti et al. (2020) and Kuchinsky et al. (2022), respectively.

The USUV/09 strain has been inoculated previously in 2-day-old chickens by Kuchinsky et al. (2021). They found that all the chickens survived and that no clinical signs of disease, including weight loss, were observed, but the individuals showed high viremia levels (i.e., >5 Log_{10} pfu/ml) (Kuchinsky et al., 2021). These viremia values could be due to the age of the individuals considering that 2-week-old chickens did not show high viremia (Chvala et al., 2005). In addition, the USUV/09 strain has been also inoculated in knockout mice (interferon α/β receptor 1 knockout (Ifnar1−/−)) showing similar pathogenicity as the African USUV strains (South Africa 1959, Uganda 2010, and Senegal 2003) and higher pathogenicity than the European USUV strain (USUV Netherlands 2016) (Kuchinsky et al., 2020).

Interestingly, the previous studies of experimental USUV infections in birds (Benzarti et al., 2020; Kuchinsky et al., 2022) point to an association of host competence and susceptibility to USUV infection with bird families, where passerines (sparrow and canary) are competent hosts and highly susceptible to USUV infection, whereas ducks and chickens (Anatidae and Phasianidae families, respectively) seem to be not competent hosts and barely susceptible to USUV infection. This is in agreement with the field observations, where most USUV detections in Europe are found in passerines. Our results observed in red-legged partridges, belonging to the Phasianidae family, are in line with these observations. However, more USUV experimental infection studies with other avian species are needed to find out which species could act as competent hosts or even as super spreaders. Likewise, differences in viremia levels or clinical signs after infection could vary depending on the USUV strain involved, as already demonstrated for WNV. Until now, to our knowledge, only one study has evaluated the susceptibility of wild birds (i.e., house sparrows) to different USUV strains (Uganda 2012 and the Netherlands 2016 belonging to Africa 3 and Europe 3 lineages, respectively), finding differences in the competence between them (Kuchinsky et al., 2022). It would be advisable to experimentally assess other recent WNV and USUV strains circulating in Europe to gain a better understanding of the transmission dynamics of these viruses in the wild.

Conclusion

In summary, we established that red-legged partridges are susceptible to the infection by WNV/08 strain, showing a similar pathogenicity as for WNV/NY99 strain. However, although red-legged partridges are susceptible to the infection by USUV/09, they are not competent hosts for the transmission of this strain. Further studies using different avian species and a variety of WNV and USUV strains co-circulating in Europe are necessary to understand the complex transmission dynamics of both viruses.

Data availability statement

The raw data supporting the conclusions of this article will be made available by the authors, without undue reservation.

Ethics statement

Animal care, handling and experimental procedures were authorized by the INIA Committee of Ethics and Animal Experimentation (Reference: 10/033826).

Author contributions

FL, MJ-C, and AV conceived and designed the study. FL, EP-R, RG-L, LH, and AV performed the methodology and the experimental infection. FL, EP-R, and RG-L analyzed the samples and the data. RGL led the writing of the manuscript. FL, RG-L, EP-R, LH, MS-S, MJ-C, and AV reviewed and contributed critically to the drafts. All authors contributed to the article and approved the submitted version.

Funding

This research was funded by the projects PI14CIII/00014 and PI19CIII_00014 from the Instituto de Salud Carlos III. RG-L was funded by a Juan de la Cierva 2019 Formación contract (FJC2019-041291-I) from the Ministry of Science and Innovation.

Acknowledgments

We thank Maria del Carmen Barbero and Cristina Cano for their help in the laboratory and during the development of the experiment.

Conflict of interest

The authors declare that the research was conducted in the absence of any commercial or financial relationships that could be construed as a potential conflict of interest.

Publisher's note

References

Aberle, S. W., Kolodziejek, J., Jungbauer, C., Stiasny, K., Aberle, J. H., Zoufaly, A., et al. (2018). Increase in human West Nile and usutu virus infections, Austria 2018. *Eurosurveillance* 23 (43), 1800545. doi: 10.2807/1560-7917

Aguilera-Sepúlveda, P., Gómez-Martín, B., Agüero, M., Jiménez-Clavero, M.Á., and Fernández-Pinero, J. (2022). A new cluster of West Nile virus lineage 1 isolated from a northern goshawk in Spain. *Transbound. Emerg. Dis.* 69 (5), 3121–3127. doi: 10.1111/tbed.14399

Bakonyi, T., and Haussig, J. M. (2020). West Nile Virus keeps on moving up in Europe. *Eurosurveillance* 25 (46), 2001938. doi: 10.2807/1560-7917

Bates, D., Mächler, M., Bolker, B., and Walker, S. (2015). Fitting linear mixed-effects models using lme4. *J. Stat. Softw.* 67 (1), 1–48. doi: 10.48550/arXiv.1406.5823

Becker, N., Jöst, H., Ziegler, U., Eiden, M., Höper, D., Emmerich, P., et al. (2012). Epizootic emergence of usutu virus in wild and captive birds in Germany. *PloS One* 7 (2), e32604. doi: 10.1371/journal.pone.0032604

Benzarti, E., Rivas, J., Sarlet, M., Franssen, M., Desmecht, D., Schmidt-Chanasit, J., et al. (2020). Experimental usutu virus infection in domestic canaries *Serinus canaria*. *Viruses* 12 (2), 164. doi: 10.3390/v12020164

Bravo-Barriga, D., Aguilera-Sepúlveda, P., Guerrero-Carvajal, F., Llorente, F., Reina, D., Pérez-Martín, J. E., et al. (2021). West Nile And usutu virus infections in wild birds admitted to rehabilitation centres in extremadura, western Spain 2017–2019. *Vet. Microbiol.* 255, 109020. doi: 10.1016/j.vetmic.2021.109020

Busquets, N., Alba, A., Allepuz, A., Aranda, C., and Nuñez, J. I. (2008). Usutu virus sequences in *Culex pipiens* (Diptera: culicidae), Spain. *Emerg. Infect. Dis.* 14 (5), 861. doi: 10.3201/eid1405.071577

Cadar, D., Lühken, R., van der Jeugd, H., Garigliany, M., Ziegler, U., Keller, M., et al. (2017). Widespread activity of multiple lineages of usutu virus, western Europe 2016. *Eurosurveillance* 22 (4), 30452. doi: 10.2807/1560-7917

Calisher, C. H., and Gould, E. A. (2003). Taxonomy of the virus family flaviviridae. *Adv. Virus Res.* 59, 1–19. doi: 10.1016/s0065-3527(03)59001-7

Calzolari, M., Gaibani, P., Bellini, R., Defilippo, F., Pierro, A., Albieri, A., et al. (2012). Mosquito, bird and human surveillance of West Nile and usutu viruses in Emilia-romagna region (Italy) in 2010. *PloS One* 7 (5), e38058. doi: 10.1371/journal.pone.0038058

Campbell, G. L., Marfin, A. A., Lanciotti, R. S., and Gubler, D. J. (2002). West Nile Virus. *Lancet Infect. Dis.* 2 (9), 519–529. doi: 10.1016/S1473-3099(02)00368-7

Castillo-Olivares, J., and Wood, J. (2004). West Nile Virus infection of horses. *Vet. Res.* 35 (4), 467–483. doi: 10.1051/vetres:2004022

Cavrini, F., Gaibani, P., Longo, G., Pierro, A. M., Rossini, G., Bonilauri, P., et al. (2009). Usutu virus infection in a patient who underwent orthotropic liver transplantation, Italy, august-September 2009. *Eurosurveillance* 14 (50), 19448. doi: 10.1080/03079450500268500

Chvala, S., Bakonyi, T., Hackl, R., Hess, M., Nowotny, N., and Weissenböck, H. (2005). Limited pathogenicity of usutu virus for the domestic chicken (*Gallus domesticus*). *Avian Pathol.* 34 (5), 392–395. doi: 10.1080/03079450500268500

Chvala, S., Bakonyi, T., Hackl, R., Hess, M., Nowotny, N., and Weissenböck, H. (2006). Limited pathogenicity of usutu virus for the domestic goose (*Anser anser f. domestica*) following experimental inoculation. *J. Vet. Med. Ser. B* 53 (4), 171–175. doi: 10.1111/j.1439-0450.2006.00942.x

Clé, M., Beck, C., Salinas, S., Lecollinet, S., Gutierrez, S., Van de Perre, P., et al. (2019). Usutu virus: a new threat? *Epidemiol. Infect.* 147, e232. doi: 10.1017/S0950268819001213

Del Amo, J., Sotelo, E., Fernández-Pinero, J., Gallardo, C., Llorente, F., Agüero, M., et al. (2013). A novel quantitative multiplex real-time RT-PCR for the simultaneous detection and differentiation of West Nile virus lineages 1 and 2, and of usutu virus. *J. Virol. Methods* 189 (2), 321–327. doi: 10.1016/j.jviromet.2013.02.019

Dridi, M., Vangeluwe, D., Lecollinet, S., van den Berg, T., and Lambrecht, B. (2013). Experimental infection of carrion crows (*Corvus corone*) with two European West Nile virus (WNV) strains. *Vet. Microbiol.* 165, 160–166. doi: 10.1016/j.vetmic.2012.12.043

Escribano-Romero, E., Jiménez de Oya, N., Camacho, M. C., Blázquez, A. B., Martín-Acebes, M. A., Risalde, M. A., et al. (2021). Previous Usutu virus exposure partially protects magpies (Pica pica) against West Nile virus disease but does not prevent horizontal transmission. *Viruses* 13 (7), 1409.

European Centre for Disease Prevention and Control (ECDC) Weekly updates (2022) *West Nile Virus transmission season*. Available at: https://www.ecdc.europa.eu/en/west-nile-fever/surveillance-and-disease-data/disease-data-ecdc (Accessed 16 January 2023).

Figuerola, J., Baouab, R. E., Soriguer, R., Fassi-Fihri, O., Llorente, F., and Jímenez-Clavero, M. A. (2009). West Nile Virus antibodies in wild birds, Morocco 2008. *Emerg. Infect. Dis.* 15 (10), 1651. doi: 10.3201/eid1510.090340

Figuerola, J., Jiménez-Clavero, M.Á., Ruíz-López, M. J., Llorente, F., Ruiz, S., Hoefer, A., et al. (2022). A one health view of the West Nile virus outbreak in Andalusia (Spain) in 2020. *Emerg. Microbes Infect.* 11, 2570–2578. doi: 10.1080/22221751.2022.2134055

Figuerola, J., Soriguer, R., Rojo, G., Tejedor, C. G., and Jimenez-Clavero, M. A. (2007). Seroconversion in wild birds and local circulation of West Nile virus, Spain. *Emerg. Infect. Dis.* 13 (12), 1915. doi: 10.3201/eid1312.070343

Fros, J. J., Miesen, P., Vogels, C. B., Gaibani, P., Sambri, V., Martina, B. E., et al. (2015). Comparative usutu and West Nile virus transmission potential by local *Culex pipiens* mosquitoes in north-western Europe. *One Health* 1, 31–36. doi: 10.1016/j.onehlt.2015.08.002

Gaibani, P., Cavrini, F., Gould, E. A., Rossini, G., Pierro, A., Landini, M. P., et al. (2013). Comparative genomic and phylogenetic analysis of the first usutu virus isolate from a human patient presenting with neurological symptoms. *PloS One* 8 (5), e64761. doi: 10.1371/journal.pone.0064761

Gaibani, P., Pierro, A., Alicino, R., Rossini, G., Cavrini, F., Landini, M. P., et al. (2012). Detection of usutu-virus-specific IgG in blood donors from northern Italy. *Vector-Borne Zoonotic Dis.* 12 (5), 431–433. doi: 10.1089/vbz.2011.0813

Gamino, V., Pérez-Ramírez, E., Gutiérrez-Guzmán, A. V., Sotelo, E., Llorente, F., Jiménez-Clavero, M.Á., et al. (2021). Pathogenesis of two Western Mediterranean West Nile virus lineage 1 isolates in experimentally infected red-legged partridges (*Alectoris rufa*). *Pathogens* 10 (6), 748. doi: 10.3390/pathogens10060748

Guerrero-Carvajal, F., Bravo-Barriga, D., Martín-Cuervo, M., Aguilera-Sepúlveda, P., Ferraguti, M., Jiménez-Clavero, M.Á., et al. (2021). Serological evidence of co-circulation of West Nile and usutu viruses in equids from western Spain. *Transbound. Emerg. Dis.* 68 (3), 1432–1444. doi: 10.1111/tbed.13810

Jiménez-Clavero, M.Á. (2012). Animal viral diseases and global change: bluetongue and West Nile fever as paradigms. *Front. Genet.* 3. doi: 10.3389/fgene.2012.00105

Jiménez-Clavero, M. A., Sotelo, E., Fernandez-Pinero, J., Llorente, F., Blanco, J. M., Rodriguez-Ramos, J., et al. (2008). West Nile Virus in golden eagles, Spain 2007. *Emerg. Infect. Dis.* 14 (9), 1489. doi: 10.3201/eid1409.080190

Jöst, H., Bialonski, A., Maus, D., Sambri, V., Eiden, M., Groschup, M. H., et al. (2011). Isolation of usutu virus in Germany. *Am. J. Trop. Med. Hyg.* 85 (3), 551. doi: 10.4269/ajtmh.2011.11-0248

Komar, N., Langevin, S., Hinten, S., Nemeth, N., Edwards, E., Hettler, D., et al. (2003). Experimental infection of north American birds with the new York 1999 strain of West Nile virus. *Emerg. Infect. Dis.* 9, 311–322. doi: 10.3201/eid0903.020628

Kuchinsky, S. C., Frere, F., Heitzman-Breen, N., Golden, J., Vázquez, A., Honaker, C. F., et al. (2021). Pathogenesis and shedding of usutu virus in juvenile chickens. *Emerg. Microbes Infect.* 10 (1), 725–738. doi: 10.1080/22221751.2021.1908850

Kuchinsky, S. C., Hawks, S. A., Mossel, E. C., Coutermarsh-Ott, S., and Duggal, N. K. (2020). Differential pathogenesis of usutu virus isolates in mice. *PloS Negl. Trop. Dis.* 14 (10), e0008765. doi: 10.1371/journal.pntd.0008765

Kuchinsky, S. C., Marano, J., Hawks, S. A., Loessberg, E., Honaker, C. F., Siegel, P. B., et al. (2022). North American house sparrows are competent for usutu virus transmission. *Msphere* 7 (6), e00295–e00222. doi: 10.1128/msphere.00295-22

Lim, S. M., Brault, A. C., van Amerongen, G., Sewbalaksing, V. D., Osterhaus, A. D. M. E., Martina, B. E. E., et al. (2014). Susceptibility of European jackdaws (*Corvus monedula*) to experimental infection with lineage 1 and 2 West Nile viruses. *J. Gen. Virol.* 95, 1320–1329. doi: 10.1099/vir.0.063651-0

Llorente, F., García-Irazábal, A., Pérez-Ramírez, E., Cano-Gómez, C., Sarasa, M., Vázquez, A., et al. (2019). Influence of flavivirus co-circulation in serological diagnostics and surveillance: a model of study using West Nile, usutu and bagaza viruses. *Transbound. Emerg. Dis.* 66 (5), 2100–2106. doi: 10.1111/tbed.13262

Llorente, F., Pérez-Ramírez, E., Fernández-Pinero, J., Soriguer, R., Figuerola, J., and Jiménez-Clavero, M.Á. (2013). Flaviviruses in game birds, southern Spain 2011–2012. *Emerg. Infect. Dis.* 19 (6), 1023. doi: 10.3201/eid1906.130122

Manarolla, G., Bakonyi, T., Gallazzi, D., Crosta, L., Weissenböck, H., Dorrestein, G. M., et al. (2010). Usutu virus in wild birds in northern Italy. *Vet. Microbiol.* 141 (1-2), 159–163. doi: 10.1016/j.vetmic.2009.07.036

Marzal, A., Ferraguti, M., Muriel, J., Magallanes, S., Ortiz, J. A., García-Longoria, L., et al. (2022). Circulation of zoonotic flaviviruses in wild passerine birds in Western Spain. *Vet. Microbiol.* 268, 109399. doi: 10.1016/j.vetmic.2022.109399

McLean, R. G., Ubico, S. R., Bourne, D., and Komar, N. (2002). "West Nile Virus in livestock and wildlife," in *Japanese Encephalitis and West Nile viruses*. Eds. J. S. Mackenzie, A. D. T. Barret and V. Deubel (Berlin: Springer), 271–308. doi: 10.1007/978-3-642-59403-8_14

Michel, F., Fischer, D., Eiden, M., Fast, C., Reuschel, M., Müller, K., et al. (2019). West Nile Virus and usutu virus monitoring of wild birds in Germany. *Int. J. Environ. Res. Public Health* 15 (1), 171. doi: 10.3390/ijerph15010171

Nagy, A., Mezei, E., Nagy, O., Bakonyi, T., Csonka, N., Kaposi, M., et al. (2019). Extraordinary increase in West Nile virus cases and first confirmed human usutu virus infection in Hungary 2018. *Eurosurveillance* 24 (28), 1900038. doi: 10.2807/1560-7917

Napp, S., Llorente, F., Beck, C., Jose-Cunilleras, E., Soler, M., Pailler-García, L., et al. (2021). Widespread circulation of flaviviruses in horses and birds in northeastern Spain (Catalonia) between 2010 and 2019. *Viruses* 13 (12), 2404. doi: 10.3390/v13122404

Nash, D., Mostashari, F., Fine, A., Miller, J., O'leary, D., Murray, K., et al. (2001). The outbreak of West Nile virus infection in the new York city area in 1999. *N Engl. J. Med.* 344 (24), 1807–1814. doi: 10.1056/NEJM200106143442401

Nikolay, B. (2015). A review of West Nile and usutu virus co-circulation in Europe: how much do transmission cycles overlap? *Trans. R. Soc. Trop. Med. Hyg.* 109 (10), 609–618. doi: 10.1093/trstmh/trv066

Pacenti, M., Sinigaglia, A., Martello, T., De Rui, M. E., Franchin, E., Pagni, S., et al. (2019). Clinical and virological findings in patients with usutu virus infection, northern ital. *Eurosurveillance* 24 (47), 1900180. doi: 10.2807/1560-7917

Payne, A. F., Binduga-Gajewska, I., Kauffman, E. B., and Kramer, L. D. (2006). Quantitation of flaviviruses by fluorescent focus assay. *J. Virol. Methods* 134 (1-2), 183–189. doi: 10.1016/j.jviromet.2006.01.003

Paz, S. (2015). Climate change impacts on West Nile virus transmission in a global context. *Philos. Trans. R. Soc. B: Biol. Sci.* 370 (1665), 20130561. doi: 10.1098/rstb.2013.0561

Pecorari, M., Longo, G., Gennari, W., Grottola, A., Sabbatini, A. M., Tagliazucchi, S., et al. (2009). First human case of usutu virus neuroinvasive infection, Italy, august-September 2009. *Eurosurveillance* 14 (50), 19446. doi: 10.2807/ese.14.50.19446-en

Pérez-Ramírez, E., Llorente, F., Del Amo, J., Nowotny, N., and Jiménez-Clavero, M.Á. (2018). Susceptibility and role as competent host of the red-legged partridge after infection with lineage 1 and 2 West Nile virus isolates of Mediterranean and central European origin. *Vet. Microbiol.* 222, 39–45. doi: 10.1016/j.vetmic.2018.06.012

Pérez-Ramírez, E., Llorente, F., and Jiménez-Clavero, M.Á. (2014). Experimental infections of wild birds with West Nile virus. *Viruses* 6, 752–781. doi: 10.3390/v6020752

R Core Team. (2016). *R: A language and environment for statistical computing*. Vienna, Austria: R Foundation for Statistical Computing. Available at: http://www.R-project.org.

Rodríguez-Alarcón, L. G. S. M., Fernández-Martínez, B., Moros, M. J. S., Vázquez, A., Pachés, P. J., Villacieros, E. G., et al. (2021). Unprecedented increase of West Nile virus neuroinvasive disease, Spain, summer 2020. *Eurosurveillance* 26 (19), 2002010. doi: 10.2807/1560-7917

Santos, P. D., Michel, F., Wylezich, C., Höper, D., Keller, M., Holicki, C. M., et al. (2022). Co-Infections: simultaneous detections of West Nile virus and usutu virus in birds from Germany. *Transbound. Emerg. Dis.* 69 (2), 776–792. doi: 10.1111/tbed.14050

Sotelo, E., Gutiérrez-Guzmán, A. V., del Amo, J., Llorente, F., El-Harrak, M., Pérez-Ramírez, E., et al. (2011). Pathogenicity of two recent Western Mediterranean West Nile virus isolates in a wild bird species indigenous to southern Europe: the red-legged partridge. *Vet. Res.* 42, 11. doi: 10.1186/1297-9716-42-11

Spedicato, M., Carmine, I., Bellacicco, A. L., Marruchella, G., Marini, V., Pisciella, M., et al. (2015). Experimental infection of rock pigeons (*Columba livia*) with three West Nile virus lineage 1 strains isolated in Italy between 2009 and 2012. *Epidemiol. Infect.* 144, 1301–1311. doi: 10.1017/S0950268815002642

Vázquez, A., Ruiz, S., Herrero, L., Moreno, J., Molero, F., Magallanes, A., et al. (2011). West Nile And usutu viruses in mosquitoes in Spain 2008–2009. *Am. J. Trop. Med. Hyg.* 85 (1), 178. doi: 10.4269/ajtmh.2011.11-0042

Vázquez, A., Sánchez-Seco, M. P., Ruiz, S., Molero, F., Hernandez, L., Moreno, J., et al. (2010). Putative new lineage of West Nile virus, Spain. *Emerg. Infect. Dis.* 16 (3), 549–5452. doi: 10.3201/eid1603.091033

Vilibic-Cavlek, T., Petrovic, T., Savic, V., Barbic, L., Tabain, I., Stevanovic, V., et al. (2020). Epidemiology of usutu virus: the European scenario. *Pathogens* 9 (9), 699. doi: 10.3390/pathogens9090699

Weissenböck, H., Kolodziejek, J., Url, A., Lussy, H., Rebel-Bauder, B., and Nowotny, N. (2002). Emergence of usutu virus, an African mosquito-borne flavivirus of the Japanese encephalitis virus group, central Europe. *Emerg. Infect. Dis.* 8 (7), 652. doi: 10.3201/eid0807.020094

Ziegler, U., Jöst, H., Müller, K., Fischer, D., Rinder, M., Tietze, D. T., et al. (2015). Epidemic spread of usutu virus in southwest Germany in 2011 to 2013 and monitoring of wild birds for usutu and West Nile viruses. *Vector-Borne Zoonotic Dis.* 15 (8), 481–488. doi: 10.1089/vbz.2014.1746

frontiers | Frontiers in Cellular and Infection Microbiology

TYPE Original Research
PUBLISHED 04 July 2023
DOI 10.3389/fcimb.2023.1155867

OPEN ACCESS

EDITED BY
Josep Quer,
Vall d'Hebron Research Institute (VHIR), Spain

REVIEWED BY
Francesca Rovida,
University of Pavia, Italy
Francesco Cerutti,
Ospedale Amedeo di Savoia, Italy

*CORRESPONDENCE
Ana Vázquez
a.vazquez@isciii.es

RECEIVED 31 January 2023
ACCEPTED 19 May 2023
PUBLISHED 04 July 2023

CITATION
Macias A, Martín P, Pérez-Olmeda M, Fernández-Martínez B, Gómez-Barroso D, Fernández E, Ramos JM, Herrero L, Rodríguez S, Delgado E, Sánchez-Seco MP, Galán M, Corbacho AJ, Jimenez M, Montero-Peña C, Valle A and Vázquez A (2023) West Nile virus emergence in humans in Extremadura, Spain 2020. *Front. Cell. Infect. Microbiol.* 13:1155867. doi: 10.3389/fcimb.2023.1155867

West Nile virus emergence in humans in Extremadura, Spain 2020

Alicia Macias[1], Paloma Martín[2], Mayte Pérez-Olmeda[3,4], Beatriz Fernández-Martínez[5,6], Diana Gómez-Barroso[5,6], Esperanza Fernández[7], Julian Mauro Ramos[8], Laura Herrero[3], Saray Rodríguez[1], Elena Delgado[7], Maria Paz Sánchez-Seco[3,4], Miguel Galán[1], Antonio Jesús Corbacho[7], Manuel Jimenez[1], Cristian Montero-Peña[9], Antonio Valle[1] and Ana Vázquez[3,6]*

[1]Servicios de Microbiología y Medicina Interna, Hospital Don Benito-Villanueva de la Serena, Don Benito, Badajoz, Spain, [2]Servicio de Microbiología , Hospital Universitario de Badajoz, Badajoz, Spain, [3]Centro Nacional de Microbiología, Instituto de Salud Carlos III (CNM-ISCIII), Madrid, Spain, [4]CIBER de Enfermedades Infecciosas (CIBERINFEC), Madrid, Spain, [5]Centro Nacional Epidemiología, Instituto de Salud Carlos III (CNE-ISCIII), Madrid, Spain, [6]CIBER de Epidemiología y Salud Pública (CIBERESP), Madrid, Spain, [7]Banco de Sangre de Extremadura, Junta de Extremadura, Mérida, Badajoz, Spain, [8]Subdirección de Epidemiología, Servicio Extremeño de Salud, Mérida, Badajoz, Spain, [9]Servicio Medicina Familiar y Comunitaria, Centro de Salud Don Benito Oeste, Hospital Don Benito-Villanueva, Don Benito, Badajoz, Spain

In Spain, the largest human West Nile virus (WNV) outbreak among humans was reported in 2020, constituting the second most important outbreak in Europe that season. Extremadura (southwestern Spain) was one of the affected areas, reporting six human cases. The first autochthonous human case in Spain was reported in Extremadura in 2004, and no other human cases were reported until 2020. In this work, we describe the first WNV human outbreak registered in Extremadura, focusing on the most important clinical aspects, diagnostic results, and control actions which followed. In 2020, from September to October, human WNV infections were diagnosed using a combination of molecular and serological methods (an in-house specific qRT-PCR and a commercial ELISA for anti-WNV IgM and IgG antibodies) and by analysing serum, urine, and/or cerebrospinal fluid samples. Serological positive serum samples were further tested using commercial kits against related flaviviruses Usutu and Tick-borne encephalitis in order to analyse serological reactivity and to confirm the results by neutralisation assays. In total, six cases of WNV infection (five with neuroinvasive disease and one with fever) were identified. Clinical presentation and laboratory findings are described. No viral RNA was detected in any of the analysed samples, but serological cross-reactivity was detected against the other tested flaviviruses. Molecular and serological methods for WNV detection in various samples as well as differential diagnosis are recommended. The largest number of human cases of WNV infection ever registered in Extremadura, Spain, occurred in 2020 in areas where circulation of WNV and other flaviviruses has been previously

reported in humans and animals. Therefore, it is necessary to enhance surveillance not only for the early detection and implementation of response measures for WNV but also for other emerging flaviviruses that could be endemic in this area.

KEYWORDS

West Nile virus, human infection, flaviviruses, diagnosis, molecular and serological methods, surveillance

Introduction

West Nile virus (WNV) is an important zoonotic virus with symptoms ranging from mild fever to severe lethal neuroinvasive disease in humans. The virus is maintained in an enzootic cycle among mosquitoes belonging to the *Culex* genus and birds, with mammals (equids and humans) being dead-end hosts. In humans, most of the infections are asymptomatic (80%) and those who develop disease, after an incubation period of 2 to 14 days, usually have mild symptoms such as fever, headache, fatigue, malaise, myalgia, arthralgia, rash, lymphadenopathy, and gastrointestinal symptoms (anorexia, nausea, vomiting, or diarrhoea) (Gray and Webb, 2014; Barzon et al., 2015; Bai et al., 2019). Less than 1% of infected cases develop a neuroinvasive disease (WNND) such as encephalitis, meningitis, and acute flaccid paralysis, frequently associated with risk factors such as aging, solid organ transplant, diabetes, hypertension, and other immunosuppression conditions related to fatal outcome (Lindsey et al., 2012). Moreover, atypical or rare presentations of WNV disease (WNVD) such us myocarditis, pancreatitis, hepatitis, cerebellitis, rhabdomyolysis, and ocular manifestations have also been described (Hasbun et al., 2016; Konjevoda et al., 2019; Velasco et al., 2020). WNVD has sometimes been associated with several sequelae, the most frequent being muscle weakness, fatigue, myalgia, memory loss, depression, and difficulty doing activities of daily living (Carson et al., 2006; Hughes et al., 2007). There is no vaccine for humans, and treatment is supportive as there are no specific antiviral drugs.

In humans, the peak of viraemia is 4–8 days post-infection (dpi). Antibodies can be detected in serum after 3–9 dpi, and the WNV IgM generally persists for over 6 months and may still be detectable for up to 1 year (Barzon et al., 2015). The laboratory-based diagnostic approaches are composed of virus isolation, RT-PCR, serology, and pathological examination. The most commonly used molecular diagnostic technique is real-time reverse transcription polymerase chain reaction (qRT-PCR), as it is a very fast and reliable technique, which also quantifies the viral genome. Serologically, diagnosis is based on the detection of IgM and IgG antibodies against WNV. As cross-reactivity with other flaviviruses may occur, the virus neutralisation tes by virus neutralisation tes against WNV remains the gold standard because of its high specificity and ability to detect and quantify neutralising antibodies to the virus (Tardei et al., 2000; Lustig et al., 2018). The limitation of this assay is that it takes a week to obtain results and, in Europe, a biosafety level 3 laboratory is required.

Since its discovery, WNV has caused human and animal disease outbreaks all over the world, except in Antarctica. In Europe, the virus is endemic and emerging in multiple countries. Over the last two decades, there have been notable increases in the number and extension of human and equine cases. Several genetic lineages of the virus have been detected (Vázquez et al., 2010), but lineages 1 and 2 have been mainly responsible for the disease in humans and equids in European countries. According to reports by the European Center for Disease Prevention and Control (ECDC), a significant increase in the number of human cases was observed in 2018 in Europe, eight times higher than in 2017 (ECDC, 2019). Most locally acquired cases were reported by Italy, Greece, and Romania, representing 39%, 20%, and 18% of EU cases, respectively. During 2020, EU/EEA and EU-neighbouring countries reported 336 locally acquired human cases of WNVD, mostly in Greece, Spain, and Italy (ECDC, 2020). Later, in 2021 (ECDC, 2022a) and 2022 (ECDC, 2022b), 139 and 965 human cases respectively were reported in Europe. In Spain, WNV fever is a notifiable disease. The first two notified human cases were detected in Andalusia in 2010 (García-Bocanegra et al., 2011), although the first known human case—diagnosed retrospectively—occurred in 2004 in Badajoz (Extremadura) (Kaptoul et al., 2007). Three additional cases were notified in Andalusia in 2016 (López-Ruiz et al., 2018), and no autochthonous human cases were reported from 2017 to 2019 in Spain. In the summer of 2020, the greatest number of WNV cases in humans in Spain was described (García San Miguel Rodríguez-Alarcón et al., 2021), with 77 cases detected in southwest Spain (71 from Andalusia and 6 from Extremadura) in areas where the virus was detected in previous years in humans, animals, and/or mosquitoes. Between 2021 and 2022, 10 human cases were reported in Spain, eight in Andalusia, and two in Catalonia, but none in Extremadura (ISCIII, 2022). Several studies in Spain have revealed the circulation of WNV in Andalusia during at least the last two decades. Moreover, the presence of WNV through seroprevalence studies is being detected in other Spanish regions (Extremadura, Catalonia, Castilla La Mancha, Castilla León, Comunidad Valenciana, and Mallorca) in birds, horses, and other mammals (Vanhomwegen et al., 2017; Napp et al., 2021; Casades-Martí et al., 2023).

In 2020 in Extremadura, where WNV human cases had not been reported since 2004, six autochthonous WNVD were described in Badajoz province. These cases were detected in areas where circulation of WNV and other flaviviruses, such as Usutu (USUV) and Tick-borne encephalitis (TBEV), has been described in birds, horses, and/or dogs (García-Bocanegra et al., 2018; Bravo-Barriga et al., 2021;

Guerrero-Carvajal et al., 2021). Moreover, in 2020, when the WNV human outbreak occurred, USUV RNA was detected in mosquitoes and USUV-specific antibodies were detected in wild birds close to rural and urban areas, which is indicative of an active circulation and represents a public health threat (Bravo-Barriga et al., 2023). In 2021, no WNV human cases or animal outbreaks were reported through the veterinary surveillance system, and in 2022, there were only three equine outbreaks in Badajoz (Ministry of Agriculture and Fisheries and Food, 2023a; Ministry of Agriculture and Fisheries and Food, 2023b).

Materials and methods

Outbreak detection

On 22/09/2020, the National Reference Laboratory for Arboviruses in Spain (NRL), of the National Center for Microbiology (NCM-ISCIII), confirmed a WNV human case in a patient in the province of Badajoz (Extremadura). In the following 4 weeks, five more cases were detected in surrounding areas, one of them by additional epidemiological investigations and retrospective serological analyses from patients with neurological disease of unknown but suspected viral aetiology. No travel history was described for the six detected WNV human cases.

The data available from the Ministry of Agriculture and Fisheries and Food (Ministry of Agriculture and Fisheries and Food, 2023a; Ministry of Agriculture and Fisheries and Food, 2023b) regarding animal surveillance and human cases were consulted, and a map was made with spatial distribution in livestock regions (sanitary areas concerning veterinary health). This map was created with free software QGIS v.3.18.

Case definition

In Spain, WNVD has been notifiable since 2010. The detection of a single case is considered a Public Health Alert. Epidemiological data are provided as soon as it is available and updated according to the evolution of the cases, following National Guidelines, which contain case definition, public health measures such us seasonal active surveillance of meningoencephalitis cases in certain regions considered at risk, and response in case of an outbreak together with standardised survey of cases. According to the National Guidelines and the European Union case definition, a WNVD human case is suspected when a person lives in/or has visited a high-risk area, or has been bitten by mosquitoes and presents at least one of the following signs or symptoms with or without fever (>38.5°C): encephalitis, meningitis, acute flaccid paralysis, or Guillain-Barré syndrome. Laboratory case definitions and diagnostic algorithms for WNV human infections are defined as laboratory-confirmed or probable cases. At least one laboratory criterion is required to confirm the case: isolation of the virus, nucleic acid detection in a clinical sample, IgM detection in cerebrospinal fluid (CSF), or WNV IgM and IgG detection in sera confirmed by the neutralisation assay. The presence of WNV-specific antibodies in a serum sample allows only probable case classification. Laboratory results need to be interpreted according to flavivirus vaccination status (European Commission, 2018; ISCIII, 2021).

Ethical statement

The cases reported in this study were investigated with routine procedures according to the national surveillance plan for WNV infection. A unique ID to ensure the anonymity of patients and no patient identifiers were included in the study. The study was approved by the Ethical Committee of ISCIII (No. CEI PI 06_2023).

Microbiological investigations

In the regional hospitals, the acute serum samples were tested by serological methods to detect recent infection due to *Borrelia* spp., *Leptospira* spp. and *Coxiella burnetii*, and by molecular methods to detect herpes simplex virus, varicella zoster virus, enterovirus, and cytomegalovirus in the central nervous system (CNS). The CSF samples were also biochemically analysed.

For WNV diagnosis, the samples were sent to the NCM-ISCIII. Molecular and serological methods were used in serum, urine, and CSF samples. The presence of WNV RNA was investigated in serum, urine, and CSF acute samples using a specific WNV qRT-PCR (Vázquez et al., 2016). Anti-WNV immunoglobulin M (IgM) and immunoglobulin G (IgG) antibodies were determined in human CSF by sera acute and convalescent samples, using WNV IgM Capture DxSelect and WNV IgG DxSelect ELISA kits (Focus Diagnostics, Cypress, California, USA).

Specimens found positive for WNV antibodies were also tested against other flaviviruses (USUV and TBEV) to exclude possible cross-reactivity. The methods used were USU IgG ELISA Euroimmun assay and TBE IgG and IgM indirect immunofluorescence assays (IFA) (Flavivirus Mosaic 1, Euroimmun, Lübeck, Germany) for TBEV. These assays were performed according to the manufacturer's instructions. WNV IgM-positive results were confirmed performing the WNV IgM assay, which was carried out in parallel in the presence and absence of antigen.

To confirm the specificity of the antibody response, positive or indeterminate sera in both WNV IgG and IgM ELISA tests were assayed by neutralisation test (NT) against WN (strain HU6365/08), USU (strain HU10279/09), and TBE (strain Neudorfl) viruses. For this purpose, samples were tested in duplicate. Briefly, serum samples were inactivated at 56°C for 30 min and then twofold dilutions (25 µl) of the samples ranging from 1:8 to 1:512 were placed in a 96-well tissue culture microplate (Nunc A/S, Roskilde, Denmark) and mixed with 25 µl containing 100 tissue culture infectivity doses (100 $TCID_{50}$) of the virus. After 1 h of incubation in a 5% CO_2 incubator at 37°C, 50 µl of a Vero E6 cell suspension containing 4×10^5 cells/ml was added to each well. Cultures were maintained for 7 days at 37°C and 5% CO_2, and microscopic evaluation of the cytopathic effect was carried out 3, 5, and 7 days after inoculation. The titres of neutralising antibodies were defined as the highest serum dilution that showed >90% neutralisation of the virus challenge. Neutralising antibody titres ≥1:16 were

considered positive. Specific responses to viruses were based on the comparison of NT titres obtained in parallel against the three flaviviruses, and the neutralising immune response observed was considered specific when NT titres for a given virus were >fourfold higher than the titre obtained for the other viruses. All these procedures were performed in a biosafety level 3 laboratory.

The WNV NAT (Nucleic Acid Testing) screening in blood donations in Extremadura was performed on individual samples using the commercial cobas® WNV Test on the cobas 6800 System (Roche Diagnostics). This screening was performed until the end of the WNV season attending to the recommendations of official organisms.

Results

Description of human cases of WNV infection

Between September and October 2020, six human cases of WNV infection were identified. The first WNV case was diagnosed on 22 September and the last one on 16 October. Symptom onset occurred between 1 and 30 September. All the patients were over 50 years old, and the average age was 64 (range 51 to 80). Two were women and four were men. No epidemiological link according to municipality of infection was found. All cases were admitted to the hospital and presented fever and other WNVD-related symptoms such as headache (n = 3), malaise (n = 2), dizziness (n = 2), diarrhoea (n = 1), vomiting (n = 1), cough (n = 1), hypertension (n = 1), and arthromyalgia (n = 1). Five of them presented WNND and the other one fever with arthromyalgia, headache, lymphopenia, and thrombopenia. Several complications such as asthenia, hypertension, unstable gait, muscle pains, bradypsychia, fever, dizziness, tremors, arthralgia, hydrocephalus, and cognitive impairment were observed, and three patients with previous pathologies presented worse disease evolution. There were no deaths, and all cases were discharged by 23 October. The mean length of stay was 16 days (range 6 to 29) (Table 1).

None of the patients had a history of travel abroad during the incubation period, and none had been vaccinated against other flaviviruses such as TBEV, yellow fever (YFV), or Japanese encephalitis (JEV).

Patients' epidemiological, clinical, and laboratory data are presented in Tables 1, 2.

Laboratory results

In total, 24 samples belonging to the six patients were analysed. The acute serum samples were negative for detecting recent infection due to *Borrelia* spp., *Leptospira* spp., *Coxiella burnetii*, herpes simplex virus, varicella zoster virus, enterovirus, and cytomegalovirus. In the CSF, the bacterial culture was negative and the CSF analysis typically showed mononuclear pleocytosis (>15 leucocytes/μl) with elevated protein concentration and a normal glucose level.

There were 15 samples (sera, CSF and urine) examined by qRT-PCR for WNV, none of which were positive (Table 2). All the cases were confirmed by detection of neutralising antibodies against WNV by the neutralisation assay in serum samples, although in four out of six cases, diagnosis was also confirmed by detection of IgM antibodies in CSF. The titre of the neutralising WNV antibodies was low, in a range from 1/16 to 1/64. A convalescent serum was obtained in four patients, and a slight rise in the neutralisation titre was found. All the human serum samples showed IgM positivity for WNV and seroconversion or a rise of the IgG level. IgM against TBEV was also tested in some acute and convalescent serum samples by IFI giving negative results, except one sample that showed positive immunofluorescent signal at 8 days post-symptom onset (dpo). However, all convalescent samples IgG positive for WNV showed cross-reactivity in IgG against TBEV and USUV, showing a high degree of cross-reactivity in these assays between these flaviviruses, but no neutralising antibodies against TBEV or USUV were detected.

Outbreak control measures

After the first human case diagnosis on 22 September, a control of the blood and organs donation system was activated, according to

TABLE 1 Summary of clinical data of the patients infected with West Nile virus in Extremadura, Spain, 2020.

Patient ID	Age ranges (years)	Gender	Symptom onset (2020)	Clinical symptoms	Comorbidity	Evolution with complications
Case 1	50-60	Female	01/09/2020	Fever, malaise, diarrhoea, dizziness, meningoencephalitis	Yes	Yes
Case 2	50-60	Female	10/09/2020	Fever, malaise, headache, vomiting, meningoencephalitis	None	No
Case 3	70-79	Male	21/09/2020	Fever and neurological involvement	Yes	Yes
Case 4	50-60	Male	06/09/2020	Fever, headache, hypertension, dizziness, meningitis	None	Yes
Case 5	70-80	Male	30/09/2020	Fever, cough, meningoencephalitis	Yes	Yes
Case 6	70-80	Male	23/09/2020	Fever, arthromyalgia, headache	None	No

10.3389/fcimb.2023.1155867

TABLE 2 Summary of the molecular and serological results obtained from the analysis carried out in the samples obtained from the patients.

	Case 1				Case 2				Case 3			Case 4			Case 5			Case 6		
Sample	CSF	Urine	Serum	Serum	CSF	Serum	Urine	Serum	CSF	Serum	Serum	CSF	Urine	Serum	CSF	Urine	Serum	CSF	Serum	Urine	Serum
days post symptom onset	6	35	35	64	6	13	13	60	6	7	>180	12	23	23	6	8	8	13	13	23	30dpi
qRT-PCR	NEG	NEG	NEG	ND	NEG	NEG	NEG	ND	NEG	NEG	ND	NEG	NEG	NEG	NEG	NEG	NEG	ND	ND	NEG	ND
WNV IgM	**POS (5.5)**	ND	**POS (4.3)**	**POS (2.7)**	**POS (5)**	**POS (7.5)**	ND	**POS (2.02)**	**POS (3.3)**	**POS (4.7)**	**POS (3.44)**	**POS (3.6)**	ND	**POS (3.6)**	NEG (0.5)	ND	**POS (5.7)**	**POS (4.84)**	**POS (5.6)**	ND	**POS (6.5)**
WNV IgG	NEG (1.1)	ND	**POS (4.8)**	**POS (4.7)**	**POS (1.9)**	**POS (2.8)**	ND	**POS (4.54)**	NEG (0.9)	**POS (1.9)**	**POS (4.43)**	NEG (1)	ND	**POS (2.74)**	NEG (0.1)	ND	**POS (2.2)**	NEG (0)	NEG (1)	ND	**POS (2.2)**
WNV NT	ND	ND	**1/64**	**1/64**	ND	**1/16**	ND	**1/64**	NEG_NEG	**1/16**	**1/64**		ND	**1/16**		ND	1/8	ND	1/8	ND	**1/16**
USUV IgG	NEG			**POS (1.3)**	NEG				NEG		**POS (1.2)**	NEG			NEG			NEG			NEG (0.5)
USUV NT	ND	ND	ND	NEG	ND	ND	ND	NEG		NEG	NEG		ND			ND	NEG	ND	ND	ND	NEG
IgM TBEV	NEG		NEG			NEG		NEG	NEG		NEG	NEG		NEG			**POS**		NEG		
IgG TBEV				**POS**							**POS**			**POS**			**POS**				**POS**
NT TBEV				NEG							NEG			NEG			NEG				NEG

CSF, cerebrospinal fluid; ELISA, enzyme-linked immunosorbent assay; IFA, immunofluorescence assay; qRT-PCR, real-time RT-PCR; ND, test was not done; NEG, negative; NT, neutralising antibody titres; POS, positive; WNV, West Nile virus; USUV, Usutu virus; TBEV, tick-borne encephalitis virus

Bold values mean that the result is positive.

the Ministry of Health regulations, the National Transplant Organization, and the European Commission directive 2014/110/UE (Scientific Committee for Transfusion Safety, 2021). Regarding the measures adopted to prevent the transmission of the virus through blood donations in risk areas, once the first confirmed WNV case was detected, all donations in the affected areas were blocked during the incubation period of the first case. Moreover, blood collections were cancelled in high-risk areas until September 29 when WNV NAT screening was introduced. This measure to control donations was maintained until the end of the virus circulation season. All the samples tested by NAT screening were negative. Moreover, an active surveillance was established by epidemiological surveillance units and Hospital Clinical Services, and all clinicians were alerted through the Extremadura Health Service. A retrospective search for possible WNVD human cases (undiagnosed meningitis and meningoencephalitis from Badajoz province) was intensified after the first case, identifying five probable cases of which one was confirmed by laboratory methods. Additional measures were activated, including information campaigns on mosquito bite prevention, cleaning potential mosquito-breeding sites, recommendations for tissue-sample handling, postmortem examination, and safety in transfusions and transplants. Additionally, at a Regional level, an entomological surveillance was established. Furthermore, at a National level, a review and update of the national guidelines for surveillance and rapid risk assessments was performed (Spanish Ministry of Health, 2020).

According to the data available from the Ministry of Agriculture and Fisheries and Food (2023a) and (2023b) regarding animal surveillance, seven cases of WNV were reported in horses belonging to three livestock regions (sanitary areas concerning veterinary health), between 4 September and 23 October in six areas in Extremadura (Caceres and Badajoz), all very close to the affected area where the human cases were detected (Figure 1). Of the seven horses, five (71%) were detected in Badajoz province and two (29%) in Caceres province. Five of them (71%) were diagnosed in September and three of them a few days before the first human case (Table 3).

FIGURE 1
Areas with WNV equine foci or human cases. Data from 2004 to 2020.

10.3389/fcimb.2023.1155867

TABLE 3 Epidemiological information of the equine and human cases in Extremadura, Spain.

Number	Province	Livestock regions (National foci)	Sensitive animals	Affected animals	Confirmation date
Equine foci					
2022/3	Badajoz	Don Benito		3	
2020/136	Cáceres	Trujillo	27	1	23/10/2020
2020/107	Badajoz	Don Benito	24	1	05/10/2020
2020/103	Badajoz	Zafra	3	1	30/09/2020
2020/102	Badajoz	Zafra	2	1	25/09/2020
2020/88	Cáceres	Trujillo	14	1	16/09/2020
2020/50	Badajoz	Don Benito	15	1	04/09/2020
2020/51	Badajoz	Don Benito	1	1	04/09/2020
2019/6	Cáceres	Trujillo	3	1	28/11/2019
2018/6	Cáceres	Coria	17	1	23/10/2018
2018/4	Cáceres	Caceres	1	1	22/10/2018
2016/72	Badajoz	Badajoz	7	1	15/11/2016
2016/70	Badajoz	Badajoz	37	1	15/11/2016
2016/67	Cáceres	Plasencia	7	1	25/10/2016
2016/44	Cáceres	Plasencia	14	1	04/10/2016
2016/43	Cáceres	Caceres	4	1	04/10/2016
2016/42	Cáceres	Trujillo	10	1	23/09/2016
2015/4	Badajoz	Don Benito	1	1	25/09/2015
Human cases					
Case 1/2020	Badajoz	Don Benito			16/10/2020
Case 2/2020	Badajoz	Don Benito			22/09/2020
Case 3/2020	Badajoz	Badajoz			05/10/2020
Case 4/2020	Badajoz	Don Benito			15/10/2020
Case 5/2020	Badajoz	Don Benito			26/10/2020
case 6/2020	Badajoz	Don Benito			16/10/2020
First case	Badajoz	Badajoz			2004

Discussion

During the 2020 WNV transmission season, Spain was the second country with more human WNV infections in Europe, registering the highest human WNV outbreak ever in the country with a total of 77 cases. Six patients were infected in Extremadura, the region where the first autochthonous human case was retrospectively identified in 2004 and no other cases had been reported until 2020. The absence of human cases reported in previous seasons in this area could be explained by a lack of clinical suspicion as most infections are asymptomatic (80%). Even when WNV infection is suspected, the diagnosis is complicated and a combination of molecular and serological assays is necessary. Generally, patients with severe clinical symptoms seek medical care, therefore the probability of detecting and reporting them is higher. In this outbreak, the six described cases exhibited fever, the most common clinical signs of the infection, and five of them (83%) presented neurological disease. Taking into account that less than 1% of infected cases develop a WNND, a high number of WNV infections would have gone undiagnosed. Thus, educational plans targeting citizens, clinicians, public health workers, and decision makers should be carried out in order to increase the awareness of WNV and other emerging diseases.

WNVD in humans is associated with mild symptoms (fever, headache, chill, malaise, myalgia, arthralgia, rash, vomiting, nausea, anorexia), most of which were present in the patients described in this outbreak. However, atypical or rare presentations such as myocarditis, pancreatitis, hepatitis, cerebellitis, rhabdomyolysis, and ocular manifestations were not observed even though the patients described in this work presented several of the risk factors related with worse disease evolution and aftermath such as the age (ranging between 50 and 80), living in rural areas in contact with animals, diabetes, hypertension, cardiovascular disease, and chronic lymphocytic leukaemia. In fact,

several sequelae have been described in some of these patients such as unstable gait, muscle pains, bradipsychia, dizziness, tremors, forgetfulness, asthenia, hydrocephalus, arthralgia, muscle paints, dyspnoea, and cognitive impairment, especially in patients with chronic morbidities. In general, age and gender are the main intrinsic predisposing factors related to WNVD. It has been reported that individuals older than 50 years of age are more susceptible to severe infections with neurological involvement and that patients older than 75 generally succumb to the infection (Gray and Webb, 2014). The latter could be explained by age-related innate immunosenescence. Regarding gender, more men have been described among WNVD cases, probably because they have more outdoor occupations and are more exposed to mosquito bites. In fact, in rural areas, WNV outbreaks and disease incidence and prevalence have been linked with agricultural activities. In the outbreak described in this work, although there were more men infected, we cannot draw conclusions due to the small number of cases. Other major risk factors are preexisting medical conditions such as cancers, cardiovascular diseases, and diabetes (chronic morbidities), and immunosuppressed individuals have a 40 times higher risk of contracting the disease and dying from WNV infection (Lindsey et al., 2012).

WNV diagnosis was possible in all cases by serological assays. From all patients, CSF, sera, and urine samples were available and analysed. Although all acute samples (<7 dpo) were available in four of the six patients, no positive results were obtained by qRT-PCR. Urine samples from different dpo (from 8 to 35) were analysed by PCR because in several studies viral RNA was detected in urine for much longer (including up to a month postinfection) than in plasma and with higher viral load (Barzon et al., 2014). However, all of the urine samples analysed in this work were negative.

In Extremadura, viral information about the WNV human and equine cases has not been available yet, even though sporadic WNV outbreaks in horses have been reported at least since 2015 (Ministry of Agriculture and Fisheries and Food, 2023a; Ministry of Agriculture and Fisheries and Food, 2023b). A recent study carried out in birds of this region (Bravo-Barriga et al., 2021) revealed WNV lineage 1 circulation, the same lineage that was detected previously in neighbouring areas in birds (Castilla La Mancha, 2007), mosquitoes (Andalusia, 2008; and 2020), and horses (Andalusia, 2010) (Sotelo et al., 2009; García-Bocanegra et al., 2011; Vázquez et al., 2011). These studies showed a high prevalence (18.23%) and active circulation of WNV in wild birds during the period 2017–2019. These seroprevalence levels are higher than those found in other European countries and very similar to those detected in birds from Doñana National Park, an endemic WNV area in Andalusia (López et al., 2011). Another study carried out in dogs in the southwest of Spain revealed the presence of neutralising antibodies against WNV and TBEV, demonstrating the circulation of these viruses in these areas (García-Bocanegra et al., 2018). Moreover, the recent detection of USUV (RNA in mosquitoes and USUV-specific antibodies in birds) and an undetermined flavivirus highlights the widespread circulation of WNV in this endemic area and its co-circulation with USUV and other flaviviruses (Bravo-Barriga et al., 2023). In the six patients studied in this work, cross-reactive IgG antibodies against USUV and TBEV were detected in all the convalescent sera samples tested, but not in the CSF. Although the presence of cross-reactive antibodies against the three flaviviruses was observed in the ELISA and IFA assays, confirmation of WNV infection was possible by neutralisation assays. Taking into account flavivirus co-circulation and the serological cross-reactivity described among these viruses, the laboratory findings should be carefully addressed and a combination of molecular and serological techniques is necessary for a complete diagnosis of this infection. Therefore, although no human infections by USUV or TBEV have been reported in Extremadura until now, when a human WNV infection is suspected in this area, a differential diagnosis should be carried out against these flaviviruses—which may also be endemic in this area—and serological cross-reactions should be excluded.

The history of detection of WNV for more than 15 years both in birds and horses, as well as the increase in human cases described in this work, indicates its establishment and spread in Extremadura, Spain. Moreover, the recent detection of USUV close to urban areas represents a public health threat that requires inclusion in the differential diagnoses in patients with compatible symptoms. Therefore, it is necessary to establish surveillance programs for these emerging flaviviruses and to develop coordinated national plans integrating multisectoral and interregional participation from a one-health approach.

Data availability statement

The original contributions presented in the study are included in the article/supplementary material. Further inquiries can be directed to the corresponding author.

Ethics statement

The studies involving human participants were reviewed and approved by Instituto de Salud Carlos III. Written informed consent for participation was not required for this study in accordance with the national legislation and the institutional requirements.

Author contributions

AV coordinated the study. AM, PM, and SR performed the laboratory screening and biochemical analysis in the regional Hospitals. AV, LH, MS-S, and MP-O performed the laboratory analysis, confirmation, and interpretation of results. AntV, MG, MJ and CM-P performed the clinical case management and description. BFM participated in the epidemiological investigations. DG-B designed and graphed the map of human and animal cases. JR, EF, ED, and AC contributed to the surveillance and epidemiological investigations. All authors contributed to the article and approved the submitted version.

Funding

This research was partially funded by the project PI19CIII_00014 from the Instituto de Salud Carlos III.

Conflict of interest

The authors declare that the research was conducted in the absence of any commercial or financial relationships that could be construed as a potential conflict of interest.

Publisher's note

References

Bai, F., Thompson, E. A., Vig, P. J. S., and Leis, A. A. (2019). Current understanding of West Nile virus clinical manifestations, immune responses, neuroinvasion, and immunotherapeutic implications. *Pathogens* 8, 193. doi: 10.3390/pathogens8040193

Barzon, L., Pacenti, M., Franchin, E., Squarzon, L., Sinigaglia, A., Ulbert, S., et al. (2014). Isolation of West Nile virus from urine samples of patients with acute infection. *J. Clin. Microbiol.* 52, 3411–3413. doi: 10.1128/JCM.01328-14

Barzon, L., Pacenti, M., Ulbert, S., and Palù, G. (2015). Latest developments and challenges in the diagnosis of human West Nile virus infection. *Expert Rev. Anti Infect. Ther.* 13, 327–342. doi: 10.1586/14787210.2015.1007044

Bravo-Barriga, D., Aguilera-Sepúlveda, P., Guerrero-Carvajal, F., Llorente, F., Reina, D., Pérez-Martín, J. E., et al. (2021). West Nile and usutu virus infections in wild birds admitted to rehabilitation centres in extremadura, western Spain 2017–2019. *Vet. Microbiol.* 255, 109020. doi: 10.1016/j.vetmic.2021.109020

Bravo-Barriga, D., Ferraguti, M., Magallanes, S., Aguilera-Sepúlveda, P., Llorente, F., Pérez-Ramírez, E., et al. (2023). Identification of usutu virus Africa 3 lineage in a survey of mosquitoes and birds from urban areas of Western Spain. *Transbound Emerg. Dis.* 2023, 10. doi: 10.1155/2023/6893677

Carson, P. J., Konewko, P., Wold, K. S., Mariani, P., Goli, S., Bergloff, P., et al. (2006). Long-term clinical and neuropsychological outcomes of West Nile virus infection. *Clin. Infect. Dis.* 43, 723–730. doi: 10.1086/506939

Casades-Martí, L., Holgado-Martín, R., Aguilera-Sepúlveda, P., Llorente, F., Pérez-Ramírez, E., Jiménez-Clavero, M. Á, et al. (2023). Risk factors for exposure of wild birds to West Nile virus in a gradient of wildlife-livestock interaction. *Pathogens* 12 (1), 83. doi: 10.3390/pathogens12010083

ECDC (2019) *West Nile Virus infection. annual epidemiological report for 2018* (Stockholm). Available at: https://www.ecdc.europa.eu/en/publications-data/west-nile-virus-infection-annual-epidemiological-report-2018 (Accessed January 29, 2023).

ECDC (2020) *Epidemiological update: West Nile virus transmission season in Europe 2020*. Available at: https://www.ecdc.europa.eu/en/news-events/epidemiological-update-west-nile-virus-transmission-season-europe-2020 (Accessed January 29, 2023).

ECDC (2022a) *Epidemiological update: West Nile virus transmission season in Europe 2021*. Available at: https://www.ecdc.europa.eu/en/news-events/epidemiological-update-west-nile-virus-transmission-season-europe-2021.

ECDC (2022b) *Weekly updates: 2022 West Nile virus transmission season*. Available at: https://www.ecdc.europa.eu/en/west-nile-fever/surveillance-and-disease-data/disease-data-ecdc.

European Commission (2018)Commission implementing decision (EU) 2018/945 of 22 June 2018 on the communicable diseases and related special health issues to be covered by epidemiological surveillance as well as relevant case definitions (Accessed January 29, 2023).

García-Bocanegra, I., Jaén-Téllez, J. A., Napp, S., Arenas-Montes, A., Fernández-Morente, M., Fernández-Molera, V., et al. (2011). West Nile Fever outbreak in horses and humans, spai. *Emerg. Infect. Dis.* 17, 2397–2399. doi: 10.3201/eid1712.110651

García-Bocanegra, I., Jurado-Tarifa, E., Cano-Terriza, D., Martínez, R., Pérez-Marín, J. E., and Lecollinet, S. (2018). Exposure to West Nile virus and tick-borne encephalitis virus in dogs in Spain. *Transbound Emerg. Dis.* 65, 765–772. doi: 10.1111/tbed.12801

García San Miguel Rodríguez-Alarcón, L., Fernández-Martínez, B., Sierra Moros, M. J., Vázquez, A., Julián Pachés, P., García Villacieros, E., et al. (2021). Unprecedented increase of West Nile virus neuroinvasive disease, Spain, summer 2020. *Eurosurveillance* 26 (19), pii=2002010. doi: 10.2807/1560-7917.ES.2021.26.19.2002010

Gray, T., and Webb, C. E. (2014). A review of the epidemiological and clinical aspects of West Nile virus. *Int. J. Gen. Med.* 7, 193–203. doi: 10.2147/IJGM.S59902

Guerrero-Carvajal, F., Bravo-Barriga, D., Martín-Cuervo, M., Aguilera-Sepúlveda, P., Ferraguti, M., Jiménez-Clavero, M. Á., et al. (2021). Serological evidence of co-circulation of West Nile and usutu viruses in equids from western Spain. *Transbound Emerg. Dis.* 68, 1432–1444. doi: 10.1111/tbed.13810

Hasbun, R., Garcia, M. N., Kellaway, J., Baker, L., Salazar, L., Woods, S. P., et al. (2016). West Nile Virus retinopathy and associations with long term neurological and neurocognitive sequelae. *PloS One* 11, e0148898. doi: 10.1371/journal.pone.0148898

Hughes, J. M., Wilson, M. E., and Sejvar, J. J. (2007). The long-term outcomes of human West Nile virus infection. *Clin. Infect. Dis.* 44, 1617–1624. doi: 10.1086/518281

ISCIII (2021) *Fiebre del nilo occidental*. Available at: https://www.isciii.es/QueHacemos/Servicios/VigilanciaSaludPublicaRENAVE/EnfermedadesTransmisibles/Documents/PROTOCOLOS/Protocolo%20vigilancia%20fiebre%20Nilo%20occidental_RENAVE.pdf (Accessed May 10, 2021).

ISCIII (2022). *Informe epidemiológico sobre la situación de la fiebre del nilo occidental en españa. años 2021 y 2022* (Instituto de Salud Carlos III: Centro Nacional de Epidemiología). Available at: https://www.isciii.es/QueHacemos/Servicios/VigilanciaSaludPublicaRENAVE/EnfermedadesTransmisibles/Documents/archivos%20A-Z/Fiebre_Nilo_Occidental/INFORME_RENAVE_FNO%202021-2022.pdf.

Kaptoul, D., Viladrich, P. F., Domingo, C., Niubó, J., Martínez-Yélamos, S., de Ory, F., et al. (2007). West Nile Virus in Spain: report of the first diagnosed case (in Spain) in a human with aseptic meningitis. *Scand. J. Infect. Dis.* 39, 70–71. doi: 10.1080/00365540600740553

Konjevoda, S., Dzelalija, B., Canovic, S., Pastar, Z., Savic, V., Tabain, I., et al. (2019). West Nile Virus retinitis in a patient with neuroinvasive disease. *Rev. Soc. Bras. Med. Trop.* 52, e20190065. doi: 10.1590/0037-8682-0065-2019

Lindsey, N. P., Staples, J. E., Lehman, J. A., and Fischer, M. (2012). Medical risk factors for severe West Nile virus disease, united states 2008–2010. *Am. J. Trop. Med. Hyg* 87, 179–184. doi: 10.4269/ajtmh.2012.12-0113

López, G., Jiménez-Clavero, M. Á., Vázquez, A., Soriguer, R., Gómez-Tejedor, C., Tenorio, A., et al. (2011). Incidence of West Nile virus in birds arriving in wildlife rehabilitation centers in southern Spain. *Vector-Borne Zoonotic Dis.* 11, 285–290. doi: 10.1089/vbz.2009.0232

López-Ruiz, N., Montaño-Remacha, M., del, C., Durán-Pla, E., Pérez-Ruiz, M., Navarro-Marí, J. M., et al. (2018). West Nile Virus outbreak in humans and epidemiological surveillance, west Andalusia, spai. *Eurosurveillance* 23 (14), pii=17-00261. doi: 10.2807/1560-7917.ES.2018.23.14.17-00261

Lustig, Y., Sofer, D., Bucris, E. D., and Mendelson, E. (2018). Surveillance and diagnosis of West Nile virus in the face of flavivirus cross-reactivity. *Front. Microbiol.* 9. doi: 10.3389/fmicb.2018.02421

Ministry of Agriculture and Fisheries and Food (2023a). Available at: https://www.mapa.gob.es/es/ganaderia/temas/sanidad-animal-higiene-ganadera/sanidad-animal/enfermedades/fiebre-nilo-occidental/F_O_Nilo.aspxhttps://www.mapa.gob.es/es/ganaderia/temas/sanidad-animal-higiene-ganadera/sanidad-animal/enfermedades/fiebre-nilo-occidental/F_O_Nilo.aspx.

Ministry of Agriculture and Fisheries and Food (2023b) *Actualización de la situación epidemiológica de la fiebre del nilo occidental (West Nile fever)*. Available at: https://www.mapa.gob.es/es/ganaderia/temas/sanidad-animal-higiene-ganadera/informefno_tcm30-435293.pdf.

Napp, S., Llorente, F., Beck, C., Jose-Cunilleras, E., Soler, M., Pailler-García, L., et al. (2021). Widespread circulation of flaviviruses in horses and birds in northeastern Spain (Catalonia) between 2010 and 2019. *Viruses* 13 (12), 2404. doi: 10.3390/v13122404

Scientific Committee for Transfusion Safety (2021) *Virus del nilo occidental* (Madrid). Available at: https://www.mscbs.gob.es/profesionales/saludPublica/medicinaTransfusional/acuerdos/docs/Virus_Nilo_Occidental.pdf (Accessed January 29, 2023).

Sotelo, E., Fernandez-Pinero, J., Llorente, F., Agüero, M., Hoefle, U., Blanco, J. M., et al. (2009). Characterization of West Nile virus isolates from Spain: new insights into the distinct West Nile virus eco-epidemiology in the Western Mediterranean. *Virology* 395, 289–297. doi: 10.1016/j.virol.2009.09.013

Spanish Ministry of Health (2020) *Meningoencefalitis por el virus del nilo occidental en españa (2a actualización-cierre de temporada)*. Available at: https://www.mscbs.gob.es/profesionales/saludPublica/ccayes/alertasActual/docs/20201203_ERR_Nilo_Occidental.pdf (Accessed January 29, 2023).

Tardei, G., Ruta, S., Chitu, V., Rossi, C., Tsai, T. F., and Cernescu, C. (2000). Evaluation of immunoglobulin m (IgM) and IgG enzyme immunoassays in serologic diagnosis of West Nile virus infection. *J. Clin. Microbiol.* 38, 2232–2239. doi: 10.1128/JCM.38.6.2232-2239.2000

Vanhomwegen, J., Beck, C., Desprès, P., Figuerola, A., García, R., Lecollinet, S., et al. (2017). Circulation of zoonotic arboviruses in equine populations of mallorca island (Spain). *Vector Borne Zoonotic Dis.* 17 (5), 340–346. doi: 10.1089/vbz.2016.2042

Vázquez, A., Herrero, L., Negredo, A., Hernández, L., Sánchez-Seco, M. P., and Tenorio, A. (2016). Real time PCR assay for detection of all known lineages of West Nile virus. *J. Virol. Methods* 236, 266–270. doi: 10.1016/j.jviromet.2016.07.026

Vázquez, A., Ruiz, S., Herrero, L., Moreno, J., Molero, F., Magallanes, A., et al. (2011). West Nile And usutu viruses in mosquitoes in Spain 2008-2009. *Am. J. Trop. Med. Hyg* 85, 178–181. doi: 10.4269/ajtmh.2011.11-0042

Vázquez, A., Sánchez-Seco, M. P., Ruiz, S., Molero, F., Hernández, L., Moreno, J., et al. (2010). Putative new lineage of West Nile virus, Spain. *Emerg. Infect. Dis.* 16, 549–552. doi: 10.3201/eid1603.091033

Velasco, M., Sánchez-Seco, M. P., Campelo, C., de Ory, F., Martin, O., Herrero, L., et al. (2020). Imported human West Nile virus lineage 2 infection in Spain: neurological and gastrointestinal complications. *Viruses* 12, 156. doi: 10.3390/v12020156

frontiers | Frontiers in Cellular and Infection Microbiology

TYPE Review
PUBLISHED 21 September 2023
DOI 10.3389/fcimb.2023.1175996

OPEN ACCESS

EDITED BY
Brijesh Rathi,
University of Delhi, India

REVIEWED BY
Pulin Kumar Gupta,
Atal Bihari Vajpayee Institute of Medical Sciences and Dr. Ram Manohar Lohia Hospital, India
Yue Han,
School of Medicine, Shanghai Jiao Tong University, China

*CORRESPONDENCE
Francisco Rodriguez-Frias
frarodri@gmail.com
Josep Quer
josep.quer@vhir.org

RECEIVED 28 February 2023
ACCEPTED 04 September 2023
PUBLISHED 21 September 2023

CITATION
Rodriguez-Frias F, Rando-Segura A and Quer J (2023) Solved the enigma of pediatric severe acute hepatitis of unknown origin?
Front. Cell. Infect. Microbiol. 13:1175996.
doi: 10.3389/fcimb.2023.1175996

Solved the enigma of pediatric severe acute hepatitis of unknown origin?

Francisco Rodriguez-Frias[1,2,3]*, Ariadna Rando-Segura[1] and Josep Quer[3,4,5]*

[1]Clinical Biochemistry Department Vall d'Hebron Institut of Research (VHIR), Vall d'Hebron Barcelona Hospital Campus, Barcelona, Spain, [2]Basic Science Department, International University of Catalonia, Barcelona, Spain, [3]Centro de Investigación Biomédica en Red de Enfermedades Hepáticas y Digestivas (CIBERehd), Instituto de Salud Carlos III, Madrid, Spain, [4]Liver Diseases-Viral Hepatitis, Liver Unit, Vall d'Hebron Institut de Recerca (VHIR), Vall d'Hebron Barcelona Hospital Campus, Barcelona, Spain, [5]Biochemistry and Molecular Biology Department, Autonomous University of Barcelona (UAB), Barcelona, Spain

Hepatitis is an inflammation of the liver whose etiology is very heterogeneous. The most common cause of hepatitis is viral infections from hepatotropic viruses, including hepatitis A, B, C, D and E. However, other factors such as infections from other agents, metabolic disorders, or autoimmune reactions can also contribute to hepatitis, albeit to a lesser extent. On April 5, 2022, the United Kingdom Health Security Agency alerted the World Health Organization (WHO) on the increased incidence of severe acute hepatitis of unknown causes (not A-E) in previously healthy young children, with symptoms of liver failure that in some cases required liver transplantation. By July 2022, 1,296 cases were reported in 37 countries. Acute hepatitis of unknown causes is not an exceptional phenomenon: in fact, it represents more than 30% of cases of acute hepatitis in children, however in the present instance the large proportion of severe cases was surprising and alarming (6% of liver transplants and almost 3% mortality). Multiple hypotheses have been proposed to explain the etiology of such higher proportion of acute hepatitis, including their co-occurrence in the context of COVID-19 pandemic. This is a review of the history of a clinical threat that has put in check a world health care system highly sensitized by the current COVID-19 pandemics, and that it looks like has ended with the arguments that the severe acute pediatric hepatitis is caused by Adeno-associated virus 2 (AAV2) infection associated with a coinfection with a helper virus (human Adenovirus HAdV or human herpesvirus 6) in susceptible children carrying HLA-class II antigen HLA-DRB1*04:01.

KEYWORDS

acute hepatitis, severity, SARS-CoV-2, adenovirus, adeno-associated virus, liver transplant, mortality

Introduction

Hepatitis is an inflammation of the liver, which can affect the portal tract or the hepatic acinus or combine both phenotypes. The causes of hepatitis are multi etiological. Initially, a possible infection by hepatotropic viruses, such as hepatitis viruses A, B, C, D and E (not A-E) was proposed as a main cause, however other infectious agents may also be responsible in a minority of patients (Box 1). Liver damage can also arise as a post-toxin event to drugs or botanicals. Other events may include excessive accumulation of fat in the hepatocytes, or NAFLD (non-alcoholic fatty liver disease)/ NASH (non-alcoholic fatty liver disease-steato-hepatitis), or autoimmunity/immune dysregulation. The diagnosis of acute hepatitis of unknown origin not A-E generally refers to liver injury caused by the exclusion of known infectious or non-infectious factors (Box 1). This disease represents over 30% of the cases of acute hepatitis in children (Alonso et al., 2017).

A new health alarm in children: another *deja vu* feeling or it is actually happening?

Today, scientific and technological advancements have reached unparalleled levels of precision, sophistication, and power, enabling us to investigate diseases that occurred in ancient times, long before historical records were even conceived (Rodríguez-Frías et al., 2021). These extraordinary advances in technology and communication, coupled with the researchers' ability of channeling their creativity, have fostered true neural networks among professionals worldwide. Irrespective of any alarming situation, this interconnected global medical community can be used to face present and future unknown clinical scenarios.

One such scenario emerged on April 5, 2022, when the United Kingdom Health Security Agency (UKHSA) alerted the World Health Organization (WHO) about a notable increased incidence of severe acute hepatitis of unknown cause among young children (UKHSA, 2022). Almost simultaneously, a similar situation was reported at the Children's Hospital of Alabama (USA), where the majority of children admitted with acute hepatitis had an unknown cause (Gutierrez Sanchez et al., 2022), raising significant concerns due to the severity of its clinical presentation and the young age of the affected children. The number of admissions in 2022 in UK, was equal or greater than the total annual admissions in previous years. Similarly, the Women's and Children's Hospital in Alabama (USA) reported an increase, with 10 cases admitted between January and March 2022 compared to 1 to 5 cases per year previously (Kelgeri et al., 2022).

Consequently to these observations, the European Center for Diseases Prevention and Control (ECDC) and the Center for Disease Control and Prevention (CDC) issued a warning about hepatitis of unknown origin in children (who/ecdc, 2022; World Health Organization (WHO), 2022). Of the 13 cases notified by the British agency to the WHO, 10 cases aroused in Scotland in children of 11 months to 5 years of age and required hospitalization. One child had an onset of symptoms in January 2022 and nine cases on March 2022. The children presented frequent non-specific gastrointestinal symptoms, such as diarrhea and vomiting, progressing to jaundice, abdominal pain, nausea, and malaise, with elevated aminotransferase (ALT) and bilirubin levels. On April 8, 2022, an UK nationwide investigation identified a total of 74 cases with similar characteristics to the original 10 cases, including high aminotransferase levels (>500 IU/L) in serum, being negative for hepatitis A to E virus infections. Conceivably, patients with milder hepatitis may have not been detected and therefore notified.

In light of the aforementioned scenarios, WHO, ECDC, CDC, and UKHSA agencies reached a consensus on the definition for the acute hepatitis, similar to the one employed in Scotland, based on exclusion of other causes of acute hepatitis. In this new definition, the category of "confirmed case" was replaced by "probable case" (Box 1). It should be noticed that all documented cases coexisted with previously reported cases, including those diagnosed under different criteria. Between April and September 14, 2022, a total of 1,296 probable cases had been reported from 37 countries/regions (Table 1), 40% of them (519) were from Europe, predominantly from Scotland and the UK (277), while 28% were from US (364),

BOX 1 Definition of cases to report and guidelines for ruling out known etiologies.

Definitions of cases. ECDC case definition. (a) *Confirmed*: A person presenting with an acute hepatitis (non hepA-E*) with serum transaminase >500 IU/l (Aspartate Transaminase-AST or Alanine Transaminase-ALT), who is 10 years and under, since 1 January 2022. (b) *Possible*: A person presenting with an acute hepatitis (non hepA-E*) with serum transaminase >500 IU/l (AST or ALT), who is 11 to 16 years, since 1 January 2022. (c) *Epi-linked:* A person presenting with an acute hepatitis (non hep A-E*) of any age who is a close contact of a confirmed case, since 1 January 2022. (*) Cases with other explanations must be discarded. WHO case definition. (a) *Confirmed case*: not available. (b) *Probable case*: A person with acute hepatitis (not A, B, C, D, E*) with serum transaminase levels >500 IU/L (AST or ALT). 16 years of age or younger, as of October 1, 2021. (*) Cases with other explanations must be discarded.

Guidelines for ruling out know etiologies. (1) PCR tests using blood/serum samples for adenovirus, enterovirus, human herpes virus 1, 2, 3, 4, 5, 6 and 7, hepatitis A, C and E virus; (2) Serological tests for hepatitis A, B, C, and E viruses, EBV, and cytomegalovirus (CMV) in addition to SARS-CoV-2; (3) Blood culture for bacteria if fever is present; (4) Panel of multiplex PCR respiratory viruses (including adenovirus, enterovirus, influenza virus, human bocavirus, and SARS-CoV-2) from the earliest possible throat swab; (5) Multiplex PCR gastrointestinal virus panel (including adenovirus, sapovirus, norovirus, enterovirus) in a stool sample; (6) Culture of stool for common bacterial enteropathogens, including Salmonella; (7) Test for adeno-associated and Adenovirus co-infection.

Serologic testing for anti-streptolysin O (ASO), throat swab culture for group A hemolytic streptococci, and serum/urine tests for leptospirosis should be considered if clinically indicated. Toxicology screening with blood and urine samples should also be considered.

TABLE 1 Distribution of the 1296 cases reported up to July 12, 2022.

Region	Number of cases	Required Liver Transplant	SARS-CoV-2 positive by PCR	Adenovirus positive by PCR	Adenovirus type 41	Deaths
America	635	26	18/222	144/325	14/28	14
Europa	519	28	56/376	225/410	62/70	3
Asia	142	1	6/62	7/62	0/3	12
TOTAL	**1296**	**55**	**78**	**209**	**31**	**22**

https://www.who.int/emergencies/disease-outbreak-news/item/2022-DON400#:~:text=Severe%20acute%20hepatitis%20of%20unknown%20aetiology%20in%20children%20%2D%20Multi%2Dcountry,-12%20July%202022&text=As%20of%208%20July%202022,case%20definition%2C%20including%2022%20deaths.

with approximately 55 cases requiring liver transplantation and 29 resulted in death (Gong et al., 2022). These data, along with the ongoing prevalence of SARS-CoV-2 infection, led the cases of severe acute hepatitis in children be considered a potentially new "health alarm".

In the last decade the evident success of vaccinations against hepatitis A and B viruses has caused a great reduction of acute infections of known origin. Nonetheless, certain viruses other than the classical hepatotropic ones (A to E) that are frequent in childhood, also present a certain hepatotropism, such as Epstein-Barr Virus (EBV), herpes simplex virus; varicella-zoster virus; human herpesvirus 6, 7, and 8; human parvovirus B19; adenoviruses; cytomegalovirus; among others (Gallegos-Orozco and Rakela-Brödner, 2010). These viruses together with other possible non-viral, toxic or autoimmune dysfunctions may cause a severe disease in a minority of patients (Box 1). In such cases, liver damage is very rapid and it is accompanied by important elevations of liver enzymes (over 100 times the upper limit of the normal range) ALT and aspartate aminotransferase (AST). In these severe cases, patients experience a rapid deterioration in their condition, resulting in significant liver function impairments such as coagulopathy, jaundice, and encephalopathy, which can ultimately progress to liver failure. In rare instances, liver failure may require transplantation, and in many patients with functional deficiencies no marked elevations of aminotransferases are observed and most of them recover due to the remarkable regenerative capacity of the liver.

In large series of children hospitalized with liver failure, most of them (between 49-64.5%) met the criteria of pediatric acute liver failure of unknown etiology or indeterminate (Squires et al., 2006; Squires et al., 2014; Leiskau et al., 2023). In a 2017 study from the Pediatric Acute Liver Failure Study Group (PALFSG) including over 1,000 children, 30% of miss-diagnosis were reported with more than 60% of cases observed in children of 1 to 5 years of age (Alonso et al., 2017). Given the extraordinary youth of the affected individuals, any possible cause should be explored including genetic and environmental triggers, able to explain the most severe cases(Centers for Disease Control and Prevention (CDC), 2022; Squires et al., 2022). As previously stated, although rare, acute hepatitis of unknown etiology in children is not a new entity, but the current alarming situation seems truly exceptional.

Currently, while the situation of acute hepatitis of unknown etiology in children remain as "open active alert", we consider helpful to provide an update as of October 27, 2022, specially focusing on the WHO European Region having important repository Historical Archives. Considering the 22 countries (HAEC 2022), 563 cases have been reported: Austria (6), Belgium (14), Bulgaria (1), Cyprus (2), Denmark (8), Finland (1), France (10), Greece (20), Ireland (29), Israel (5), Italy (47), Latvia (1), Luxembourg (1), Netherlands (16), Norway (6), Poland (22), Portugal (26), Republic of Moldova (1), Serbia (1), Spain (54), Sweden (12) and the United Kingdom (280) (Ministerio de Sanidad, 2022; who/ecdc, 2022). The epidemiological curve shows the cases by date of symptoms onset (381 cases), date of hospitalization (159 cases) and date of notification at the national level. The cases (numbers) by week in Europe as of October 27 are shown in Figure 1 (Pan et al., 2022; World Health Organization (WHO), 2022), showing that there was a notable increase in cases from week 12, remaining stable until week 18 with 28 to 39 cases reported per week. Although late reporting may affect recent case numbers, there was a steady decline in weekly reported cases starting from week 18. The majority of patients (75.7%) were five years old or younger. In Europe, there were seven deaths related to the disease out of the 364 reported cases. Among the reported cases, 98 (26.9%) required admission to the Intensive Care Unit. Out of the 313 cases with available information, 24 cases (7.7%) underwent a liver transplant. Among 440 cases analyzed for different adenovirus detection, 231 (52.5%) tested positive. The highest positivity rate was observed in whole blood samples (49.5%). Adenovirus typing information was only available for eleven cases: type 31 (n = 1), type 40 (n = 3), type 41 (n = 5) and other types (n = 2). Among 384 cases analyzed for SARS-CoV-2 detection using PCR, 40 (10.4%) were positive. However, serology results for SARS-CoV-2 were available for only 109 cases, with a higher frequency of 68 (62.4%) positive cases. In addition, out of 162 cases with vaccination data against COVID-19, 143 (88.3%) were not vaccinated (Ministerio de Sanidad, 2022).

A global predisposition based on gender and ethnicity was observed. In Spain, the Health Alerts and Emergencies Coordination Center (HAECC) issued a report on April 22, 2022, regarding "Alert of severe acute hepatitis of unknown causes, non A-E, in children under 10 years in UK. Situation in Spain". The report stated that as of November 10, there were 59 unrelated cases of liver failure in children under investigation in Spain, with 48 of them being 10 years old or younger. No cases with epidemiological link were found. A microbiological study of 59 cases, confirmed the absence of known causes of hepatitis in 32 of them (viruses A to E, leptospira, parvovirus B19, herpes simplex, and varicella zoster virus, were negative) (Ministerio de Sanidad, 2022). When the 32

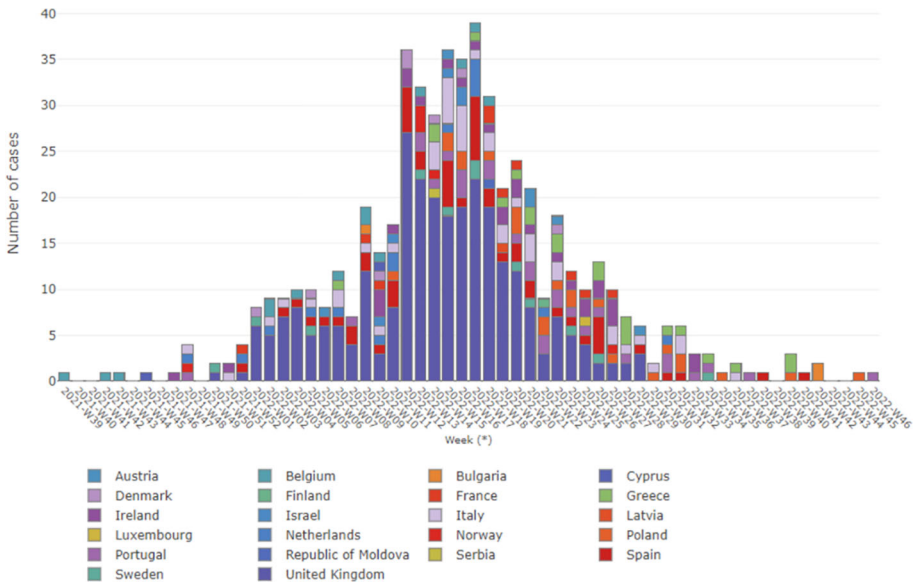

FIGURE 1
Severe acute hepatitis in children, in Europe WHO region, by week. Data updated up to 27 October 2022, and obtained from WHO (World Health Organization (WHO), 2022).

cases were analysed for herpes virus, 8 patients (25%) were found positive for herpes viruses, 6 of them for cytomegalovirus (CMV), 1 was herpes type 6 and the last was epstein-barr virus (EBV) plus herpes type 7. Additionally, 15 out of the 32 cases (47%) were positive for adenovirus, and 3 cases resulted positive for enterovirus in serum (one of them typed by metagenomics as coxsackie B4). Further analysis of the 15 adenovirus-positive cases revealed infection of type-2 adenovirus (1 case), and type-41 adenovirus (1 case) using metagenomics. In addition, 4 other adenoviruses (two types 5 and two types 41) were identified using PCR/partial sequencing. In addition, using metagenomics, 8 cases of adenovirus revealed the adeno associated, dependovirus-parvovirus A (AAV), and 2 cases were AAV type 2. Interestingly, AAVtype 2 has not been previously associated with any human pathology. Additionally, other viruses of known pathogenic interest have been found: 1 coronavirus NL63, 1 echovirus 11, 3 sapporo virus, and 2 parechovirus. Multiple pathogens were found in 15 cases, while no pathogens were found in 10 cases. The HAECC report in Spain concluded that adenovirus was commonly detected in severe acute hepatitis of unknown causes.

It is worth mentioning that the liver histology of autoimmune hepatitis is very similar to that induced by drugs or toxins, characterized by the presence of eosinophils. Hepatitis has been reported as part of a multisystem inflammatory syndrome in children (MIS-C) (Heinz et al., 2020; Xu et al., 2020). While it is well-known that influenza viruses, coronavirus, herpesvirus, CMV and EBV virus can cause hepatitis in both immunocompetent and immunocompromised adults and children (Spengler, 2020), none of the aforementioned viruses can be associated with the current case of severe acute hepatitis in pediatric patients. Regarding the management of clinical patients, the majority of children with severe acute hepatitis typically achieve full recovery with supportive care. However, it is important to acknowledge that the clinical course of the disease can be unpredictable, and in rare instances, it may progress to acute liver failure. Therefore, it is crucial for clinicians to be well-informed about the signs that indicate disease severity progression and to stablish a threshold for referring patients to a liver transplant center (Leiskau et al., 2023) (Box 1).

Was SARS-CoV-2 infection a critical cofactor for the development of severe acute hepatitis in children?

The prevalence of induced hepatic dysfunction including “cytokine storm” injury (Li and Fan, 2020; Trevenzoli et al., 2020), increased susceptibility to HAdVs contagion or a greater virulence of the adenovirus caused by the concurrent SARS-CoV-2 infection(Brodin and Arditi, 2022), hyper immunization-related factors (Avci and Abasiyanik, 2021; Bril et al., 2021; Rocco et al., 2021; Vuille-Lessard et al., 2021), molecular mimicry (Lai et al., 2022), and auto-inflammatory dysregulation caused by the virus itself (Vojdani and Kharrazian, 2020; Bril et al., 2021; Rocco et al., 2021; Vuille-Lessard et al., 2021), have supported a potential relationship between SARS-CoV-2 infection and the severe acute hepatitis in children. However, only 15% of the children with available data in Europe and 10% of cases in USA, meet the conditions (World Health Organization (WHO), 2022). For example, in the previously mentioned series of 44 children from the same hospital in Birmingham, Al, USA, only one child tested positive for SARS-CoV-2, 6-8 weeks prior a seizure episode (Kelgeri et al., 2022). For acute hepatitis, only 11 of 39 children were positive for SARS-CoV-2 at admission.

The increase in severe acute hepatitis coincided with the moment in which the Delta variant alternated with the Omicron variant. The latter was described to cause gastrointestinal symptoms in children, such as vomiting, diarrhea, abdominal pain, and anorexia, suggesting an increase in intestinal tropism of SARS-CoV-2 that overlaps with the described ACE2 expression in the small intestine (Zhang et al., 2022). Interestingly, despite the high expression of ACE2 in hepatocytes and cholangiocytes, and that the viral tropism for the liver and the underlying mechanisms have been stablished (Wanner et al., 2022), the hepatic involvement of COVID-19 is very rare (Louis et al., 2022). This observation appears to rule out a direct implication of Omicron infection and non A-E acute hepatitis cases. However, concomitant infections of Omicron with HAdV-F41, or Adeno Associated Virus 2 (AAV2) was proposed by Grand (Grand, 2022). An attractive hypothesis suggests that SARS-CoV-2 may be acting as a superantigen, suggesting that these cases of severe acute hepatitis in children infected by SARS-CoV-2 could be caused by a previous HAdV-F41 infection in the intestine (Brodin and Arditi, 2022). This idea stems from the description of cases where severe hepatitis resulted from a multisystem inflammatory syndrome (MIS) observed in children with COVID-19 (Cantor et al., 2020). However, MIS typically occurs 3-4 weeks after the peak of COVID-19, and 60% of seropositive children with MIS have no detectable virus, indicating that MIS may result from the immune response following the infection (Verdoni et al., 2020). It is worth noting the persistence of SARS-CoV-2 viral RNA in the gastrointestinal tract of children compared to adults, potentially leading to repeated activation of the immune system (Wong et al., 2021; Xing et al., 2020; UKHSA, 2022). The SARS-CoV2 envelope glycoprotein S (Spike) contains a sequence with structural motif similar to a bacterial "superantigen" (enterotoxin B from Staphylococcus aureus) (Cheng et al., 2020), capable of directly binding to T cell receptors and triggering excessive and uncontrolled activation of the immune system (Brown and Bhardwaj, 2021; Noval Rivas et al., 2021; Ramaswamy et al., 2021; Sacco et al., 2022). Analogous to HIV-1 patients, children previously infected with SARS-CoV-2 may experience repetitive immune activation due to the prolonged presence of SARS-CoV-2 in the gastrointestinal tract (Brodin, 2022; Xia et al., 2022). Consequently, if, normally, the immune system activates less than 0.001% of the available T lymphocytes, in the presence of a superantigen up to 30% T lymphocytes are activated, generating a massive release of proinflammatory cytokines (Brodin, 2022), similarly to what has been reported for multiple bacterial toxins or viral molecules (Pérez-Gracia et al., 2022). Under these conditions, children may become susceptible to other viral infections, and repeated activation by adenovirus coinfection could increase the risk of toxic shock and liver damage (Yarovinsky et al., 2005; Brodin and Arditi, 2022). This scenario may arise from the interaction between the SARS-CoV-2 superantigen and a host sensitized with HAdV-41F (Brodin and Arditi, 2022). MIS is observed in a small proportion of children, appearing a few weeks or months after disease onset, even in cases of mild disease, leading to hepatitis that requires hospitalization in 40% of cases. It has been suggested that the deterioration of the intestinal barrier associated with these infections allows the viruses to enter the bloodstream, triggering inflammation (Cantor et al., 2020; Yonker et al., 2021). Animal studies have demonstrated that HAdVs infection sensitizes subjects to subsequent staphylococcal enterotoxin B-mediated toxic shock, resulting in liver failure and death. This phenomenon may be attributed to HAdV-induced type 1 immune dysregulation, characterized by excessive production of IFN-γ and IFN-γ-mediated hepatocyte apoptosis (Yarovinsky et al., 2005). Therefore, it is suggested that severe acute hepatitis in children could have a similar mechanism, resulting from HAdVs infection with intestinal trophism in children previously infected with SARS-CoV-2 (Brodin and Arditi, 2022).

Despite initially appearing as an enticing hypothesis, the relationship of the disease with the SARS-CoV-2 infection was not confirmed (Brodin and Arditi, 2022; Pérez-Gracia et al., 2022). Moreover, the recent study by Ho et al., has confirmed that that there is no direct link between COVID-19 and the occurrence of acute hepatitis (Ho et al., 2023), thereby debunking the captivating "superantigen" hypothesis.

The contribution of HAdV as potential triggers of severe acute hepatitis in children?

Adenovirus infections have been frequently reported in countries where cases of severe acute hepatitis have been documented, with approximately 90% of affected children testing positive for human adenovirus (HAdVs) in the two cohorts from Alabama (USA) and the United Kingdom (UK). Adenoviruses (family *Adenoviridae)* are 90–100 nm non enveloped viruses, with an icosahedral nucleocapsid containing a linear genome (double-stranded, ds) dsDNA that ranges between 26 and 48 Kb. These agents have a broad variety of vertebrate hosts. In humans, more than 50 distinct adenovirus serotypes are recognized associated to illnesses that range from the common cold to life-threatening multi-organ disease in people with a weakened immune system (Lynch et al., 2011). Currently, 88 human adenoviruses (HAdVs) of seven species have been defined (Human Adenovirus A to G) associated with different conditions (Benkő et al., 2022).

Adenovirus serotypes 40-41 have a higher affinity for the gastrointestinal tract among the different adenovirus species, being HAdV-41 infection one of the most frequent causes of viral gastroenteritis in children. These serotypes have been reported in immunosuppressed individuals related to numerous conditions such as hematopoietic stem cell transplantation, solid organ transplantation, human immunodeficiency virus infection, chemotherapy, and congenital hepatitis, or immunodeficiency syndromes (Rocholl et al., 2004; Ozbay Hoşnut et al., 2008; Khalifa et al., 2022). Despite, they are not associated to hepatitis in immunocompetent children (Rocholl et al., 2004; Hough et al., 2005; Kawashima et al., 2015), multi organ infections with HAdVs, including hepatitis, from very focal to very extensive, have been reported occasionally in immunocompetent newborns (Schaberg et al., 2017). In the case of immunocompromised adults, hepatitis caused by these adenovirus is lethal, while in pediatric patients lethality is approximately 60-65% (Ronan et al., 2014).

It is noticeable that all 9 children in the Alabama series and 27 of the 30 children who underwent molecular testing in the UK study, tested positive for HAdV human adenovirus type F41 (HAdV-F41) (Karpen, 2022; UKHSA, 2022). Indeed, HAdV has been detected in whole blood specimens, with the high positivity rate of 69% in EU, suggesting its role as a pathogenic microorganism. According to UK respiratory infection surveillance data, a significant increase in the rate of HAdVs infection in healthy children has been observed in recent weeks compared to previous years, especially in children from 1 to 9 years of age (UKHSA, 2022). Remarkably, serum viral load values of HAdV-F41 in patients with progression to liver failure, especially those who required liver transplantation, were substantially higher compared to patients who recovered spontaneously: median of 20,722 versus 2,733 viral copies/mL (Kelgeri et al., 2022). Altogether these reports represent adequate evidence that HAdV-F41 may have been involved as a cause for pediatric liver failure (Garnett et al., 2009).

However, some questions arise regarding the aforementioned observations. The ECDC report indicates that more than 25% of children with severe acute hepatitis tested positive for HAdVs infection in their respiratory, serum or stool samples (who/ecdc, 2022). However, concerns about the accuracy of these findings are raised due to the detection of positive throat swabs in 11% of healthy children in the same ECDC report. Furthermore, studies have shown that some children may test positive for adenovirus only in whole blood and at very low concentrations (Leen and Rooney, 2005; Djeneba et al., 2007; Song et al., 2016). Histological studies of liver biopsies from affected patients also fail to provide evidence of hepatocellular adenoviral infection (Gutierrez Sanchez et al., 2022). It is important to note that the standard reference method for diagnosing HAdVs-related hepatitis is the detection of the virus in inclusion bodies in liver biopsies (Schaberg et al., 2017), which have not been found in the reported cases mentioned above. Finally, the absence of adenovirus in hepatocytes, but the presence of severe liver injury leading to acute liver failure, may be related to an abnormal immune response of the host's hepatic immune system (Pérez-Gracia et al., 2022) (Rocholl et al., 2004; Ozbay Hoşnut et al., 2008; Khalifa et al., 2022).

In summary, the previous reports indicate that 90% of affected children tested positive for human adenovirus in two cohorts from USA and the UK. Additionally, adenovirus positivity was found in 55% of cases in Europe and 45% in the USA (World Health Organization (WHO), 2022). This finding provides sufficient evidences that HAdVs may be involved, in some way, in causing severe acute hepatitis in children.

The contribution of HAdV in association with AAV2 as a cause of severe acute hepatitis in children

AAV2 is a single-stranded DNA virus with 4675 nucleotides which belongs to the family *Parvoviridae, genus Dependoparvovirus* (ICTV, 2023). The AAV2 virus has a broad tissue tropism that can only replicate in the presence of a "helper" virus, often a Human Adenoviruses (HAdV), but also herpesvirus or even human papillomavirus for productive replication in mammalian cells (Casto et al., 1967; Buller et al., 1981; Carter, 2004; Samulski and Muzyczka, 2014). AAV itself did not cause any disease in the absence of helper virus, AAVs can give rise to latent infections where the viral DNA is maintained as circular episomes or is integrated in the chromosomal DNA (Muzyczka and Berns, 2001; Kerr et al., 2006; Samulski and Muzyczka, 2014). Although contact with AAVs is nearly universal, with more than 70% of the population having antibodies to AAV1–3 and AAV5, the presence of viral DNA has been detected in only a small proportion of cases. In fact, AAVs infection has not been linked to any specific human disease and typically elicits a mild immune response. Even immunocompromised patients exhibit very low levels of viremia, and there is limited evidence to suggest that AAVs cause clinical symptoms. These observations indicate that AAVs do not play, by itself, a pathogenic role in organ-specific diseases or in highly immunocompromised populations (Heugel et al., 2011).

Surprisingly, a recent study carried out in Scotland, detected the AAV2 virus in plasma of 9 out of 9 children and in the liver of 4 out of 4 patients, but no positivity was found in serum/plasma of 13 age-matched healthy controls (Ho et al., 2023). In addition, 12 children infected with adenovirus (HAdV) with normal liver function were found negative for AAV, and similarly, the HAdV was not detected in 33 hospitalized children with hepatitis of other etiologies. In this study HAdV (species C and F) and human herpesvirus 6B (HHV6B) have been detected in 6 out of 9 and 3 out of 9 affected cases respectively, including in 3 out of 4 and 2 out of 4 liver biopsies.

In the same report, it was observed that 8 out of 9 patients had the HLA-DRB1* 04: 41 class II allele, present at a much lower frequency in the general Scottish population, indicative of an association of this allele with the increased susceptibility to infection with the above mentioned viruses (Ho et al., 2023).

In this context, prolonged lockdowns have been proposed as a factor limiting children's exposure to HAdVs and AAV, potentially reducing their natural immunity. Sequencing data indicate no amino acid differences in the E1A, E2A and E4 HAdVs proteins, and no relevant differences have been reported in the AAV2 (AAVv66) capsid that could impact their tropism. Nevertheless, patients displayed some dissimilarities compared to healthy controls (Grand, 2022; Gutierrez Sanchez et al., 2022; Morfopoulou et al., 2022; Ho et al., 2023). On the other hand, alterations in AAVv66 have been observed diminishing its ability to bind heparin. These changes may account for increased virion stability, production, evasion of neutralizing antibodies, enhanced tissue spread, and improved transduction potential to the central nervous system (Hsu et al., 2020; Ho et al., 2023).

The evidence for the presence of HAdV41 in many cases of severe acute hepatitis in children is strong, and recent studies provide unequivocal confirmation of AAV2 involvement. These findings suggest that HAdVs may potentially act as a helper virus for AAV2 (Leiskau et al., 2023), with/without eventual mutations in the AAV2 genome (Grand, 2022; Morfopoulou et al., 2022; Ho et al., 2023).

Technological solutions based on high-throughput sequencing methodologies have improved the chances of detecting DNA and RNA viruses in a clinical sample. Using metagenomic (Ibañez-Lligoña et al., 2023) to identify both RNA and DNA viruses next-generation sequencing (NGS) on NextSeq500 (Illumina) platform, and target enrichment NGS using VirCapSeq-VERT Capture probes, together with reverse transcription-polymerase chain reaction (RT-PCR), serology and *in situ* hybridisation(ISH), Ho et al. detected recent infection with AAV2 in the plasma and liver samples of 81% of the Scottish pediatric hepatitis cases and only in 7% of controls. Interestingly, an increase in HAdV diagnoses in Scotland directly preceded the outbreak of unknown severe hepatitis in children of a similar age (UKHSA, 2022). A helper virus is required to support AAV2 replication, and AAV2 RNA was detected within ballooned hepatocytes suggesting the presence of replicating virus. Moreover, authors found a strong association between affected children and the Human Leucocyte Antigen (HLA) class II DRB1*04:01 allele, since it was identified in 93% (25/27) cases compared with the background frequency of 10/64 (16%) in study controls (Ho et al., 2023), and only 0.11% in UK unrelated biobank samples.

To summarize

Regarding the etiology of Pediatric Severe Acute Hepatitis, recent publication emphasizes that there is no link between COVID-19 and the current outbreak, contradicting previous suggestions. Autoimmune disease is also deemed less likely due to the absence of autoantibodies in affected cases and atypical histology in liver specimens. Results from Ho et al. strongly indicate a plausible association between concurrent HAdV infection and coinfected or reactivated AAV2 infection, leading to severe acute hepatitis in susceptible children carrying the HLA class II allele HLA-DRB1*04:01. This study paves the way for population-level investigations into the role of AAV2 and a helper virus (such as HAdV and/or HHV6B) of pediatric severe acute hepatitis with an unknown etiology.

Author contributions

The three authors FR-F, JQ and AR-S have significantly contributed in designing, collecting information and writing the manuscript. All authors approved the submitted version.

Funding

This study was partially supported by Pla Estratègic de Recerca i Innovació en Salut (PERIS)—Direcció General de Recerca i Innovació en Salut (DGRIS), Catalan Health Ministry, Generalitat de Catalunya; Centro para el Desarrollo Tecnológico Industrial (CDTI) from the Spanish Ministry of Economy and Business, grant number IDI-20200297; Projects PI19/00301, PI20/01692 and PI22/00258 funded by Instituto de Salud Carlos III (ISCIII) and co-funded by the European Union and Gilead's biomedical re-search projects GLD21/00006, GLD22/00080.

Acknowledgments

We thank Dra. Rosanna Paciucci for English language support.

Conflict of interest

The authors declare that the research was conducted in the absence of any commercial or financial relationships that could be construed as a potential conflict of interest.

Publisher's note

References

Alonso, E. M., Horslen, S. P., Behrens, E. M., and Doo, E. (2017). Pediatric acute liver failure of undetermined cause: a research workshop. *Hepatology* 65, 1026–1037. doi: 10.1002/hep.28944

Avci, E., and Abasiyanik, F. (2021). Autoimmune hepatitis after SARS-CoV-2 vaccine: New-onset or flare-up? *J. Autoimmun.* 125, 102745. doi: 10.1016/j.jaut.2021.102745

Benkő, M., Aoki, K., Arnberg, N., Davison, A. J., Echavarría, M., Hess, M., et al. (2022). ICTV virus taxonomy profile: adenoviridae 2022. *J. Gen. Virol.* 103 (3), 001721. doi: 10.1099/jgv.0.001721

Bril, F., Al Diffalha, S., Dean, M., and Fettig, D. M. (2021). Autoimmune hepatitis developing after coronavirus disease 2019 (COVID-19) vaccine: Causality or casualty? *J. Hepatol.* 75, 222–224. doi: 10.1016/j.jhep.2021.04.003

Brodin, P. (2022). SARS-CoV-2 infections in children: Understanding diverse outcomes. *Immunity* 55, 201–209. doi: 10.1016/j.immuni.2022.01.014

Brodin, P., and Arditi, M. (2022). Severe acute hepatitis in children: investigate SARS-CoV-2 superantigens. *Lancet Gastroenterol. Hepatol.* 7, 594–595. doi: 10.1016/S2468-1253(22)00166-2

Brown, M., and Bhardwaj, N. (2021). Super(antigen) target for SARS-CoV-2. *Nat. Rev. Immunol.* 21, 72. doi: 10.1038/s41577-021-00502-5

Buller, R. M., Janik, J. E., Sebring, E. D., and Rose, J. A. (1981). Herpes simplex virus types 1 and 2 completely help adenovirus-associated virus replication. *J. Virol.* 40, 241–247. doi: 10.1128/JVI.40.1.241-247.1981

Cantor, A., Miller, J., Zachariah, P., DaSilva, B., Margolis, K., and Martinez, M. (2020). Acute hepatitis is a prominent presentation of the multisystem inflammatory syndrome in children: a single-center report. *Hepatology* 72, 1522–1527. doi: 10.1002/hep.31526

Carter, B. J. (2004). Adeno-associated virus and the development of adeno-associated virus vectors: a historical perspective. *Mol. Ther.* 10, 981–989. doi: 10.1016/j.ymthe.2004.09.011

Casto, B. C., Atchison, R. W., and Hammon, W. M. (1967). Studies on the relationship between adeno-associated virus type I (AAV-1) and adenoviruses. I. Replication of AAV-1 in certain cell cultures and its effect on helper adenovirus. *Virology* 32, 52–59. doi: 10.1016/0042-6822(67)90251-6

Centers for Disease Control and Prevention (CDC) (2022) *Children with Hepatitis of Unknown Cause*. Available at: https://www.cdc.gov/ncird/investigation/hepatitis-unknown-cause/overview-what-to-know.html (Accessed 22 February 2023).

Cheng, M. H., Zhang, S., Porritt, R. A., Noval Rivas, M., Paschold, L., Willscher, E., et al. (2020). Superantigenic character of an insert unique to SARS-CoV-2 spike supported by skewed TCR repertoire in patients with hyperinflammation. *Proc. Natl. Acad. Sci. U.S.A.* 117, 25254–25262. doi: 10.1073/pnas.2010722117

Djeneba, O., Damintoti, K., Denise, I., Christelle, N. W. M., Virgilio, P., Adrien, B., et al. (2007). Prevalence of rotavirus, adenovirus and enteric parasites among pediatric patients attending Saint Camille Medical Centre in Ouagadougou. *Pakistan J. Biol. Sci. PJBS* 10, 4266–4270. doi: 10.3923/pjbs.2007.4266.4270

Gallegos-Orozco, J. F., and Rakela-Brödner, J. (2010). Hepatitis viruses: not always what it seems to be. *Rev. Med. Chil.* 138, 1302–1311. doi: 10.4067/S0034-98872010001100016

Garnett, C. T., Talekar, G., Mahr, J. A., Huang, W., Zhang, Y., Ornelles, D. A., et al. (2009). Latent species C adenoviruses in human tonsil tissues. *J. Virol.* 83, 2417–2428. doi: 10.1128/JVI.02392-08

Gong, K., Xu, X., Yao, J., Ye, S., Yu, X., Tu, H., et al. (2022). Acute hepatitis of unknown origin in children: A combination of factors. *Front. Pharmacol.* 13. doi: 10.3389/fphar.2022.1056385

Grand, R. J. (2022). A link between severe hepatitis in children and adenovirus 41 and adeno-associated virus 2 infections. *J. Gen. Virol.* 103(11). doi: 10.1099/jgv.0.001783

Gutierrez Sanchez, L. H., Shiau, H., Baker, J. M., Saaybi, S., Buchfellner, M., Britt, W., et al. (2022). A case series of children with acute hepatitis and human adenovirus infection. *N. Engl. J. Med.* 387, 620–630. doi: 10.1056/NEJMoa2206294

Heinz, N., Griesemer, A., Kinney, J., Vittorio, J., Lagana, S. M., Goldner, D., et al. (2020). A case of an Infant with SARS-CoV-2 hepatitis early after liver transplantation. *Pediatr. Transplant.* 24, e13778. doi: 10.1111/petr.13778

Heugel, J., Boeckh, M., Huang, M.-L., Dierks, B., Hackman, R., Fredricks, D., et al. (2011). Detection of adeno-associated virus viremia in hematopoietic cell transplant recipients. *J. Infect. Dis.* 204, 1746–1749. doi: 10.1093/infdis/jir655

Ho, A., Orton, R., Tayler, R., Asamaphan, P., Herder, V., Davis, C., et al. (2023). Adeno-associated virus 2 infection in children with non-A-E hepatitis. *Nature* 617 (7961), 555–563. doi: 10.1038/s41586-023-05948-2

Hough, R., Chetwood, A., Sinfield, R., Welch, J., and Vora, A. (2005). Fatal adenovirus hepatitis during standard chemotherapy for childhood acute lymphoblastic leukemia. *J. Pediatr. Hematol. Oncol.* 27, 67–72. doi: 10.1097/01.mph.0000153958.95486.6f

Hsu, H.-L., Brown, A., Loveland, A. B., Lotun, A., Xu, M., Luo, L., et al. (2020). Structural characterization of a novel human adeno-associated virus capsid with neurotropic properties. *Nat. Commun.* 11, 3279. doi: 10.1038/s41467-020-17047-1

Ibañez-Lligoña, M., Colomer-Castell, S., González-Sánchez, A., Gregori, J., Campos, C., Garcia-Cehic, D., et al. (2023). Bioinformatic tools for NGS-based metagenomics to improve the clinical diagnosis of emerging, re-emerging and new viruses. *Viruses* 15 (12), 587. doi: 10.3390/v15020587

ICTV (2023) *Family: Parvoviridae*. Available at: https://ictv.global/report/chapter/parvoviridae/parvoviridae/dependoparvovirus (Accessed 31 March 2023).

Karpen, S. J. (2022). Acute hepatitis in children in 2022 - human adenovirus 41? *N. Engl. J. Med.* 387, 656–657. doi: 10.1056/NEJMe2208409

Kawashima, N., Muramatsu, H., Okuno, Y., Torii, Y., Kawada, J., Narita, A., et al. (2015). Fulminant adenovirus hepatitis after hematopoietic stem cell transplant: Retrospective real-time PCR analysis for adenovirus DNA in two cases. *J. Infect. Chemother. Off. J. Japan Soc Chemother.* 21, 857–863. doi: 10.1016/j.jiac.2015.08.018

Kelgeri, C., Couper, M., Gupte, G. L., Brant, A., Patel, M., Johansen, L., et al. (2022). Clinical spectrum of children with acute hepatitis of unknown cause. *N. Engl. J. Med.* 387, 611–619. doi: 10.1056/NEJMoa2206704

Kerr, J. R., Cotmore, S. F., and Bloom, M. E. (2006). *Parvoviruses* (1st. ed.). (London: CRC Press). doi: 10.1201/b13393

Khalifa, A., Andreias, L., and Velpari, S. (2022). Adenovirus hepatitis in immunocompetent adults. *J. Investig. Med. High impact Case Rep.* 10, 23247096221079190. doi: 10.1177/23247096221079192

Lai, Y.-C., Cheng, Y.-W., Chao, C.-H., Chang, Y.-Y., Chen, C.-D., Tsai, W.-J., et al. (2022). Antigenic cross-reactivity between SARS-CoV-2 S1-RBD and its receptor ACE2. *Front. Immunol.* 13. doi: 10.3389/fimmu.2022.868724

Leen, A. M., and Rooney, C. M. (2005). Adenovirus as an emerging pathogen in immunocompromised patients. *Br. J. Haematol.* 128, 135–144. doi: 10.1111/j.1365-2141.2004.05218.x

Leiskau, C., Tsaka, S., Meyer-Ruhnke, L., Mutschler, F. E., Pfister, E.-D., Lainka, E., et al. (2023). Acute severe non-A-E-hepatitis of unknown origin in children - a 30-year retrospective observational study from north-west Germany. *J. Hepatol.* 78, 971–978. doi: 10.1016/j.jhep.2022.12.012

Li, J., and Fan, J.-G. (2020). Characteristics and mechanism of liver injury in 2019 coronavirus disease. *J. Clin. Transl. Hepatol.* 8, 13–17. doi: 10.14218/JCTH.2020.00019

Louis, T. J., Qasem, A., Abdelli, L. S., and Naser, S. A. (2022). Extra-pulmonary complications in SARS-CoV-2 infection: a comprehensive multi organ-system review. *Microorganisms* 10 (1), 153. doi: 10.3390/microorganisms10010153

Lynch, J. P., Fishbein, M., and Echavarria, M. (2011). Adenovirus. *Semin. Respir. Crit. Care Med.* 32, 494–511. doi: 10.1055/s-0031-1283287

Ministerio de Sanidad (2022) *Severe acute non-A-E hepatitis of unknown cause in children under 16 years of age. Final situation report (Spanish) 28.12.2022*. Available at: https://www.sanidad.gob.es/profesionales/saludPublica/ccayes/alertasActual/hepatitis.htm (Accessed 22 February 2023).

Morfopoulou, S., Buddle, S., Torres Montaguth, O. E., Atkinson, L., Guerra-Assunção, J. A., Storey, N., et al. (2022). Genomic investigations of acute hepatitis of unknown aetiology in children. *medRxiv* 2022, 22277963. doi: 10.1101/2022.07.28.22277963

Muzyczka, N., and Berns, K. I. (2001). Parvoviridae: the viruses and their replication. in *Fields Virol.*, D. M. Knipe, P. M. Howley, D. E. Griffen, R. A. Lamb, M. A. Martin, B. Roizman and S. E. Straus (ed.). Lippincott Williams and Wilkins: Philadelphia, Pa" p. 2327–2359.

Noval Rivas, M., Porritt, R. A., Cheng, M. H., Bahar, I., and Arditi, M. (2021). COVID-19-associated multisystem inflammatory syndrome in children (MIS-C): a novel disease that mimics toxic shock syndrome-the superantigen hypothesis. *J. Allergy Clin. Immunol.* 147, 57–59. doi: 10.1016/j.jaci.2020.10.008

Ozbay Hoşnut, F., Canan, O., Ozçay, F., and Bilezikçi, B. (2008). Adenovirus infection as possible cause of acute liver failure in a healthy child: a case report. *Turkish J. Gastroenterol. Off. J. Turkish Soc Gastroenterol.* 19, 281–283.

Pan, L.-X., Wang, G.-Y., Zhong, J.-H., and Fan, X.-H. (2022). Current knowledge about the outbreak of acute severe hepatitis of unknown origin among children. *J. Clin. Transl. Res.* 8, 470–475.

Pérez-Gracia, M. T., Tarín-Pelló, A., and Suay-García, B. (2022). Severe acute hepatitis of unknown origin in children: what do we know today? *J. Clin. Transl. Hepatol.* 10, 711–717. doi: 10.14218/JCTH.2022.00244

Ramaswamy, A., Brodsky, N. N., Sumida, T. S., Comi, M., Asashima, H., Hoehn, K. B., et al. (2021). Immune dysregulation and autoreactivity correlate with disease severity in SARS-CoV-2-associated multisystem inflammatory syndrome in children. *Immunity* 54, 1083–1095.e7. doi: 10.1016/j.immuni.2021.04.003

Rocco, A., Sgamato, C., Compare, D., and Nardone, G. (2021). Autoimmune hepatitis following SARS-CoV-2 vaccine: May not be a casuality. *J. Hepatol.* 75, 728–729. doi: 10.1016/j.jhep.2021.05.038

Rocholl, C., Gerber, K., Daly, J., Pavia, A. T., and Byington, C. L. (2004). Adenoviral infections in children: the impact of rapid diagnosis. *Pediatrics* 113, e51–e56. doi: 10.1542/peds.113.1.e51

Rodríguez-Frías, F., Quer, J., Tabernero, D., Cortese, M. F., Garcia-Garcia, S., Rando-Segura, A., et al. (2021). Microorganisms as shapers of human civilization, from pandemics to even our genomes: villains or friends? A historical approach. *Microorganisms* 9 (12), 2518. doi: 10.3390/microorganisms9122518

Ronan, B. A., Agrwal, N., Carey, E. J., De Petris, G., Kusne, S., Seville, M. T., et al. (2014). Fulminant hepatitis due to human adenovirus. *Infection* 42, 105–111. doi: 10.1007/s15010-013-0527-7

Sacco, K., Castagnoli, R., Vakkilainen, S., Liu, C., Delmonte, O. M., Oguz, C., et al. (2022). Immunopathological signatures in multisystem inflammatory syndrome in children and pediatric COVID-19. *Nat. Med.* 28, 1050–1062. doi: 10.1038/s41591-022-01724-3

Samulski, R. J., and Muzyczka, N. (2014). AAV-mediated gene therapy for research and therapeutic purposes. *Annu. Rev. Virol.* 1, 427–451. doi: 10.1146/annurev-virology-031413-085355

Schaberg, K. B., Kambham, N., Sibley, R. K., and Higgins, J. P. T. (2017). Adenovirus hepatitis: clinicopathologic analysis of 12 consecutive cases from a single institution. *Am. J. Surg. Pathol.* 41, 810–819. doi: 10.1097/PAS.0000000000000834

Song, E., Wang, H., Kajon, A. E., Salamon, D., Dong, S., Ramilo, O., et al. (2016). Diagnosis of pediatric acute adenovirus infections: is a positive PCR sufficient? *Pediatr. Infect. Dis. J.* 35, 827–834. doi: 10.1097/INF.0000000000001119

Spengler, U. (2020). Liver disease associated with non-hepatitis viruses. *Encycl. Gastroenterol.*, 363–376. doi: 10.1016/B978-0-12-801238-3.65782-3

Squires, J. E., Alonso, E. M., Ibrahim, S. H., Kasper, V., Kehar, M., Martinez, M., et al. (2022). North american society for pediatric gastroenterology, hepatology, and nutrition position paper on the diagnosis and management of pediatric acute liver failure. *J. Pediatr. Gastroenterol. Nutr.* 74, 138–158. doi: 10.1097/MPG.0000000000003268

Squires, R. H., Ng, V., Romero, R., Ekong, U., Hardikar, W., Emre, S., et al. (2014). Evaluation of the pediatric patient for liver transplantation: 2014 practice guideline by the American Association for the Study of Liver Diseases, American Society of Transplantation and the North American Society for Pediatric Gastroenterology, Hepatol. *J. Pediatr. Gastroenterol. Nutr.* 59, 112–131. doi: 10.1097/MPG.0000000000000431

Squires, R. H. J., Shneider, B. L., Bucuvalas, J., Alonso, E., Sokol, R. J., Narkewicz, M. R., et al. (2006). Acute liver failure in children: the first 348 patients in the pediatric acute liver failure study group. *J. Pediatr.* 148, 652–658. doi: 10.1016/j.jpeds.2005.12.051

Trevenzoli, M., Guarnaccia, A., Alberici, I., Fassan, M., Di Meco, E., Farinati, F., et al. (2020). SARS-CoV-2 and hepatitis. *J. Gastrointestin. Liver Dis.* 29, 473–475. doi: 10.15403/jgld-2747

UKHSA (2022) *Investigation into acute hepatitis of unknown aetiology in children in England. Tec. Brief. 4.* Available at: https://www.gov.uk/government/publications/acute-h.

Verdoni, L., Mazza, A., Gervasoni, A., Martelli, L., Ruggeri, M., Ciuffreda, M., et al. (2020). An outbreak of severe Kawasaki-like disease at the Italian epicentre of the SARS-CoV-2 epidemic: an observational cohort study. *Lancet (London England)* 395, 1771–1778. doi: 10.1016/S0140-6736(20)31103-X

Vojdani, A., and Kharrazian, D. (2020). Potential antigenic cross-reactivity between SARS-CoV-2 and human tissue with a possible link to an increase in autoimmune diseases. *Clin. Immunol.* 217, 108480. doi: 10.1016/j.clim.2020.108480

Vuille-Lessard, É., Montani, M., Bosch, J., and Semmo, N. (2021). Autoimmune hepatitis triggered by SARS-CoV-2 vaccination. *J. Autoimmun.* 123, 102710. doi: 10.1016/j.jaut.2021.102710

Wanner, N., Andrieux, G., Badia-I-Mompel, P., Edler, C., Pfefferle, S., Lindenmeyer, M. T., et al. (2022). Molecular consequences of SARS-CoV-2 liver tropism. *Nat. Metab.* 4, 310–319. doi: 10.1038/s42255-022-00552-6

who/ecdc (2022) *Joint ECDC-WHO Regional Office for Europe Hepatitis of Unknown Origin in Children Surveillance Bulletin*. Available at: https://cdn.ecdc.europa.eu/novhep-surveillance/ (Accessed 22 February 2023).

Wong, Y. C., Lau, S. Y., Wang To, K. K., Mok, B. W. Y., Li, X., Wang, P., et al. (2021). Natural transmission of bat-like severe acute respiratory syndrome coronavirus 2 without proline-arginine-arginine-alanine variants in coronavirus disease 2019 patients. *Clin. Infect. Dis.* 73 (2), e437-e444. doi: 10.1093/cid/ciaa953

World Health Organization (WHO) (2022) *Severe acute hepatitis of unknown aetiology in children - Multi-country*. Available at: https://www.who.int/emergencies/disease-outbreak-news/item/2022-DON400 (Accessed 22 February 2023).

Xia, P., Xing, X.-D., Yang, C.-X., Liao, X.-J., Liu, F.-H., Huang, H.-H., et al. (2022). Activation-induced pyroptosis contributes to the loss of MAIT cells in chronic HIV-1 infected patients. *Mil. Med. Res.* 9, 24. doi: 10.1186/s40779-022-00384-1

Xing, Y.-H., Ni, W., Wu, Q., Li, W.-J., Li, G.-J., Wang, W.-D., et al. (2020). Prolonged viral shedding in feces of pediatric patients with coronavirus disease 2019. *J. Microbiol. Immunol. Infect.* 53, 473–480. doi: 10.1016/j.jmii.2020.03.021

Xu, L., Liu, J., Lu, M., Yang, D., and Zheng, X. (2020). Liver injury during highly pathogenic human coronavirus infections. *Liver Int. Off. J. Int. Assoc. Study Liver* 40, 998–1004. doi: 10.1111/liv.14435

Yarovinsky, T. O., Mohning, M. P., Bradford, M. A., Monick, M. M., and Hunninghake, G. W. (2005). Increased sensitivity to staphylococcal enterotoxin B following adenoviral infection. *Infect. Immun.* 73, 3375–3384. doi: 10.1128/IAI.73.6.3375-3384.2005

Yonker, L. M., Gilboa, T., Ogata, A. F., Senussi, Y., Lazarovits, R., Boribong, B. P., et al. (2021). Multisystem inflammatory syndrome in children is driven by zonulin-dependent loss of gut mucosal barrier. *J. Clin. Invest.* 131 (14), e149633. doi: 10.1172/JCI149633

Zhang, L.-Y., Huang, L.-S., Yue, Y.-H., Fawaz, R., Lim, J. K., and Fan, J.-G. (2022). Acute hepatitis of unknown origin in children: early observations from the 2022 outbreak. *J. Clin. Transl. Hepatol.* 10, 522–530. doi: 10.14218/JCTH.2022.00281

frontiers | Frontiers in Cellular and Infection Microbiology

TYPE Original Research
PUBLISHED 21 September 2023
DOI 10.3389/fcimb.2023.1177270

OPEN ACCESS

EDITED BY
Josep Quer,
Vall d'Hebron University Hospital, Spain

REVIEWED BY
Benjamin Anthony Krishna,
University of Cambridge, United Kingdom
Adrien Breiman,
Université de Nantes, France
Gerardo Santos-López,
Instituto Mexicano del Seguro Social (IMSS), Mexico

*CORRESPONDENCE
Rafael Delgado
rafael.delgado@salud.madrid.org

RECEIVED 01 March 2023
ACCEPTED 28 August 2023
PUBLISHED 21 September 2023

CITATION
Labiod N, Luczkowiak J, Tapia MM, Lasala F and Delgado R (2023) The role of DC-SIGN as a trans-receptor in infection by MERS-CoV. *Front. Cell. Infect. Microbiol.* 13:1177270. doi: 10.3389/fcimb.2023.1177270

The role of DC-SIGN as a trans-receptor in infection by MERS-CoV

Nuria Labiod[1], Joanna Luczkowiak[1], María M. Tapia[1], Fátima Lasala[1] and Rafael Delgado[1,2,3]*

[1]Department of Microbiology, Instituto de Investigación Hospital Universitario 12 de Octubre (Imas12), Madrid, Spain, [2]Departamento de Medicina, Facultad de Medicina, Universidad Complutense, Madrid, Spain, [3]CIBERINFEC, Instituto de Salud Carlos III, Madrid, Spain

DC-SIGN is a C-type lectin expressed in myeloid cells such as immature dendritic cells and macrophages. Through glycan recognition in viral envelope glycoproteins, DC-SIGN has been shown to act as a receptor for a number of viral agents such as HIV, Ebola virus, SARS-CoV, and SARS-CoV-2. Using a system of Vesicular Stomatitis Virus pseudotyped with MERS-CoV spike protein, here, we show that DC-SIGN is partially responsible for MERS-CoV infection of dendritic cells and that DC-SIGN efficiently mediates trans-infection of MERS-CoV from dendritic cells to susceptible cells, indicating a potential role of DC-SIGN in MERS-CoV dissemination and pathogenesis.

KEYWORDS

MERS-CoV, Coronaviruses, DC-SIGN, receptors, dendritic cell

Introduction

In the last 20 years, three coronaviruses have been identified as highly pathogenic for humans, which are severe acute respiratory syndrome coronavirus (SARS-CoV), Middle East respiratory syndrome coronavirus (MERS-CoV), and severe acute respiratory syndrome coronavirus 2 (SARS–CoV–2). In June 2012, a highly pathogenic coronavirus was identified at a hospital in Jeddah, Saudi Arabia, and later it was named Middle East respiratory syndrome coronavirus (MERS-CoV) (Zaki et al., 2012). The mortality rate of the virus was estimated at approximately 40% (Al Awaidy & Khamis, 2019). Dipeptidyl peptidase 4 (DPP4) has been demonstrated to be the functional cellular receptor for MERS-CoV (Raj et al., 2013). DPP4 or CD26 is primarily expressed on the surface of certain cell types, including epithelial cells in the respiratory tract, endothelial cells, and immune cells such as monocyte-derived DC (Mo-DC) (Scobey et al., 2013; Zhong et al., 2013; Chu et al., 2014). The importance of viral receptors has been thoroughly researched and it is a key factor in interpreting the pathogeny of the virus (Raj et al., 2013).

In these scenarios, the viral receptors present on dendritic cells (DCs) become interesting. DCs are found in the skin and mucosal tissue (van Kooyk, 2008) and circulate through extracellular spaces, actively surveying the presence of foreign antigens. They are considered the first line of defense against pathogenic invasion due to their

abundant expression of various receptors on their cell surface. These include pattern recognition receptors (PRRs) such as Toll-like receptors (TLRs) and C-type lectin receptors (CLRs) that recognize structures with a high mannose content (Lundberg & Rydnert, 2014).

It has been evidenced that the expression of the C-type lectin DC-SIGN (Dendritic cell-specific ICAM-3-grabbing nonintegrin) on dendritic cells plays an important role in the entry and dissemination processes of various viruses, such as the human immunodeficiency virus (HIV), which is one of the most studied cases. Conventional HIV infection involves virus binding to the CD4 receptor, followed by interaction with co-receptors such as CCR5 or CXCR4 on CD4+ T lymphocytes to initiate direct infection or cis infection. However, there is an alternative pathway. In dendritic cells, DC-SIGN recognizes the high mannose region of the HIV gp120 protein, conferring upon dendritic cells the ability to facilitate trans-infection. This means that dendritic cells can capture the virus and transmit it to susceptible cells that express the necessary receptors for viral entry. It has been shown that this mechanism represents a significant route of virus dissemination from mucosal surfaces to replication in T cells present in secondary lymphoid organs through the interaction of DC-SIGN with immature dendritic cells (Geijtenbeek et al., 2000).

These host binding factors also play a crucial role in viral infection mechanisms as they increase the density of viral particles on cell surfaces, promoting their adhesion and consequently facilitating access to the real receptors (Thépaut et al., 2021). These mechanisms that facilitate trans-infection, where secondary presentation through non-permissive cells avoid immunological recognition, play a relevant role not only in HIV but have also been described in other viruses such as SARS-CoV, SARS-CoV-2, Ebola virus, or Dengue (Alvarez et al., 2002; Tassaneetrithep et al., 2003; Jeffers et al., 2004; Léger et al., 2016; Guo et al., 2021; Lempp et al., 2021; Thépaut et al., 2021).

Therefore, this study aimed to explore the role of DC-SIGN present in dendritic cells in the viral infection and dissemination mechanisms of MERS-CoV.

Materials and methods

Cell lines

African Green Monkey Cell Line (Vero E6) and Baby hamster kidney cells (BHK-21, 12-14-17 MAW, Kerafast, Boston, MA) were cultured in Dulbecco´s modified Eagle medium (DMEM) supplemented with 10% heat-inactivated fetal bovine serum (FBS), 25 µg/mL gentamycin, and 2 mM L-glutamine.

Production of human monocyte-derived dendritic cells

Blood samples were obtained from healthy human donors (Hospital Universitario 12 de Octubre, Madrid, Spain) subject to informed consent and IRB approval. Peripheral blood mononuclear cells (PBMCs) were isolated by Ficoll density gradient centrifugation (Ficoll Paque, GE17-5442-02, Sigma-Aldrich). To generate monocyte-derived dendritic cells (MDDCs), CD14+ monocytes were purified using anti-human CD14 antibody-labeled magnetic beads and iron-based LS columns (Miltenyi Biotec) and used directly for further differentiation into dendritic cells (Domínguez-Soto et al., 2011). Differentiation to immature MDDCs was achieved by incubation at 37°C with 5% CO2 for 7 days and subsequent activation with cytokines GM-CSF (1000 U/mL) and IL-4 (500 U/mL) (Miltenyi Biotec) every other day.

Production of pseudotyped recombinant Vesicular Stomatitis Virus

rVSV-luc pseudotypes (PSV) were generated following a published protocol (Whitt, 2010). First, BHK-21cells were transfected using Lipofectamine 3000 (Fisher Scientific) to express the different viral envelope glycoproteins: Ebola virus Makona Glycoprotein (EBOV-GP, GenBank KM233102.1) and S protein of MERS-CoV (NC_019843) were synthesized and cloned into pcDNA3.1 by GeneArt AG technology (Life Technologies, Regensburg, Germany); S protein of SARS-CoV-2 (codon-optimized; kindly provided by J. García-Arriaza, CNB-CSIC, Spain) or S protein of SARS-CoV (SinoBiological, Cat: VG40150-G-N) were cloned into a pCMV/hygro vector. After 24 h, transfected cells were inoculated with a replication-deficient rVSV-luc pseudotype (MOI: 3–5) (Kerafast, Boston, MA). After 1 h incubation at 37°C, cells were washed exhaustively with PBS and then DMEM supplemented with 5% heat-inactivated FBS, and 25 µg/mL gentamycin and 2 mM L-glutamine were added. PSV were collected 24 h post-inoculation, clarified from cellular debris by centrifugation, and stored at -80°C. Infectious titers were estimated as tissue culture infectious doses by limiting dilution of rVSV-luc-pseudotypes on Vero E6 cells. Luciferase activity was determined by luciferase assay (Steady-Glo Luciferase Assay System, Promega).

Antibodies and inhibitors

The antibodies used in the experiments were Mouse IgG2a Isotype Control (Invitrogen), MERS Coronavirus Spike Protein neutralizing Antibody MA5-29975 (Invitrogen), Invitrogen CD26 Monoclonal Antibody (BA5b) (Invitrogen), Human DC-SIGN +DC-SIGNR Antibody (R&D Systems), PE anti-human CD209 (DC-SIGN) Antibody (Biolegend), and CD26 Monoclonal Antibody (BA5b) PE (Invitrogen). As a lectin-binding control, mannan from Saccharomyces cerevisiae (Sigma-Aldrich) was used. Mannan is used in experiments to inhibit C-type lectin receptors, such as DC-SIGN due to its ability to block the interaction between these receptors and viral or pathogenic ligands. Being a complex polysaccharide, mannan competes with the binding sites of the receptors, acting as a decoy and preventing the attachment of infectious agents to host cells (Jan et al., 2018).

Direct (in cis) cellular infection with PSV

primary cells MDDCs ($5x10^4$) were challenged with MERS-CoV, SARS-CoV, SARS-CoV-2, EBOV-GP pseudotyped recombinant viruses (MOI: 0.5–2), mannan, and different antibodies (Figure 1). After 24 h of incubation, cells were washed twice with PBS and lysed for luciferase assay.

Trans-infection assays with PSV

For trans-infection studies, MDDCs ($5x10^4$) were challenged with recombinant MERS-CoV, SARS-CoV, SARS-CoV-2, or EBOV-GP pseudotyped viruses (MOI: 0.5–2) and incubated for 2h with rotation (Figure 2). The antibodies were incubated with the MDDC cells 40 minutes prior to virus exposure, except for the

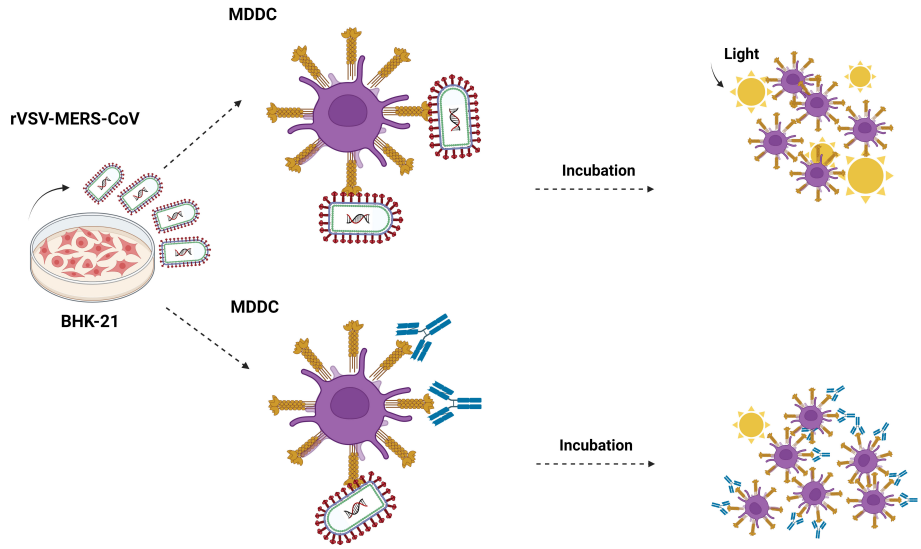

FIGURE 1
Cis-infection in monocyte-derived dendritic cells. Outline of the direct infection assay. MDDC cells are exposed to recombinant rVSV MERS-CoV, EBOV, SARS-CoV, and SARS-CoV-2 pseudotypes, and also in the presence of mannan, isotype control antibody, anti-DC/L-SIGN, anti-DPP4, and neutralizing anti-MERS antibodies. After 24 hours, the cells are washed and lysed for the luciferase assay. Made with Biorender.com.

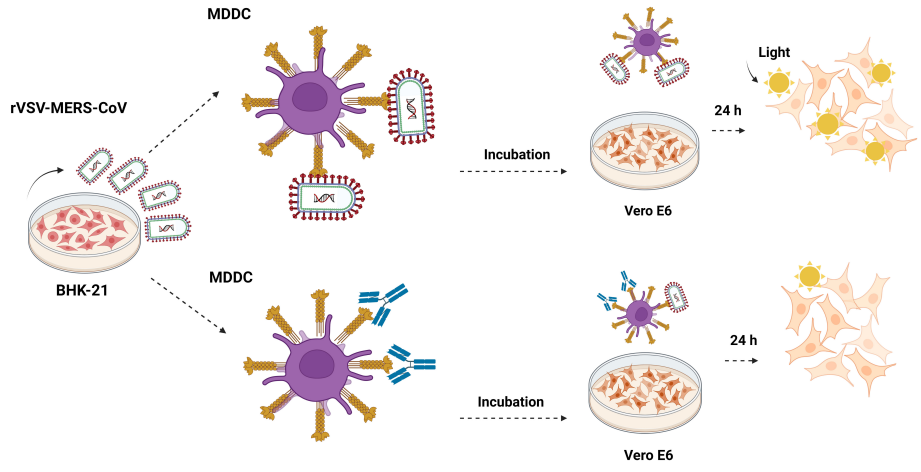

FIGURE 2
Trans-infection in monocyte-derived dendritic cells. Outline of the trans-infection assay. MDDC cells are exposed to recombinant rVSV MERS-CoV, EBOV, SARS-CoV, and SARS-CoV-2 pseudotypes, and also in the presence of mannan, isotype control antibody, anti-DC/L-SIGN, anti-DPP4, and neutralizing anti-MERS antibodies and incubated for 2h. After the incubation time, cells were centrifuged at 1200 rpm for 5 minutes and washed six times with PBS. MDDCs were then resuspended in RPMI medium and co-cultivated with adherent Vero E6 cells. After 24 hours, the cells were washed and lysed for the luciferase assay. They were made with Biorender.com.

neutralizing antibody against MERS, which was incubated with the virus for 40 minutes before the addition of the cells. After the incubation time, cells were then centrifuged at 1200 rpm for 5 minutes and washed six times with PBS supplemented with 0.5% bovine serum albumin (BSA) and 1 mM CaCl2 to ensure the removal of unbound virus from the cell receptor. The inclusion of CaCl2 in the wash buffer helps to maintain the integrity and functionality of DC-SIGN during the experimental procedures. After that, MDDCs were then resuspended in RPMI medium and co-cultivated with adherent Vero E6 cells ($1.5x10^5$ cells/well) on a 24-well plate. After 24h, the supernatant was removed and the monolayer of Vero E6 was washed with PBS six times and lysed for luciferase assay. These washes were performed to remove the co-cultivated dendritic cells from the Vero E6 cells and ensure that the infection observed in the Vero E6 cells was due to the trans-infection process and not direct infection that may occur in the MDDC cells. In order to control this variable, a parallel trans-infection experiment with MERS-CoV was also conducted on MDDC cells under the same conditions. After the incubation period, the dendritic cells were not co-cultivated with the Vero E6 target cells following the washes with PBS. The levels of RLU/s in the infection readout after 24 hours indicate the amount of MERS-CoV that had successfully entered through direct infection in the dendritic cells during the two-hour incubation period.

Verification of DC-SIGN's role as a trans-receptor for MERS-CoV

The duration of migration for a dendritic cell from the mucosal layers where MERS-CoV could potentially adhere to a deeper tissue where infection initiation occurs remains uncertain. To enhance our comprehension of this biological phenomenon, a trans-infection assay was conducted, incorporating varying time intervals between attachment and infection. In order to monitor the viral entry of MERS-CoV into MDDCs during these incubation periods, an infection assay was carried out under identical conditions. Trypsin treatment: To discern between viral attachment and entry into the cell, a trypsin treatment experiment (Hanley et al., 2010) was conducted on MDDCs both before and after exposure to the MERS-CoV virus. This was performed to ascertain whether trans-infection was stopped.

Results

DC-SIGN does not act as a direct receptor for MERS-CoV

MERS-CoV PSV demonstrated a clear capability to infect MDDC in cis, and levels of infection were reduced in the presence of anti-DC/L-SIGN although it was not significant, and it was reduced by mannan (Figure 1). Cis infection of MDDC with SARS-CoV-1 and SARS-CoV-2 PSV displayed a total absence of infection, whereas EBOV PSV exhibited clear infection of MDDC that was inhibited by anti-DC-SIGN as demonstrated before (Alvarez et al., 2002).

The isotype control antibody employed alongside the anti-DC/L-SIGN and anti-DPP4 antibodies confirmed the specificity of the primary antibody binding, ruling out any potential effects from other protein interactions or nonspecific Fc receptor binding. Cis infection by MERS-CoV in the presence of anti-DPP4 antibody exhibited a significant reduction, thereby demonstrating the utilization as a direct cellular receptor by MERS-CoV. Infection with MERS-CoV was completely abolished in the presence of its neutralizing antibody (Figure 3).

The results showed percentages (%) considering cis-infection in the absence of antibodies as 100% of infection.

To evaluate the effectiveness of these antibodies, a cis infection assay was conducted in human 293T cells and African green monkey Vero E6 cells.

The results showed that 293T cells were infected by MERS-CoV and SARS-CoV-2. MERS-CoV and SARS-CoV-2 infections in 293T were not inhibited by isotype control antibody; however, infection with MERS-CoV in the presence of the anti-DPP4 antibody showed a significant reduction, unlike SARS-CoV-2 where the infection persisted. Additionally, MERS-CoV infection has been inhibited in the presence of the neutralizing antibody (Supplementary Figure 1).

On the other hand, cis-infection showed that Vero E6 cells were infected by MERS-CoV and SARS-CoV-2 and this infection was not inhibited by isotype control antibody. Infection with MERS-CoV in the presence of the anti-DPP4 antibody did not show a significant reduction due to the anti-DPP4 antibody being a human antibody. Additionally, MERS-CoV infection has been inhibited in the presence of the neutralizing antibody (Supplementary Figure 2).

DC-SIGN acts as a trans-receptor for MERS-CoV

The trans-infection assay in MDDC with MERS-CoV PSV led to high levels of infection and anti-DC-SIGN exhibited a significant reduction in infectivity showing that DC-SIGN promoted an efficient trans-infection by MERS-CoV from MDDC to Vero E6 cells (Figure 4). Similar DC-SIGN-specific trans-infection was also shown for SARS-CoV, SARS-CoV-2, and EBOV PSV.

An isotype control antibody was used for both anti-DC/L-SIGN and anti-DPP4 antibodies to confirm that the binding of the primary antibody is specific and not the result of other protein interactions or non-specific binding of the Fc receptor. The trans-infection mediated by MERS-CoV was entirely suppressed when its neutralizing antibody was present, and the control of inhibition of infection mediated by lectin receptors mannan reduced the trans-infection. Finally, trans-infection by MERS-CoV in the presence of the anti-DPP4 antibody did not show a significant reduction.

On a separate note, to control the viral entry of MERS-CoV into MDDCs during these incubation periods, a concurrent trans-infection experiment involving MDDC cells was also carried out using identical conditions. Subsequent to the incubation phase, the dendritic cells were not co-cultured with the Vero E6 target cells after PBS washes. The levels of relative light units per second (RLU/s) in

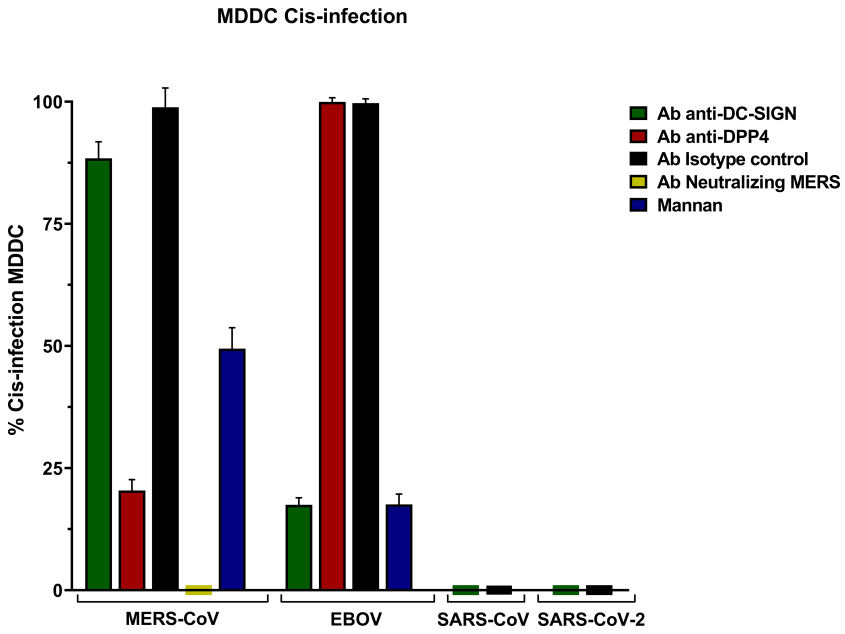

FIGURE 3
Cis-infection in Monocyte-derived Dendritic Cells (MDDC) with pseudoviruses based in rVSV-luc. Percentage of cis-infection in MDDCs, with SARS-CoV-2, SARS-CoV, MERS-CoV, and EBOV-GP, compared with infection in the absence of antibodies. Bars represent the mean SEM of the mean of four independent experiments with cells from two different donors performed in duplicates. Data were compared among multiple independent groups using one-way ANOVA (P= <0,0001) using GraphPad Prism v8. Cis-infection values are expressed as Percentage (%).

the infection readout after 24 hours demonstrated minimal infection by MERS-CoV, in comparison with the levels of trans-infection in Vero E6 (Supplementary Figure 3).

To further explore the role of DC-SIGN as a trans-receptor for MERS-CoV, an infection assay was conducted under identical conditions at different time points. The assay demonstrated effective trans-infection at 2, 6, and 12 hours, with the highest binding observed at the six-hour mark. The parallel assay in MDDCs revealed that viral entry into the cells increases with the incubation time, albeit remaining modest in comparison to the

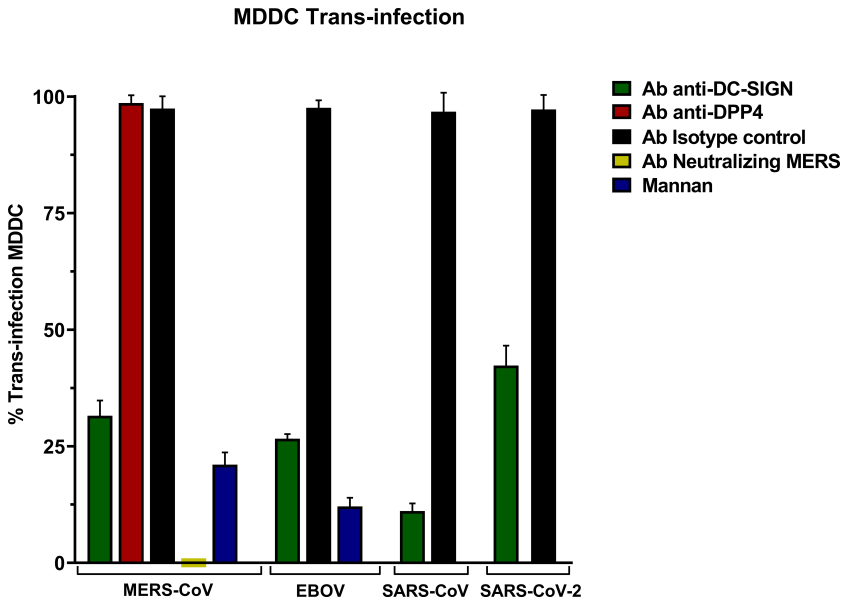

FIGURE 4
Trans-Infection in Monocyte-derived Dendritic Cells (MDDC) with pseudoviruses based in rVSV-luc. Percentage of trans-infection in MDDCs with SARS-CoV-2, SARS-CoV, MERS-CoV, and EBOV-GP compared with trans-infection in the absence of antibodies. Bars represent the mean SEM of the mean of four independent experiments with cells from two different donors performed in duplicates. Data were compared among multiple independent groups using one-way ANOVA (P= <0,0001) using GraphPad Prism v8. Trans-infection values are expressed as Percentage (%).

levels of trans-infection observed in Vero E6 cells (Supplementary Figure 4).

The results of the trypsin treatment experiment followed by PBS washing demonstrated that trans-infection is halted when MDDCs are treated both before exposure to the MERS-CoV virus and after virus attachment. There were no significant differences between pre-incubation and post-incubation trypsin treatment during the trans-infection assay (Supplementary Figure 5).

Analysis of receptor expression levels

PE anti-human CD209 (DC-SIGN) Antibody (Biolegend) and CD26 Monoclonal Antibody (BA5b) PE (Invitrogen) were employed to quantify the expression of the DC-SIGN receptor (Supplementary Figure 6) and DPP4 receptor (Supplementary Figure 7) on Monocyte-Derived Dendritic Cells (MDDCs). The expression was analyzed by flow cytometry in a Cytek Aurora with FlowJo V10.7.1 software.

Discussion

We studied the interaction of DC-SIGN with MERS-CoV. DC-SIGN, also named CD209 or dendritic cell-specific (DC) intercellular adhesion molecule-3-grabbing non-integrin (ICAM-3), is expressed in immature dendritic cells of peripheral tissues that we can find in diverse places such as the tonsils, mucous tissues, lymph nodes, monocyte-derived DCs, and spleen (Geijtenbeek et al., 2002). This type-C lectin recognizes highly glycosylated ligands present in pathogens such as viruses and human tissues through the recognition of carbohydrates mediated by the receptor's CDR (Soilleux et al., 2002). It has been proved that DC-SIGN expressed in DCs has an important role in the entry and dissemination of different viruses like the known case of the human immunodeficiency virus (HIV). Even though DC-SIGN is not a direct receptor of this virus for the viral entry for it does not mediate in the host cell, it confers to DCs the ability to facilitate trans-infection, that is, to capture the virus and transmit it to permissive cells that express the necessary receptors for the viral entry. This mechanism has been demonstrated as an important route for the dissemination of the virus from mucous surfaces to its replication in T cells present in secondary lymphoid organs by binding to DC-SIGN in immature DCs (Geijtenbeek et al., 2000). These binding factors of the host are key elements in viral infection mechanisms for they increase the density of viral particles at the cell surfaces, increasing its adhesion to them and thus boosting the access to their real receptors (Thépaut et al., 2021). These mechanisms facilitate trans-infection where a secondary presentation by non-permissive cells evading the immunological recognition system plays a role not only for HIV but for other viruses as well.

Even though in the bibliography the interaction between DC-SIGN lectin and MERS-CoV is described (Campana et al., 2020; Rahimi, 2020; Chapoval & Keegan, 2021), until now no study has experimentally proved such interaction. We have studied if MERS-CoV, whose canonical receptor is dipeptidyl peptidase-4 protein (DPP4), could have DC-SIGN as an alternative receptor for cis or trans-infection.

A study by Chu et al. (2014) proved productive infection by MERS in dendritic cells. Those patients who were infected with MERS-CoV, in clinical terms, developed coagulopathy, multiorgan dysfunction, lymphopenia, neutrophilia, and thrombocytopenia. It is worth mentioning that the virus is not only detected in the respiratory system but also in the urine, blood, and feces of infected people, which would support a systemic dissemination of the virus. For this reason, in people infected with MERS-CoV, monocyte-derived macrophages and dendritic cells could act as potential dissemination carriers by facilitating viral spread to the lymph nodes where, due to the interaction with T cells, they would boost the storm of cytokines and/or chemokines, imitating the scenery in SARS-CoV-1, worsening the clinical profile of the infected individual. In that study, they proved the existence of a productive infection in dendritic cells by MERS-CoV, which is something that does not happen in SARS-CoV (Chu et al., 2014).

The present study aims to explore if MERS-CoV can use DC-SIGN as a direct receptor, in this way partially explaining the productive infection demonstrated in dendritic cells in the direct infection of the virus discussed by Chu et al., or if it can also act, as it does in SARS-CoV-1 and SARS-CoV-2, as a binding factor, as well as its possible role in viral dissemination.

Cis-infection showed infection of dendritic cells by MERS-CoV PSV; however, anti-DC-SIGN could not significantly reduce infection indicating that this is not dependent on DC-SIGN though the decrease in the levels of infection in the presence of mannan indicates that a lectin receptor might be involved.

Trans-infection assays with MDDCs showed an increase in the infection values of target Vero E6 cells and a significant decrease in the presence of anti-DC-SIGN, indicating that the lectin is acting as a trans-receptor for MERS-CoV. The exact mechanism of how trans-infection occurs and the subsequent spread of the virus to other cells is still being studied. It is possible that the virus, once captured by dendritic cells, can be transported to other cells through various mechanisms, such as cell-to-cell contact or the release of viral particles.

The biological relevance of the interaction of DC-SIGN with MERS-CoV through the trans-infection process in the pathogenesis of severe respiratory disease remains to be explored.

Data availability statement

The raw data supporting the conclusions of this article will be made available by the authors, without undue reservation.

Ethics statement

The studies involving humans were approved by Comité Investigación Clínica Hospital Universitario 12 de Octubre (Reference CEIm 20/157). The studies were conducted in

accordance with the local legislation and institutional requirements. The human samples used in this study were acquired from Blood samples were obtained from healthy human donors (Hospital Universitario 12 de Octubre, Madrid, Spain) under informed consent and IRB approval. Written informed consent for participation was not required from the participants or the participants' legal guardians/next of kin in accordance with the national legislation and institutional requirements.

Author contributions

NL performed the experiments. JL, FL and MMT collaborated in research. RD directed the investigation. NL and RD wrote the paper. All authors contributed to the article and approved the submitted version.

Funding

This work was supported by grants from the Instituto de Investigación Carlos III, ISCIII, CIBERINFEC, and FIS PI2100989 by the European Commission; Horizon Europe Framework programme: Project EPIC-CROWN-2 ID: 101046084; Fundación Caixa-Health Research (Project StopEbola HR18-00469); Comunidad de Madrid Retar-A COVID P2022/BMD-7274 and PAII62/21-ANTICIPA/2021-23 to RD.

Conflict of interest

The authors declare that the research was conducted in the absence of any commercial or financial relationships that could be construed as a potential conflict of interest.

Publisher's note

All claims expressed in this article are solely those of the authors and do not necessarily represent those of their affiliated organizations, or those of the publisher, the editors and the reviewers. Any product that may be evaluated in this article, or claim that may be made by its manufacturer, is not guaranteed or endorsed by the publisher.

Supplementary material

The Supplementary Material for this article can be found online at: https://www.frontiersin.org/articles/10.3389/fcimb.2023.1177270/full#supplementary-material

References

Al Awaidy, S. T., and Khamis, F. (2019). Middle east respiratory syndrome coronavirus (MERS-CoV) in Oman: Current situation and going forward. *In Oman Med. J.* 34 (3), 181–183. doi: 10.5001/omj.2019.36

Alvarez, C. P., Lasala, F., Carrillo, J., Muñiz, O., Corbí, A. L., and Delgado, R. (2002). C-Type Lectins DC-SIGN and L-SIGN Mediate Cellular Entry by Ebola Virus in cis and in trans. *J. Virol.* 76, 13, 6841–6844. doi: 10.1128/JVI.76.13.6841

Campana, P., Parisi, V., Leosco, D., Bencivenga, D., Della Ragione, F., and Borriello, A. (2020). Dendritic cells and SARS-CoV-2 infection: Still an unclarified connection. *Cells* 9 (9), 2046. doi: 10.3390/cells9092046

Chapoval, S. P., and Keegan, A. D. (2021). Perspectives and potential approaches for targeting neuropilin 1 in SARS-CoV-2 infection. *Mol. Med.* 27 (1), 162. doi: 10.1186/s10020-021-00423-y

Chu, H., Zhou, J., Wong, B. H.-Y., Li, C., Cheng, Z.-S., Lin, X., et al. (2014). Productive replication of Middle East respiratory syndrome coronavirus in monocyte-derived dendritic cells modulates innate immune response. *Virology* 454–455, 197–205. doi: 10.1016/j.virol.2014.02.018

Domínguez-Soto, A., Sierra-Filardi, E., Puig-Kröger, A., Pérez-Maceda, B., Gómez-Aguado, F., Corcuera, M. T., et al. (2011). Dendritic cell-specific ICAM-3-grabbing nonintegrin expression on M2-polarized and tumor-associated macrophages is macrophage-CSF dependent and enhanced by tumor-derived IL-6 and IL-10. *J. Immunol. (Baltimore Md. : 1950)* 186 (4), 2192–2200. doi: 10.4049/jimmunol.1000475

Geijtenbeek, T. B. H., Engering, A., and van Kooyk, Y. (2002). DC-SIGN, a C-type lectin on dendritic cells that unveils many aspects of dendritic cell biology. *J. Leukocyte Biol.* 71 (6), 921–931. doi: 10.1189/jlb.71.6.921

Geijtenbeek, T. B. H., Kwon, D. S., Torensma, R., van Vliet, S. J., van Duijnhoven, G. C., Middel, J., et al. (2000). DC-SIGN , a dendritic cell – specific HIV-1-binding protein that enhances trans -infection of T cells. *Cell* 100, 587–597. doi: 10.1016/s0092-8674(00)80694-7

Guo, L., Liang, Y., Li, H., Zheng, H., Yang, Z., Chen, Y., et al. (2021). Epigenetic glycosylation of SARS-CoV-2 impact viral infection through DC&L-SIGN receptors. *IScience* 24 (12), 103426. doi: 10.1016/j.isci.2021.103426

Hanley, T. M., Blay Puryear, W., Gummuluru, S., and Viglianti, G. A. (2010). PPARgamma and LXR signaling inhibit dendritic cell-mediated HIV-1 capture and trans-infection. *PLoS Pathog.* 6 (7), e1000981. doi: 10.1371/journal.ppat.1000981

Jan, M., Upadhyay, C., Alcami Pertejo, J., Hioe, C. E., and Arora, S. K. (2018). Heterogeneity in glycan composition on the surface of HIV-1 envelope determines virus sensitivity to lectins. *PLoS One* 13 (3), e0194498. doi: 10.1371/journal.pone.0194498

Jeffers, S. A., Tusell, S. M., Gillim-Ross, L., Hemmila, E. M., Achenbach, J. E., Babcock, G. J., et al. (2004). CD209L (L-SIGN) is a receptor for severe acute respiratory syndrome coronavirus. *Proc. Natl. Acad. Sci. U. S. A.* 101 (44), 15748–15753. doi: 10.1073/pnas.0403812101

Léger, P., Tetard, M., Youness, B., Cordes, N., Rouxel, R. N., Flamand, M., et al. (2016). Differential use of the C-type lectins L-SIGN and DC-SIGN for phlebovirus endocytosis. *Traffic* 17 (6), 639–656. doi: 10.1111/tra.12393

Lempp, F. A., Soriaga, L., Montiel-ruiz, M., Benigni, F., Noack, J., Park, Y., et al. (2021). Lectins enhance SARS-CoV-2 infection and influence neutralizing antibodies. *Nature* 598, 342–347. doi: 10.1038/s41586-021-03925-1

Lundberg, K., and Rydnert, F. (2014). Human blood dendritic cell subsets exhibit discriminative pattern recognition receptor profiles. *Immunology* 142, 279–288. doi: 10.1111/imm.12252

Rahimi, N. (2020). C-type lectin CD209L/L-SIGN and CD209/DC-SIGN: Cell adhesion molecules turned to pathogen recognition receptors. *Biology* 10 (1), 1. doi: 10.3390/biology10010001

Raj, V. S., Mou, H., Smits, S. L., Dekkers, D. H. W., Müller, M. A., Dijkman, R., et al. (2013). Dipeptidyl peptidase 4 is a functional receptor for the emerging human coronavirus-EMC. *Nature* 495 (7440), 251–254. doi: 10.1038/nature12005

Scobey, T., Yount, B. L., Sims, A. C., Donaldson, E. F., Agnihothram, S. S., Menachery, V. D., et al. (2013). Reverse genetics with a full-length infectious cDNA of the Middle East respiratory syndrome coronavirus. *Proc. Natl. Acad. Sci. U. S. A.* 110 (40), 16157–16162. doi: 10.1073/pnas.1311542110

Soilleux, E. J., Morris, L. S., Leslie, G., Chehimi, J., Luo, Q., Levroney, E., et al. (2002). Constitutive and induced expression of DC-SIGN on dendritic cell and macrophage subpopulations in *situ* and in *vitro*. *J. Leukocyte Biol.* 71 (3), 445–457. doi: 10.1189/jlb.71.3.445

Tassaneetrithep, B., Burgess, T. H., Granelli-piperno, A., Trumpfheller, C., Finke, J., Sun, W., et al. (2003). DC-SIGN (CD209) mediates dengue virus infection of. *J. Exp. Med.* 197, 823–829. doi: 10.1084/jem.20021840

Thépaut, M., Luczkowiak, J., Vivès, C., Labiod, N., Bally, I., Lasala, F., et al. (2021). DC/L-SIGN recognition of spike glycoprotein promotes SARS-CoV-2 trans-infection and can be inhibited by a glycomimetic antagonist. *PLoS Pathog.* 17 (5), 1–27. doi: 10.1371/journal.ppat.1009576

van Kooyk, Y. (2008). C-type lectins on dendritic cells: Key modulators for the induction of immune responses. *Biochem. Soc. Trans.* 36 (6), 1478–1481. doi: 10.1042/BST0361478

Whitt, M. A. (2010). Generation of VSV pseudotypes using recombinant ΔG-VSV for studies on virus entry, identification of entry inhibitors, and immune responses to vaccines. *J. Virological Methods* 169 (2), 365–374. doi: 10.1016/j.jviromet.2010.08.006

Zaki, A. M., van Boheemen, S., Bestebroer, T. M., Osterhaus, A. D. M. E., and Fouchier, R. A. M. (2012). Isolation of a novel coronavirus from a man with pneumonia in Saudi Arabia. *New Engl. J. Med.* 367 (19), 1814–1820. doi: 10.1056/NEJMoa1211721

Zhong, J., Rao, X., Deiuliis, J., Braunstein, Z., Narula, V., Hazey, J., et al. (2013). A potential role for dendritic cell/macrophage-expressing DPP4 in obesity-induced visceral inflammation. *Diabetes* 62 (1), 149–157. doi: 10.2337/db12-0230

frontiers | Frontiers in Cellular and Infection Microbiology

TYPE Original Research
PUBLISHED 06 December 2023
DOI 10.3389/fcimb.2023.1163569

OPEN ACCESS

EDITED BY
Ana Falcón,
Algenex, Spain

REVIEWED BY
Rohit K Jangra,
LSU Health Sciences Center-Shreveport, United States
Moona Huttunen,
University of Jyväskylä, Finland

*CORRESPONDENCE
Miguel Ángel Cuesta-Geijo
cuesta.miguelangel@inia.csic.es

RECEIVED 17 February 2023
ACCEPTED 13 November 2023
PUBLISHED 06 December 2023

CITATION
Barrado-Gil L, García-Dorival I, Galindo I, Alonso C and Cuesta-Geijo MÁ (2023) Insights into the function of ESCRT complex and LBPA in ASFV infection. *Front. Cell. Infect. Microbiol.* 13:1163569. doi: 10.3389/fcimb.2023.1163569

Insights into the function of ESCRT complex and LBPA in ASFV infection

Lucía Barrado-Gil, Isabel García-Dorival, Inmaculada Galindo, Covadonga Alonso and Miguel Ángel Cuesta-Geijo*

Departmento Biotecnología, INIA-CSIC, Centro Nacional Instituto Nacional de Investigación y Tecnología Agraria y Alimentaria, Madrid, Spain

The African swine fever virus (ASFV) is strongly dependent on an intact endocytic pathway and a certain cellular membrane remodeling for infection, possibly regulated by the endosomal sorting complexes required for transport (ESCRT). The ESCRT machinery is mainly involved in the coordination of membrane dynamics; hence, several viruses exploit this complex and its accessory proteins VPS4 and ALIX for their own benefit. In this work, we found that shRNA-mediated knockdown of VPS4A decreased ASFV replication and viral titers, and this silencing resulted in an enhanced expression of ESCRT-0 component HRS. ASFV infection slightly increased HRS expression but not under VPS4A depletion conditions. Interestingly, VPS4A silencing did not have an impact on ALIX expression, which was significantly overexpressed upon ASFV infection. Further analysis revealed that ALIX silencing impaired ASFV infection at late stages of the viral cycle, including replication and viral production. In addition to ESCRT, the accessory protein ALIX is involved in endosomal membrane dynamics in a lysobisphosphatydic acid (LBPA) and Ca^{2+}-dependent manner, which is relevant for intraluminal vesicle (ILV) biogenesis and endosomal homeostasis. Moreover, LBPA interacts with NPC2 and/or ALIX to regulate cellular cholesterol traffic, and would affect ASFV infection. Thus, we show that LBPA blocking impacted ASFV infection at both early and late infection, suggesting a function for this unconventional phospholipid in the ASFV viral cycle. Here, we found for the first time that silencing of VPS4A and ALIX affects the infection later on, and blocking LBPA function reduces ASFV infectivity at early and later stages of the viral cycle, while ALIX was overexpressed upon infection. These data suggested the relevance of ESCRT-related proteins in ASFV infection.

KEYWORDS

ESCRT, LBPA, Alix, Vps4, multivesicular bodies, NPC1, ASFV, African swine fever virus

1 Introduction

Currently, African swine fever (ASF) is considered as a major emerging threat since it has increased its incidence and spread over Central and Eastern Europe to Southeast Asia, America, and Oceania, causing high economic burden and impact on animal health (Alonso et al., 2018; Mighell and Ward, 2021; Schambow et al., 2022). ASF usually results in hemorrhagic fever in domestic pigs and wild boar, with a case fatality rate close to 100%. The etiological agent causing ASF is the African swine fever virus (ASFV), the only member of the *Asfarviridae* family and also part of the nucleocytoplasmic large DNA virus (NCLDV) group, including *Mimiviridae*, *Poxviridae*, *Iridoviridae*, faustoviruses, pandoraviruses, and pacmanviruses (Andreani et al., 2017; Koonin and Yutin, 2019; Koonin et al., 2020). The development of strategies to prevent and control ASFV is a major challenge due to the dearth of commercial vaccines or antiviral treatments as well as the existence of wildlife reservoirs contributing to its impact and increasing difficulties to control the disease. Subsequently, animal movement restrictions and slaughtering of infected animals are the only possible solutions during the outbreaks (Costard et al., 2009; Urbano and Ferreira, 2022). In this scenario, it is necessary to continue to decipher the mechanisms underlying ASFV infection.

ASF virions are icosahedral multi-layered structures of approximately 200 nm in diameter, comprising a DNA-containing nucleoid, which is then surrounded by the core shell or matrix. In the internal face of the inner viral membrane, the capsid is assembled around this internal membrane. Lastly, a further envelope is acquired when the virus buds out at the host cell plasma membrane. The external envelope is not essential for viral infection. New details have been recently unveiled about the complexity of the virion structure (Liu et al., 2019; Wang et al., 2019; Andres et al., 2020).

ASFV enters the cell via clathrin- and dynamin-mediated endocytosis (Hernaez and Alonso, 2010; Galindo et al., 2015) and macropinocytosis (Sanchez et al., 2012; Hernaez et al., 2016). The late endosome is a crucial compartment for viral fusion, involving the NPC intracellular cholesterol transporter 1 (NPC1) (Matamoros et al., 2020; Cuesta-Geijo et al., 2022). Fusion would allow penetration towards the cytosol to finally start replication (Cuesta-Geijo et al., 2012; Sanchez et al., 2017). The viral factories made by ASFV are highly complex structures, induced by profound reorganization of the organelles that comprise membranes recruited from the endosomal pathway (Cuesta-Geijo et al., 2017) and the secretory pathway, which may contribute to the induction of cellular stress responses. ASFV mature particles utilize the cytoskeletal network to egress from the viral factory to the cell surface (Carvalho et al., 1988; Jouvenet et al., 2004), a travel depending on the late structural protein E120R (Andres et al., 2001).

The endosomal sorting complex required for transport (ESCRT) machinery is crucial for various cellular membrane-reorganization events including membrane remodeling, sealing, or repair, as required in several viral infections (Vietri et al., 2020; Olmos, 2022). In fact, enveloped retroviruses (HIV) and +strand RNA viruses (such as filo-, arena-, radon-, and paramyxoviruses) redirect cellular ESCRT proteins to the plasma membrane, leading to budding and fission of the viral particles from infected cells (McCullough et al., 2013; Vietri et al., 2020). In addition, the ESCRT machinery leads the constitution of the viral replication complex of a variety of viral families that require alterations of cellular membranes for successful replication (Torii et al., 2020; Meng and Lever, 2021). A closely related virus, such as Vaccinia virus (VACV), hijacks ESCRT to facilitate virus maturation, egress, and spread by ESCRT-mediated VACV wrapping. Moreover, multivesicular bodies (MVBs) serve as a major non-cisternae membrane source for the formation of intracellular enveloped viruses (IEVs) (Huttunen et al., 2021).

The ESCRT complex comprises four core complexes called ESCRT-0, ESCRT-I, ESCRT-II, and ESCRT-III, plus the vacuolar protein sorting-associated protein 4 (VPS4) and additional accessory proteins such as ALG-2 interacting protein X (ALIX) homodimer (Katzmann et al., 2001; Babst et al., 2002; Saksena et al., 2009; Schoneberg et al., 2017). ESCRT subunits are activated as a cascade, starting with ESCRT-0 (HRS) that recruits ESCRT-I, while, in turn, ESCRT-I interacts with the ESCRT-II complex. Then, ESCRT-II initiates the formation of the ESCRT-III complex that needs energy to depolymerize (Korbei, 2022; Olmos, 2022). ATPase VPS4, which has the isoforms VPS4A and VPS4B, hydrolyzes ATP to provide the necessary energy to recycle ESCRT-III (Babst et al., 1998). VPS4 balance out cytosolic ESCRT-III and allows a change of ESCRT-III filaments during the membrane scission process (Adell et al., 2014; Mierzwa et al., 2017; McCullough et al., 2018).

As mentioned before, ALIX is a crucial actor in ESCRT dynamics. It is a cytosolic protein identified on the basis of its association with pro-apoptotic signaling (Vito et al., 1999). However, ALIX regulates other cellular mechanisms, including endocytic membrane trafficking, cell adhesion, and cytoskeletal remodeling (Odorizzi, 2006). In addition, several viral families exploit ALIX for budding (Carlton et al., 2008; Zhai et al., 2011; Votteler and Sundquist, 2013) or replication (Fujii et al., 2009; Liu et al., 2022). This ability to participate in a variety of activities relies in its domain architecture, which allows ALIX to interact with the ESCRT-I subunit TSG101 (Strack et al., 2003; von Schwedler et al., 2003), and the ESCRT-III subunit CHMP4 (Odorizzi, 2006; Fisher et al., 2007; Usami et al., 2007).

ALIX tightly collaborates with LBPA, an unconventional and specific phospholipid localized primarily at the inner late endosome/lysosome (LE/LY) membranes, being crucial for intraluminal vesicle (ILV) formation in a Ca^{2+}-dependent manner (Bissig et al., 2013). Moreover, lysobisphosphatydic acid (LBPA) is involved in the sorting and efflux of LE/LY components, including cholesterol intracellular traffic (Kobayashi et al., 1998; Kobayashi et al., 1999; Gruenberg, 2003; Mobius et al., 2003; Matsuo et al., 2004; Hullin-Matsuda et al., 2007). An obligate direct interaction with the cholesterol transporter NPC2 has been recently revealed, establishing the essential functional nature of NPC2–LBPA interactions in the egress of cholesterol from the LE/LY compartment. Of note is that the importance of the host cholesterol pools in viral fusion and replication including ASFV has been described (Ilnytska et al., 2013; Cuesta-Geijo et al., 2016; McCauliff et al., 2019; Ballout et al., 2020).

Our study gives indications suggesting that these protein machineries affecting cellular membrane dynamics could have a role in the ASFV infection cycle, unveiling lines of evidence about the relevance of ESCRT machinery-related proteins VPS4A and ALIX, as well as the LBPA lipid, as potential new therapeutical targets to combat the infection.

2 Materials and methods

2.1 Cell culture

The Vero (ATCC CCL-81; renal fibroblasts) cell line was cultured in Dulbecco's modified Eagle medium (DMEM) 1% penicillin-streptomycin (P/S), and 2 mM GlutaMAX (Gibco, Gaithersburg, MD, USA) and supplemented with 5% heat-inactivated fetal bovine serum (FBS). FBS was reduced to 2% in the inoculum at the time of viral adsorption and throughout the infection process. All these mammalian cells were grown at 37°C and 5% CO2 conditions.

2.2 Viruses and infection

We used the Vero-adapted and non-pathogenic ASFV isolate Ba71V (Enjuanes et al., 1976) and fluorescent recombinant viruses Ba71V-30GFP (BPP30GFP) (Barrado-Gil et al., 2017) and Ba71V-Bp54GFP (B54GFP) (Hernaez et al., 2006). BPP30GFP expresses the GFP gene under the promoter of the early viral p30 protein (Barrado-Gil et al., 2017). Recombinant B54GFP expresses GFP as a fusion protein of viral p54, which is an early/late protein that mainly accumulates at the viral replication sites (Rodriguez et al., 1994; Hernaez et al., 2006). ASFV viral stocks were propagated and titrated by plaque assay in Vero cells, as previously described (Enjuanes et al., 1976). When using the recombinant viruses BPP30GFP or B54GFP, green fluorescent plaques were observed 4 days after infection under the fluorescence microscope. ASFV stocks were partially purified using a sucrose cushion (40%) in PBS at 68,000 × g for 50 min at 4°C and were further used at a multiplicity of infection (MOI) of 1 unless otherwise indicated.

2.3 Generation of stable cell lines

To generate Vero cells deficient in VPS4A or ALIX, we used the commercial lentiviral vector containing shRNA to interfere with VPS4A (TRCN000012998) or ALIX (TRCN0000343595), respectively, obtained from Merck (Darmstadt, Germany). A TRC1 pLKO.1-puro empty shRNA was used as control. Lentiviral particles were produced by transfection of HEK293T cells (seeded in 60-mm dishes) with 5 µg of lentiviral vectors, 3 µg of the human immunodeficiency virus (HIV) gag-pol expressing plasmid, and 3 µg of vesicular stomatitis virus-G glycoprotein using Lipofectamine 2000 (Life Technologies, Carlsbad, CA, USA). Supernatants containing the lentivirus were harvested at 48 and 72 h post transfection, 0.45 µm-filtered, and used to transduce Vero cells, which were subsequently selected for puromycin resistance (Life Technologies, 10 µg/mL).

2.4 Antibodies

The following rabbit antibodies were used: VPS4A (H-165) (SCBT, sc-32922), Lamp-1 (Abcam, ab24170), ALIX (Abcam, ab88388), ALIX (Proteintech, 12422-1-AP), or HRS (CST, #14346). Mouse monoclonal antibodies used were as follows: ALIX (Q19) (sc-49268), EEA1 (BD Biosciences, 610457), CD63 (H5C6) (Novus Biologicals, NBP2-42225), p150 (Ingenasa, 17AH2), p72 (Ingenasa,1BC11), p72 (Ingenasa, 18BG3), p30 (a gift from J.M. Escribano, Algenex, Madrid, Spain), or LBPA (6C4) (Echelon Biosciences, Z-SLBPA). ALIX (Q19) (SCBT, sc-9268) was the goat antibody used.

2.5 Flow cytometry

Vero cells were infected with recombinant ASFV BPP30GFP or B54GFP at a MOI of 1 pfu/cell for 16 h. Cells were washed with PBS, harvested with Trypsin-EDTA (Gibco, Gaithersburg, MD, USA), and then washed and collected with flow cytometry buffer (PBS, 0.01% sodium azide, and 0.1% bovine serum albumin). In order to determine the percentage of infected cells per condition (infection efficiency), 10,000 cells per time point were scored using a FACS Canto II flow cytometer (BD Sciences, Franklin Lakes, NJ, USA) and analyzed using the FlowJo software. Infected cell percentages obtained were normalized to values found in control samples.

2.6 Western blot analysis

Cells were seeded in six-well plates and infected with ASFV at a MOI of 1 pfu/cell. Protein lysates were separated based on electrophoretic mobility in sodium dodecyl sulfate polyacrylamide gels (SDS-PAGE) under reducing conditions and transferred to nitrocellulose membranes (Amersham Biosciences, Amersham, UK). Membranes were blocked with 5% skimmed milk powder in PBS–0.05% Tween-20 (Sigma-Aldrich, Saint Louis, MO, USA) for 1 h and further incubated with primary antibody at 4°C overnight. Finally, immunoblot was incubated with suitable horseradish peroxidase-conjugated secondary antibodies for 1 h at room temperature. Protein expression was analyzed using the molecular imager Chemidoc XRS plus Imaging System. Bands were quantified by densitometry and normalized using the Image Lab software (Bio-Rad, Hercules, CA, USA).

2.7 Immunofluorescence

Vero cells were seeded at a variable density onto 12-mm glass coverslips in 24-well plates before infection. Then, cells were washed with PBS and fixed with 4% paraformaldehyde (PFA) for 15 min. After washing with PBS, cells were permeabilized with 0.1%

Triton X-100 in PBS for 10 min. Then, coverslips were washed with PBS and incubated in 2% bovine serum albumin (BSA, Sigma) diluted in PBS for 1 h. Slides were then incubated at room temperature for 1 h in primary antibody diluted in PBS–BSA 1%. Appropriate secondary antibodies conjugated to either Alexa Fluor-488 or -594 (Thermo Fisher, Waltham, MA, USA) were used and cell nuclei were detected with TO-PRO-3 (Thermo Fisher Scientific). Coverslips were mounted on glass slides using ProLong Gold (Thermo Fisher Scientific). Cells were visualized using a TCS SPE confocal microscope (Leica) and image acquisition was performed with a Leica Application Suite Advanced Fluorescence software (LAS AF).

2.8 Immunofluorescence quantitative analysis

Fluorescence labeling of ALIX antibody was measured using ImageJ 1.53c (NIH). Specific ROIs (regions of interest) were designed for 20 cells per condition, and cytoplasmic fluorescence signal above a certain threshold (adjusted as background) was quantified. Results were expressed as the average of intensity and, relative to values detected in control samples, arbitrarily assigned a value of one.

To quantify the amount of LBPA accumulated close to the viral factory, we used the ImageJ plug-in "Fluorescence Ratio" kindly provided by Dr. Sánchez Sorzano (CNB, Madrid, Spain) (Rincon et al., 2011) that allows us to obtain the fluorescence intensity detected at a particular area of the cell related to other areas. The plugin takes into account the fluorescence provided by the background. In our experiment, we computed the ratio between the fluorescence at the viral factory in the perinuclear region and the total cytoplasm of each cell. We measured the intensity in 30 individual cells per condition (MOCK or infected).

2.9 Virus titration

Vero cells were infected with Ba71V or BPP30GFP at a MOI of 1 pfu/cell. After 24 h or 48 h of infection, total viruses from cell lysates and supernatants were collected and titrated by plaque assay in triplicate samples on monolayers of Vero cells. Intracellular virus titers were obtained by repeatedly freezing and thawing infected cells. Vero cells were infected with 10-fold serial dilutions from samples and viral adsorption lasted 90 min in 2% FBS at 37°C. The viral inoculum was then removed and a 1:1 ratio of 2% low-melting-point agarose and complete 2X EMEM was added. Plaque visualization was possible at 10 days after staining with violet crystal. When using the recombinant BPP30GFP, green fluorescent plaques were observed 4 days after infection.

2.10 Quantitative real-time PCR

DNA from Vero cells infected with ASFV at an MOI of 1 pfu/cell for 16 h was purified using the DNAeasy blood and tissue kit (Qiagen) following the manufacturer's protocol. DNA concentration was measured using a Nanodrop spectrophotometer. The qPCR assay amplifies a region of the p72 viral gene, as described previously (King et al., 2003). The amplification mixture was 200 ng of DNA template added to a final reaction mixture of 20 µL containing 50 pmol sense primers, 50 pmol anti-sense primer, 5 pmol of probe, and 10 µL of Premix Ex Taq (2×) (Takara Bio, Shiga, Japan). Each sample was included in triplicate and values were normalized to standard positive controls. Reactions were performed using the ABI 7500 Fast Real-Time PCR System (Applied Biosystems) with the following parameters: 94°C for 10 min and 45 cycles of 94°C for 10 s and 58°C for 60 s.

2.11 RNA extraction and quantitative PCR analysis

RNA was extracted from Vero cells grown in six-well plates using the RNeasy RNA extraction kit (Qiagen, Hilden, Germany) according to the manufacturer's protocol. For retrotranscription, a QuantiTect Reverse Transcription kit (Qiagen) was used to synthesize cDNA, also following the manufacturer's protocol. cDNA (250 ng) was the template for real-time PCR using the QuantiTect SYBR Green PCR Kit (Qiagen). Reactions were performed using the ABI 7500 Fast Real-Time PCR System (Applied Biosystems, Waltham, MA, USA). Expression of VPS4A was analyzed by using Hs_VPS4A_1_SGQuantiTect Primer Assay QT00022029 (Qiagen) and normalized to an internal control (18S ribosome subunit) to yield the fold expression.

2.12 Statistical analysis

The experimental data were analyzed by one-way ANOVA by GraphPad Prism 6 software. For multiple comparisons, Bonferroni's correction was applied. When comparing two sample means, an unpaired Student's *t*-test was performed. Values were expressed in bar graphs as mean ± SD of at least three independent experiments unless otherwise noted. A $p < 0.05$ was considered as statistically significant.

3 Results

3.1 Role of VPS4A in ASFV infection

To determine the impact of the ESCRT complex on ASFV infection, we silenced the expression of VPS4A using shRNA as described above. The reduction of VPS4A expression levels was confirmed by Western blot (Figures 1A, B) and RT-qPCR (Figure 1C). After assessing the silencing, we were interested in identifying whether VPS4A interfered in ASFV infectivity. Wild-type, empty shRNA (empty) and VPS4A shRNA (shVPS4A) Vero cells were infected with ASFV BPP30GFP, a recombinant virus that expresses the GFP protein under the early viral protein promoter p30. No effect was detected at early stages post-infection by flow cytometry using this

10.3389/fcimb.2023.1163569

tagged recombinant virus (Figure 1D). However, when cells were infected with recombinant virus B54GFP, expressing GFP as a p54 fusion protein resulted in an inhibition of the infectivity. In fact, the silencing of VPS4A reduced the percentage of fluorescent cells when measured by flow cytometry at 16 h post infection compared to empty cells (Figure 1E). In agreement with the result shown in Figure 1E, we obtained a significant decrease of ASFV replication in shVPS4A cells analyzed by quantitative PCR (Figure 1F). In order to gain knowledge of the impact of VPS4A silencing in the last stage of ASFV infection, wild-type, empty, and shVPS4A Vero cells were infected with BPP30GFP in order to quantify the amount of intracellular virus produced in each condition, and also evaluate the amount of virus released to the extracellular space. After 24 h of infection, intracellular (IC) and extracellular (EC) virus production were analyzed. Cellular pellets and supernatants were collected and titrated by plaque assay in Vero cells as described in *Materials and Methods*. As shown in Figure 1G, no significant differences were observed when titrating IC viral production generated in Vero, empty, and shVPS4A Vero cells. Interestingly, the shVPS4A cell line produced less EC viral particles compared to empty Vero cells (Figure 1H).

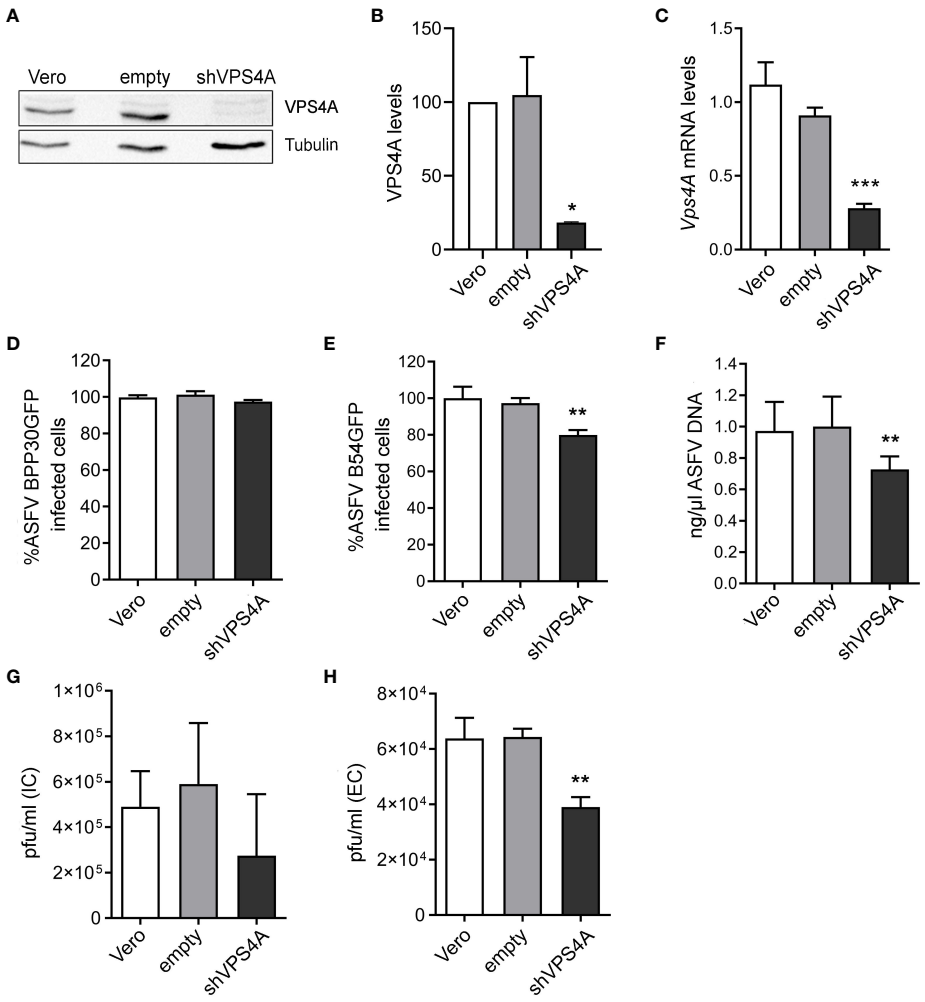

FIGURE 1
Impact of VPS4A silencing in several infection parameters. **(A)** Representative immunoblot of VPS4A in Vero cells transduced with lentiviral particles encoding VPS4A shRNA (shVPS4A) or empty shRNA (empty) and wild-type Vero cells (Vero) as controls. **(B)** Densitometric analysis of VPS4A expression in WB using alpha-tubulin as loading control and compared with empty values. **(C)** VPS4A mRNA levels analyzed by qPCR using VPS4A-specific primers. Ribosomal protein 18S was used as control. Data are presented as a fold compared to empty cells. **(D)** Infectivity of BPP30GFP (1 pfu/mL) in Vero cells at 16 hpi measured by flow cytometry (GFP fluorescence percentage relative to empty control). **(E)** Percentage of B54GFP-infected cells (GFP fluorescence relative to empty control) at 16 hpi in Vero cells. **(F)** Quantification of ASFV genome copy number by real-time PCR 16 hpi and normalized to empty values. Data are presented as a fold and normalized to empty values. **(G)** Virus titration by plaque assay of intracellular (IC) virions generated in wild-type, empty, or shVPS4A Vero cells infected with BPP30GFP at a MOI of 1 pfu/mL for 24 (h) **(H)** Virus titration by plaque assay of extracellular (EC) virions generated in wild-type, empty, or shVPS4A Vero cells infected with BPP30GFP at a MOI of 1 pfu/mL for 24 hpi. Statistically significant differences are indicated by asterisks (*$p < 0.05$; **$p < 0.01$; ***$p < 0.001$).

3.2 Effect of VPS4A silencing in the redistribution of endosomal membranes during ASFV infection

Previous studies have shown a reorganization of endosomal traffic and endosomal membranes remodeling close to the viral replication site or viral factory (VF) (Cuesta-Geijo et al., 2017) that could be eventually altered under the inhibition of the ESCRT component VPS4A. The ASFV VF is the site where the viral replication takes place, and it is visualized as a perinuclear structure by confocal microscopy.

Empty and shVPS4A Vero cells were infected with ASFV for 16 hpi. Cells were fixed and assayed with immunofluorescence to detect the early endosome marker EEA1, the MVB marker CD63, and the lysosomal marker Lamp1. As previously described, immunofluorescence images showed EEA1-labeled early endosomes around the VF. The VF was recognized by the labeling with the structural viral protein p150 at 16 hpi in infected empty cells (Figure 2A). Silencing of VPS4A maintained EEA1 recruitment close to the VFs (Figure 2A). In CD63 labeling, we detected a diffuse cytoplasmic localization of MVBs in mock empty cells (Figure 2B), while CD63 repositioned close to the VF in infected empty cells. A similar pattern was found in mock- as well as ASFV-infected shVPS4A cells (Figure 2B). When visualizing the reorganization of lysosomes in the absence of VPS4A, no alteration was observed either in mock-infected or in ASFV-infected cells, when comparing empty and shVPS4A cell lines (Figure 2C). In summary, no alterations in the distribution of cellular vesicles were detected in either mock or infected cells under VPS4A silencing conditions.

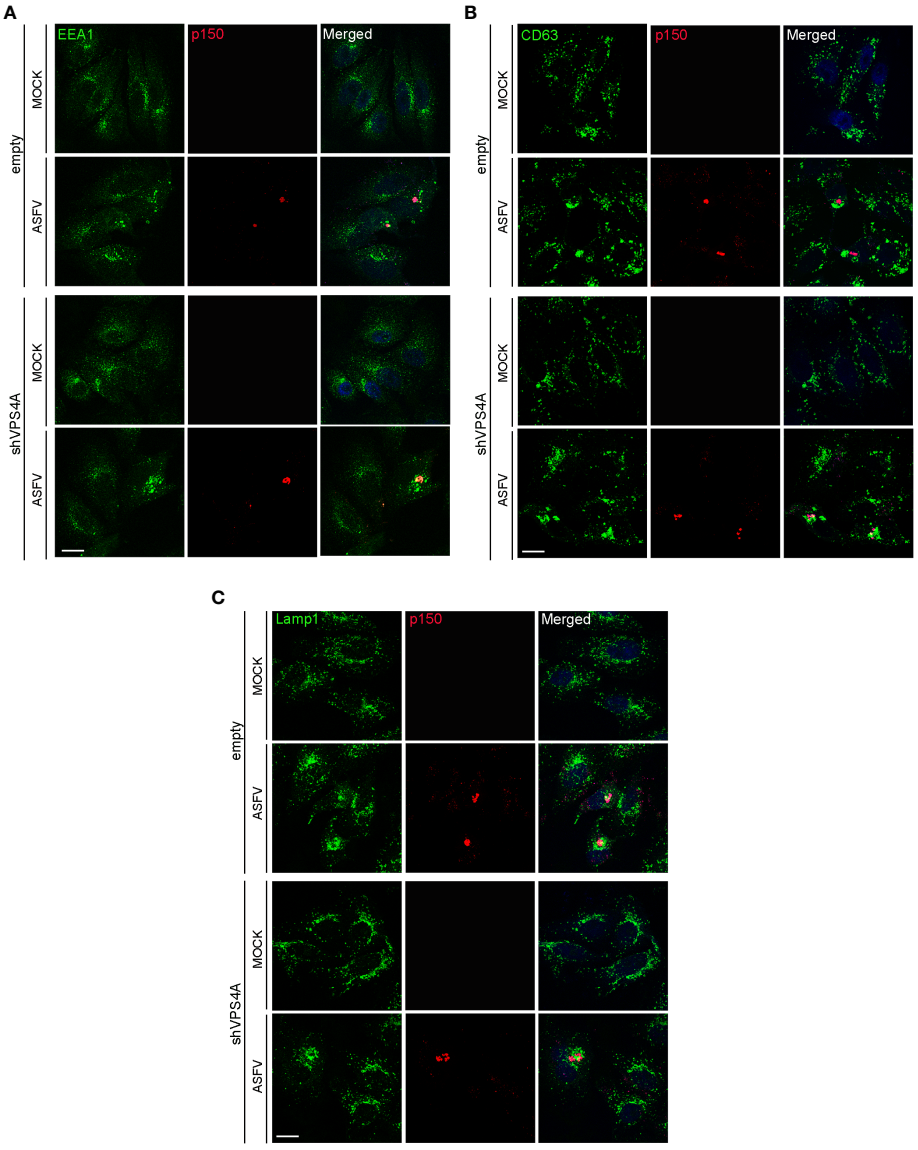

FIGURE 2
VPS4A and vesicle reorganization at viral factories. Representative confocal images of empty and shVPS4A Vero cells uninfected (MOCK) or infected with Ba71V at a MOI of 1 pfu/cell for 16 (h) After fixation, cells were stained for viral core protein p150 (red), DNA (TO-PRO-3, blue), and vesicle membrane marker EEA1 (green) **(A)**, CD63 (green) **(B)**, or Lamp1 (green) **(C)**. Scale bar: 20 μm.

3.3 Impact of VPS4A silencing in ALIX expression during ASFV infection

To gain insight into how silencing VPS4A could affect other ESCRT components and ASFV infection, we focus on HRS (ESCRT-0) and the adaptor protein ALIX, a crucial player for several virus models to pursue a successful infection (Le Blanc et al., 2005; Munshi et al., 2007; Pattanakitsakul et al., 2010; Pasqual et al., 2011; Jiang et al., 2020). This protein participates in actin assembly and membrane remodeling processes settled by ESCRT-III (McCullough et al., 2018; Qiu et al., 2022), which are relevant for several viruses (Lin et al., 2022). We infected wild-type, empty, and shVPS4A Vero cells with ASFV at a MOI of 1 pfu/cell and they were harvested at 16 hpi. Western blot analysis showed a tendency towards the increase of ESCRT-0 component HRS in silenced VPS4A cells, slightly dependent on ASFV infection (Figure 3A). Similar data were observed in Vero wild-type cells, used as control. When studying ALIX expression, we observed an increase in cells infected with ASFV at 16 hpi compared to mock cells. This increment was independent of the silencing of VPS4A (Figure 3B). Finally, we monitored the pattern of ALIX during ASFV infection in both empty and shVPS4A Vero cells by immunofluorescence (Figure 3C). In agreement with immunoblot experiments, infected shVPS4A cells (lower panel, Figure 3C)

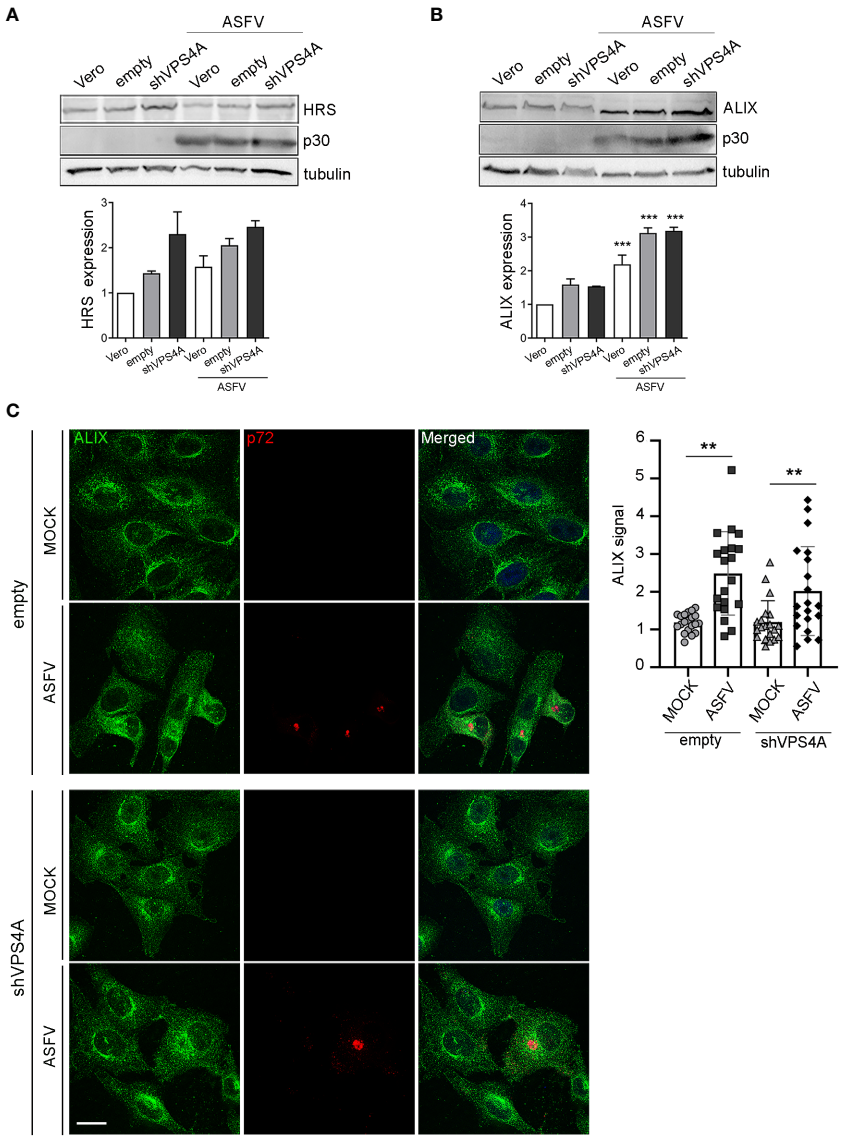

FIGURE 3
ALIX expression in cells lacking VPS4A. **(A, B)** Representative immunoblot and densitometric analysis of HRS expression **(A)** or ALIX expression **(B)** in MOCK and infected samples harvested at 16 hpi (MOI of 1 pfu/cell) for wild-type Vero cells (Vero), empty shRNA (empty), or VPS4A shRNA (VPS4A). ASFV infection was detected by using viral protein p30. Alpha-tubulin was used as loading control. Data are presented as mean ± SD of densitometry values from two independent experiments. **(C)** Illustrative confocal images of empty (upper panel) and shVPS4A (lower panel) Vero cells stained with ALIX (green). Viral factories were detected with the antibody against p72 (red) and DNA with TO-PRO-3 (blue). Quantification of ALIX staining in MOCK or infected (ASFV) in empty and shVPS4A cell lines. Each dot represents a single cell (n = 20). Scale bar: 20 μm. Statistically significant differences are indicated by asterisks (**p < 0.01; ***p < 0.001).

showed a higher ALIX labeling than mock shVPS4A cells (lower panel, Figure 3C). Similar results were obtained from empty cells (upper panel, Figure 3C). ALIX distribution around viral factory (labeled with p72) was detected in both cell lines (Figure 3C). These results point out that HRS is dependent on VPS4A silencing but weakly on ASFV infection. Conversely, ALIX overexpression occurs under infection conditions and it is not related to VPS4A depletion.

3.4 ASFV replication and virus production are impacted by ALIX knockdown

Using a validated shRNA targeting ALIX, we conducted RNA silencing of the protein in Vero cells to investigate the function of ALIX in ASFV infection. Immunoblotting of cell lysates revealed that gene knockdown reduced protein expression of ALIX at 10% after silencing (Figures 4A, B).

After that, cells were infected with ASFV. As observed in Figure 4C, viral internalization of ASFV BPP30GFP was not affected, since early viral protein expression p30 was unaltered after ALIX knockdown, detected through GFP by flow cytometry. Conversely, the late viral protein p54 decreased under silencing conditions (Figure 4D). Indeed, we confirmed this by observing a significant decrease of ASFV replication in shALIX Vero cells by using qPCR (Figure 4E).

To further assess a function for ALIX at later stages at the viral cycle, we analyzed the viral production by the plaque assay. In agreement with viral replication results, silencing of ALIX triggered a 1.5 log reduction in intracellular viral titer, as well as in extracellular viral titer in shALIX Vero cells compared to empty Vero cells (Figures 4F, G).

3.5 LBPA plays a role in ASFV infection

Enhanced expression of ALIX and its role in ASFV infection lead us to study the possible involvement of lysobisphosphatidic acid (LBPA), an unconventional lipid that interacts with ALIX, in regulating endosomal homeostasis and cholesterol efflux from the LE, which are crucial for ASFV infection.(McCauliff et al., 2019). To test the effect of LBPA in ASFV entry and infection, we used the blocking monoclonal antibody LBPA 6C4 that inhibits LBPA activity (Kobayashi et al., 1998) and LBPA–ALIX interaction (Pattanakitsakul et al., 2010). We first tested the correct LBPA antibody internalization (Figure 5A). Thus, Vero cells were incubated with anti-LBPA antibody

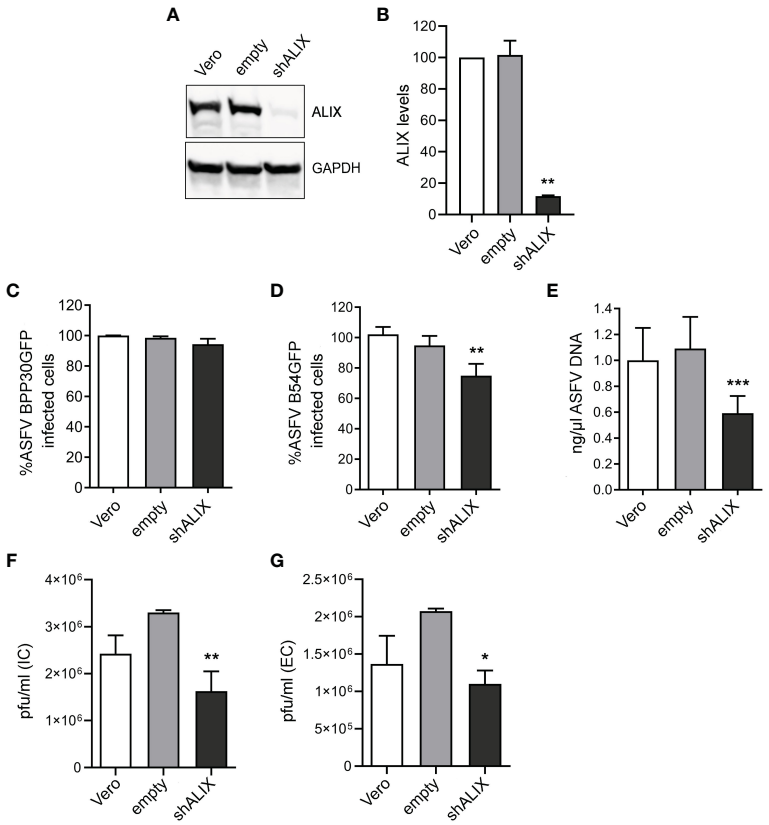

FIGURE 4
ALIX depletion affects ASFV infection. **(A, B)** Representative immunoblot of ALIX in Vero cells transduced with lentiviral particles encoding ALIX shRNA (shVPS4A) or empty shRNA (empty) and wild-type Vero cells (Vero) as controls. **(B)** Densitometric analysis of ALIX expression in WB using GAPDH as loading control and compared with empty values. Data are presented as mean ± SD of densitometry values from two independent experiments. **(C, D)** Flow cytometry of wild-type, empty, and shALIX Vero cells infected with fluorescent recombinant ASFV BPP30GFP **(C)** or B54GFP **(D)** at a MOI of 1 pfu/mL for 16 hpi. **(E)** Quantification of ASFV DNA by qPCR at 16 hpi. Data are presented as a fold and normalized to empty values. **(F, G)** Virus titration by plaque assay of intracellular (IC) and extracellular (EC) virions generated in wild-type, empty, or shALIX Vero cells infected with BPP30GFP at a MOI of 0.1 pfu/mL for 48 h, respectively. Statistically significant differences are indicated by asterisks (*$p < 0.05$; **$p < 0.01$; ***$p < 0.001$).

for 24 h and subsequently infected with BPP30GFP (MOI of 1 pfu/cell). Pre-incubation with anti-LBPA antibody resulted in a significant decrease of ASFV entry at 6 hpi, as observed when we analyzed the percentage of GFP-positive cells by flow cytometry (Figure 5B). In concordance with the previous results, we detected a higher impact of LBPA blocking at later stages of the infection, reaching almost 50% of inhibition in Vero cells treated and infected with B54GFP (Figure 5C). Our observations of reduced ASFV infectivity under LBPA antibody treatment was further supported by a decrease in total viral production (Figure 5D). Finally, we illustrated the pattern of endogenous LBPA by staining Vero-infected cells at 16 hpi and processing them by confocal microscopy. As shown in Figure 5E, LBPA staining distributed with the same pattern as late endosomes, around the viral factories in infected cells colocalizing with p150-labeled replication sites. Quantification of the amount of LBPA clustered around the viral factory (determined as a ratio fluorescence intensity close to the VF/total fluorescence) showed that LBPA accumulates specifically around VFs compared to the cytoplasm in infected cells (ASFV). In uninfected cells (MOCK), LBPA signal distribution was more homogeneous in the perinuclear region and cytoplasm (Figure 5E).

4 Discussion

Increasing lines of evidence indicate that several viruses usurp the cellular ESCRT machinery at several infection stages (Votteler and Sundquist, 2013; Weissenhorn et al., 2013; Scourfield and Martin-Serrano, 2017). However, it is still unknown whether ESCRT proteins could participate in ASFV infection.

ESCRT-III functions are coordinated by the AAA-ATPase VPS4, which regulates the exchange of subunits during ESCRT-III polymerization and disassembly upon membrane remodeling and membrane scission (Davies et al., 2010; Adell and Teis, 2011; Adell et al., 2017; Pfitzner et al., 2020; Vietri et al., 2020). In addition, several virus families exploit VPS4 for a successful infection. This protein has a relevant function in the generation of the virion envelope of herpesvirus in the nucleus of infected cells (Crump et al., 2007; Pawliczek and Crump, 2009; Yadav et al., 2017), and alterations in this protein impair the egress of viral particles through the inner nuclear membrane (Lee et al., 2012; Arii et al., 2018). Classical swine fever virus, Echovirus 1, or Arenavirus also require VPS4 function for their infection (Karjalainen et al., 2011; Pasqual et al., 2011; Liu et al., 2022), and recently, the relevance for VPS4 in HIV budding has been shown (Harel et al., 2022). Nevertheless, in other enveloped viruses, VPS4 has merely an ESCRT-III recycling function (Diaz et al., 2015), or it is needless, as shown for flavivirus replication (Tabata et al., 2016). Consistent with a central role for VPS4 in several viral infections, we proceed to evaluate the impact of silencing VPS4A in ASFV infection. ASFV replication was affected when silencing VPS4A expression in cells, mainly at later stages of the viral cycle. Changes in the level of VPS4A did not impair ASFV infectivity at early stages; therefore, VPS4A silencing suggests an implication for a later stage in viral infection. It could be possible that VPS4A assists the viral progeny

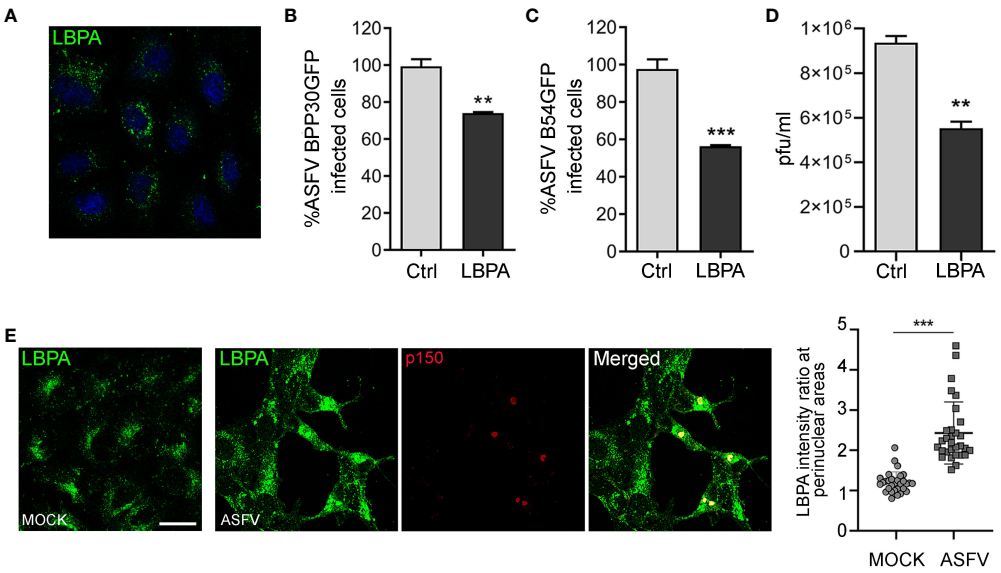

FIGURE 5
LBPA affects ASFV infection. Vero cells were pre-incubated with no antibody (Ctrl) or 50 μg/mL monoclonal antibody anti-LBPA for 24 (h) **(A)** LBPA internalization was processed for immunofluorescence and analyzed by confocal microscopy **(B, C)** Cells were then infected with recombinant virus BPP30GFP or B54GFP. In treated samples (LBPA), a virus adsorption period (90 min at 37°C) was conducted in the presence of the Ab. After washing out unbound viral particles, Vero cells were incubated at 37°C in fresh medium. **(B)** Infectivity of BPP30GFP (1 pfu/mL) in Vero cells at 6 hpi measured by flow cytometry (GFP fluorescence percentage relative to control). **(C)** Percentage of B54GFP-infected cells (GFP fluorescence relative to empty control) at 16 hpi in Vero cells. **(D)** Total ASFV production quantified by plaque assay of Vero cells untreated (Ctrl) or incubated with LBPA for 24 h and infected with ASFV. **(E)** Vero cells infected with ASFV for 16 h and staining with anti-LBPA antibody (green) and core protein p150 (red). Graph shows the quantification of LBPA staining in the perinuclear area related to the cytoplasm in MOCK and infected Vero cells. Each dot in the graph represents the ratio of fluorescence measured at the perinuclear region related to the cytoplasm per cell (n = 30 per condition). Scale bar: 20 μm. Statistically significant differences are indicated by asterisks (**$p < 0.01$; ***$p < 0.001$).

assembly during the virion membrane acquisition, as occurs with Vaccinia virus, a closely related nucleocytoplasmic DNA virus (Huttunen et al., 2021). In fact, VPS4A silencing reduced extracellular virus production; hence, this would suggest a potential role for this ESCRT protein in ASFV budding, similarly to HIV-1 (Kieffer et al., 2008; Harel et al., 2022).

The redistribution of membranes, analyzed through endosomal and lysosomal markers, remained altered in infected cells, without any evident effect in the redistribution of vesicle membranes under VPS4A silencing. A plausible reason for this finding could be a functional redundancy between VPS4A and VPS4B that would compensate for the lack of VPS4A at particular infection stages, as has previously been described for other ESCRT components such as CHMP2 or CHMP4 families in flavivirus infection (Tabata et al., 2016).

The ESCRT-0 component HRS initially guides ubiquitinated membrane proteins from early endosomes into ILVs of the MVBs (Vietri et al., 2020). ASFV weakly increased HRS expression; however, virions that traffic through endosomes would occur independently of ILVs, since ILVs have a smaller size than ASFV virions and require the acidic pH of LEs to decapsidate (Cuesta-Geijo et al., 2012). Thus, this requirement of HRS in ASFV infection is not yet well understood.

The accessory ESCRT protein ALIX exerts multiple functions, including endosomal homeostasis in cooperation with other ESCRT components (Gupta et al., 2020; Tran et al., 2022). Contrarily to HRS, ASFV-infected cells overexpressed and relocated ALIX around the viral factory independently of VPS4A silencing. As ALIX was recruited to the viral factory, we hypothesized that the protein could have a role during ASFV infection, supporting later stages during the viral cycle as replication, viral production, or egress, as occurs in flavivirus infection (Tran et al., 2022), HIV-1 (Fujii et al., 2009), or classical swine fever infection (Liu et al., 2022). This assumption was supported by a reduction of p54 expression and viral copy number during replication in cells lacking ALIX. According to these data, viral production was altered, as indicated by the reduction in intracellular and extracellular viral titer. We could speculate about the involvement of ALIX in viral morphogenesis and viral egress since intracellular and extracellular titers were affected, or it could be also a consequence of a defective viral replication. Thereby, since replication is affected and intracellular and extracellular plaque assay results are comparable, with no severe effects in titer, ALIX could support viral replication, but it has a modest role in viral production and budding. Further studies need to be conducted to clarify this issue.

Besides its role with ESCRT, ALIX controls ILV formation in the MVB and LE dynamics through the interaction with LBPA by an exposed site in the ALIX Bro1 domain in a Ca^{2+}-dependent manner (Williams and Urbe, 2007; Bissig and Gruenberg, 2014). Interestingly, it has been recently reported that ASFV triggers the activation of calcium-signaling pathways in endosomes (Galindo et al., 2021).

LBPA is specifically located particularly in the inner leaflet of late endosomes and a variety of viruses, such as dengue virus or vesicular stomatitis virus, take advantage of this molecule for membrane fusion at entry. In fact, pretreatment with anti-LBPA antibody reduces dengue and Arenavirus infection (Pattanakitsakul et al., 2010; Zaitseva et al., 2010; Roth and Whittaker, 2011). We impaired LBPA function by preincubating cells with a blocking function monoclonal antibody against LBPA prior to ASFV infection, which affects endosomal/MVBs homeostasis or back fusion events altering the cholesterol efflux necessary for ASFV infection (Bissig and Gruenberg, 2014; Gruenberg, 2020; Cuesta-Geijo et al., 2022). Our data support the idea that LBPA blocking treatment prior to infection reduces ASFV infectivity at early and late stages post-infection, thus affecting virions trafficking through endosomes, replication, and also viral production. This indicates how LBPA controls ASFV infectivity and viral production, probably by affecting cholesterol efflux, in an ALIX unrelated process, since ALIX knockdown did not alter early protein expression during ASFV infection.

Cholesterol traffic and the main intracellular cholesterol transporters NPC1 and 2 are relevant in ASFV infectivity and replication (Cuesta-Geijo et al., 2022). Thus, the direct interaction between NPC2 and LBPA to regulate cholesterol efflux could possibly affect earlier stages of ASFV infection (McCauliff et al., 2019). Furthermore, LBPA is redistributed to perinuclear locations, where ASFV replication occurs, supporting a function in viral infection at later stages.

Interestingly, recent works have shown that LBPA is important for the life cycle of SARS-CoV-2 (Carriere et al., 2020; Luquain-Costaz et al., 2020), but more studies are required to unveil its mechanism of action in the infection. Our results would support that ASFV needs an efficient cholesterol transport that depends on LBPA and NPC proteins from early steps of the infection, while the LBPA–ALIX interaction, related to ILV formation and back fusion, would remain in the background, since ASF virions fuse with the LE (Cuesta-Geijo et al., 2012; Hernaez et al., 2016).

In summary, our results point out for the first time the involvement of ESCRT-related proteins such as VPS4A, ALIX, and the unconventional phospholipid LBPA in ASFV infection. These molecules are tightly linked to the maintenance of endocytic pathway homeostasis, and their functions impact the infectivity and replication of ASFV. The results presented constitute an interesting opening for addressing the specific function of these proteins in future works, unveiling potential new therapeutic molecules with a putative antiviral activity.

Data availability statement

The original contributions presented in the study are included in the article/supplementary material. Further inquiries can be directed to the corresponding author.

Author contributions

CA and MC-G contributed to conception and design of the study. B-GL and MC-G conducted experimentation and CA validation. ID and IG conducted the image quantification and formal analysis. CA was responsible for the funding of the project. All authors wrote sections of the manuscript. All authors contributed to manuscript revision and approved the submitted version.

Funding

The author(s) declare financial support was received for the research, authorship, and/or publication of this article. This research was partially supported through the European Commission, Horizon 2020 Framework Programme European Union ASFVInt ERANET-2021-0017 co-funded by Spanish Ministry of Science and Innovation PCI2021-121939/AEI/10.13039/501100011033 (https://www.ciencia.gob.es/); "La Caixa" Banking Foundation award number LCF/PR/HR19/52160012, Spain; and the Spanish Ministry of Science and Innovation, Spain PID2021-122825OB. This research work was also funded by the European Commission–NextGenerationEU (Regulation EU 2020/2094), through CSIC's Global Health Platform (PTI SaludGlobal).

Conflict of interest

The authors declare that the research was conducted in the absence of any commercial or financial relationships that could be construed as a potential conflict of interest.

Publisher's note

References

Adell, M. A., and Teis, D. (2011). Assembly and disassembly of the ESCRT-III membrane scission complex. *FEBS Lett.* 585 (20), 3191–3196. doi: 10.1016/j.febslet.2011.09.001

Adell, M. A. Y., Migliano, S. M., Upadhyayula, S., Bykov, Y. S., Sprenger, S., Pakdel, M., et al. (2017). Recruitment dynamics of ESCRT-III and Vps4 to endosomes and implications for reverse membrane budding. *Elife* 6, e31652. doi: 10.7554/eLife.31652

Adell, M. A., Vogel, G. F., Pakdel, M., Muller, M., Lindner, H., Hess, M. W., et al. (2014). Coordinated binding of Vps4 to ESCRT-III drives membrane neck constriction during MVB vesicle formation. *J. Cell Biol.* 205 (1), 33–49. doi: 10.1083/jcb.201310114

Alonso, C., Borca, M., Dixon, L., Revilla, Y., Rodriguez, F., Escribano, J. M., et al. (2018). ICTV virus taxonomy profile: asfarviridae. *J. Gen. Virol.* 99 (5), 613–614. doi: 10.1099/jgv.0.001049

Andreani, J., Khalil, J. Y. B., Sevvana, M., Benamar, S., Di Pinto, F., Bitam, I., et al. (2017). Pacmanvirus, a new giant icosahedral virus at the crossroads between asfarviridae and faustoviruses. *J. Virol.* 91 (14), e00212-17. doi: 10.1128/JVI.00212-17

Andres, G., Charro, D., Matamoros, T., Dillard, R. S., and Abrescia, N. G. A. (2020). The cryo-EM structure of African swine fever virus unravels a unique architecture comprising two icosahedral protein capsids and two lipoprotein membranes. *J. Biol. Chem.* 295 (1), 1–12. doi: 10.1074/jbc.AC119.011196

Andres, G., Garcia-Escudero, R., Vinuela, E., Salas, M. L., and Rodriguez, J. M. (2001). African swine fever virus structural protein pE120R is essential for virus transport from assembly sites to plasma membrane but not for infectivity. *J. Virol.* 75 (15), 6758–6768. doi: 10.1128/JVI.75.15.6758-6768.2001

Arii, J., Watanabe, M., Maeda, F., Tokai-Nishizumi, N., Chihara, T., Miura, M., et al. (2018). ESCRT-III mediates budding across the inner nuclear membrane and regulates its integrity. *Nat. Commun.* 9 (1), 3379. doi: 10.1038/s41467-018-05889-9

Babst, M., Katzmann, D. J., Snyder, W. B., Wendland, B., and Emr, S. D. (2002). Endosome-associated complex, ESCRT-II, recruits transport machinery for protein sorting at the multivesicular body. *Dev. Cell* 3 (2), 283–289. doi: 10.1016/s1534-5807(02)00219-8

Babst, M., Wendland, B., Estepa, E. J., and Emr, S. D. (1998). The Vps4p AAA ATPase regulates membrane association of a Vps protein complex required for normal endosome function. *EMBO J.* 17 (11), 2982–2993. doi: 10.1093/emboj/17.11.2982

Ballout, R. A., Sviridov, D., Bukrinsky, M. I., and Remaley, A. T. (2020). The lysosome: A potential juncture between SARS-CoV-2 infectivity and Niemann-Pick disease type C, with therapeutic implications. *FASEB J.* 34 (6), 7253–7264. doi: 10.1096/fj.202000654R

Barrado-Gil, L., Galindo, I., Martinez-Alonso, D., Viedma, S., and Alonso, C. (2017). The ubiquitin-proteasome system is required for African swine fever replication. *PloS One* 12 (12), e0189741. doi: 10.1371/journal.pone.0189741

Bissig, C., and Gruenberg, J. (2014). ALIX and the multivesicular endosome: ALIX in Wonderland. *Trends Cell Biol.* 24 (1), 19–25. doi: 10.1016/j.tcb.2013.10.009

Bissig, C., Lenoir, M., Velluz, M. C., Kufareva, I., Abagyan, R., Overduin, M., et al. (2013). Viral infection controlled by a calcium-dependent lipid-binding module in ALIX. *Dev. Cell* 25 (4), 364–373. doi: 10.1016/j.devcel.2013.04.003

Carlton, J. G., Agromayor, M., and Martin-Serrano, J. (2008). Differential requirements for Alix and ESCRT-III in cytokinesis and HIV-1 release. *Proc. Natl. Acad. Sci. U.S.A.* 105 (30), 10541–10546. doi: 10.1073/pnas.0802008105

Carriere, F., Longhi, S., and Record, M. (2020). The endosomal lipid bis (monoacylglycero) phosphate as a potential key player in the mechanism of action of chloroquine against SARS-COV-2 and other enveloped viruses hijacking the endocytic pathway. *Biochimie* 179, 237–246. doi: 10.1016/j.biochi.2020.05.013

Carvalho, Z. G., De Matos, A. P., and Rodrigues-Pousada, C. (1988). Association of African swine fever virus with the cytoskeleton. *Virus Res.* 11 (2), 175–192. doi: 10.1016/0168-1702(88)90042-1

Costard, S., Wieland, B., de Glanville, W., Jori, F., Rowlands, R., Vosloo, W., et al. (2009). African swine fever: how can global spread be prevented? *Philos. Trans. R Soc. Lond B Biol. Sci.* 364 (1530), 2683–2696. doi: 10.1098/rstb.2009.0098

Crump, C. M., Yates, C., and Minson, T. (2007). Herpes simplex virus type 1 cytoplasmic envelopment requires functional Vps4. *J. Virol.* 81 (14), 7380–7387. doi: 10.1128/JVI.00222-07

Cuesta-Geijo, M. A., Barrado-Gil, L., Galindo, I., Munoz-Moreno, R., and Alonso, C. (2017). Redistribution of endosomal membranes to the african swine fever virus replication site. *Viruses* 9 (6), 133. doi: 10.3390/v9060133

Cuesta-Geijo, M. A., Chiappi, M., Galindo, I., Barrado-Gil, L., Munoz-Moreno, R., Carrascosa, J. L., et al. (2016). Cholesterol flux is required for endosomal progression of african swine fever virions during the initial establishment of infection. *J. Virol.* 90 (3), 1534–1543. doi: 10.1128/JVI.02694-15

Cuesta-Geijo, M. A., Galindo, I., Hernaez, B., Quetglas, J. I., Dalmau-Mena, I., and Alonso, C. (2012). Endosomal maturation, Rab7 GTPase and phosphoinositides in African swine fever virus entry. *PloS One* 7 (11), e48853. doi: 10.1371/journal.pone.0048853

Cuesta-Geijo, M. A., Garcia-Dorival, I., Del Puerto, A., Urquiza, J., Galindo, I., Barrado-Gil, L., et al. (2022). New insights into the role of endosomal proteins for African swine fever virus infection. *PloS Pathog.* 18 (1), e1009784. doi: 10.1371/journal.ppat.1009784

Davies, B. A., Azmi, I. F., Payne, J., Shestakova, A., Horazdovsky, B. F., Babst, M., et al. (2010). Coordination of substrate binding and ATP hydrolysis in Vps4-mediated ESCRT-III disassembly. *Mol. Biol. Cell* 21 (19), 3396–3408. doi: 10.1091/mbc.E10-06-0512

Diaz, A., Zhang, J., Ollwerther, A., Wang, X., and Ahlquist, P. (2015). Host ESCRT proteins are required for bromovirus RNA replication compartment assembly and function. *PloS Pathog.* 11 (3), e1004742. doi: 10.1371/journal.ppat.1004742

Enjuanes, L., Carrascosa, A. L., Moreno, M. A., and Vinuela, E. (1976). Titration of African swine fever (ASF) virus. *J. Gen. Virol.* 32 (3), 471–477. doi: 10.1099/0022-1317-32-3-471

Fisher, R. D., Chung, H. Y., Zhai, Q., Robinson, H., Sundquist, W. I., and Hill, C. P. (2007). Structural and biochemical studies of ALIX/AIP1 and its role in retrovirus budding. *Cell* 128 (5), 841–852. doi: 10.1016/j.cell.2007.01.035

Fujii, K., Munshi, U. M., Ablan, S. D., Demirov, D. G., Soheilian, F., Nagashima, K., et al. (2009). Functional role of Alix in HIV-1 replication. *Virology* 391 (2), 284–292. doi: 10.1016/j.virol.2009.06.016

Galindo, I., Cuesta-Geijo, M. A., Hlavova, K., Munoz-Moreno, R., Barrado-Gil, L., Dominguez, J., et al. (2015). African swine fever virus infects macrophages, the natural host cells, via clathrin- and cholesterol-dependent endocytosis. *Virus Res.* 200, 45–55. doi: 10.1016/j.virusres.2015.01.022

Galindo, I., Garaigorta, U., Lasala, F., Cuesta-Geijo, M. A., Bueno, P., Gil, C., et al. (2021). Antiviral drugs targeting endosomal membrane proteins inhibit distant animal and human pathogenic viruses. *Antiviral Res.* 186, 104990. doi: 10.1016/j.antiviral.2020.104990

Gruenberg, J. (2003). Lipids in endocytic membrane transport and sorting. *Curr. Opin. Cell Biol.* 15 (4), 382–388. doi: 10.1016/s0955-0674(03)00078-4

Gruenberg, J. (2020). Life in the lumen: The multivesicular endosome. *Traffic* 21 (1), 76–93. doi: 10.1111/tra.12715

Gupta, S., Bendjennat, M., and Saffarian, S. (2020). Abrogating ALIX interactions results in stuttering of the ESCRT machinery. *Viruses* 12 (9), 1032. doi: 10.3390/v12091032

Harel, S., Altaras, Y., Nachmias, D., Rotem-Dai, N., Dvilansky, I., Elia, N., et al. (2022). Analysis of individual HIV-1 budding event using fast AFM reveals a multiplexed role for VPS4. *Biophys. J.* 121 (21), 4229–4238. doi: 10.1016/j.bpj.2022.08.035

Hernaez, B., and Alonso, C. (2010). Dynamin- and clathrin-dependent endocytosis in African swine fever virus entry. *J. Virol.* 84 (4), 2100–2109. doi: 10.1128/JVI.01557-09

Hernaez, B., Escribano, J. M., and Alonso, C. (2006). Visualization of the African swine fever virus infection in living cells by incorporation into the virus particle of green fluorescent protein-p54 membrane protein chimera. *Virology* 350 (1), 1–14. doi: 10.1016/j.virol.2006.01.021

Hernaez, B., Guerra, M., Salas, M. L., and Andres, G. (2016). African swine fever virus undergoes outer envelope disruption, capsid disassembly and inner envelope fusion before core release from multivesicular endosomes. *PloS Pathog.* 12 (4), e1005595. doi: 10.1371/journal.ppat.1005595

Hullin-Matsuda, F., Kawasaki, K., Delton-Vandenbroucke, I., Xu, Y., Nishijima, M., Lagarde, M., et al. (2007). *De novo* biosynthesis of the late endosome lipid, bis (monoacylglycero)phosphate. *J. Lipid Res.* 48 (9), 1997–2008. doi: 10.1194/jlr.M700154-JLR200

Huttunen, M., Samolej, J., Evans, R. J., Yakimovich, A., White, I. J., Kriston-Vizi, J., et al. (2021). Vaccinia virus hijacks ESCRT-mediated multivesicular body formation for virus egress. *Life Sci. Alliance* 4 (8), e202000910. doi: 10.26508/lsa.202000910

Ilnytska, O., Santiana, M., Hsu, N. Y., Du, W. L., Chen, Y. H., Viktorova, E. G., et al. (2013). Enteroviruses harness the cellular endocytic machinery to remodel the host cell cholesterol landscape for effective viral replication. *Cell Host Microbe* 14 (3), 281–293. doi: 10.1016/j.chom.2013.08.002

Jiang, W., Ma, P., Deng, L., Liu, Z., Wang, X., Liu, X., et al. (2020). Hepatitis A virus structural protein pX interacts with ALIX and promotes the secretion of virions and foreign proteins through exosome-like vesicles. *J. Extracell Vesicles* 9 (1), 1716513. doi: 10.1080/20013078.2020.1716513

Jouvenet, N., Monaghan, P., Way, M., and Wileman, T. (2004). Transport of African swine fever virus from assembly sites to the plasma membrane is dependent on microtubules and conventional kinesin. *J. Virol.* 78 (15), 7990–8001. doi: 10.1128/JVI.78.15.7990-8001.2004

Karjalainen, M., Rintanen, N., Lehkonen, M., Kallio, K., Maki, A., Hellstrom, K., et al. (2011). Echovirus 1 infection depends on biogenesis of novel multivesicular bodies. *Cell Microbiol.* 13 (12), 1975–1995. doi: 10.1111/j.1462-5822.2011.01685.x

Katzmann, D. J., Babst, M., and Emr, S. D. (2001). Ubiquitin-dependent sorting into the multivesicular body pathway requires the function of a conserved endosomal protein sorting complex, ESCRT-I. *Cell* 106 (2), 145–155. doi: 10.1016/s0092-8674(01)00434-2

Kieffer, C., Skalicky, J. J., Morita, E., De Domenico, I., Ward, D. M., Kaplan, J., et al. (2008). Two distinct modes of ESCRT-III recognition are required for VPS4 functions in lysosomal protein targeting and HIV-1 budding. *Dev. Cell* 15 (1), 62–73. doi: 10.1016/j.devcel.2008.05.014

King, D. P., Reid, S. M., Hutchings, G. H., Grierson, S. S., Wilkinson, P. J., Dixon, L. K., et al. (2003). Development of a TaqMan PCR assay with internal amplification control for the detection of African swine fever virus. *J. Virol. Methods* 107 (1), 53–61. doi: 10.1016/s0166-0934(02)00189-1

Kobayashi, T., Beuchat, M. H., Lindsay, M., Frias, S., Palmiter, R. D., Sakuraba, H., et al. (1999). Late endosomal membranes rich in lysobisphosphatidic acid regulate cholesterol transport. *Nat. Cell Biol.* 1 (2), 113–118. doi: 10.1038/10084

Kobayashi, T., Stang, E., Fang, K. S., de Moerloose, P., Parton, R. G., and Gruenberg, J. (1998). A lipid associated with the antiphospholipid syndrome regulates endosome structure and function. *Nature* 392 (6672), 193–197. doi: 10.1038/32440

Koonin, E. V., Dolja, V. V., Krupovic, M., Varsani, A., Wolf, Y. I., Yutin, N., et al. (2020). Global organization and proposed megataxonomy of the virus world. *Microbiol. Mol. Biol. Rev.* 84 (2), e00061-19. doi: 10.1128/MMBR.00061-19

Koonin, E. V., and Yutin, N. (2019). Evolution of the large nucleocytoplasmic DNA viruses of eukaryotes and convergent origins of viral gigantism. *Adv. Virus Res.* 103, 167–202. doi: 10.1016/bs.aivir.2018.09.002

Korbei, B. (2022). Ubiquitination of the ubiquitin-binding machinery: how early ESCRT components are controlled. *Essays Biochem.* 66 (2), 169–177. doi: 10.1042/EBC20210042

Le Blanc, I., Luyet, P. P., Pons, V., Ferguson, C., Emans, N., Petiot, A., et al. (2005). Endosome-to-cytosol transport of viral nucleocapsids. *Nat. Cell Biol.* 7 (7), 653–664. doi: 10.1038/ncb1269

Lee, C. P., Liu, P. T., Kung, H. N., Su, M. T., Chua, H. H., Chang, Y. H., et al. (2012). The ESCRT machinery is recruited by the viral BFRF1 protein to the nucleus-associated membrane for the maturation of Epstein-Barr Virus. *PloS Pathog.* 8 (9), e1002904. doi: 10.1371/journal.ppat.1002904

Lin, C. Y., Urbina, A. N., Wang, W. H., Thitithanyanont, A., and Wang, S. F. (2022). Virus hijacks host proteins and machinery for assembly and budding, with HIV-1 as an example. *Viruses* 14 (7), 1528. doi: 10.3390/v14071528

Liu, C. C., Liu, Y. Y., Zhou, J. F., Chen, X., Chen, H., Hu, J. H., et al. (2022). Cellular ESCRT components are recruited to regulate the endocytic trafficking and RNA replication compartment assembly during classical swine fever virus infection. *PloS Pathog.* 18 (2), e1010294. doi: 10.1371/journal.ppat.1010294

Liu, S., Luo, Y., Wang, Y., Li, S., Zhao, Z., Bi, Y., et al. (2019). Cryo-EM structure of the african swine fever virus. *Cell Host Microbe* 26 (6), 836-843.e833. doi: 10.1016/j.chom.2019.11.004

Luquain-Costaz, C., Rabia, M., Hullin-Matsuda, F., and Delton, I. (2020). Bis (monoacylglycero)phosphate, an important actor in the host endocytic machinery hijacked by SARS-CoV-2 and related viruses. *Biochimie* 179, 247–256. doi: 10.1016/j.biochi.2020.10.018

Matamoros, T., Alejo, A., Rodriguez, J. M., Hernaez, B., Guerra, M., Fraile-Ramos, A., et al. (2020). African swine fever virus protein pE199L mediates virus entry by enabling membrane fusion and core penetration. *mBio* 11 (4), e00789-20. doi: 10.1128/mBio.00789-20

Matsuo, H., Chevallier, J., Mayran, N., Le Blanc, I., Ferguson, C., Faure, J., et al. (2004). Role of LBPA and Alix in multivesicular liposome formation and endosome organization. *Science* 303 (5657), 531–534. doi: 10.1126/science.1092425

McCauliff, L. A., Langan, A., Li, R., Ilnytska, O., Bose, D., Waghalter, M., et al. (2019). Intracellular cholesterol trafficking is dependent upon NPC2 interaction with lysobisphosphatidic acid. *Elife* 8, e50832. doi: 10.7554/eLife.50832

McCullough, J., Colf, L. A., and Sundquist, W. I. (2013). Membrane fission reactions of the mammalian ESCRT pathway. *Annu. Rev. Biochem.* 82, 663–692. doi: 10.1146/annurev-biochem-072909-101058

McCullough, J., Frost, A., and Sundquist, W. I. (2018). Structures, functions, and dynamics of ESCRT-III/vps4 membrane remodeling and fission complexes. *Annu. Rev. Cell Dev. Biol.* 34, 85–109. doi: 10.1146/annurev-cellbio-100616-060600

Meng, B., and Lever, A. M. L. (2021). The interplay between ESCRT and viral factors in the enveloped virus life cycle. *Viruses* 13 (2), 324. doi: 10.3390/v13020324

Mierzwa, B. E., Chiaruttini, N., Redondo-Morata, L., von Filseck, J. M., Konig, J., Larios, J., et al. (2017). Dynamic subunit turnover in ESCRT-III assemblies is regulated by Vps4 to mediate membrane remodelling during cytokinesis. *Nat. Cell Biol.* 19 (7), 787–798. doi: 10.1038/ncb3559

Mighell, E., and Ward, M. P. (2021). African Swine Fever spread across Asia 2018-2019. *Transbound Emerg. Dis.* 68 (5), 2722–2732. doi: 10.1111/tbed.14039

Mobius, W., van Donselaar, E., Ohno-Iwashita, Y., Shimada, Y., Heijnen, H. F., Slot, J. W., et al. (2003). Recycling compartments and the internal vesicles of multivesicular bodies harbor most of the cholesterol found in the endocytic pathway. *Traffic* 4 (4), 222–231. doi: 10.1034/j.1600-0854.2003.00072.x

Munshi, U. M., Kim, J., Nagashima, K., Hurley, J. H., and Freed, E. O. (2007). An Alix fragment potently inhibits HIV-1 budding: characterization of binding to retroviral YPXL late domains. *J. Biol. Chem.* 282 (6), 3847–3855. doi: 10.1074/jbc.M607489200

Odorizzi, G. (2006). The multiple personalities of Alix. *J. Cell Sci.* 119 (Pt 15), 3025–3032. doi: 10.1242/jcs.03072

Olmos, Y. (2022). The ESCRT machinery: remodeling, repairing, and sealing membranes. *Membranes (Basel)* 12 (6), 633. doi: 10.3390/membranes12060633

Pasqual, G., Rojek, J. M., Masin, M., Chatton, J. Y., and Kunz, S. (2011). Old world arenaviruses enter the host cell via the multivesicular body and depend on the endosomal sorting complex required for transport. *PloS Pathog.* 7 (9), e1002232. doi: 10.1371/journal.ppat.1002232

Pattanakitsakul, S. N., Poungsawai, J., Kanlaya, R., Sinchaikul, S., Chen, S. T., and Thongboonkerd, V. (2010). Association of Alix with late endosomal lysobisphosphatidic acid is important for dengue virus infection in human endothelial cells. *J. Proteome Res.* 9 (9), 4640–4648. doi: 10.1021/pr100357f

Pawliczek, T., and Crump, C. M. (2009). Herpes simplex virus type 1 production requires a functional ESCRT-III complex but is independent of TSG101 and ALIX expression. *J. Virol.* 83 (21), 11254–11264. doi: 10.1128/JVI.00574-09

Pfitzner, A. K., Mercier, V., Jiang, X., Moser von Filseck, J., Baum, B., Saric, A., et al. (2020). An ESCRT-III polymerization sequence drives membrane deformation and fission. *Cell* 182 (5), 1140-1155.e1118. doi: 10.1016/j.cell.2020.07.021

Qiu, X., Campos, Y., van de Vlekkert, D., Gomero, E., Tanwar, A. C., Kalathur, R., et al. (2022). Distinct functions of dimeric and monomeric scaffold protein Alix in regulating F-actin assembly and loading of exosomal cargo. *J. Biol. Chem.* 298 (10), 102425. doi: 10.1016/j.jbc.2022.102425

Rincon, E., Saez de Guinoa, J., Gharbi, S. I., Sorzano, C. O., Carrasco, Y. R., and Merida, I. (2011). Translocation dynamics of sorting nexin 27 in activated T cells. *J. Cell Sci.* 124 (Pt 5), 776–788. doi: 10.1242/jcs.072447

Rodriguez, F., Alcaraz, C., Eiras, A., Yanez, R. J., Rodriguez, J. M., Alonso, C., et al. (1994). Characterization and molecular basis of heterogeneity of the African swine fever virus envelope protein p54. *J. Virol.* 68 (11), 7244–7252. doi: 10.1128/JVI.68.11.7244-7252.1994

Roth, S. L., and Whittaker, G. R. (2011). Promotion of vesicular stomatitis virus fusion by the endosome-specific phospholipid bis(monoacylglycero)phosphate (BMP). *FEBS Lett.* 585 (6), 865–869. doi: 10.1016/j.febslet.2011.02.015

Saksena, S., Wahlman, J., Teis, D., Johnson, A. E., and Emr, S. D. (2009). Functional reconstitution of ESCRT-III assembly and disassembly. *Cell* 136 (1), 97–109. doi: 10.1016/j.cell.2008.11.013

Sanchez, E. G., Perez-Nunez, D., and Revilla, Y. (2017). Mechanisms of entry and endosomal pathway of african swine fever virus. *Vaccines (Basel)* 5 (4), 42. doi: 10.3390/vaccines5040042

Sanchez, E. G., Quintas, A., Perez-Nunez, D., Nogal, M., Barroso, S., Carrascosa, A. L., et al. (2012). African swine fever virus uses macropinocytosis to enter host cells. *PloS Pathog.* 8 (6), e1002754. doi: 10.1371/journal.ppat.1002754

Schambow, R., Reyes, R., Morales, J., Diaz, A., and Perez, A. M. (2022). A qualitative assessment of alternative eradication strategies for African swine fever in the Dominican Republic. *Front. Vet. Sci.* 9. doi: 10.3389/fvets.2022.1054271

Schoneberg, J., Lee, I. H., Iwasa, J. H., and Hurley, J. H. (2017). Reverse-topology membrane scission by the ESCRT proteins. *Nat. Rev. Mol. Cell Biol.* 18 (1), 5–17. doi: 10.1038/nrm.2016.121

Scourfield, E. J., and Martin-Serrano, J. (2017). Growing functions of the ESCRT machinery in cell biology and viral replication. *Biochem. Soc. Trans.* 45 (3), 613–634. doi: 10.1042/BST20160479

Strack, B., Calistri, A., Craig, S., Popova, E., and Gottlinger, H. G. (2003). AIP1/ALIX is a binding partner for HIV-1 p6 and EIAV p9 functioning in virus budding. *Cell* 114 (6), 689–699. doi: 10.1016/s0092-8674(03)00653-6

Tabata, K., Arimoto, M., Arakawa, M., Nara, A., Saito, K., Omori, H., et al. (2016). Unique requirement for ESCRT factors in flavivirus particle formation on the endoplasmic reticulum. *Cell Rep.* 16 (9), 2339–2347. doi: 10.1016/j.celrep.2016.07.068

Torii, S., Orba, Y., Sasaki, M., Tabata, K., Wada, Y., Carr, M., et al. (2020). Host ESCRT factors are recruited during chikungunya virus infection and are required for the intracellular viral replication cycle. *J. Biol. Chem.* 295 (23), 7941–7957. doi: 10.1074/jbc.RA119.012303

Tran, P. T., Chiramel, A. I., Johansson, M., and Melik, W. (2022). Roles of ESCRT proteins ALIX and CHMP4A and their interplay with interferon-stimulated gene 15 during tick-borne flavivirus infection. *J. Virol.* 96 (3), e0162421. doi: 10.1128/JVI.01624-21

Urbano, A. C., and Ferreira, F. (2022). African swine fever control and prevention: an update on vaccine development. *Emerg. Microbes Infect.* 11 (1), 2021–2033. doi: 10.1080/22221751.2022.2108342

Usami, Y., Popov, S., and Gottlinger, H. G. (2007). Potent rescue of human immunodeficiency virus type 1 late domain mutants by ALIX/AIP1 depends on its CHMP4 binding site. *J. Virol.* 81 (12), 6614–6622. doi: 10.1128/JVI.00314-07

Vietri, M., Radulovic, M., and Stenmark, H. (2020). The many functions of ESCRTs. *Nat. Rev. Mol. Cell Biol.* 21 (1), 25–42. doi: 10.1038/s41580-019-0177-4

Vito, P., Pellegrini, L., Guiet, C., and D'Adamio, L. (1999). Cloning of AIP1, a novel protein that associates with the apoptosis-linked gene ALG-2 in a Ca2+-dependent reaction. *J. Biol. Chem.* 274 (3), 1533–1540. doi: 10.1074/jbc.274.3.1533

von Schwedler, U. K., Stuchell, M., Muller, B., Ward, D. M., Chung, H. Y., Morita, E., et al. (2003). The protein network of HIV budding. *Cell* 114 (6), 701–713. doi: 10.1016/s0092-8674(03)00714-1

Votteler, J., and Sundquist, W. I. (2013). Virus budding and the ESCRT pathway. *Cell Host Microbe* 14 (3), 232–241. doi: 10.1016/j.chom.2013.08.012

Wang, N., Zhao, D., Wang, J., Zhang, Y., Wang, M., Gao, Y., et al. (2019). Architecture of African swine fever virus and implications for viral assembly. *Science* 366 (6465), 640–644. doi: 10.1126/science.aaz1439

Weissenhorn, W., Poudevigne, E., Effantin, G., and Bassereau, P. (2013). How to get out: ssRNA enveloped viruses and membrane fission. *Curr. Opin. Virol.* 3 (2), 159–167. doi: 10.1016/j.coviro.2013.03.011

Williams, R. L., and Urbe, S. (2007). The emerging shape of the ESCRT machinery. *Nat. Rev. Mol. Cell Biol.* 8 (5), 355–368. doi: 10.1038/nrm2162

Yadav, S., Libotte, F., Buono, E., Valia, S., Farina, G. A., Faggioni, A., et al. (2017). EBV early lytic protein BFRF1 alters emerin distribution and post-translational modification. *Virus Res.* 232, 113–122. doi: 10.1016/j.virusres.2017.02.010

Zaitseva, E., Yang, S. T., Melikov, K., Pourmal, S., and Chernomordik, L. V. (2010). Dengue virus ensures its fusion in late endosomes using compartment-specific lipids. *PloS Pathog.* 6 (10), e1001131. doi: 10.1371/journal.ppat.1001131

Zhai, Q., Landesman, M. B., Chung, H. Y., Dierkers, A., Jeffries, C. M., Trewhella, J., et al. (2011). Activation of the retroviral budding factor ALIX. *J. Virol.* 85 (17), 9222–9226. doi: 10.1128/JVI.02653-10

Frontiers in
Cellular and Infection Microbiology

Investigates how microorganisms interact with their hosts

Explores bacteria, fungi, parasites, viruses, endosymbionts, prions and all microbial pathogens as well as the microbiota and its effect on health and disease in various hosts.

Discover the latest Research Topics

See more →

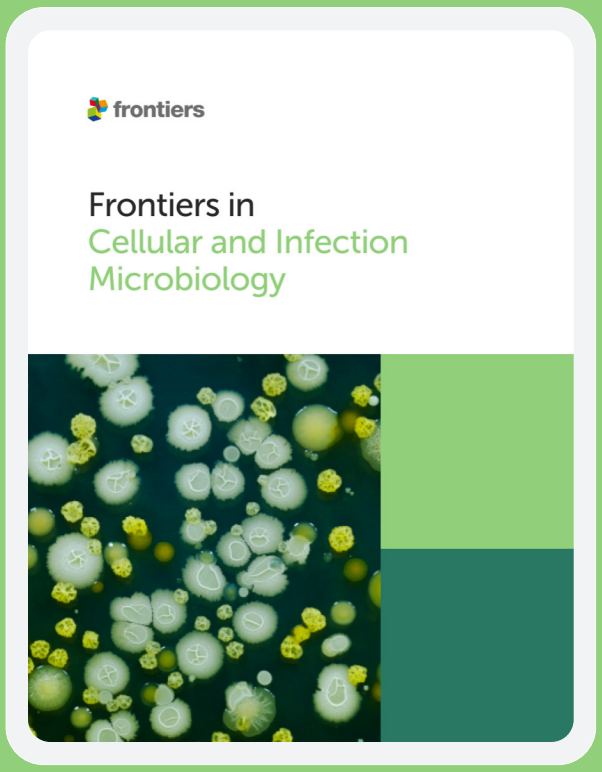

Frontiers

Avenue du Tribunal-Fédéral 34
1005 Lausanne, Switzerland
frontiersin.org

Contact us

+41 (0)21 510 17 00
frontiersin.org/about/contact